Urban Flood Simulation by Coupling a Hydrodynamic Model with a Hydrological Model

Hongbin Zhang

A thesis submitted for the degree of Doctor of Philosophy

School of Civil Engineering and Geosciences
Faculty of Science, Agriculture and Engineering
Newcastle University
Newcastle upon Tyne
UK

July 2014

Declaration

I hereby certify that this work is my own, except where otherwise acknowledged, and that it has not been submitted previously for a degree or other qualification at this, or any other university.

Signature:

Hongbin Zhang

03/07/2014

Abstract

This work introduces a new integrated flood modelling tool in urban areas by coupling a hydrodynamic model with a hydrological model in order to overcome the drawbacks of each individual modelling approach, i.e. high computational costs usually associated with hydrodynamic models and less detailed physical representations of the underlying flow processes corresponding to hydrological models.

Crucial to the simulation process is to first divide the catchment hydraulic and hydrological zones where the corresponding model is then applied. In the hydrological zones that have more homogeneous land cover and relatively simple topography, a conceptual lumped model is applied to obtain the surface runoff, which is then routed by a group of pre-acquired 'unit hydrographs' to the zone border, for high-resolution flood routing in the hydraulic zones with complex topographic features, including roads, buildings, etc. In hydraulic zones, a full 2D hydrodynamic model is applied to provide more detailed flooding information e.g. water depth, flow velocity and arrival time.

The new integrated flood modelling tool is validated in Morpeth, the North East of England by reproducing the September 2008 flood event during which the town was severely inundated following an intense rainfall event. Moreover, the coupled model is investigated and evaluated according to the effects from temporal and spatial resolutions, friction, rainfall, infiltration, buildings and coupling methods. In addition, the model is also employed to implement flood damage estimations with different scenarios of the upstream storage and flood defences in the town centre.

Whilst producing similar accuracy, the new model is shown to be much more efficient compared with the hydrodynamic model depending on the hydrological zone percentage. These encouraging results indicate that the new modelling tool could be robust and efficient for practitioners to perform flood modelling, damage estimation, risk assessment and flood management in urban areas and large-scale catchments.

Acknowledgements

First of all I would like to express my deepest gratitude to my supervisor, Professor Qiuhua Liang, for his guidance throughout. He has supported, encouraged and provided me with constructive criticism right through my PhD study. I have also learnt a rigorous scientific approach and a positive philosophy of life from his example that will be beneficial in my future career and life. At the same time I have appreciated the patient instruction and helpful suggestions of my other supervisors, Professor Chris Kilsby and Professor Lan Li. All three professors have enabled me to complete this PhD thesis.

I would like to acknowledge, too, the financial sponsorship of 'The School of Civil Engineering and Geosciences' and 'The Chinese Scholarship Council' for the first three years. Then for the fourth year of my PhD study 'The Henry Lester Trust Limited' and 'The Great Britain-China Educational Trust' took over the financial expenditure. Without all their funding, I could not have afforded the four years of study overseas.

There are other individuals who have given me their time and effort so that I could complete my research. Dr. Geoff Parkin has given me access to observed data and shared useful information with me about the research site. The Environmental Agency and Morpeth Flood Scheme Team have provided me with a range of useful data, too. These sources are the base for and a prerequisite of my thesis. Additionally, I have to thank for the technical support from my colleagues, Jingming Hou, Luke Smith, Yueling Wang, Rong Zhang, Steve Birkinshaw, Reza Amouzgar, Martin Robertson and Laura Hanson as well as Samantha Mahaffey for proof reading this thesis.

Life is always punctuated by ups and downs, which have been ever-present over the past four years, so I have cherished the selfless and unwavering love from my parents, my Aunty Lirong and my best friend, Huiyong Li. When the way forward has been difficult, they have been constantly encouraging me to persevere. So I would like to dedicate this thesis to them as a token of my appreciation of all they have done for me. Besides them, I would also like to thank my dear friends, Miao Wang, Roger Darsley, Norma Darsley, Lili Zhang, Jingchun Wang, Alexander Nicolson, Xiaohao Shi, Xilin Xia, Guang Gao, Ciprian Spatar, Mengfei Yang, Dan McBride, Pan Chen, Yu Huang, You Luo, Lei Cui, Xueguan Song, Wenbin Liu, Jia Jia, Huibo Liu, not forgetting the

care shown by Dr. Sophie Weatherhead and the nurses in the Royal Victoria Infirmary, Newcastle.

My final acknowledgement is for the services offered by the computing technicians, administrative staff and librarians at Newcastle University, especially Graham Patterson, Melissa Ware, Hannah Lynn, Lynn Patterson and Ruth Vater.

Abbreviations

1D	One-dimensional
2D	Two-dimensional
3D	Three-dimensional
ADI	Alternating Direction Implicit
ADO	above Ordnance datum
AMR	Adaptive Mesh Refinement
ANN	Artificial Neural Network
API	Application Processing Interface
ArcGIS	A GIS for working with maps and geographic information
ARMA	Auto-Regressive Moving Average
AUD	Australia dollar
CEH	Centre for Ecology and Hydrology
CFL	Courant-Friedrichs-Lewy
CNY	Chinese Yuan
CPU	Central Processing Unit
CUDA	Compute Unified Device Architecture
DDF	Depth-Duration-Frequency
DEFRA	Department for Environment, Food and Rural Affairs
DEM	Digital Elevation Model
DIVAST	Diffuse Source Vertical Analytical Solute Transport Model
DSM	Digital Surface Model
DTM	Digital Terrain Model
DWM	Diffusion Wave Model
EA	Environment Agency
EPSRC	Engineering and Physical Sciences Research Council
ESRI	Environmental Systems Research Institute
FDM	Finite Difference Method
FEH	Flood Estimation Handbook
FEM	Finite Element Method
FHRC	Flood Hazard Research Centre
FRMRC	Flood Risk Management Research Consortium
FSR	Flood Studies Report

FVM	Finite Volume Method
GBP	Great Britain Pound
GIS	Geographic Information System
GNSS	Global Navigation Satellite System
GPGPU	General-Purpose Graphics Processing Units
GPS	Global Positioning System
GPU	Graphics Processing Unit
HBV	Hydrologiska Byråns Vattenbalansavdelning (Swedish)
HEC-RAS	Hydrologic Engineering Center - River Analysis System
HLLC	Harten Lax and van Leer-Contact
HOST	Hydrology of Soil Type
HYMAS	Hydrological Model Application System
ID	Identification
IDF	Intensity-Duration-Frequency
IHDM	Institute of Hydrology Distributed Model
InterpOSe	A software to process Ordnance Survey MasterMap files
IPCC	Intergovernmental Panel on Climate Change
ISIS	A commercial model by CH2M HILL engineering company
IUDM	Integrated Urban Drainage Management
JBA	Jeremy Benn Associates
JFLOW	A 2D flood model by JBA consulting company
LiDAR	Light Detection and Ranging
MIKE	A series of commercial models by the Danish Hydraulics Institute
MPI	Message Passing Interface
NVIDIA	An American global technology company
ODE	Ordinary Differential Equation
OpenCL	Open Computing Language
OpenMP	Open Multiple Processing
OS	Ordnance Survey
PVM	Parallel Virtual Machine
RAF	Royal Air Force
ReFH	Revitalised Flood Hydrograph
RMA2	Resource Management Association-2 (a hydraulic model)
RNLI	Royal National Lifeboat Institution

SAR	Synthetic Aperture Radar
SHE	Système Hydrologique Européen (French)
SWAT	Soil Water Assessment Tool
SWM	Stanford Watershed Model
SWMPs	Surface Water Management Plans
TBR	Tipping Bucket Rain gauge
TELEMAC	A commercial model by the Division for Research and Development of the French Electricity Board
TOPMODEL	A topography-based hydrological model
TUFLOW	Two-dimensional Unsteady FLOW
TVD	Total variation diminishing
TWI	Topographic Wetness Index
UH	Unit Hydrograph
USDA	United States Department of Agriculture
WBM	Water Balance Model
ZIM	Zero Inertial Model

Notations

A	cross-sectional area
AREA	catchment area (km)
B	benchmark dataset
BF_0	initial base flow (m^3/s)
BFIHOST	base flow index from 'Hydrology of Soil Types' classification
BL	base flow recession constant
BR	ratio of base flow recharge to runoff
C	DDF curve parameter
C_f	bed roughness coefficient
C_{ini}	initial soil moisture content (mm)
$C_{\max}$	maximum soil moisture content (mm)
C_r	Courant number
D	design rainfall duration (hours)
D_1	DDF curve parameter
D_2	DDF curve parameter
D_3	DDF curve parameter
dis	distance between rain gauges and the town centre
DPLBAR	mean drainage path length (km)
DPSBAR	mean drainage path slope ($m\ km^{-1}$)
E	east interface of a cell
E_0	DDF curve parameter
EE	evapotranspiration
$\mathbf{f}$	flux vector in x-direction in shallow water equations
f	infiltration
F	DDF curve parameter
F^1	first fit statistic
F^2	second fit statistic
FF	cumulative depth of infiltration
$\mathbf{g}$	fluxes vector in y-direction in shallow water equations
g	gravitational acceleration
GE	global error of water depth

h	water depth
$\bar{h}$	water depth before non-negativity depth reconstruction
i	cell index in x-direction
I	position at inner boundary
ii	index of rain gauges
j	cell index in y-direction
k	time level
K_s	saturated hydraulic conductivity
Ks_1	saturated hydraulic conductivity for clay loam
Ks_2	saturated hydraulic conductivity for sandy clay loam
L	left hand side of cell interface
M	modelling results
n	Manning coefficient
N	the north interface of a cell
nn	total number of rain gauges
NN	total number of computational cells
O	position at outer boundary (ghost cell)
P	counter used in fit statistics
pow	power of inverse distance
PP	rainfall
$PROPWET$	proportion of time when soil moisture deficit was less than or equal to 6 mm during the period 1961-1990
q_x	unit width discharge in x-direction
Q_x	discharge in x-direction
$\overline{q_x}$	unit width discharge in x-direction before non-negativity depth reconstruction
q_y	unit width discharge in y-direction
Q_y	discharge in y-direction
$\overline{q_y}$	unit width discharge in y-direction before non-negativity depth reconstruction
R	right hand side of cell interface
$RMSE$	Root Mean Square Error
RR	surface runoff
$\mathbf{s}$	vector of source terms in shallow water equations
S	south interface of a cell

$\boldsymbol{S_0}$	vector of slope source term in shallow water equations
S_{0x}	second component of vector $\boldsymbol{S_0}$ or the slope source term of 1D momentum equation
S_{0y}	third component of vector $\boldsymbol{S_0}$
SAAR	1961-1990 standard-period average annual rainfall (mm)
$\mathbf{S}_f$	vector of bed friction source terms in shallow water equations
S_{fx}	second component of vector $\mathbf{S}_f$ or the friction source term of 1D momentum equation
S_{fy}	third component of vector $\mathbf{S}_f$
ss	external source term in shallow water equations
SS	maximum surface storage
t	time
T_p	time-to-peak of unit hydrograph (hours)
$\mathbf{u}$	vector of conservative variables in shallow water equations
u	depth-averaged velocity in x-direction
$\bar{u}$	depth-averaged velocity in x-direction before and after non-negativity depth reconstruction
$URBEXT_{1990}$	extent of urban and suburban land cover (year 1990)
uu	normal velocity
v	depth-averaged velocity in y-direction
$\bar{v}$	depth-averaged velocity in y-direction before and after non-negativity depth reconstruction
va	modelling flow variables
$\hat{va}$	benchmark flow variables
vv	tangential velocity
w	weight of rain gauges
W	west interface of a cell
x	Cartesian coordinate
y	Cartesian coordinate
z_b	bed elevation
$\overline{z_b}$	bed elevation before non-negativity depth reconstruction
Δq_x	increment of q_x
Δt	time step

Δx	cell size in *x*-direction
Δy	cell size in *y*-direction
Δz	difference between the actual and calculated water level in the condition where a flow hits a wall
η	water level
$\bar{\eta}$	water level before non-negativity depth reconstruction
θ_s	saturated moisture content
θ_a	initial moisture content
ρ	density of water
τ_{bx}	bed friction stress term in *x*-direction in shallow water equations
τ_{by}	bed friction stress term in *y*-direction in shallow water equations
ψ_f	matric pressure at the wetting front

Table of Contents

List of Figures

List of Tables

Chapter 1 Introduction

1.1 Background

A flood is defined as a temporary covering of water on land not normally covered by water (The European Union, 2007). It is also defined in Oxford dictionary that an overflow of a large amount of water beyond its normal limits, especially over what is normally dry land. Floods are generally categorised by their causes, and these categories comprise of: fluvial floods, pluvial floods, coastal floods, sewer floods and groundwater floods. Fluvial floods spread over the floodplain along watercourses, and are usually caused by breaching or overtopping boundaries, e.g. flood defences. Pluvial floods arise from intense precipitation falling over impermeable or saturated surfaces with inadequate drainage capacity. Coastal floods are associated with unusually high tides or surges which may be triggered by storms, earthquakes, etc. Sewer floods occur when sewer systems are blocked or their capacity is insufficient. Groundwater floods generally result from the rise of groundwater tables above ground surface levels after prolonged heavy rainfall. A flood event could be a joint occurrence caused by any number of these reasons.

Floods can help improve soil fertility, maintain natural irrigation, replenish wetland ecosystems and recharge groundwater. However, floods also have plenty of adverse impacts. In many countries and regions, flooding is one of the most frequent and the most destructive natural disasters which can cause huge economic, social, environmental and ecological losses, and even threaten human lives. For instance, flooding can damage properties, farmland, infrastructure and transportation, interrupt power supplies, and also cause pollution. The indirect effects of flooding may lead to water supply shortages, spread of diseases, loss of food stockpiles and psychological damage (König *et al.*, 2002).

A growing number of severe floods have been witnessed over the past two decades in the UK. In the autumn of 2000, tropical cyclones caused heavy rainfall and consequently severe flooding across the UK. The worst affected areas were Kent and Sussex in October; and Shropshire, Worcestershire and Yorkshire in November. The successive series of floods caused two deaths and the inundation of 7,406 properties with a total economic loss of £500 million (Met Office, 2014). In January 2005, Carlisle

experienced the worst flood since 1822, in which 1,844 properties were flooded and 2,700 homes were affected. The flood directly caused three deaths and over £400 million of economic losses. Two years later, England and Wales were hit by severe flooding which caused 14 deaths and left thousands of people suffering prolonged misery. More than 55,000 homes and 6,000 businesses were flooded, resulting in the highest number of search-and-rescue missions in the UK since the Second World War (Marsh and Hannaford, 2007). Furthermore, the Association of British Insurers (2007) noted that 165,000 claims totalling £3 billion were reported. In September 2008, serious flooding hit the North East of England, and in the town of Morpeth alone, approximately 1,000 properties were inundated. Nationwide flood events occurred during the course of 2012 and through the winter into 2013 which caused at least nine deaths and the economic loss of about £1 billion. In Tyne and Wear, on 28th June 2012, 50mm rain fell in around two hours, equivalent to the average rainfall for the whole month of June. The heavy storm occurred during the afternoon rush hour, resulting in widespread travel chaos. Notably, the Central Railway Station and the Metro system were closed, and many buses were either seriously delayed or cancelled. The flood also lead to around 500 properties suffering internal flooding (Newcastle City Council, 2013). A more recent flood episode in the UK occurred between December 2013 and January 2014 as a result of clustered and persistent storms. The exceptional winter storms triggered the highest tide in eastern and southern England since January 1953 requiring substantial evacuation efforts, as seen in Lincolnshire, and causing wetland damage, such as in Norfolk. Thereafter, high rainfall and a sharp increase in river flow were witnessed in South West England followed by severe floodplain inundations, which caused major disruptions to households, businesses and infrastructure. Furthermore, in Sussex and Hampshire, groundwater flooding occurred. The delayed response to the rainfall contributed further flooding in vulnerable aquifer areas (Met Office, 2014).

Flooding is not exclusive to the UK, but is also an international problem. China has experienced many devastating flood events during the last several decades due to either natural weather patterns or human conflict. The flood event of 1998 is an example, almost the whole catchment area of the Yangze River and also the Songhua River experienced intense and prolonged rainfall leading to severe floodplain inundation, and the economic loss of over 150 billion Yuan (1 GBP ≈ 15 CNY in 1998). A recent significant flood event in China was the ‘7.21 Beijing flood’ in 2012, which caused 79

deaths and the economic loss of 11.64 billion Yuan (1 GBP ≈ 10 CNY in 2012). In Europe, extreme flooding occurred after consistent heavy rain in late May and early June 2013, which primarily hit Germany, Czech Republic and Austria. Additionally, Switzerland, Slovakia, Belarus, Poland, Hungary and Serbia were affected to a lesser extent. The east coast of Australia has also suffered from flooding problems. For example, in December 2010, a series of floods affected Queensland, forcing the evacuation of thousands of people. Damage was estimated at around 2.38 billion Australian dollars (1 GBP ≈ 1.5 AUD in 2010). Other flood-prone countries include United States, Bangladesh, India, Pakistan, and Thailand, etc.

The increase in flood risk is generally caused by two main reasons: climate changes and human activities (Ashley *et al.*, 2007). Researchers are increasingly concerned in exploring the effects of climate changes (Hunt, 2002; Dale, 2005; Lehner *et al.*, 2006), and the topic has also been a focus amongst governments around the world. The Intergovernmental Panel on Climate Change (IPCC) (2007) concluded that global warming would lead to increasing probability of extreme events including severe droughts, heavy storms, substantial sea level rise and changing weather patterns, and the changes in precipitation and temperature would cause changes in runoff. Met Office (2009) also indicated that global warming and the subsequent climate changes would result in more frequent and more intense heat waves, floods, storms, droughts and wildfires. In the UK, the future changes in precipitation are highly uncertain which results in the uncertainty of flood wave formations. Quantifying the changes in flooding driven by climate change is still a very challenging research topic.

Intensive human activities are another reason of the increasing flood risks. Public and private developments physically change floodplains, interfere with the spatial distributions of water resources, and also put pressures on other natural resources. Deforestation and urbanization inevitably lead to land cover degradation and the reduction of water storage capacity, which subsequently increases the vulnerability of cities to floods. Hundecha and Bárdossy (2004) indicated an obvious increase in surface flow during a summer storm as a result of urbanisation. Waheed and Chukwuemeka (2010) investigated the Kaduna river floodplain, and concluded that increasing urbanisation was the main cause of the more frequent flood events.

The Department for Environment, Food and Rural Affairs (DEFRA) (2011) reported that around 5.2 million (one in six) residential and commercial properties in England

were estimated to be in areas of high flood risk in 2009. With the progression of climate changes and human activities, it is predicted that over the next 100 years, river and coastal flood risks could increase between two and 20 times, and the resulting annual economic losses in the UK could increase from about £1.4 billion to £21 billion by the 2080s (Evans *et al.*, 2004). However, people continue to reside in flood plains even when they are aware of the increasing flood risk because the proximity to water bodies is beneficial for water supplies, agriculture, transportation and trading. For this reason, a compromise must be made between the benefits of living in floodplains and vulnerability to the danger of flooding. The Environment Agency (2009a) showed that 55% of residents living in flood prone areas in England realised the risks of flooding and three out of five of them had taken actions to prepare for potential flooding and minimise their losses. Completely eliminating flood risks is technically and economically impossible, so the management of flood risk is recommended to avoid or mitigate the adverse impacts of floods on individuals and communities (Pitt, 2008).

1.2 Flood Risk Management

Flood risk management in many countries and regions has been established to monitor, warn, control and prevent flooding, and the management expenditure is generally far less than the losses caused by floods. The European Union has promoted flood risk management plans through the Floods Directive (The European Union, 2007), and its member states, including the UK, are obliged to assess whether their coast lines and water courses are at risk from flooding, to map the extent of flood risk in these areas, and to take measures to reduce the flood risk. The Flood and Water Management Act of 2010 requires local authorities in the UK to produce Surface Water Management Plans (SWMPs) for areas with high flood risk. The ‘Making Space for Water’ programme was initiated by DEFRA (2005) in order to improve flood risk management methods, and mitigate environmental, social and economic pressures. In addition, the UK Flood Risk Management Research Consortium (FRMRC) was set up and supported by Engineering and Physical Sciences Research Council (EPSRC) along with other funders, to support multi-disciplinary research in order to enhance flood risk management.

Assessing flood risk is an indispensable step in flood risk management. The information about when, where and to what extent floods will occur should be estimated by different modelling tools. This kind of information can help generate flood risk maps, aid in development planning and design, and in the preparation of emergency plans. The Pitt

review (2008) suggested that the Environment Agency should cooperate with other institutions to develop techniques and tools to model surface water flooding.

There are two main kinds of modelling methods to assess flood risks: physical models and mathematical models. Physical models simulate the physical processes of floods through experiments. With the recent advance in computational power and increase in the availability of data, mathematical models which conceptualise flooding problems into numerical approximations are now being widely used. Among the mathematical models, hydraulic models solving the governing flow equations, derived from mass and momentum conservation, are the most popular. These models are able to simulate the propagation of flood waves along river channels and over floodplains with complex topography, and provide important flood information including: inundation extent, water depth, flow velocity and arrival time. In practice, the majority of floods can be considered as shallow flows for which vertical flow acceleration can be neglected leading to a 2D representation of the flow. A number of researchers have shown that 2D hydraulic models are capable of providing sufficient details of gradually varying flow (e.g. Bates and de Roo, 2000; Yu and Lane, 2006a; Hunter *et al.*, 2007). Among these models, full 2D hydrodynamic models solving the full shallow water equations have proved to be the most effective in representing flows in different regimes including subcritical flows, transcritical flows, supercritical flows and shock-like flow discontinuities, and are accurate in dealing with wetting-drying problems over a complex domain topography (e.g. Anastasiou and Chan, 1997; Liang *et al.*, 2008; Ai and Jin, 2009; Kesserwani and Liang, 2010).

1.3 Urban Flood Simulations

Urban areas are usually subject to flooding from a number of sources including fluvial flooding, pluvial flooding, sewer flooding, coastal flooding and even groundwater flooding. Compared with flooding in rural areas, greater runoff can be produced in urban areas owing to the large areas of impermeable surfaces which place more pressure on drainage networks. Furthermore, urban areas are more vulnerable to flooding and may suffer more losses due to dense populations and well developed infrastructure. The concept of Integrated Urban Drainage Management (IUDM) has been introduced to consider flooding from all sources in urban areas (DEFRA, 2005). Robust flood modelling tools are in demand to predict flooding and manage flood routes in urban

areas (Evans *et al.*, 2004). The aforementioned full 2D hydrodynamic models could be an effective tool for these purposes (Hunter *et al.*, 2008).

One of the major requirements for urban flood modelling is to represent urban landscape features including urban topography as well as structural features such as buildings and fences which are important with regard to the flow direction and flood attenuation. Recently, topographic data, available through Light Detection And Ranging (LiDAR) combined with Ordnance Survey (OS) MasterMap land use data, has made it possible to describe urban landscape variations in a high-resolution digital form. Yu and Lane (2006a) have demonstrated that a reduction in resolution may have considerable influence on the representation of fine-scale structures and hence affect simulation results. For example, the loss of representation of paths between buildings may lead to false flow directions. Evans (2010) has investigated the problem of to what extent resolution can be decreased whilst maintaining the representation of the urban landscape features. In general, modelling of urban flooding must be carried out at a resolution of better than 5×5 metres or so (Mark *et al.*, 2004).

The aforementioned full 2D hydrodynamic models, which are based on mass and momentum conservation, can provide a detailed physical description of flood waves, but generally require sophisticated computational methods to provide reliable and stable numerical solutions. This inevitably incurs considerable computational cost especially for high- resolution simulations in urban areas. The balance between computational accuracy and efficiency needs to be achieved in practical applications to urban flood simulations.

1.4 Research Gap

Substantial research efforts have been made to improve the computational efficiency of full 2D hydrodynamic models. Hydraulic models with reduced complexity achieve better computational efficiency by omitting certain terms in the full momentum equations (e.g. Bates and de Roo, 2000; Hunter *et al.*, 2007). Adaptive mesh refinement techniques can adjust mesh resolution according to surface features and flow regimes (e.g. Berger and Colella, 1989; Liang, 2012), and thereby improve the computational efficiency. Recently, parallel programming approaches (e.g. Neal *et al.*, 2009; Smith and Liang, 2013) have been utilised to better harness computing power, and achieve a significant acceleration in processing time. The above methods have been widely used,

but there are still several limitations. Reduced complexity hydraulic models may be less effective to simulate complex flow regimes; with dynamically adaptive mesh refinement techniques it can be difficult to achieve mass conservation and well-balanced conditions at the same time; and all three of the above methods are much less efficient when applied to large-scale catchments.

Hydrological models are another type of mathematical model. They are widely used in rural catchments which cost less computational time by representing less detailed physical processes, but can provide reasonable simulating capability. Coupling hydrodynamic models with hydrological models may overcome the shortcomings of either type of the modelling approaches. The main shortcomings of the two approaches are: high computational cost usually associated with hydrodynamic models and a less detailed physical representation of underlying flow processes corresponding to hydrological models. Enhanced computational efficiency in urban flood simulations is therefore expected at the price of losing a detailed physical description of underlying processes in the certain parts of the floodplain. Moreover, hydrological models can reproduce the runoff production processes, which hydrodynamic models are generally incapable of, including precipitation, evapotranspiration, infiltration and interception, etc. Although hydrodynamic and hydrological models have been separately used in many practical applications, coupling of these two types of models for urban flood simulations are still not many in literature. The current coupled models generally only consider a point link, such as a river inlet, between hydrological model and hydrodynamic model. There is a need to appropriately couple the hydrodynamic and hydrological models to offer more effective urban flood simulations by considering surface runoff from the hydrological zones to flooding in hydraulic zones, and also save computational costs.

1.5 Aim and Objectives

The aim of this work is to develop a robust and efficient tool for practitioners to perform urban flood modelling by coupling a hydrodynamic model with a hydrological model.

The aims can be specified into the following objectives:

1) Review the main hydrodynamic models, hydrological models and existing methods to balance computational accuracy and efficiency.

2) Collect and process data for the selected research site.

3) Develop an approach to divide the research site into hydraulic and hydrological zones according to the design flood event and land cover.

4) Develop a coupled hydrodynamic and hydrological model.

5) Configure the coupled model for paralleling computing with Open Multiple Processing (OpenMP).

6) Validate the coupled model through a selected flood event in the research site.

7) Evaluate the effect on the coupled model from modelling resolutions, bed friction, rainfall, infiltration, buildings and coupling methods, etc.

8) Implement the flood damage estimation under different scenarios of the upstream storage and flood defences in the research site.

9) Identify the limitations of the coupled model and indicate the need for future research.

1.6 Thesis Outline

Chapter 1 briefly introduces the background of flood risk management, discusses the problems in urban flood simulations, explains the aim and objectives of this work and outlines the thesis structure.

Chapter 2 presents a comprehensive literature review of the main hydrodynamic models, hydrological models and existing methods to balance computational accuracy and efficiency.

Chapter 3 describes the methodology which is employed in this work, mainly including the descriptions of the selected hydrodynamic model and hydrological model as well as the coupling methods.

Chapter 4 introduces the research site to which the coupled model is applied. In addition, it addresses data needs, and describes the data collection and processing.

Chapter 5 focuses on the presentation and discussion of the modelling results.

Chapter 6 draws conclusions upon the current research and identifies future work.

Chapter 2 Literature Review

In this chapter, full 2D hydrodynamic models are firstly reviewed in the context of flood modelling. Despite the satisfactory computational accuracy they achieved, the high computational cost is the main disadvantage, limiting their practical applications for large-scale simulations that cover a whole city or catchment. Different means to improve the computational efficiency of full 2D hydrodynamic models are thereafter discussed, of which coupling hydrodynamic models with hydrological models is a promising way to resolve this problem. Herein, the main types of hydrological models and existing coupling methods are reviewed and discussed. Finally, a new coupled model is proposed, and relevant techniques employed in this model are also reviewed.

2.1 Full 2D Hydrodynamic Models

Hydraulic models may be classified into one, two and three-dimensional models. 1D hydraulic models generalise a river channel into a number of cross sections perpendicular to the channel centreline, and the floodplain is regarded as extended cross sections. These models can provide good descriptions of flood routing for in-bank flows and are widely used in practice. Examples of well-known 1D hydraulic modelling systems include ISIS (Halcrow & Wallingford, 1997), MIKE11 (Danish Hydraulic Institute, 2001) and HEC-RAS (US Army Corps of Engineers, 2010). However, due to the high level of simplification, 1D models are incapable of accurately reproducing floodplain inundations and flows over complex topography. On the contrary, 3D hydraulic models, like FLUENT (Fluent Incorporated Company, 2006) and MIKE 3 (Danish Hydraulic Institute, 2011), involve full representations of flow processes in three-dimensions. These models may potentially provide better representation of the physical flow processes and hence more accurate results, but they are also computationally demanding due to the complex model structures. In reality, for the majority of floods, water depth can be considered small, compared to the wave length and horizontal dimensions of the physical domain. The vertical variation of flow velocity may be neglected to give rise to a two-dimensional approximation. Therefore, 2D shallow water models are adequate to provide sufficient details for most flood events.

Among 2D hydraulic models with different levels of complexity, hydrodynamic models that consider the full terms of shallow water equations have proved to be powerful in modelling transient flow phenomena with high computational accuracy. Examples of the commercial full 2D hydrodynamic models include TELEMAC-2D (Division for Research and Development of the French Electricity Board, 2000), MIKE21 (Danish Hydraulic Institute, 2011), RMA2 (US Army Engineer Research and Development Center, 2006), TUFLOW (BMT WBM, 2010), DIVAST (Dillon, 1988) and so on. MIKE21 and TUFLOW adopt the Alternating Direction Implicit (ADI) technique to integrate the governing equations of mass and momentum conservation in the time-space domain, which work well when flows are slow and smooth. However, the ADI technique is inadequate to describe supercritical flows or transcritical flows that can be commonly found in dam breaks, levee breaches and flash floods (Liang *et al.*, 2007b). DIVAST utilises the finite difference method (FDM) (Fennema and Chaudhry, 1990) to solve full 2D shallow water equations; while RMA2 and TELEMAC-2D adopt the finite element method (FEM) (Bates and Anderson, 1993). However, compared with the finite volume method (FVM) (Zhao *et al.*, 1994; Caleffi *et al.*, 2003), it is usually difficult for FDM to maintain local mass and momentum conservation, and is time-consuming for the FEM to construct shock-capturing schemes.

A robust full 2D hydrodynamic model for flood simulations should be：

- Able to simulate different types of flow including transcritical flows, subcritical flows, supercritical flows, shock-like flow discontinuities, and tidal surges
- Well-balanced to cope with complex topographic features in a natural terrain, and this means that the fluxes and slope source terms are balanced without spurious momentums (Greenberg and Leroux, 1996)
- Effective and accurate in dealing with wetting and drying without predicting negative water depths

Liang (2010) has developed such a robust model, in which, the well-balanced full 2D shallow water equations are explicitly solved by a Godunov-type finite volume scheme (Alcrudo and Garcia-Navarro, 1993) with the interface fluxes evaluated by Harten Lax and van Leer-Contact (HLLC) approximate Riemann solver (Toro *et al.*, 1994), and numerical stability of the model is controlled by the Courant-Friedrichs-Lewy (CFL) criterion. Additionally, a non-negative water depth reconstruction approach is used to

deal with the wetting and drying front. In order to avoid spurious oscillations an implicit scheme is utilised to discretise the friction source term. This full 2D hydrodynamic model has been validated (Liang, 2011; Wang *et al.*, 2011a) for different flow regimes, and to trace wetting and drying fronts over complex bed topography, preventing negative depth predictions. Other full 2D hydrodynamic models, e.g. which are equipped with a Godunov-type finite volume scheme (Begnudelli and Sanders, 2007; Song *et al.*, 2011; Hou *et al.*, 2013) or TVD-MacCormack finite different scheme (Liang *et al.*, 2007c) may also meet the above criteria for robust models.

Even if full 2D hydrodynamic models can simulate and predict floods with relatively high computational accuracy, there is a common problem in practice that they may be computationally expensive, especially in the following conditions for flood risk assessment:

- Flood simulations for a large-scale catchment
- High-resolution simulations for urban inundations
- The prediction of flood frequency with a large number of simulations, e.g. Monte Carlo method (Rahman *et al.*, 2002).

In such cases, measures need to be taken to improve the computational efficiency of full 2D hydrodynamic models.

2.2 Hydrological Models

There are several different classification methods for hydrological models, including linear or non-linear; stochastic or deterministic; lumped or distributed (Beven, 2012).

With regard to the representations of physical processes, hydrological models can be classified into empirical, conceptual and physically based models. This is one of the most often used classification methods.

Empirical models or black-box models describe a real system with a mathematical relationship between the input e.g precipitation and output e.g. outflow hydrograph with parameters that may not have physical meanings, but the relationship is based on statistics and implicitly represents the underlying physical system. Empirical models are straightforward and easy to be implemented, and are quite useful in the catchments with sufficient data. The ARMA (Auto-Regressive Moving Average) model (Tesfaye *et al.*,

2006) and ANN (Artificial Neural Network) model (Hsu *et al.*, 1995) belong to this category.

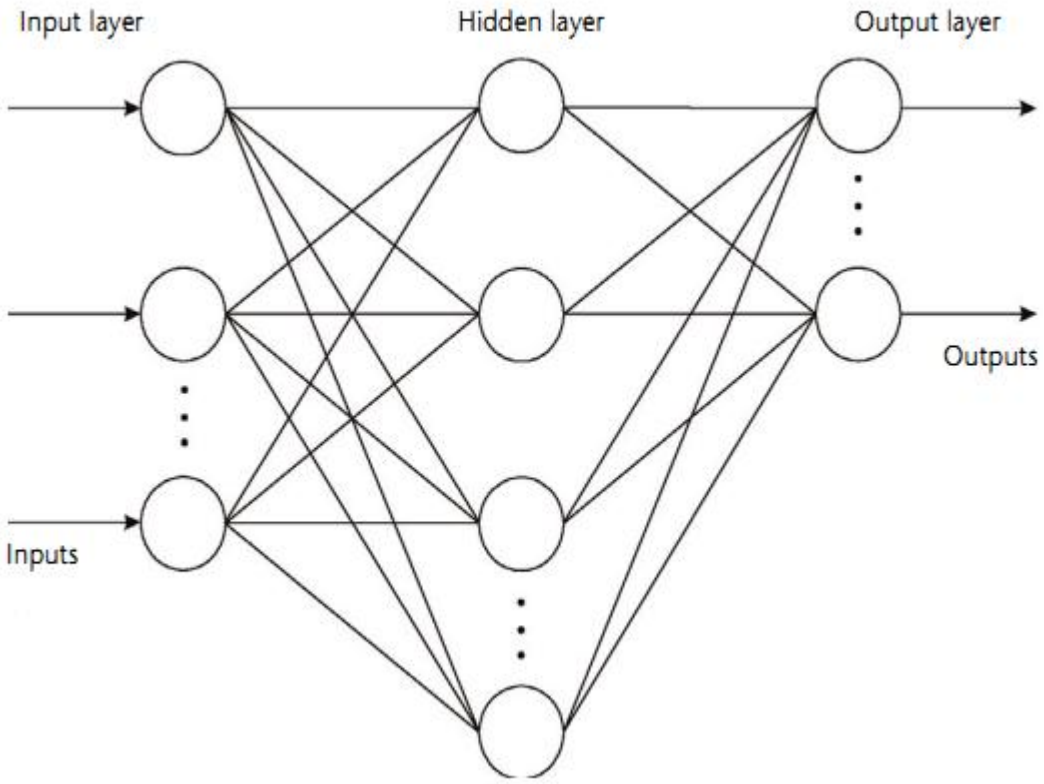

Figure 2.1 Structure of the ANN model (Kumar *et al.*, 2012).

Conceptual models or grey-box models representing limited processes in the hydrological system are a trade-off between empirical and physically based models. Conceptual models simplify hydrological processes by a series of conceptual elements. These can be described by non-linear reservoir equations, considering physical representations in a highly simplified form. Conceptual models are quite popular because they are much easier to set up than physically based models, and can provide more reliable simulations than empirical models. Examples of this type of models are SWM (Stanford Watershed Model) (Crawford and Linsley, 1966) and HBV (Hydrologiska Byråns Vattenbalansavdelning) model (Bergström, 1995).

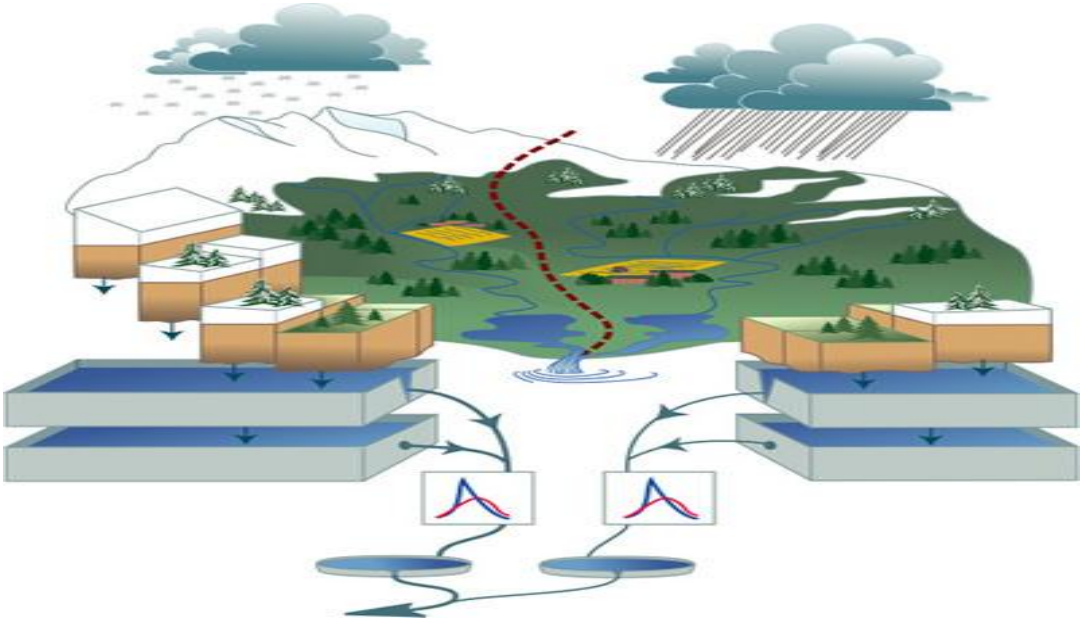

Figure 2.2 Schematic diagram of HBV model (SMHI, 2006).

Physically based models or white box models describe hydrological processes by considering as many physical processes as necessary. Based on the governing physical theory, these models are complicated to develop, which require a considerable amount of data and computational time as well as heavy work on parameterisation. SHE (Système Hydrologique Européen) model (Abbott *et al.*, 1986) and IHDM (Institute of Hydrology distributed model) (Beven *et al.*, 1987) are two examples of this class.

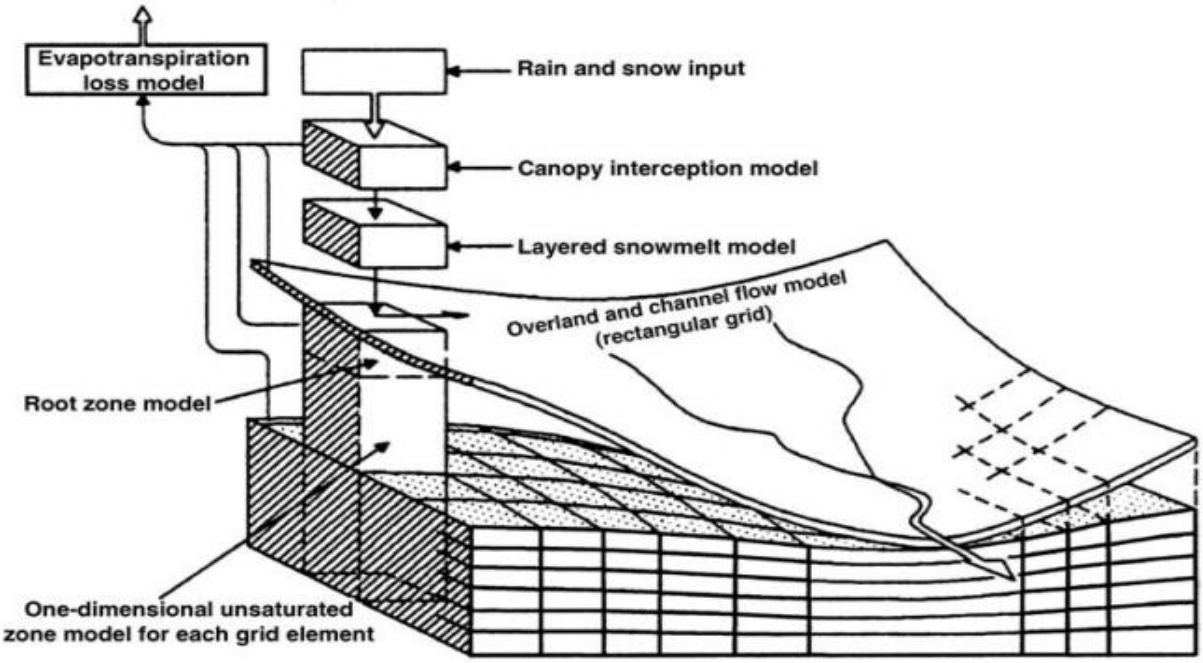

Figure 2.3 Schematic diagram of a grid-based catchment discretisation as in SHE model (Refsgaard and Storm, 1995).

Another classification method is according to the spatial scale of catchments. In this aspect, hydrological models can be classified into lumped, semi-distributed and distributed models.

Lumped models treat the whole catchment as a homogenous unit ignoring spatial variations, so heterogeneities can not be represented by catchment-averaged parameters. The lumped models are usually used to fill missing data and extend existing data. There are many lumped models available in literature, e.g. SWM (Stanford Watershed Model) (Crawford and Linsley, 1966), IUH (the Institute of Hydrology) Lumped Model (Nash and Sutcliffe, 1970).

Semi-distributed models lie between lumped and distributed models. These calculate the average runoff production in sub-catchments, and route the runoff within and between sub-catchments to the outlet of the whole catchment. Kite and Kouwen (1992) validated that semi-distributed models outperformed lumped models because they related the parameter values to different sub-catchment conditions, and hence produced a more reasonable representation of the whole catchment. HBV model, HYMAS (Hydrological Model Application System) (Hughes and Sami, 1994), SWAT (Soil Water Assessment Tool) model (Arnold *et al.*, 1998) and TOPMODEL (Beven and Kirkby, 1979) are examples of this class.

Distributed models, or fully distributed models divide the whole catchment into cells where calculations are implemented. Therefore, the spatial variations of catchments can be better considered compared with semi-distributed models. The aforementioned SHE model and IHDM are two examples of distributed models.

Based on the above review, in general physically based distributed models are the most powerful among different hydrological models because physical processes and spatial variations are well represented. However, like hydrodynamic models, they are difficult to develop and cost much computational time.

2.3 Main Approaches to Improve Computational Efficiency

Many efforts in balancing computational accuracy and efficiency have been reported in literature, and these may be classified into mathematical, numerical and computing methods.

2.3.1 *Simplified models*

A number of simplified models for inundation modelling, which aim to improve computational efficiency by omitting certain terms in the momentum equations of the full 2D shallow water formulation and using less complex numerical schemes, have proliferated over the last decades (e.g. Bates and de Roo, 2000; Hunter *et al.*, 2007; Bates *et al.*, 2010). These models solve the kinematic, diffusion and partial inertial equations, which can be regarded as a progression in complexity towards full dynamic equations, and provide the different levels of simulating abilities (Hunter *et al.*, 2007).

Taking 1D momentum equation as an example, it can be used to demonstrate the different levels of complexity of the dynamic equations:

$$\underbrace{\underbrace{\underbrace{\underbrace{\frac{1}{A}\frac{\partial}{\partial x}\left(\frac{Q_x^{\,2}}{A}\right)}_{\text{Dynamic wave}}+\frac{1}{A}\frac{\partial Q_x}{\partial t}}_{\text{Partial inertial wave}}+g\frac{\partial h}{\partial x}}_{\text{Diffusion wave}}-g(S_{0x}-S_{fx})}_{\text{Kinematic wave}}=0\,, \tag{2.1}$$

where t denotes time; x is the Cartesian coordinate; Q_x is the discharges; A is the cross-sectional area; h is the water depth; g is the gravity acceleration; S_{0x} is the slope term, and S_{fx} is the friction force term.

The most basic form of the momentum equation (Cunge *et al.*, 1980) is the kinematic wave approximation which neglects dynamic and pressure terms by assuming that flows are primarily influenced by gravity, and the frictional force is balanced with the gravity force. The kinematic wave theory was developed by Lighthill and Whitham (1955a; 1955b) and used to describe the propagation of flood waves in long rivers. Almost at the same time, developed an approximate method with the kinematic wave assumption for routing steady and uniform flows in open channels with any shape of cross section. Both sets of research can be credited as the first proposals of the kinematic wave approximation. Since then the kinematic wave theory has been applied to a variety of hydrological processes (Singh, 1996; Singh, 2001). Examples of its application involve overland and channel flows, base flows, movement of glaciers, erosion and sediment transport, etc. However, this theory can only give a reasonable level of accuracy for simple flow regimes.

A more practical simplification is the diffusion wave approximation achieved by eliminating the dynamic terms of the momentum equations for simulating steady but non-uniform open channel flows. The diffusion wave concept was firstly introduced by Cunge *et al*. (1980). Govindaraju *et al*. (1988a; 1988b) did a lot of research on the diffusion wave approximation, and obtained an analytical approximation in the form of a cubic approximation providing upper and lower boundaries for its applications. Parlange *et al*. (1989) for the first time compared the predictive results under steady state conditions from the kinematic wave approximation and the diffusion wave approximation, and investigated the differences between them. A number of successful diffusion wave models (DWMs) or zero inertial models (ZIMs) for flood simulations have been reported in literature (e.g. Cunge *et al.*, 1980; Bates and de Roo, 2000; Horritt and Bates, 2001; Horritt and Bates, 2002; Bradbrook *et al.*, 2004; Yu, 2005; Yu and Lane, 2006a; Yu and Lane, 2006b; Hunter *et al.*, 2008; Wang *et al.*, 2011b). Among these models, LISFLOOD-FP (Bates and de Roo, 2000) and JFLOW (Bradbrook *et al.*, 2004) are two popular ones. Despite their successes, concerns have been raised over the lack of inertial terms. One such concern may involve the control of time steps. 'Chequerboard' type oscillations may be generated, as shown in Figure 2.4, unless the constant time step is small enough, where water in one particular cell drains into the adjacent cell in a single large time step and flows back again in the next time step (Cunge *et al.*, 1980).

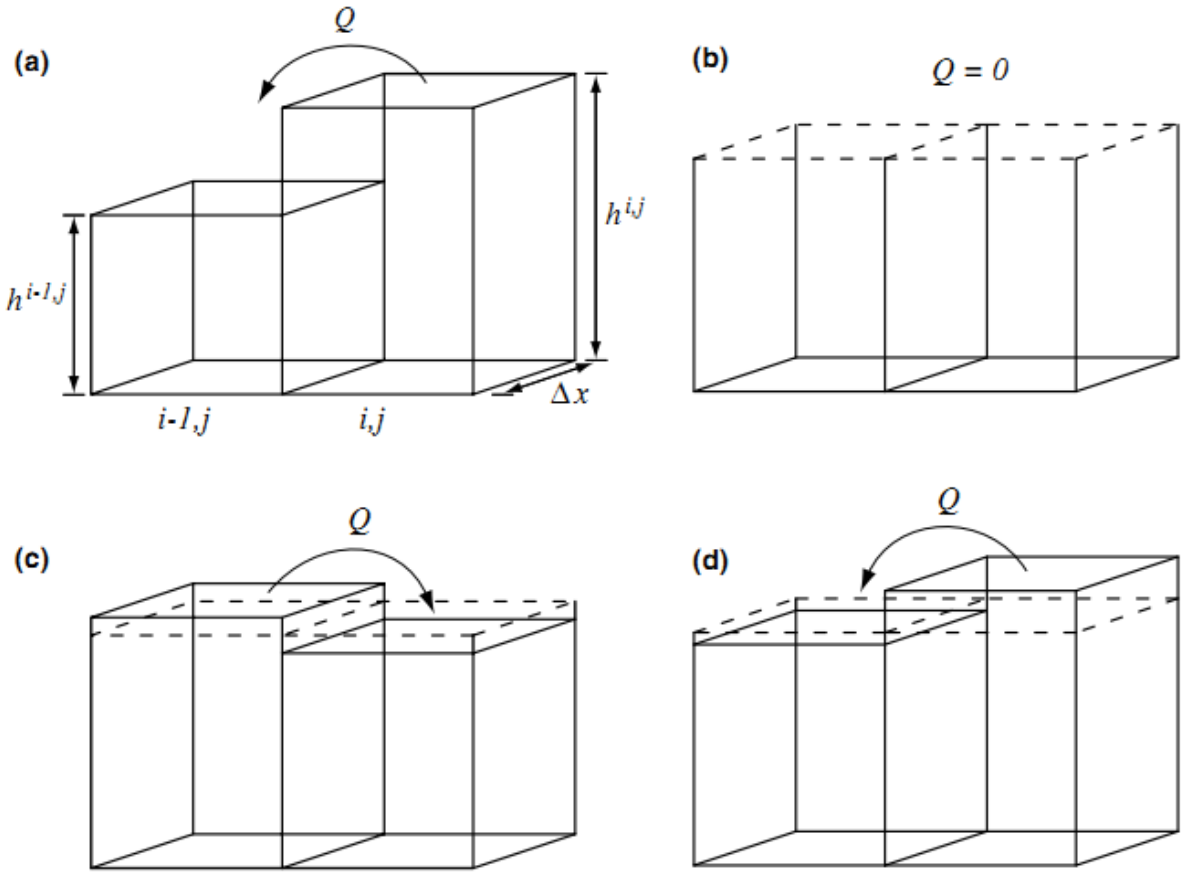

Figure 2.4 Illustration of chequerboard oscillations between two adjacent cells (Hunter *et al.*, 2005).

To avoid this instability, a flow limiter, which sets the maximum flow that can occur between cells, is required. This prevents too much water from leaving a given cell in a single time step. However, the flow limiter displays a strong dependence on the selected cell size and time step, but is not sensitive to the bed friction. The adaptive time stepping proposed by Hunter *et al.* (2005) may be an alternative to the flow limiter, where an optimum time step is calculated in every iteration, by using the Von Neumann condition. This time step is therefore adaptive during the course of a simulation and independent of the initial choice of the time step. However, later work by Hunter *et al.* (2006) found the computational cost increased dramatically when the adaptive stepping scheme was implemented for higher-resolution grids because the optimum time step reduced quadratically with decreasing cell sizes. Due to the necessity for a stricter time step control to maintain stability, the effect of diffusion wave approximations in saving computational time is not obvious for higher-resolution simulations.

Hunter *et al.* (2008) suggested that inclusion of inertial terms in diffusion wave equations may allow the use of a larger time step, and consequently less computational

time. Inertial terms consist of two parts: the local acceleration term and the convective acceleration term. Based on the diffusion wave approximation, a partial inertial model (also known as local inertial model, or simple inertial model) has been set up by including the local acceleration term which makes the water being modelled less likely to cause oscillations. The convective acceleration term is excluded because in many floodplains flow advection is relatively unimportant especially for gradually varying flow conditions (Hunter *et al.*, 2007; Bates *et al.*, 2010). This model has been validated by several numerical cases against field data, analytical solutions, and the solutions of simplified and full shallow water equations. (Dottori and Todini, 2011; Fewtrell *et al.*, 2011; Neal *et al.*, 2011; de Almeida *et al.*, 2012). The behaviour in saving computational time for higher-resolution simulations compared with the diffusion wave approach is satisfactory. In addition, the partial inertial scheme performs better in computational efficiency than the dynamic wave scheme due to the omission of convective acceleration terms. De Almeida and Bates (2013) presented an extended view on the application of the partial inertial approximation to several flow problems, showing the scheme could provide relatively accurate and efficient results to the lower range of subcritical flows and the upper range with mild water depth gradients.

In summary, reduced complexity models are designed to perform specific tasks by ignoring certain flow processes. In general, the simplified equations and numerical schemes remove computational burdens and thereby are less computationally expensive compared with full 2D shallow water equations. Yet it should be understood that the aforementioned simplified forms of full 2D shallow water equations have their own limitations and only account for parts of the hydraulic processes. Table 2.1 summarises the hydraulic conditions which different forms of the shallow water equations account for. When a flood event involves complex flow regimes, e.g. transcritical flows, supercritical flows or shock-like flow discontinuities, full 2D shallow water equations are essential to correctly evaluate the flooding processes. In these cases, alternative ways to reduce computational burdens for full 2D hydrodynamic models are required.

Flow conditions	Kinematic wave	Diffusion wave	Partial inertial wave	Dynamic wave
Wave translation	Yes	Yes	Yes	Yes
Backwater	No	Yes	Yes	Yes
Wave attenuation	No	Yes	Yes	Yes
Flow acceleration	No	No	Partially	Yes
Shock-like flow	No	No	No	Yes

Table 2.1 Different levels of account for the different forms of shallow water equations.

2.3.2 *Adaptive mesh refinement techniques*

An effective way to improve the computational efficiency of full 2D hydrodynamic models is to optimise computational nodes by using adaptive mesh refinement (AMR) techniques (Berger and Oliger, 1984; Berger and Colella, 1989). The basic idea is to produce higher-resolution meshes and reproduce local flow phenomena in regions of interest such as boundaries, around shocks and areas with complicated topography or structures. For the remaining parts of the domain lower-resolution computational meshes are maintained. Higher computational efficiency can be therefore achieved with significantly fewer overall computational nodes, when compared with their uniform mesh-based counterparts. AMR techniques can be performed on either structured or unstructured meshes. Unstructured meshes are extensively used owing to the high flexibility and robustness for dealing with complex domain geometries and boundaries (Sleigh *et al.*, 1998; Skoula *et al.*, 2006). However, the associated data structures are generally more complicated. For example, the information of both nodes and faces needs to be sorted and stored, and a connectivity matrix is required to define the adjacent neighbours for each control volume. Furthermore, refinements based on unstructured meshes require significant computational effort in order to find neighbouring nodes and also ensure local grid quality. These drawbacks may be avoided or mitigated by using structured meshes.

There are several techniques for structured mesh-based refinements, three of which are based on Cartesian grids: the block-structured method (Berger and Oliger, 1984; Ivanenko and Muratova, 2000; Baeza and Mulet, 2006), the hierarchical method (Rogers *et al.*, 2001; Rogers *et al.*, 2003; Liang *et al.*, 2004; Krámer and Józsa, 2007; Liang and Borthwick, 2009) and the cell-based structured method (Ji *et al.*, 2010).

However, all these methods implement local mesh refinements by using data structures with different levels of complexity, and inevitably necessitate computational overheads to store and search these data structures. It is desirable to develop a data structure free method to minimize the overheads for manipulating local mesh refinements. Recently, Liang (2012) proposed a new AMR method with no data structures needed, where all neighbours of each cell are determined entirely by a simple algebraic relationship. As a result, the computational cost may be reduced compared with the aforementioned AMR methods with data structures.

Despite the successes of AMR methods in saving computational time for full 2D hydrodynamic models, the difficulty in maintaining mass conservation and well-balanced conditions to some extent limits the development of this kind of method for a wider range of applications (Popinet, 2012; Hou *et al.*, 2014).

2.3.3 *Parallel computing*

With the rapid development of computing resources, it is becoming popular to enhance the modelling efficiency through different computing architectures, of which parallel computing is one of the most popular techniques. Parallel computing allows independent parts of a program to be executed simultaneously by processors, and thereby significantly saving computational time.

There are two main architectures to implement parallelisation including distributed memory and shared memory. For the distributed memory architecture, each processor has its own private memory and is connected to other processors through networks. Different processors are used as parts of a large cluster to calculate different elements of a whole task utilising high-throughput computing systems to facilitate the work (e.g. Condor, Cloud). This architecture is usually used to deal with coarse-grain parallelism where the target domain is decomposed into a set of subdomains, and then distributed to different processors. Tran and Hluchy (2004) introduced the approach to parallelising flooding models under the distributed memory architecture(Yu, 2010). An attempt at domain decomposition for the finite volume scheme in computational fluid dynamics was made by Pau and Sanders (2006b) with a multi-computer system. In this kind of configuration, the memory is scalable with the number of processors which means an increase in the number of processors will lead to an increase in memory sizes proportionally. However, data communication between processors needs to be dealt

with by message passing libraries such as Message Passing Interface (MPI) (Pau and Sanders, 2006a)and Parallel Virtual Machine (PVM) (Kowalik, 1994). For example, in the Godunov-type finite volume scheme, data on cells and their neighbours are required at each time step, but the information for neighbouring cells is not available for cells along boundaries if the domain is decomposed. In this case, the data interchange between subdomains is needed which is relatively difficult to implement.

The alternative architecture of parallel computing is the shared memory architecture, in which multi-processors operate independently while still having access to a global memory space. It is generally used to deal with fine-grain parallelism which is achieved by distributing iterations over different processors. Neal *et al.* (2009) implemented a parallel version of the LISFLOOD-FP hydraulic model based on the application programming interface of OpenMP, demonstrating the parallel speed-up in domains with different sizes and resolutions. The primary advantage of using the shared memory parallelisation is that it is very simple to implement without largely changing existing serial codes. The disadvantage is the lack of scalability between memory and processors. Current trends seem to indicate that the hybrid distributed-shared memory architecture (Rabenseifner *et al.*, 2009) will prevail in the future, but the increased complexity is a main disadvantage.

Mapping general-purpose computation onto Graphics Processing Units (GPUs) requires the use of graphics hardware to solve applications which are not necessarily of graphic nature. This is called General-Purpose GPU (GPGPU). Compared to Central Processing Units (CPUs), there are typically much more computing units in GPUs, which leads to great improvements in computational efficiency. A validated CPU-based flood model was converted to NVIDIA's CUDA version and run on two different NVIDIA graphics cards, which showed that equipping with GPUs increased the model's performance, with speed-ups ranging from 3x to 6x on GeForce 8400GS, and 50x to 135x on Tesla T10 (Shankar *et al.*, 2010). Smith and Liang (2013) employed OpenCL to develop a GPU-accelerated shallow flow modelling tool, which provided greater compatibility between different devices and hardware configurations than other popular alternatives, such as CUDA, with comparable performance levels. Similar to CPU-based parallelisation, the GPU-based one can also be conducted following the shared memory or distributed memory architecture. However, neither of them is easy to be implemented due to the complexity of using GPUs. The original serial codes need to be dramatically

updated to fit the requirement of GPU-based configurations. Besides, the data exchanges between GPUs and CPUs also require special considerations.

2.3.4 *Coupling hydraulic and hydrological models*

Apart from hydraulic models, other types of modelling tools such as hydrological models have been widely used to simulate and predict flows especially in rural catchments. The main advantage of hydrological models against hydraulic models is that they usually necessitate much less computational time due to a less detailed physical representation of underlying flow processes. The computational efficiency of hydraulic models may be improved at the price of losing detailed physical descriptions of certain parts of a catchment by coupling hydrological models. Furthermore, hydrological models can simulate the runoff production processes, which hydrodynamic models are usually not able to, including precipitation, evapotranspiration, infiltration and interception, etc.

There are three main types of methods for coupling hydraulic and hydrological models: external coupling, internal coupling and full coupling (Morita and Yen, 2002).

The simplest and most common type is external coupling which usually employs the pre-acquired hydrograph from hydrological models as the upstream and/or lateral boundary for the hydraulic models, to provide a one-way but seamless transition (Anselmo *et al.*, 1996; Correia *et al.*, 1998; Lastra *et al.*, 2008; Gül *et al.*, 2010; Bravo *et al.*, 2012). This coupling type is widely applied in routing flow propagation through complicated river network systems (Whiteaker *et al.*, 2006; Lian *et al.*, 2007; Bonnifait *et al.*, 2009; Mejia and Reed, 2011; Paiva *et al.*, 2011; Kim *et al.*, 2012; Lerat *et al.*, 2012). The upstream and lateral inflow in the river network can be obtained from hydrological models, while 1D hydraulic models are then used to reproduce the flow propagation within the river network. The reason why hydrological models are not utilised for simulating open channel flow is that they usually use simple flow routing methods focusing only on flood wave delays and attenuation such as the linear reservoir model (Coe, 2000) and Muskingum method (Chow, 1973). Another application of this coupling type is to simulate the inundation of ungauged urban catchments. Hydrological models offer the upstream inflow and/or lateral boundary for 2D hydraulic models to simulate the inundation within urban catchments. The hydraulic models can thereafter offer boundary conditions to downstream catchments for another hydrological

simulation (Moramarco *et al.*, 2005). A similar idea of this coupling method has also been used in simulating water quality variables in rivers (Debele *et al.*, 2008; Prinsen and Becker, 2011).

Internal coupling has also been reported in literature (Thompson, 2004), and the governing equations for hydraulic models and hydrological models can be solved separately, with information at the shared boundaries updated and exchanged at each computational time step (Morita and Yen, 2002). Thompson (2004) linked MIKE-SHE hydrological model and MIKE 11 hydraulic model by several prescribed points along the river. Water levels calculated from MIKE 11 can be transferred to MIKE-SHE, and overland flows calculated by MIKE-SHE can be fed back to MIKE 11 by these points throughout the simulation.

There is little literature which reports full coupling, due to the complication of reformulating governing equations for a coupled model and solving them as a whole.

2.4 Developing a Coupled Model

This study presents a new method for coupling hydraulic models with hydrological models in urban catchments which falls into the external coupling category. During a simulation, hydraulic and hydrological zones are firstly specified according to a design flood event and land cover where the corresponding model is applied. The runoff calculated by a lumped conceptual model, known as a Water Balance Model (WBM) (Walker and Zhang, 2002), in hydrological zones is routed with a group of pre-acquired 'unit hydrographs' to the hydraulic cells at shared boundaries for higher-resolution simulations utilising the full 2D hydrodynamic model (Liang, 2010) in hydraulic zones.

Compared with the current coupled models introduced in sub-section 2.3.4, the new coupled model in this study has following advantages:

1) Dividing hydraulic and hydrological zones according to a design flood event and land cover is more reasonable for external coupling models because the division generally ensures one-way coupling where flows only occur from hydrological zones to hydraulic zones.

2) Using a lumped conceptual hydrological model can improve computational efficiency as well as maintain reasonable representations of hydrological processes.

3) Distributed overland flows into hydraulic zones are well estimated by using a series of ‘unit hydrographs’ which are generated by pre-running a hydrodynamic model.

4) The selected hydrodynamic model is able to simulate complex flow regimes, and deal with wetting and drying fronts over a complex topography preventing negative depth predictions.

5) Inside hydraulic zones, hydrological elements such as precipitation and infiltration are also considered as the external source term of the continuity equation.

6) Buildings in hydraulic zones are represented to consider their blockage effects and the effects of precipitation on their roofs.

Herein, the techniques employed in this coupled model are briefly reviewed.

2.4.1 *Catchment division*

The most straightforward way to divide catchments into hydraulic and hydrological zones is based on bed elevation. Areas with relatively higher bed elevations can be preliminarily specified as hydrological zones, whilst other areas can be considered hydraulic zones. However, this method only offers a very rough division. A more thorough method is to use a Topographic Wetness Index (TWI) to represent the influence of topography on the propagation of floods (Beven and Kirkby, 1979; Ambroise *et al.*, 1996; Ma *et al.*, 2010). TWI considers not only bed elevations, but also takes into account local slopes. Hydrological zones are usually specified for areas with higher elevations and steeper slopes because they are less likely to be inundated, and the remaining areas are specified as hydraulic zones. However, the selection of TWI threshold value highly depends on experience. A more practical system, employed in this work, is to pre-run the hydraulic model on a lower-resolution grid with design rainfall and design hydrograph as the input, producing a rough flood extent map with a certain return period. The areas which are not inundated can be preliminarily specified as hydrological zones; whilst the rest of the domain specified as hydraulic zones. The preliminary division can be thereafter adjusted according to land cover data.

2.4.2 *Design rainfall and hydrograph*

The Intensity-Duration-Frequency (IDF) curves or Depth-Duration-Frequency (DDF) curves are a set of curves describing the relationship between rainfall intensity/rainfall depth and duration for different return periods. These are widely applied in estimating

the design rainfall. Each region may have different IDF/DDF curves depending on local meteorological and hydrological conditions. Faulkner (1999) proposed a DDF model with three concatenated line segments to represent rainfall changes with durations and return periods, and offered three formulae to evaluate the design rainfall for different durations. Other methods to construct IDF/DDF curves may involve using isopluvial maps (Reich, 1963; Froehlich, 2010) or more complex statistical models (Madsen *et al.*, 2002; Ariff *et al.*, 2012). However, these methods produce either rainfall depth or rainfall intensity for the whole duration without analysing the distribution of the rainfall within the duration. A method within the Flood Studies Report (FSR) rainfall-runoff model (Houghton-Carr, 1999), based on recommended design rainfall profiles and cumulative profiles for the UK, is capable of distributing the rainfall depth for a given duration and a required return period and obtaining a UK design hyetograph.

The design peak flow can be estimated in the easiest way, using a rational equation with the assumption that the frequency of the peak flow is equal to the frequency of the average rainfall intensity (Froehlich, 2010). A generalised logistic distribution using an L-moment method to evaluate the parameters has been introduced in the Flood Estimation Handbook (FEH) to produce flood frequency curves which represent a relationship between peak flows and return periods (Robson and Reed, 1999). However, these methods only focus on the design peak flow, and other attributes such as flood volumes and durations are not investigated.

In many practical cases, the full design hydrograph is of interest. The relationship between peak flows and hydrograph volumes has been analysed from recorded data, and a large set of annual maxima synthetic hydrographs that keep the distributions of peaks, volumes and durations have been generated for reservoir design (Mediero *et al.*, 2010). Another two popular methods to obtain design hydrographs are event-based method (Kjeldsen, 2007a) and continuous simulation method (Boughton and Droop, 2003). The former is to apply a design hyetograph into a rainfall-runoff model and obtain the corresponding design hydrograph with the same return period. The latter is to select the maximum annual hydrograph from a long synthetic runoff-time series which is obtained from a continuous simulation by a rainfall-runoff model with long synthetic rainfall time series as the input. These two methods have been examined and compared in terms of the peaks, volumes and durations of design hydrographs (Grimaldi *et al.*, 2012). Despite that the event-based approach may underestimate the volume and duration of

the resulting hydrograph (Grimaldi *et al.*, 2012), it is still widely adopted due to its simplicity and the wide availability of IDF/DDF curves. In the UK, an event-based Revitalised Flood Hydrograph (ReFH) Model, to estimate design hydrographs, has been proposed in FEH and widely tested in practical use (Kjeldsen, 2007a).

2.4.3 *Digital Elevation Model*

Digital Elevation Models (DEMs) play an important role in flood simulations. Field surveys and photogrammetry are traditional methods of obtaining terrain data which are both time consuming and labour-intensive. Nowadays, the LiDAR system, based on a combination of laser scanner, Global Positioning System (GPS) and an inertial measurement unit installed onto an aircraft, has become a main tool in obtaining high-resolution digital elevation data (Raber *et al.*, 2007). In the last decade, LiDAR has been significantly enhanced with laser pulse rates up to 100 kHz which improve data resolution from 3m to 25 cm, and reduce vertical elevation errors to 5 cm in relation to root mean square errors (*RMSE*s) (Fewtrell *et al.*, 2011). The direct products of the LiDAR system are Digital Surface Models (DSMs), which contain all features the laser beam strikes, including man-made objects (e.g. buildings, road lamps and bridges) and vegetation (Barber and Shortridge, 2005). Through different filter methods, all elements on the top of bare grounds can be removed and Digital Terrain Models (DTMs) are thereby produced. Both DTM and DSM need to be improved when used in flood simulations. For DTMs, the main surface features, like buildings, which may affect flood propagations, should be added to better represent floodplains. While for DSMs, surface features that may cause disturbance should be removed, such as bridges, bypasses and tree canopies along rivers.

2.4.4 *The representations of buildings*

Urban areas consist of many buildings which can not be neglected in order to reproduce accurate inundation results. There are several approaches representing buildings in urban flood simulations.

Chen *et al.* (2012) introduced the building coverage ratio and the conveyance reduction factor to consider the effect of buildings in overland flow modelling based on the coarse grid. One drawback is that extra work needs to be done to calculate building areas and the maximum occupancy ratios of buildings on computational cell boundaries.

Another approach to represent buildings is to raise the friction coefficient for cells where buildings are located in order to consider the resistance they cause. The location of buildings can be identified using OS MasterMap land cover data. The value of the friction coefficient depends on the density of buildings (Syme, 2008). However, the selection of specific values is difficult and subjective, and a thorough model calibration is required.

Liang *et al.* (2007a) and Soares-Frazão *et al.* (2008) introduced the concept of porosity into the shallow water equations and provided another way to represent buildings. The amount of water flowing through buildings is determined by the building porosity. This method can reflect the fact that buildings may allow flows to enter through doors and windows. However, porosity values are hard to specify and usually require time consuming calibrations.

The 'raised building method' involves the raising of bed elevations where buildings are located to a reasonable height in DTMs, or to filter out other features while keeping buildings in DSMs. Fewtrell *et al.* (2008) used this method to compare the model behaviours based on different grid resolution. A similar approach is called 'threshold method' where a building is represented by a threshold of elevation above which water will occupy (Schubert and Sanders, 2012). The main limitation of these methods are that 3D flow patterns may be produced locally around buildings, which may not be properly described by 2D shallow water equations.

'Blocked building method' is an alternative method which takes building cells out from the domain and insert a solid wall boundary around building outlines. Schubert *et al.* (2008) used this method to evaluate the effect of buildings showing that it could outperform 'no building' simulations especially in high-resolution modelling. Extra consideration should be taken over the rainfall occurring on the top of the buildings.

2.4.5 *Flood damage estimation*

Flood damage is the economic cost which is caused by floods. In the UK, current annual average flood damage is estimated at £1.4 billion (Foresight, 2014). The future flood damage is anticipated to be more serious in the UK. There is a wide range of research on flood damages to human health, infrastructure, buildings, vehicles and the environment (Jonkman and Kelman, 2005; Jonkman *et al.*, 2008; Penning-Rowsell *et al.*, 2010; Xia *et al.*, 2011).

Flood damages can be generally estimated by flood damage functions, which are based on the relationship between the economic damage and flood characteristics (mainly flood depth). Damage functions are derived from practical data in different countries, for different flood types. In the UK, The Flood Hazard Research Centre (FHRC) has collected information about flood impact and has developed the flood damage estimation method, which provides guidance on appraising flood damage, including the economic loss relating to urban properties and infrastructure, etc. (Penning-Rowsell *et al.*, 2010)

2.5 Summary

In this chapter, different ways to improve computational efficiency of full 2D hydrodynamic models have been reviewed. Simplified models are useful and relatively easy to be implemented. However, they are incapable of reproducing flood events that involve complex flow regimes, because certain terms in the momentum equations within the full shallow water formulation have been neglected. This problem can be avoided by combining full 2D hydrodynamic models with AMR or parallel computing techniques. For AMR, it is sometimes difficult to maintain mass conservation and well-balance conditions. Parallel computing techniques have proliferated recently with the development of computing resources. One such technique, the CPU-based OpenMP technique, is used in this study because of the ease of implementation and minimal code changes required for parallelisation.

Another idea to improve computation efficiency is to couple full 2D hydrodynamic models with hydrological models. Different methods to couple models have been reviewed, among which, the external coupling type is the most often used one. In this work, a new coupling method of this type has been proposed. On one hand, a full 2D shallow flow model (Liang, 2010), which can simulate complex flow regimes, and deal with wetting and drying fronts over the complex bed topography preventing negative depth predictions, has been employed for high-resolution flood simulations in hydraulic zones. On the other hand, a lumped conceptual hydrological model known as Water Balance Model (WBM) (Walker and Zhang, 2002) and a ‘unit hydrograph’ method, which are quite simple and straightforward, have been used in hydrological zones, providing overland inflows to hydraulic zones through cells at the shared boundary. The advantages of the new coupled model are also listed. Finally, other techniques relating to the proposed coupled model have been reviewed.

Chapter 3 Methodology

This chapter describes the main methods that are used in this study. Hydrological analysis is adopted to determine the specific sub-catchments which are of interest and will be used for modelling. These sub-catchments can be divided into hydraulic zones and hydrological zones according to a design flood event and land cover data. Thereafter, the details of the hydraulic model, hydrological model and coupling method are provided, followed by details of the model acceleration through the parallel computing technique. Finally, the flood damage estimation method is introduced to evaluate the economic losses caused by floods.

3.1 Hydrological Analysis

Hydrological analysis can help in understanding how water flows across an area, and is often used to obtain flow directions, extract stream information and delineate sub-catchments. In this study, ESRI's ArcGIS Hydrology Tool is utilised to implement the hydrological analysis in order to extract from the whole catchment the sub-catchments of interest, in which the research urban area is located. Sub-catchments are used as the computational domain as it is not necessary to run the models on the whole catchment when boundary conditions for the sub-catchments are known. Furthermore, it usually incurs high computational costs for models to be implemented over a large domain area especially when based on a relatively fine grid.

Hydrological analysis is mainly based on the topography. Depressions, also called sinks, in DTMs, can be divided into 'real' and 'fake' depressions. The 'real' depressions are essentially those locations with lower ground elevation than the surrounding areas, typically including pools, reservoirs, etc. The 'fake depressions' are typically caused by data errors, which should be identified and filled prior to hydrological analysis (Figure 3.1).

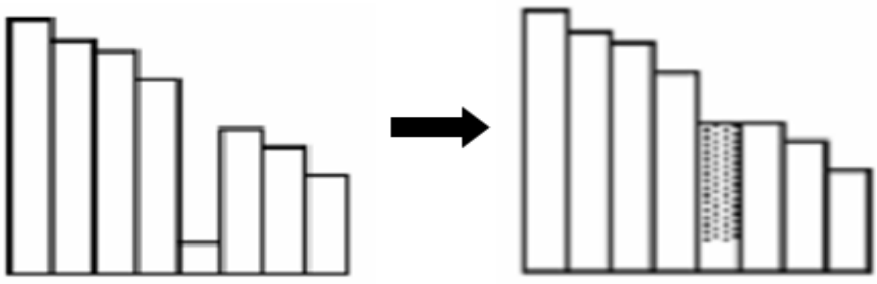

Figure 3.1 Filling the depressions in the DTM.

Flow directions can be obtained from the filled DTM by the so-called ‘D8 method’ which assumes water in one cell can only flow into its neighbouring cell with the steepest slope (Jenson and Domingue, 1988). Figure 3.2 shows the eight values that represent the eight neighbouring cells into which water can flow in the ‘D8 method’. The flow directions that 1, 2, 4, 8, 16, 32, 64 and 128 represent are to the east, southeast, south, southwest, west, northwest, north and northeast, respectively.

32	**64**	**128**
16		**1**
8	**4**	**2**

Figure 3.2 Flow direction values in the ‘D8 method’.

Flow accumulation values which represent the accumulated flow to each cell can be calculated by accumulating the weight for all cells that flow into each downslope cell. A stream network is then created by specifying a threshold for the accumulated flow, above which the corresponding cell is regarded as a stream cell. The stream network is combined with the flow directions to calculate the stream links, which link streams by the Strahler stream order (Strahler, 1952) and allocate each stream an individual number. In Strahler’s stream order system, the upstream segment of a stream network is considered low within the stream order, with the next segment downstream regarded as its parent and thus higher within the stream order. However, lower order segments joining a segment with higher order do not change the order of the higher stream (Figure 3.3). Sub-catchments are finally extracted by analysing the stream links and the flow directions.

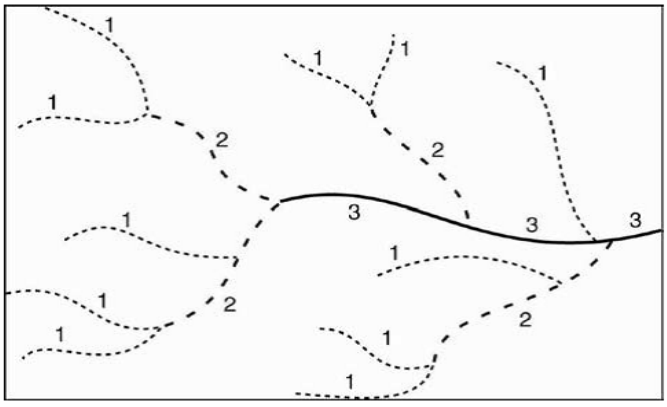

Figure 3.3 Strahler stream order classification method (Strahler, 1952).

3.2 Catchment Division

After the specific sub-catchments are extracted, hydraulic and hydrological zones should be specified where the corresponding model may be then applied respectively. In this work, a full 2D shallow flow model (Liang, 2010) is used with design rainfall and design hydrograph as the input to produce a design flood event. The sub-catchments are then divided into hydraulic and hydrological zones according to the inundation extent of a design flood event and land cover data.

3.2.1 *Design rainfall*

Design rainfall is estimated from DDF curves. The details of DDF curves for the UK can be found in the Flood Estimation Handbook (FEH) (Faulkner, 1999). Herein, a brief description is provided. In a DDF curve, rainfall duration is taken on a logarithmic scale along the *x*-axis, and rainfall depth is taken on a logarithmic scale along the *y*-axis. There are a group of curves for different return periods. From these curves, rainfall depth for a certain duration at a certain return period can be obtained. Figure 3.4 shows such a set of DDF curves.

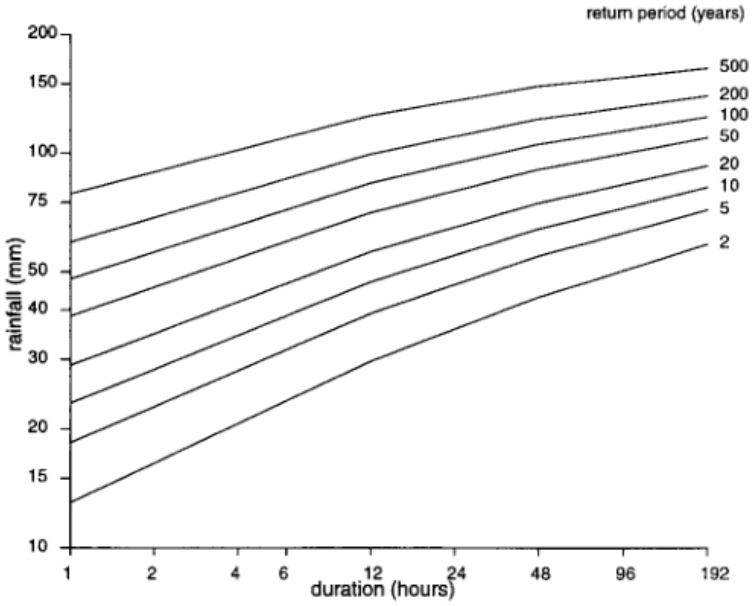

Figure 3.4 An example of DDF curves (Faulkner, 1999).

In Figure 3.4, the shape and location of the lines are defined by six parameters C, D_1, D_2, D_3 E_0, F. Herein, C, D_1, D_2, D_3 define the curve slope, and E_0, F define the intercept of the curve with the *y*-axis. There are two sets of estimated values available for these parameters for UK catchments on the FEH CD-ROM 3 (CEH, 2009). One is the averaged values of the selected catchment for calculating the average rainfall depth on

the catchment; the other is the value for the 1 km grid point which can be used to estimate the rainfall depth at a certain point in the catchment.

The design rainfall duration *D* (hours) is evaluated by:

$$D = T_p \times (1 + SAAR/1000), \tag{3.1}$$

where *Tp* is time-to-peak of unit hydrograph (hours); and *SAAR* is 1961-1990 standard-period average annual rainfall (mm).

$$T_p = 1.56 PROPWET^{-1.09} DPLBAR^{0.60} (1 + URBEXT_{1990})^{-3.34} DPSBAR^{-0.28}, \tag{3.2}$$

where *PROPWET* is the proportion of time when soil moisture deficit was less than or equal to 6 mm during the period 1961-1990; *DPLBAR* is the mean drainage path length (km); $URBEXT_{1990}$ is the extent of urban and suburban land cover (year 1990); and *DPSBAR* is the mean drainage path slope (m km^{-1}).

Design rainfall depth can be distributed within the design duration using an appropriate design rainfall profile. In rural catchments, a 75% winter profile has been adopted as the reference, which on average shows higher peaks than 75% of UK winter storms (Houghton-Carr, 1999). In urban catchments, 50% summer profile has been adopted as the reference, which on average shows higher peaks than 50% of UK summer storms (Houghton-Carr, 1999). These two symmetrical and bell-shaped rainfall profiles and the corresponding cumulative profiles are shown in Figure 3.5.

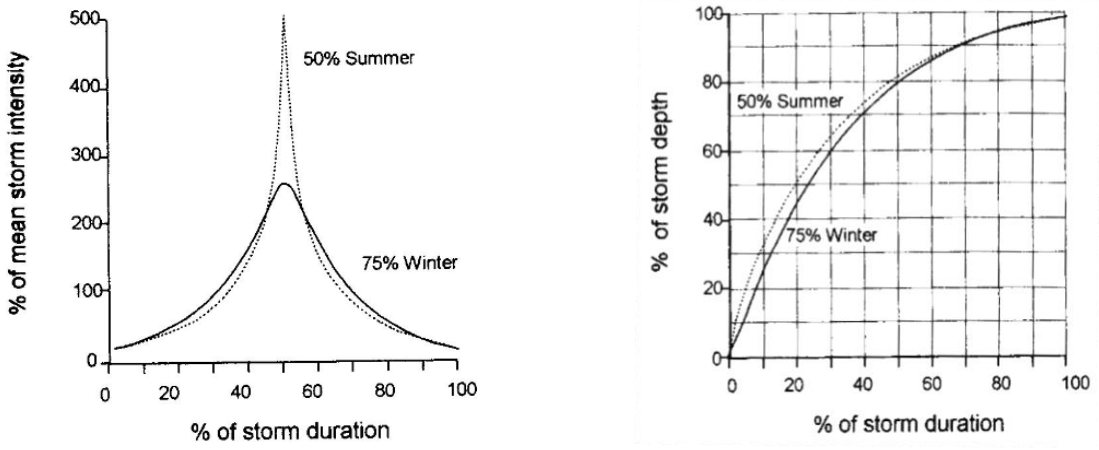

(a) (b)

Figure 3.5 Recommended design rainfall profiles (a) and cumulative profiles (b) for summer and winter (Houghton-Carr, 1999).

The above methods are used to generate a design rainfall hyetograph within design duration for a certain return period, where a seasonal correction factor and an areal reduction factor can be applied to consider the effects from seasons and areas.

3.2.2 *Design hydrograph*

A lumped conceptual rainfall-runoff model, the Revitalised Flood Hydrograph (ReFH) model (Kjeldsen, 2007b), is used in this study to produce the inflow design hydrograph based on upstream design rainfall and initial soil moisture content. The ReFH model is considered to be an updated version of the FSR/FEH model (Houghton-Carr, 1999). Particularly, the ReFH model has improved the description of hydrological processes and undated the analytical techniques.

After the estimates of upstream design rainfall, further estimates of net rainfall, runoff routing and base flows are implemented by three components of the ReFH model: the loss model, the routing model and the base flow model. The loss model is used to calculate the fractional rainfall that is turned into the direct runoff, which is then routed to the outlet of the upstream catchment by a unit hydrograph in the routing model. The total flow at the outlet is thus calculated by adding the direct flow and the base flow. The hydrograph at the outlet of the upstream catchment also acts as the inflow hydrograph for the research domain. The structure of ReFH model is shown in Figure 3.6.

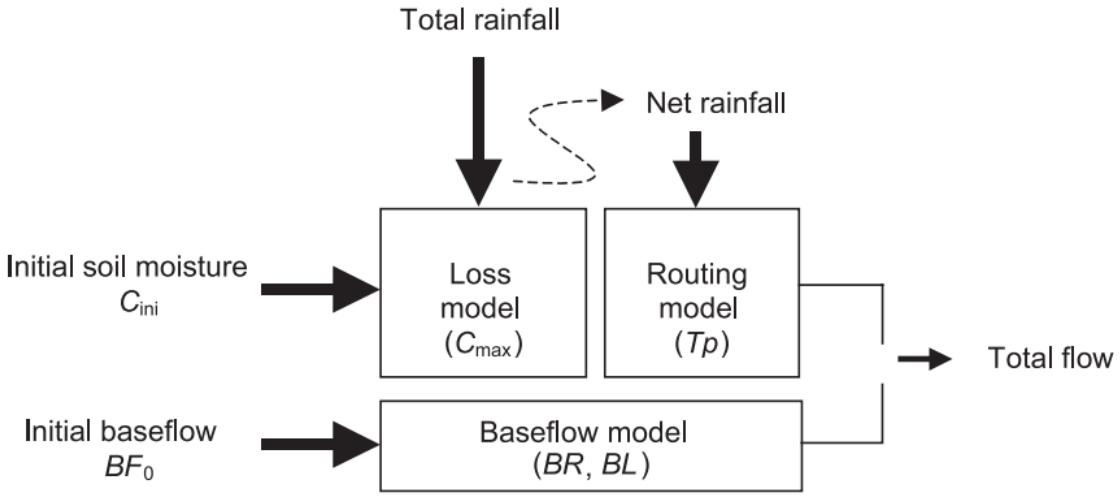

Figure 3.6 The schematization of ReFH model (Kjeldsen, 2007b).

There are six parameters in ReFH model: C_{ini} is the initial soil moisture content (mm); C_{max} is the maximum soil moisture content (mm); BF_0 is the initial base flow (m^3/s); *BR*

is the ratio of base flow recharge to runoff; *BL* is the base flow recession constant; and *Tp* is time-to-peak of unit hydrograph (hours).

These parameters are estimated by catchment descriptors from FEH CD-ROM 3. The relationship between the ReFH model parameters and catchment descriptors are listed in Equations 3.2-3.5 (Kjeldsen, 2007b):

$$C_{\max} = 596.7 BFIHOST^{0.95} PROPWET^{-0.24}, \quad (3.3)$$

$$BL = 25.5 BFIHOST^{0.47} DPLBAR^{0.21} PROPWET^{-0.53} (1 + URBEXT_{1990})^{-3.01}, \quad (3.4)$$

$$BR = 3.75 BFIHOST^{1.08} PROPWET^{0.36}, \quad (3.5)$$

where *BFIHOST* is the base flow index from the 'Hydrology of Soil Types' classification (Boorman *et al.*, 1995).

To support the dissemination of the ReFH model, the Environment Agency funded the Centre for Ecology and Hydrology (CEH) to develop a series of software tools including a ReFH spreadsheet (CEH, 2005) which is employed in this study. By importing upstream catchment descriptors from FEH CD-ROM 3 and setting flood return periods, time steps and design duration, etc. an upstream design rainfall hyetograph can be obtained as mentioned in sub-section 3.2.1. Thereafter, an inflow design hydrograph can be generated by running the model with the design upstream rainfall hyetograph as the input.

3.2.3 *Hydraulic and hydrological zones*

Before actual simulations, the full 2D shallow flow model (Liang, 2010) is utilised with design rainfall in the research domain and an inflow design hydrograph as the inputs to produce a design flood event. To save computational time, this work can be implemented in a lower-resolution grid, which does not largely affect the inundation results. The areas inundated by fluvial floods in a design flood event are preliminarily regarded as hydraulic zones, while the rest of the domain is specified as hydrological zones. For the type of one-way external coupling, flow from hydraulic zones to hydrological zones is not expected. Therefore, areas less likely to be inundated, with relatively higher elevations and steeper local slopes, are usually specified as hydrological zones.

The preliminary division can be further adjusted according to the land cover data. Green land (e.g. parks and golf courses) may be specified as hydrological zones, while hydraulic zones may cover impermeable surfaces in urban areas (e.g. rivers, roads, squares).

Notably, however, catchment division is still to some extent subjective and based on the modeller's experience, even though inundation extent and land cover are still important references. An example of this would be when determining whether local inundations are caused by fluvial or pluvial floods, or dividing an area which is mixed with buildings and grassland. Consequently, there are no absolutely correct division schemes, and different modellers may give slightly different divisions.

3.3 Hydraulic Models

In this section, the full 2D shallow flow model (Liang, 2010), the original partial inertial model (PIM) (Bates *et al.*, 2010), and two improved PIMs (Zhang *et al.*, 2014) are introduced and compared in terms of modelling accuracy and efficiency.

3.3.1 *Full 2D shallow flow model*

With the assumption of hydrostatic pressure, and omitting the viscous terms, the well-balanced shallow water equations in differential hyperbolic conservation form can be written as:

$$\frac{\partial \mathbf{u}}{\partial t}+\frac{\partial \mathbf{f}}{\partial x}+\frac{\partial \mathbf{g}}{\partial y}=\mathbf{s}\,. \tag{3.6}$$

The vectors representing conservative variables, fluxes and source terms are given by (Liang and Borthwick, 2009):

$$\mathbf{u}=\begin{bmatrix}\eta\\ uh\\ vh\end{bmatrix},\qquad \mathbf{f}=\begin{bmatrix}uh\\ u^2h+\frac{1}{2}g(\eta^2-2\eta z_b)\\ uvh\end{bmatrix},$$
$$\mathbf{g}=\begin{bmatrix}vh\\ uvh\\ v^2h+\frac{1}{2}g(\eta^2-2\eta z_b)\end{bmatrix},\qquad \mathbf{s}=\begin{bmatrix}ss\\ -\frac{\tau_{bx}}{\rho}-g\eta\frac{\partial z_b}{\partial x}\\ -\frac{\tau_{by}}{\rho}-g\eta\frac{\partial z_b}{\partial y}\end{bmatrix}, \tag{3.7}$$

where t denotes time; x and y are the Cartesian coordinates; η represents water level; uh and vh are the unit width discharges; h, u and v are the water depth and velocity

components in the two Cartesian directions, respectively; and *ss* is the external source term in shallow water equations. The density of water is given by ρ; z_b is the bed elevation; and g is the gravitational acceleration.

The effect of bed roughness on flows is determined by the bed friction stress terms τ_{bx} and τ_{by}, which can be estimated using:

$$\tau_{bx} = \rho C_f u\sqrt{u^2+v^2} \text{ , and } \tau_{by} = \rho C_f v\sqrt{u^2+v^2} \text{ .} \quad (3.8)$$

The bed roughness coefficient C_f can be evaluated using $C_f = gn^2 \big/ h^{1/3}$, where n is the Manning coefficient. C_f is equal to zero in dry areas with $h < 10^{-10}$ m.

The above shallow water equations are solved using a finite volume shock-capturing Godunov-type scheme (Toro, 2001), and an explicit time-marching conservative formula is used to discretise Equation 3.6 and update the flow variables to the next time step:

$$\mathbf{u}_{i,j}^{k+1} = \mathbf{u}_{i,j}^{k} - \frac{\Delta t}{\Delta x}\left(\mathbf{f}_{i+1/2,j} - \mathbf{f}_{i-1/2,j}\right) - \frac{\Delta t}{\Delta y}\left(\mathbf{g}_{i,j+1/2} - \mathbf{g}_{i,j-1/2}\right) + \Delta t \mathbf{s}_{i,j} \text{ ,} \quad (3.9)$$

where k is the time level; i and j are cell indexes in the x- and y-direction; Δx and Δy correspond to cell size in the x- and y- direction; and Δt is the time step.

Herein, first-order approximations for the face values of flow variables are used, with a non-negative depth reconstruction technique for wetting and drying (Liang, 2010), and fluxes through the four interfaces of each computational cell are evaluated by HLLC approximate Riemann solver (Toro, 2001).

In order to update the flow variables to a new time step, the source terms should be evaluated in the proper way. There are three kinds of source terms in Equation 3.6: external source terms, bed slope source terms and bed friction source terms. The external source terms may be rainfall, infiltration, etc. The bed slope source terms can be discretised by a central-differencing scheme (Liang, 2010). The bed friction source terms can be explicitly solved by Equation 3.8, but the friction forces may be exaggerated to reverse the flow direction when the bed roughness coefficient C_f is large enough, caused by either a very large Manning coefficient or very shallow water depth near the wet-dry front. To avoid such numerical instability, a splitting-point implicit

scheme (Bussing and Murman, 1988; Fiedler and Ramirez, 2000) is used to evaluate the bed friction source terms (Liang and Marche, 2009; Liang, 2010).

Despite the use of an implicit scheme to calculate the bed friction source terms, the overall numerical scheme to solve Equation 3.6 is explicit, and its numerical stability is governed by the CFL criterion (Courant *et al.*, 1967). The time step, Δt, may be expressed by the following formula:

$$\Delta t = C_r \min(\Delta t_x, \Delta t_y) . \tag{3.11}$$

with

$$\Delta t_x = \min_{i,j} \frac{\Delta x_{i,j}}{|u_{i,j}| + \sqrt{g h_{i,j}}} \quad \text{and} \quad \Delta t_y = \min_{i,j} \frac{\Delta y_{i,j}}{|v_{i,j}| + \sqrt{g h_{i,j}}} . \tag{3.12}$$

where the Courant number is specified in the range $0 < C_r \leq 1$.

Two types of boundary conditions are imposed in this study, i.e. open and slip boundary conditions.

In open boundary conditions, the gradients of flow variables are assumed to be zero at the boundary:

$$h_O = h_I , \quad uu_O = uu_I , \quad vv_O = vv_I . \tag{3.13}$$

In slip boundary conditions, the normal velocity as well as the gradients of the water level and the tangential velocity is required to be zero at the boundary:

$$h_O = h_I , \quad uu_O = -uu_I , \quad vv_O = vv_I , \tag{3.14}$$

where *uu* is the normal velocity; *vv* is the tangential velocity; and subscripts *O* and *I* represent the cell at outer boundary and inner boundary, respectively.

3.3.2 *Partial inertial models (***PIMs***)*

The PIMs solve the same continuity equation as the full 2D shallow flow model：

$$\frac{\partial \eta}{\partial t} + \frac{\partial q_x}{\partial x} + \frac{\partial q_y}{\partial y} = ss , \tag{3.15}$$

where $q_x = uh$ and $q_y = vh$ are the unit width discharges.

These unit width discharges are approximated using a simplified formula derived from the full momentum equation. The diffusion wave approximation indicates that the dynamic terms of the full momentum equations become insignificant and may be neglected without significantly affecting the physical description of many slow-varying overland flows (Hunter *et al.*, 2007). In this work, the simplified momentum formula proposed by Bates *et al*. (2010) is adopted, which is derived from the above diffusion wave assumption by retaining some of the inertial effects.

Assuming that the convection acceleration terms are negligible, the momentum equation can be simplified to become:

$$\frac{\partial q_x}{\partial t} + gh\frac{\partial (h + z_b)}{\partial x} + \frac{gn^2 q_x \|q\|}{h^{7/3}} = 0, \tag{3.16}$$

where $\frac{\partial q_x}{\partial t}$ is the local acceleration term; $gh\frac{\partial h}{\partial x}$ is the pressure force term; $gh\frac{\partial z_b}{\partial x}$ is the slope source term representing the gravitational effect; and $\frac{gn^2 q_x \|q\|}{h^{7/3}}$ is the friction source term. An explicitly discretised equation for q_x may be derived as follows:

$$q_x^{t+\Delta t} = q_x^t - gh^t \Delta t \left[\frac{\Delta \eta^t}{\Delta x} + \frac{n^2 q_x^t \|q^t\|}{h^{t\ 10/3}} \right], \tag{3.17}$$

where $\Delta\eta$ calculates the local difference in water level and $\|q\|$ returns the magnitude of q. Replacing q_x^t in the friction term with $q_x^{t+\Delta t}$ to form a linear equation for the unknown $q_x^{t+\Delta t}$ creates a semi-implicit scheme to achieve better numerical stability (Bates *et al.*, 2010); Equation 3.17 may then be rearranged to give:

$$q_x^{t+\Delta t} = \frac{q_x^t - gh^t \Delta t \frac{\Delta \eta^t}{\Delta x}}{1 + g\Delta t n^2 \|q^t\| / h^{t^{7/3}}}. \tag{3.18}$$

This semi-implicit scheme can prevent the flow from changing direction under the condition of extremely high-friction force, which an explicit scheme can not. It also avoids the heavy computational burden of an iterative full-implicit scheme.

From Equation 3.18, the well-balanced scheme can be preserved because zero velocities and invariant water surface gradient in still water can keep the water motionless at the next time step.

At each time step during a simulation, q_x and q_y (which may be similarly derived) are updated using Equation 3.18 and combined with Equation 3.15 to update the water level. In this work, Equation 3.15 is solved using a FVM based on the structured grid, which results in the following time-marching formula for updating the water level at a new time step:

$$\eta_{i,j}^{k+1} = \eta_{i,j}^{k} - \Delta t\left(\frac{q_{xE}^{\,k+1} - q_{xW}^{\,k+1}}{\Delta x} + \frac{q_{y_N}^{\,k+1} - q_{y_S}^{\,k+1}}{\Delta y} \right) + ss^{k}\,, \tag{3.19}$$

where subscripts *E*, *W*, *N*, *S* represent the east, west, north and south interface of a cell, respectively.

Taking the eastern interface as an example, q_{xE} is estimated using Equation 3.18 as:

$$q_{xE}^{\,k+1} = \frac{q_{xE} - gh_E \Delta t \dfrac{\eta_E^R - \eta_E^L}{\Delta x}}{1 + g\Delta t n^2 \left\| q_E \right\| / h_E^{7/3}}\,. \tag{3.20}$$

Herein, the values of flow variables on the right-hand-side are obtained at time level *k*. The fluxes through the other three cell interfaces at time level *k* can be evaluated in a similar way. Subsequently, the updated discharges at the centre of cell (*i*, *j*) are simply evaluated by averaging the two associated fluxes:

$$q_{x_{i,j}}^{\,k+1} = \left(q_{xE}^{\,k+1} + q_{xW}^{\,k+1} \right)/2 \text{ and } q_{y_{i,j}}^{\,k+1} = \left(q_{y_N}^{\,k+1} + q_{y_S}^{\,k+1} \right)/2\,. \tag{3.21}$$

In order to estimate the interface values of the flow variables in Equation 3.20, the face values at the left and right sides of the interface may firstly be approximated to be the same as the corresponding cell-centred values, which leads to a first order numerical scheme (Zhang *et al.*, 2013). The left face values of the eastern interface are therefore given by:

$$\bar{\eta}_E^{\,L} = \eta_{i,j},\ \bar{h}_E^{\,L} = h_{i,j},\ \bar{z}_{b\,E}^{\,L} = \bar{\eta}_E^{\,L} - \bar{h}_E^{\,L},\ \bar{q}_{xE}^{\,L} = q_{xEi,j}\,. \tag{3.22}$$

Similarly, the corresponding right face values are:

$$\bar{\eta}_E^{\,R} = \eta_{i+1,j},\ \bar{h}_E^{\,R} = h_{i+1,j},\ \bar{z}_{b\,E}^{\,R} = \bar{\eta}_E^{\,R} - \bar{h}_E^{\,R},\ \bar{q}_{xE}^{\,R} = q_{xWi+1,j}\,. \tag{3.23}$$

The corresponding velocity components are then evaluated by:

$$\bar{u}_E^L = \bar{q}_{xE}^L \big/ \bar{h}_E^L, \quad \bar{u}_E^R = \bar{q}_{xE}^R \big/ \bar{h}_E^R. \tag{3.24}$$

In a dry cell (defined as $h < 10^{-10}$ m) (Brufau and García-Navarro, 2003), the velocities are set to be zero directly and not evaluated by Equation 3.24.

The original PIM reconstructs water depth at the interface by taking the difference between the maximum water level and the maximum bed elevation at either side of the interface as:

$$h_E = \max(\bar{\eta}_E^L, \bar{\eta}_E^R) - \max(\bar{z}_{bE}^L, \bar{z}_{bE}^R). \tag{3.25}$$

This reconstruction maintains non-negative water depth in most situations. However, high velocities and negative water depth may still occur when the water surface gradient is large. For example, as shown in Figure 3.7 (b) when the difference between water levels at the left and right side of an interface becomes too large, a large flux can be generated as a result of Equation 3.20, which in turn calculates a negative water depth from Equation 3.19. In order to ensure non-negative water depth, water level, instead of water depth, should be reconstructed.

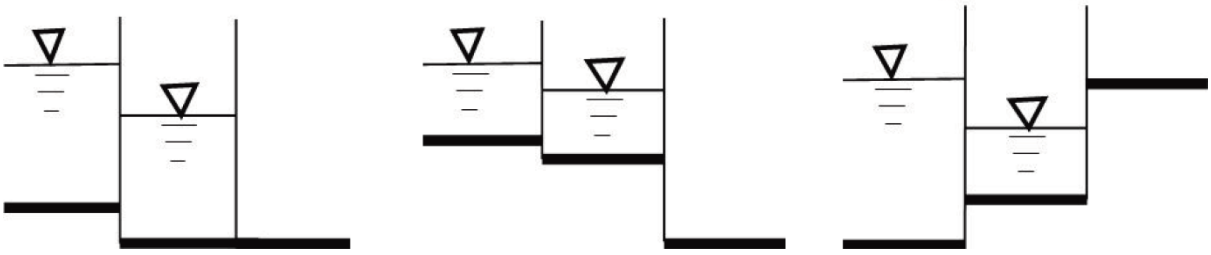

(a) (b) (c)

Figure 3.7 Three generalised configurations for wetting and drying.

A single value of bed elevation at a cell interface is defined (Audusse *et al.*, 2004) as:

$$z_{bE} = \max(\bar{z}_{bE}^L, \bar{z}_{bE}^R). \tag{3.26}$$

The water depths at either side of the interface are then reconstructed as:

$$h_E^L = \max(0, \bar{\eta}_E^L - z_{bE}), \quad h_E^R = \max(0, \bar{\eta}_E^R - z_{bE}). \tag{3.27}$$

This ensures non-negative water depth. Based on Equations 3.26 and 3.27, the corresponding water level and unit width discharges are then reconstructed as:

$$\eta_E^L = h_E^L + z_{bE},\ \eta_E^R = h_E^R + z_{bE},$$
$$q_{xE}^{\ L} = \bar{u}_E^L h_E^L,\ q_{xE}^{\ R} = \bar{u}_E^R h_E^R. \tag{3.28}$$

In the above reconstruction, it is evident that the water level coincides with the bed elevation in a dry cell. If the dry cell has a bed elevation higher than the water level in a neighbouring cell, as shown in Figure 3.7 (c), a spurious flux will be calculated between the dry cell and the adjacent wet cell due to the higher water level on the dry side. To avoid this unphysical numerical flux, other than reconstructing the bed elevation and water levels by following Equations 3.26-3.28, the difference between the fake and actual water level must be identified and subtracted from the reconstructed values. A general formula for specifying this difference is given as follows:

$$\Delta z = \max\left(0,\ (z_{bE} - \bar{\eta}_E^L)\right). \tag{3.29}$$

The associated bed elevation and water levels are subsequently modified by subtracting Δz from their original values as:

$$z_{bE} - \Delta z \rightarrow z_{bE},\ \eta_E^L - \Delta z \rightarrow \eta_E^L,\ \eta_E^R - \Delta z \rightarrow \eta_E^R. \tag{3.30}$$

These modified face values are then substituted into the right-hand side of Equation 3.20 to calculate the flux, for which the interface values of the water depth and discharge (h_E and q_{xE}) are also required. Similar to the original PIM, the maximum water depth from either side of the interface is used in this work. When deciding the interface discharge q_{xE}, two options are available and tested herein:

1) Take the maximum unit width discharge at either side of the interface:

When $q_{xE}^{\ L}$ and $q_{xE}^{\ R} \geq 0$:

$$q_{xE} = \max(q_{xE}^{\ L}, q_{xE}^{\ R}). \tag{3.31}$$

When $q_{xE}^{\ L}$ and $q_{xE}^{\ R} < 0$:

$$q_{xE} = \min(q_{xE}^{\ L}, q_{xE}^{\ R}). \tag{3.32}$$

This is essentially the same scheme as in the original PIM. Using the larger values in flux calculation may help to partly overcome the negative effect of neglecting the convective acceleration terms in the momentum equation. Together with the new non-negative depth reconstruction, as proposed in the current work, this model is hereafter referred to as 'improved PIM1', and will be used to demonstrate the improvement achieved as a result of the water level reconstruction.

2) Take the average unit width discharge of both sides of the interface:

$$q_{xE} = (q_{xE}^{L} + q_{xE}^{R})/2 . \tag{3.32}$$

A mathematical proof has shown that the original PIM is not able to produce a stable solution for domains dominated by large areas of low-friction land, and the adoption of an average face value of discharge may mitigate this problem by introducing extra numerical diffusion (de Almeida *et al.*, 2012). Combined with the current water level reconstruction, this new scheme is referred to as 'improved PIM2' in the rest of the text, which will be tested for low-friction simulations.

The time steps of PIMs are controlled by CFL criterion (Equations 3.11 and 3.12), and two boundary conditions are imposed, i.e. open and slip boundary conditions (Equations 3.13 and 3.14).

3.3.3 *Model comparison*

In this sub-section, the full 2D shallow flow model, the original PIM, the 'improved PIM1' and the 'improved PIM2' are compared in terms of both accuracy and efficiency by applying them to simulate a hypothetical inundation event at Thamesmead, located at the south bank of the Thames River in the UK. The comparisons in more test cases can be found in the work of Zhang *et al.* (2014). In all of the simulations, g = 9.81 m/s^2 is used. All simulations are performed on a standard personal desktop with an Intel$^{(R)}$ Core$^{(TM)}$ i5 CPU.

Relative Root Mean Square Error (*RMSE*) and fit statistics (F^1 and F^2) are employed in this work to quantitatively analyse the results. Other statistics may include overall accuracy, Nash and Sutcliffe efficiency, mean residual, etc.

The relative *RMSE* is calculated by:

$$RMSE = \sqrt{\frac{\sum_{i,j}\left(\frac{va_{i,j} - \hat{va}_{i,j}}{\hat{va}_{i,j}}\right)^2}{NN}}, \tag{3.33}$$

where *va* represents any modelling flow variables including water level, water depth, flow velocity, etc; while $\hat{va}$ denotes any benchmark flow variables; *NN* is the total number of computational cells.

Fit statistics are used to evaluate the simulation of wet (1)/dry (0) states. The critical water depth to divide wet or dry states is set to be 0.1 m in this study (Aronica *et al.*, 2002). F^1 represents the percentage of the cells with the matched wet-dry state between modelling results (*M*) and benchmark dataset (*B*):

$$F^1 = \frac{\sum_{i,j} P_{i,j}^{B_0M_0} + \sum_{i,j} P_{i,j}^{B_1M_1}}{NN}. \tag{3.34}$$

When the cell states are both wet, $P_{i,j}^{B_1M_1}$ is given a value of 1, and otherwise $P_{i,j}^{B_1M_1}$ is given a value of 0. When the cell states are both dry, $P_{i,j}^{B_0M_0}$ is given a value of 1, and otherwise $P_{i,j}^{B_0M_0}$ is given a value of 0. F^1 ranges between 0 for no cells, with the wet-dry state matched between modelling results and benchmark dataset, and 1 for a perfect match of wet-dry states. There is a drawback in using F^1 for the condition that the inundation area is much smaller than the whole domain area, because the large non-flooding area within the domain may result in large values for $\sum P_{i,j}^{B_0M_0}$ and F^1, which will overestimate the model performance.

Another fit statistic F^2 is used to estimate the percentage of the matched flood extent between modelling results (*M*) and benchmark dataset (*B*):

$$F^2 = \frac{\sum_{i,j} P_{i,j}^{B_1M_1}}{\sum_{i,j} P_{i,j}^{B_1M_1} + \sum_{i,j} P_{i,j}^{B_1M_0} + \sum_{i,j} P_{i,j}^{B_0M_1}}. \tag{3.35}$$

When the benchmark cell state is wet and the modelling cell state is dry, $P_{i,j}^{B_1M_0}$ is given a value of 1, and otherwise $P_{i,j}^{B_1M_0}$ is given a value of 0. When the benchmark cell state is dry and the modelling cell state is wet, $P_{i,j}^{B_0M_1}$ is given a value of 1, and otherwise $P_{i,j}^{B_0M_1}$ is given a value of 0. F^2 varies between 0, when there is no matched flood extent

between modelling results and benchmark data, and 1 for a perfect match of the flood extent. F^2 focuses only on the active floodplain in the domain, and hence avoids the aforementioned drawback of F^1.

A processed 10 m bare-earth DTM as shown in Figure 3.8 is used to represent the selected 9000 m × 4000 m floodplain. A 150 m wide breach in the embankment is assumed to generate an inundation event. The flow hydrograph through the breach is shown in Figure 3.9. The whole floodplain with open boundary conditions is discretised by a uniform grid with 900 × 400 cells and a constant Manning coefficient n = 0.035 $m^{-1/3}s$ is applied (Liang *et al.*, 2008).

Figure 3.8 Thamesmead floodplain map.

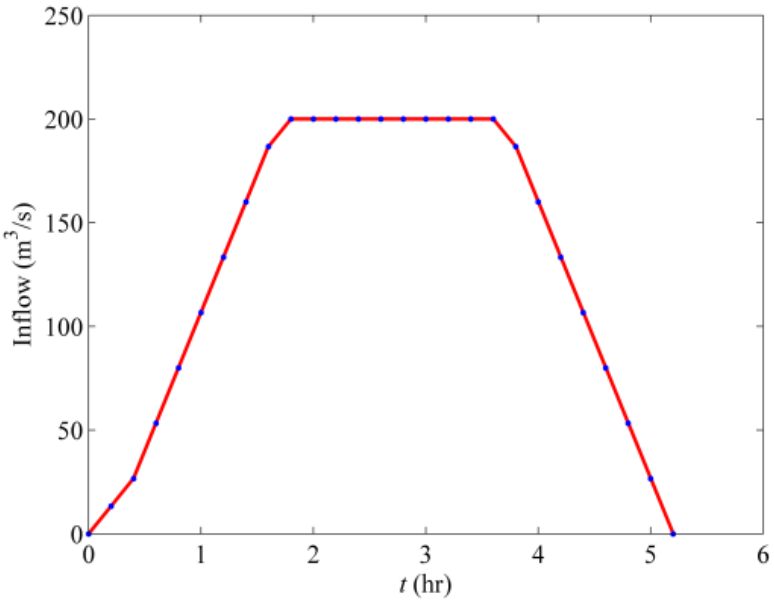

Figure 3.9 Thamesmead inflow hydrograph.

Figure 3.10 displays the inundation maps at t = 10 hours produced by the four models, respectively. Full 2D shallow flow model is utilised as a reference as there is no measured data available for this case. With regard to flood extents, the original PIM and the 'improved PIM1' are in close agreement with the full 2D shallow flow model, but the 'improved PIM2' produces a smaller flood extent. This is related to the different methods these models employ to calculate the interface fluxes. In practical applications, the convective acceleration is generally in the same direction as the velocity and hence accelerates the flow, so the omission of convective acceleration terms usually slows down the flow propagation. Therefore using the maximum face value of discharge to calculate the interface fluxes can reduce, to some extent, the effect of omitting the convective acceleration terms. This generates more satisfactory results than taking the average face value in this case. In addition, for practical applications the bed friction is normally large enough to stabilise the solution, and taking the average face value as the interface flux may introduce unwanted numerical diffusion and slow down flow propagation. Because of this, the flux calculation scheme, as implemented in 'improved PIM2', may not be recommended for realistic flood simulations.

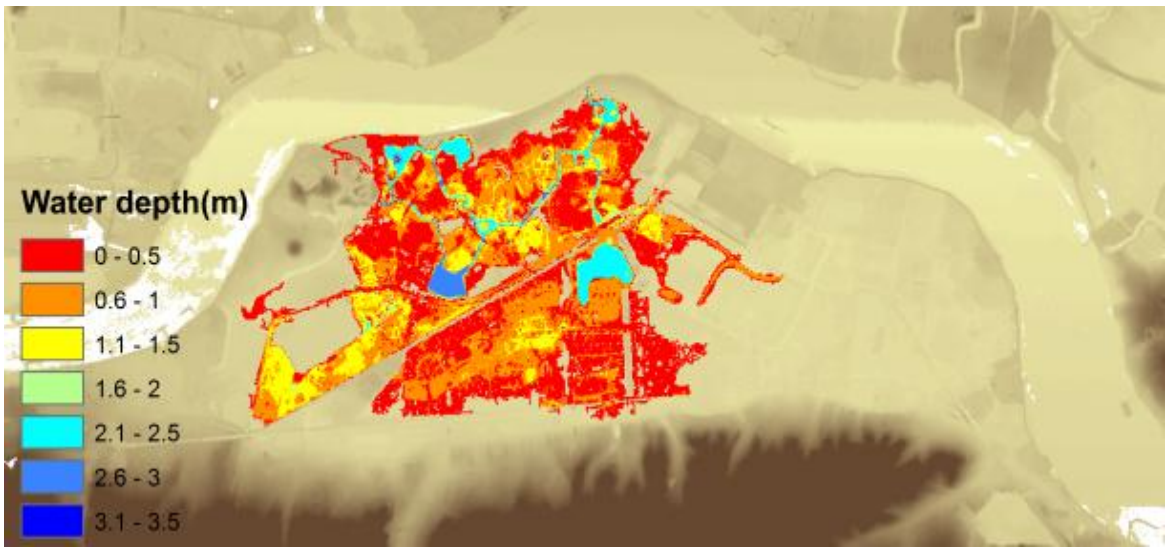

(a)

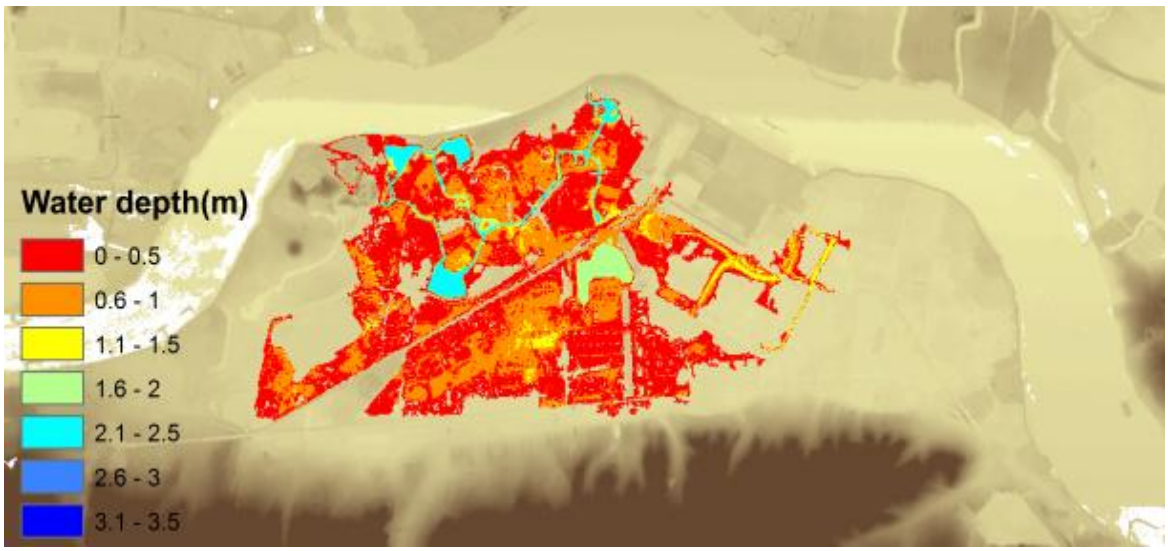

(b)

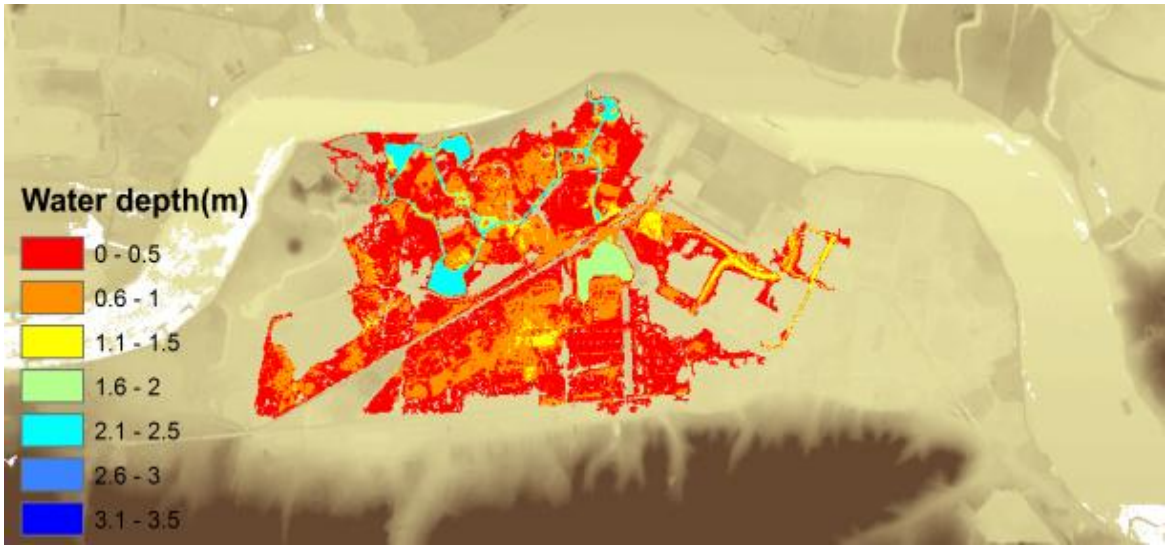

(c)

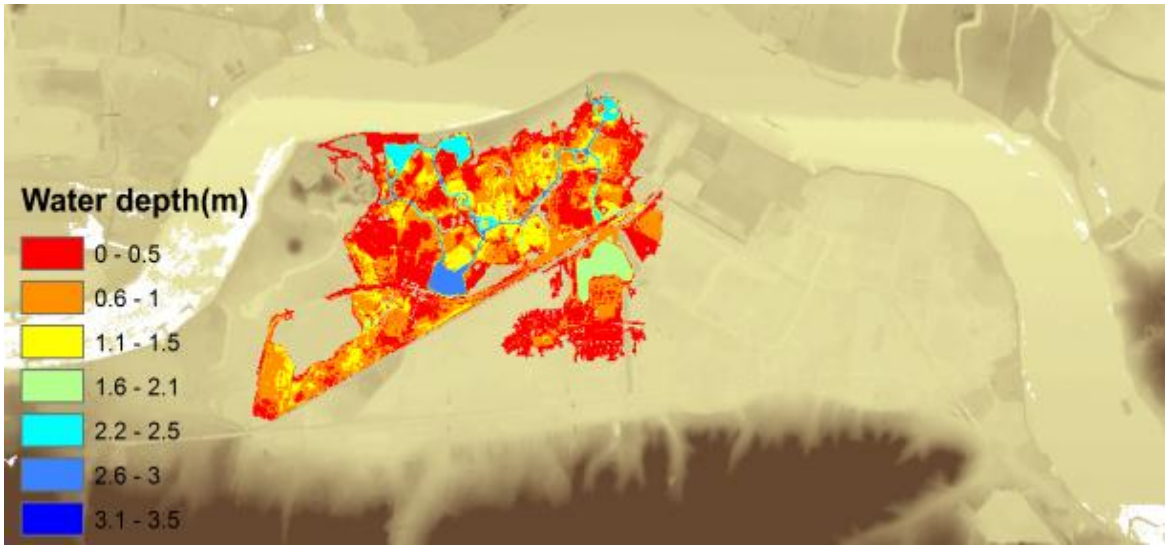

(d)

Figure 3.10 Thamesmead inundation: inundation maps predicted by the full 2D shallow flow model (a), original PIM (b), 'improved PIM1' (c) and 'improved PIM2'(d).

In order to further compare the simulation results, the temporal changes in water depth and flow velocity are recorded at four gauge points as indicated in Figure 3.8 and compared in Figure 3.11 and Figure 3.12. Generally, the water depth and velocity predicted by the three PIMs follow the trend, as predicted by the full 2D shallow flow model, but deviation between the results is also evident, especially for the 'improved PIM2'. Excellent agreement can be found between the original PIM and 'improved PIM1' in both water depth and flow velocity predictions, which implies that for practical conditions, where the bed slope and flow hydrodynamics change gently, the original PIM may be capable of producing non-negative water depths without the need for water level reconstruction. But obviously, this conclusion can only be drawn case by case.

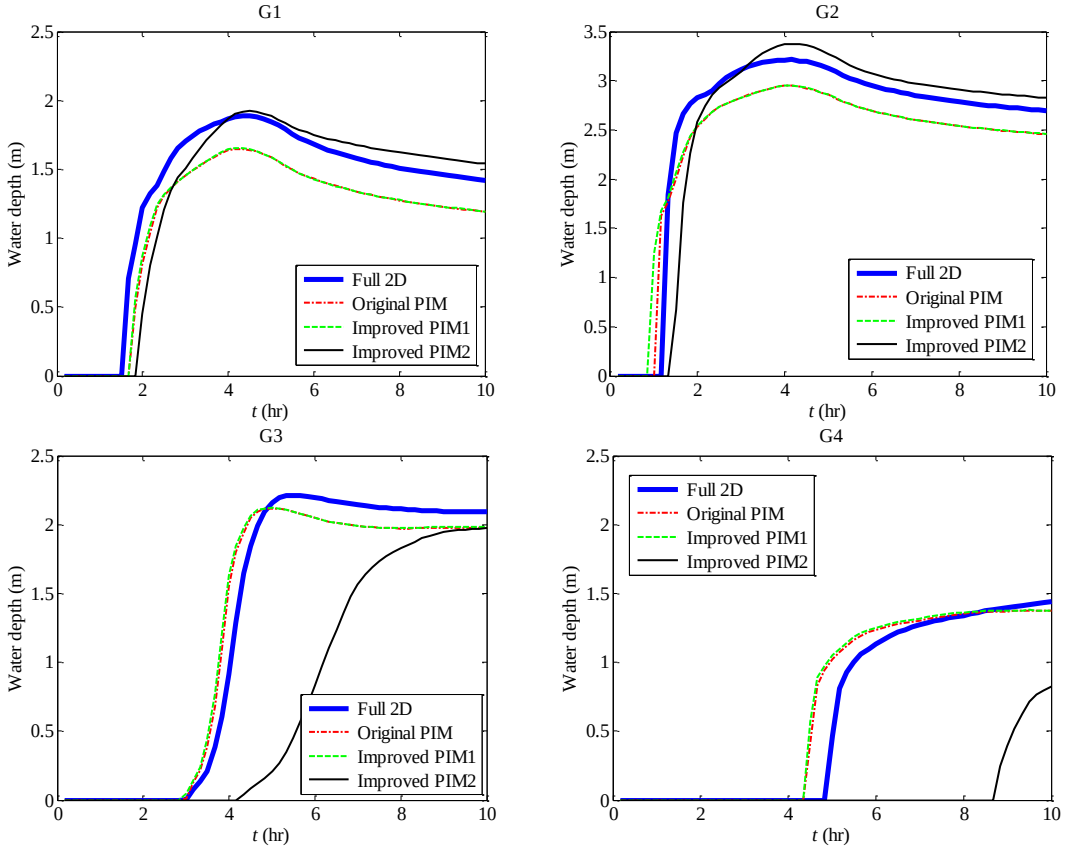

Figure 3.11 Thamesmead inundation: temporal change in the water depth at four gauge points.

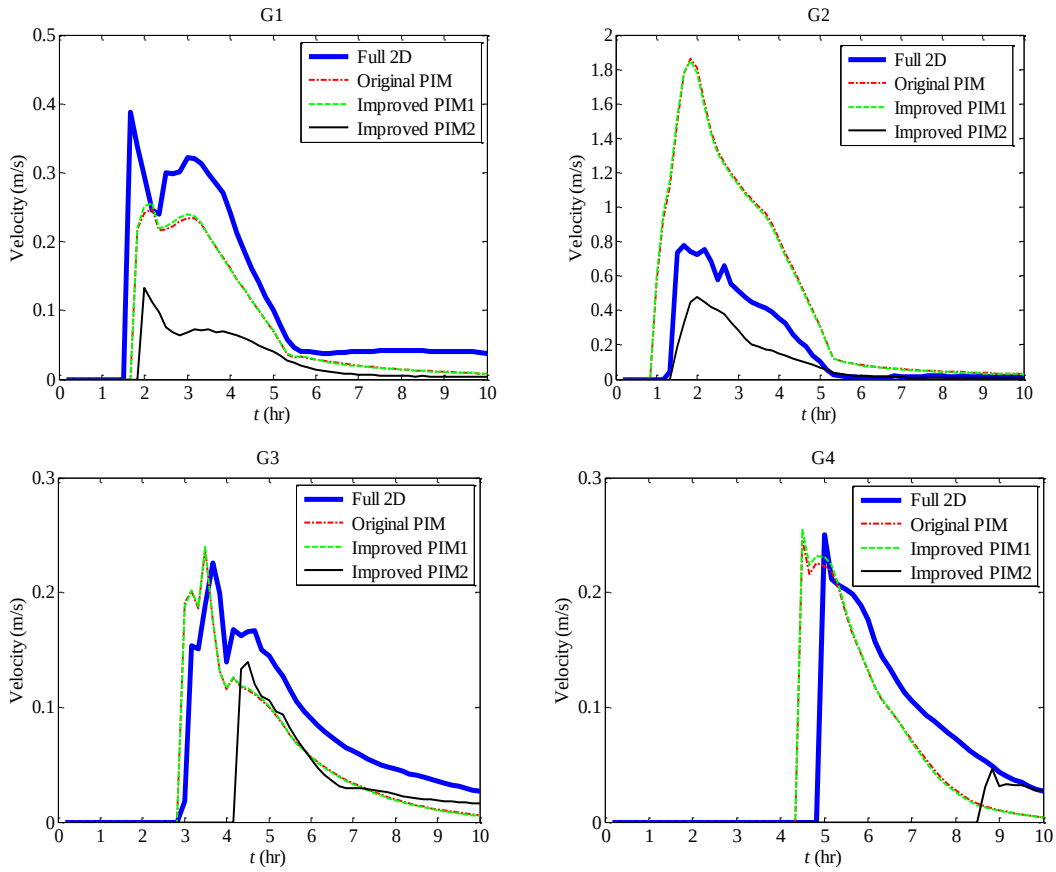

Figure 3.12 Thamesmead inundation: temporal change in flow velocity at four gauge points.

To further quantify the performance of the three PIMs, the relative *RMSE* and fit statistics (F^1 and F^2) are calculated for the whole simulation and plotted in Figure 3.13 and Figure 3.14, with the numerical solution from the full 2D shallow flow model given as a reference. As can be seen in Figure 3.13(a), the relative *RMSE* of the water depth for the original PIM and 'improved PIM1' is below 25%. The behaviour of the 'improved PIM2' is less satisfactory, with the maximum relative *RMSE* reaching nearly 30%. Meanwhile, the capability of all three PIMs is not satisfactory in resolving the flow velocity, as shown in Figure 3.13(b), where the error may sometimes reach above 100%. Again, the omission of convective acceleration terms is the main reason why these PIMs can not give reasonable predictions in the flow velocity. From the fit statistics (F^1 and F^2) presented in Figure 3.14, it can be seen that the correct state of wet-dry cells predicted by the original PIM can match up to 96% with the full 2D shallow flow model, and the flood extents predicted by these two models agree over 70% for most of the simulation. The 'improved PIM1' is able to produce equally good results as the original PIM, but the 'improved PIM2' results are generally less impressive, compared with the other two PIMs. With respect to the computational time,

the original PIM, ‘improved PIM1’, ‘improved PIM2’ and full 2D shallow flow model took 3,491s, 3,574s, 3,576s and 4,717s, respectively, to complete the 10-hour simulation. The ‘improved PIM1’ and ‘improved PIM2’ require 2.3% more computational time than the original PIM and 1.3 times as fast as the full 2D shallow flow model.

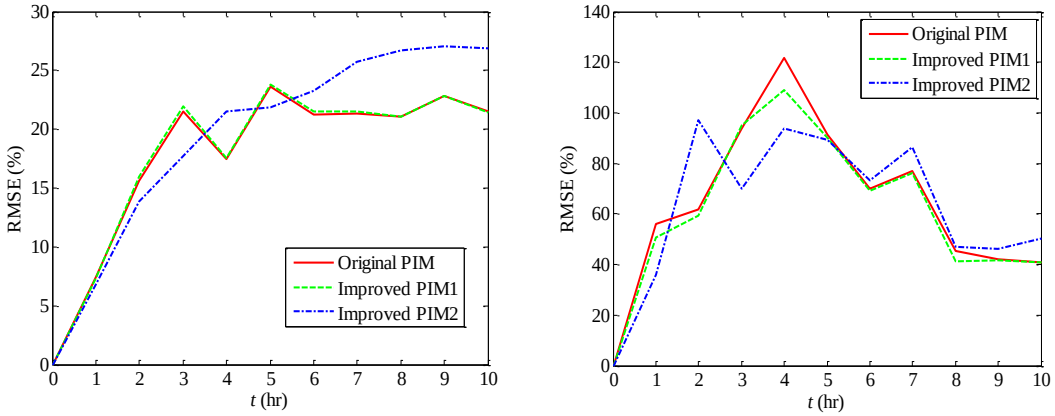

(a) (b)

Figure 3.13 Thamesmead inundation: time histories of the relative *RMSE* for the water depth (a) and flow velocity (b).

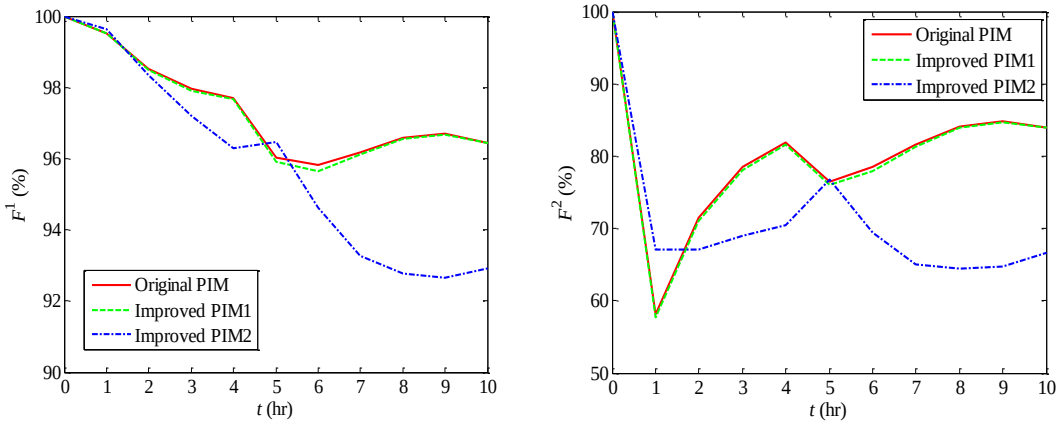

(a) (b)

Figure 3.14 Thamesmead inundation: time histories of F^1 (a) and F^2 (b).

In summary, the original PIM and ‘improved PIM1’ featuring different face value reconstruction techniques can produce similar simulation results without causing negative depth in practical conditions with a gentle bed slope and water gradient. Their performances are satisfactory in terms of predicting water depths and flood extents, when compared with the full 2D shallow flow model. Additionally, for practical applications the bed friction is normally large enough to stabilise the solution. The ‘improved PIM2’ may introduce unwanted numerical diffusion and slow down flow propagation; therefore, it may not be recommended for practical flood simulations. In

terms of computational cost, due to the use of simplified governing equations and corresponding simple numerical scheme, PIMs can be 1.3 times as fast as the full 2D shallow flow model. However, this marginal efficiency improvement is obtained at the price of a relatively obvious loss in accuracy, particularly for the velocities. As a consequence, this work will select the full 2D shallow flow model for coupling purposes.

3.4 Hydrological Model

In this study, the lump conceptual Water Balance Model (WBM) (Walker and Zhang, 2002) is utilised to calculate runoff production because of its simplicity and high efficiency. In the coupling method to be introduced in Section 3.6, the full 2D shallow flow model can also be coupled with other hydrological models which offer different levels of complexity.

A conceptual view of the WBM model is shown in Figure 3.15, in which the catchment is treated as a container with an input, e.g. rainfall, and outputs, e.g. infiltration and evapotranspiration. The capacity of the container is the maximum surface storage of the catchment, which mainly depends on surface ponding and plant interception, etc. Once the water volume inside the container exceeds its capacity, surface runoff will immediately occur. Interflow and base flow are not considered in this study for simplification.

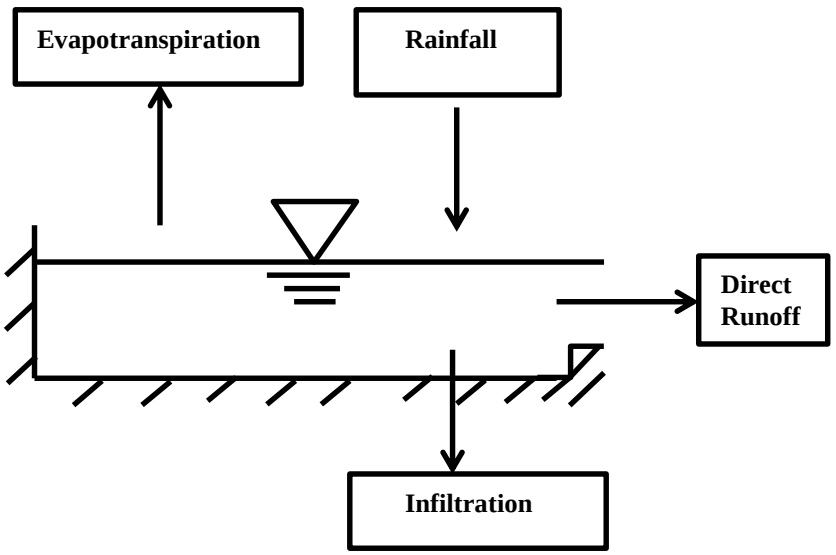

Figure 3.15 The conceptual representation of the Water Balance Model.

The surface runoff per unit time can be evaluated by:

$$RR = PP - EE - f - SS\,, \tag{3.36}$$

where *RR* is the surface runoff; *PP* is the rainfall; *EE* is the evapotranspiration; *f* is the infiltration; and *SS* is the maximum surface storage.

Noticeably, Equation 3.36 can not only be applied to hydrological zones for calculating the lumped runoff production, they can also be used in hydraulic zones to consider hydrological processes in each hydraulic cell. Thereafter they can be combined with the full 2D shallow flow model, with runoff production acting as the external source term.
The hydrological elements in Equation 3.36 may be further simplified. Since this study concerns an event-based inundation across a relatively small urban catchment, evapotranspiration can be considered negligible. Additionally, the maximum surface storage can also be ignored since the areas which are classified as hydrological zones, as well as an individual cell in hydraulic zones, are usually covered by homogeneous topographic features. Infiltration in impermeable areas including rooftops is assumed to be zero, and in permeable areas it is estimated by the Green-Ampt equation (Heber Green and Ampt, 1911).

$$f = \frac{dFF}{dt} = -K_s\left(\psi_f \frac{\theta_s - \theta_a}{FF} + 1\right), \tag{3.37}$$

where *FF* is the cumulative depth of infiltration; K_s is the soil saturated hydraulic conductivity; ψ_f is the matric pressure at the wetting front; θ_a is the initial moisture content; θ_s is the saturated moisture content. The parameter values for different soil textures can be referred to (Rawls *et al.*, 1982; Rawls and Brakensiek, 1985). In addition, a sensitivity analysis needs to be implemented.

3.5 Building Representation

In this work, the buildings are represented by two methods, i.e. the 'raised building method' and the 'blocked building method', with rainfall on building tops distributed in a hydraulic and hydrological way, respectively.

In the 'raised building method', bed elevations are raised by 10 meters where buildings are located. This height is a rough estimate of the average building height in the UK, but the value does not to be 10 meters, as long as it is high enough to prevent submerge. During the simulation, bed elevations are reconstructed as introduced in sub-section 3.3.2 so that rain falling on the top of buildings can be routed by the full 2D shallow

flow model to the neighbouring cells without generating unrealistically large velocity (Sampson *et al.*, 2013).

In the 'blocked building method', buildings are blocked out from the domain and a solid wall is inserted around the building. Rainfall on building tops is proportionally distributed to the neighbouring cells, and the neighbouring cells receive the distribution as an external source term. Figure 3.16 demonstrates some typical conditions of rainfall distributions. Buildings are represented in blue tones, and their neighbouring cells are represented in orange tones. The different orange tones represent different rainfall depth. Condition (a) may sometimes happen when building polygons in an OS MasterMap are converted into building rasters (see details in sub-section 4.3.4), and need to be eliminated from the domain by raising the central cell to the same elevation as the surrounding buildings. Conditions (b), (c) and (d) show rainfall distributions for a single building, and the proportion distributed to the neighbouring cells depends on the amount of building cells they are next to. For example, the central cell in Condition (d) is adjacent to three building cells and hence receives three portions of the total rainfall on the top of its neighbouring building. Conditions (e) and (f) demonstrate rainfall distributions for more than one building. The communal neighbouring cells of different buildings can obtain rainfall distributions from all buildings they are next to. The proportion also depends on the amount of neighbouring building cells they are next to. For example, in Condition (e), the central cell can receive rainfall distributions from its left and right neighbouring buildings with one portion from each. This rainfall distribution is a hydrological method.

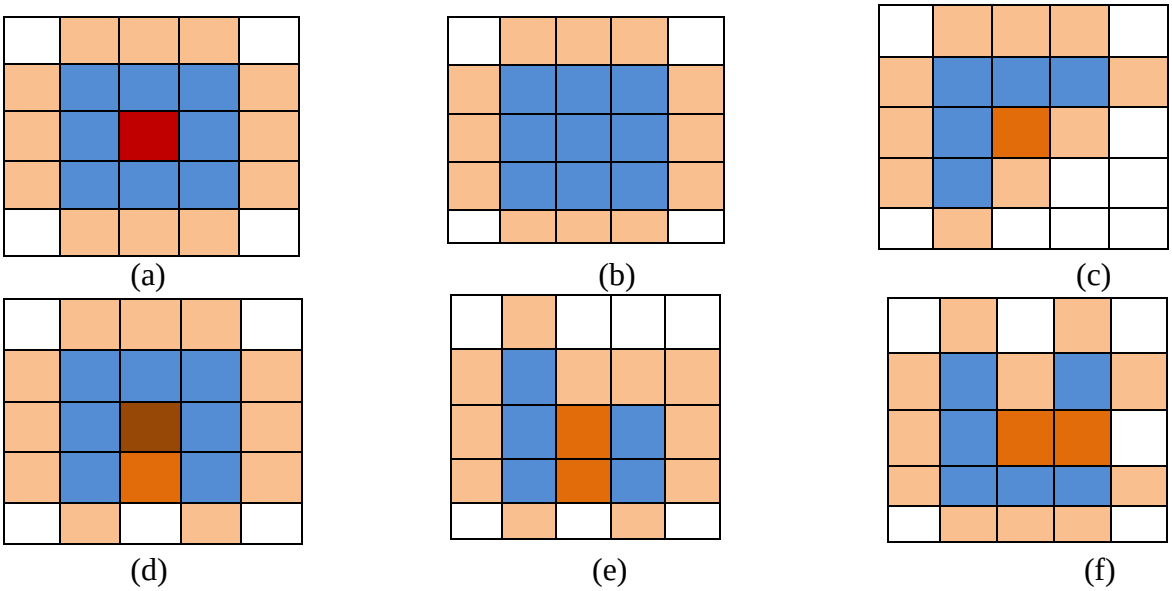

Figure 3.16 Typical conditions of rainfall distributions on building tops.

3.6 Coupling Method

The external coupling method is utilised in this study, which generally employs the surface runoff hydrograph from the hydrological model as the upstream and/or lateral boundary for the hydraulic model, to provide a one-way but seamless transition. Herein, the 'unit hydrographs' ('UH') for zone border cells are pre-generated by running a spatially-distributed hydrodynamic model in the hydrological zones (the left part in Figure 3.17). Thereafter, surface runoff production in hydrological zones is calculated using the WBM hydrological model. The resulting runoff production is then routed, by the UH method, to the hydraulic cells at the border of hydraulic and hydrological zones for the following higher-resolution simulations by the full 2D shallow flow model in hydraulic zones (the right part in Figure 3.17). The flow from hydraulic zones to hydrological zones is not considered because, when dividing the catchment in Section 3.2, the hydrological zones are specified as those areas that are unlikely to be inundated due to their relatively high bed elevations and steep slopes.

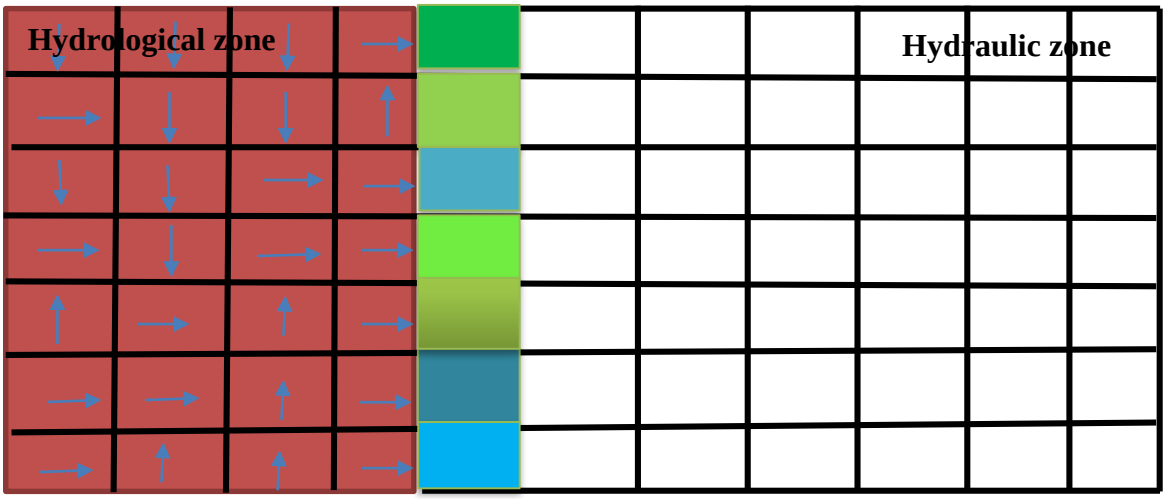

(a)

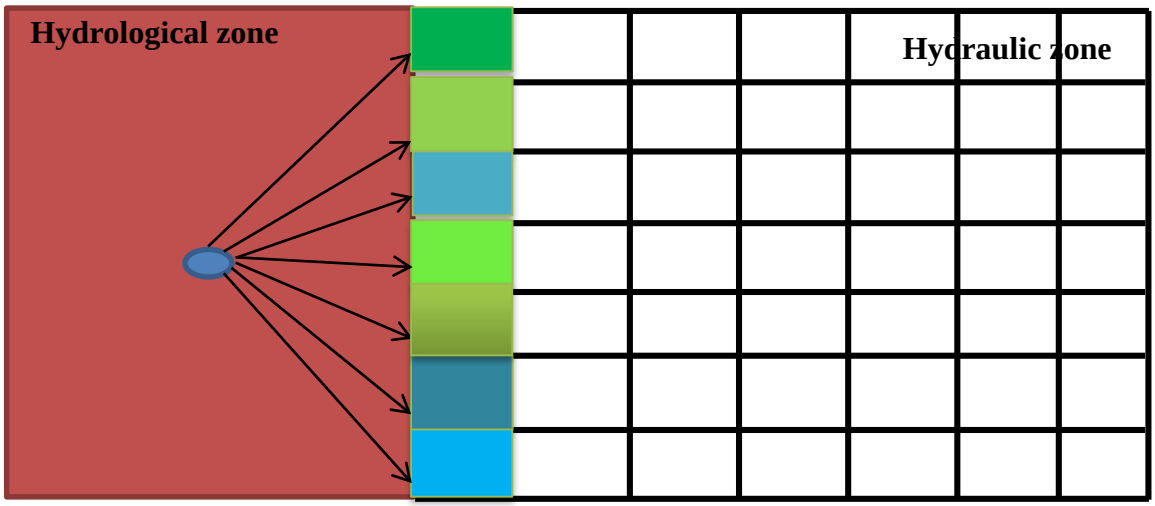

(b)

Figure 3.17 The schematization of the coupling method: pre-run (a) and post-run (b).

The unit hydrograph is usually the hypothetical response of a catchment at the outlet to a unit input of uniform net rainfall. In this work, the concept of a unit hydrograph has been extended, and is not only limited to the catchment outlet, but also to the catchment zone border. In order to generate a 'unit hydrograph' at the zone border, the hypothetical net rainfall (10mm for 15 minutes) is applied to the hydrological zones, and the full 2D shallow flow model is used to simulate the surface flow and record hydrographs at each bordering cell. These hypothetical hydrographs can be regarded as a group of generalised unit hydrographs. During real simulations, these 'unit hydrographs' can be scaled and superimposed according to real runoff production in the hydrological zones (shown in Figure 3.18), and provide accumulative hydrographs along the zone border. As the directions of these accumulative hydrographs are unknown, they are taken as external source terms in the full 2D shallow flow model for simulations in hydraulic zones.

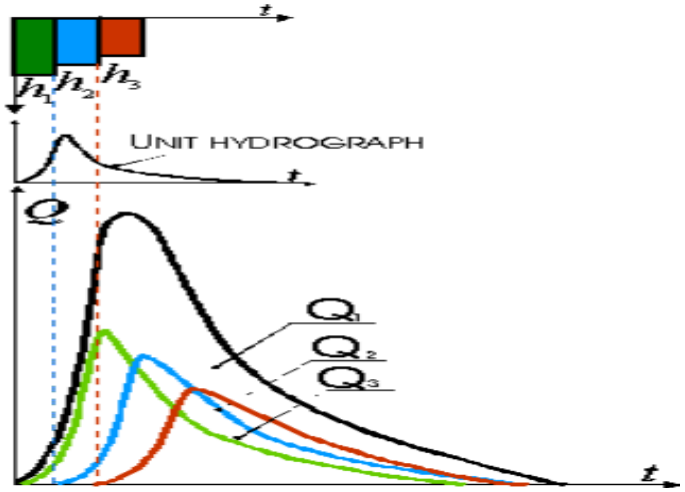

Figure 3.18 The unit hydrograph method (VICAIRE, 2006).

As well as the ‘UH’ method, another routing method is to use the ArcGIS Hydrology Tool. Each cell at the zone border accumulates flows from a certain number of upstream cells, and the accumulated flow can be calculated based on the topography and the flow direction, as introduced in Section 3.1. Subsequently, the lumped surface runoff in hydrological zones can be distributed to bordering cells in proportion to their accumulated flow as the external source term in the hydrodynamic model. The main drawback of this method is that the travel time of runoff is neglected, and this method is thus only employed as an alternative to the ‘UH’ method for comparison purposes.

3.7 Model Validation

In this work, the hydrodynamic model and hydrological model are not separately validated because each model is only used to simulate flood events in parts of the catchment, and may not generate overall modelling results individually. If the coupled model is validated, the corresponding hydrodynamic model and hydrological model are also regarded to be validated.

Ideally, validation of the coupled model would be done by comparing model results with observed field data. However, such a dataset sometimes is only limited to a certain number of locations. In order to validate the coupled model globally, other than observed field data, spatially distributed data from post-event investigations can be employed as benchmarks data sets, as well as results from the full 2D hydrodynamic model. The potential limitations of post-event investigation data are introduced in Chapter 4.

Relative Root Mean Square Error (*RMSE*) and Fit Statistics (F^1 and F^2) which have been introduced in Section 3.3 are employed to assess the global performances of the coupled model.

3.8 Model Parallelisation

In this work, the coupled model is further accelerated by combining OpenMP, owing to the ease of implementation and minimal code changes required to conduct parallel simulations.

OpenMP is an Application Processing Interface (API) that contains a collection of complier directives, library routines and environment variables for shared memory parallel programming with C, C++ or Fortran, in most operating systems including

Windows NT and Unix, etc. It is jointly defined and endorsed by a group of major computer hardware and software vendors. In this study, OpenMP 2.5 is used which was released in 2005. Since then, more advanced versions have been released with the latest version of OpenMP 4.0 in 2013. However, additional functions, such as task level parallelization are attempted in the current study.

OpenMP uses a fork-join model for parallel executions (Hermanns, 2002), shown in Figure 3.19. An OpenMP program begins with a serial process, and the code is executed by only one thread until this master thread encounters a parallel region. A team of parallel threads are then created with unique thread numbers starting from zero. The program is executed in parallel by these threads. After the parallel region, the code is executed again by only one thread. Figure 3.20 demonstrates a general OpenMP code structure.

In this study, OpenMP is implemented in the Intel Visual Fortran Studio environment. The original Fortran code is updated by adding several OpenMP directives, and this is relatively easy to do compared with other parallel computing techniques, such as GPU-based parallelisation. The code blocks that can be computed in parallel, within the full 2D shallow flow model and the coupled model, may involve evaluating the wet/dry state of cells, obtaining bed friction source terms, calculating flow variables in a new time step and updating flow variables, because in these blocks the calculation in each cell of the domain is independent and can be done simultaneously.

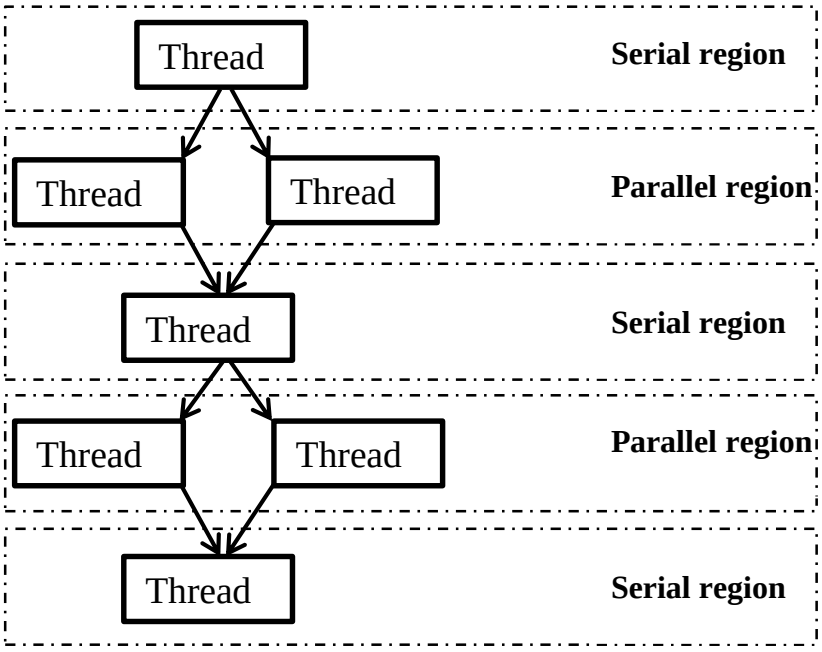

Figure 3.19 The fork-join model used by OpenMP.

```
PROGRAM HELLO
INTEGER VAR1, VAR2, VAR3
Serial Code
……
Beginning of a parallel section.
!$OMP PARALLEL PRIVATE(VAR1, VAR2), SHARED(VAR3)
Parallel section executed by all threads
……
!$OMP END PARALLEL
All threads join master thread
Resume serial code
……
END
```

Figure 3.20 The general OpenMP code structure.

3.9 Flood Damage Estimation

Flood damage estimation is implemented in this work in order to explore the impact of alleviation options. The Flood Hazard Research Centre (FHRC) depth-damage curves (Penning-Rowsell *et al.*, 2010) are employed to estimate the flood damages. In this study, only building damages are considered. The curves for residential buildings and commercial buildings are illustrated in Figure 3.21. These curves are obtained by FHRC through collecting a huge amount of information about the economic losses caused by inundations of different kinds of buildings in the UK, and these curves are sector-averaged.

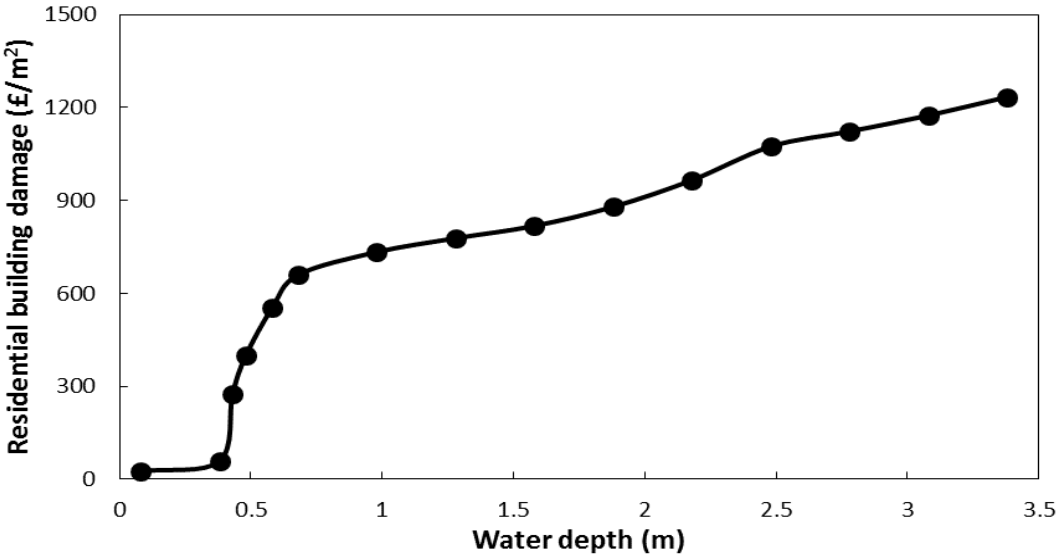

(a)

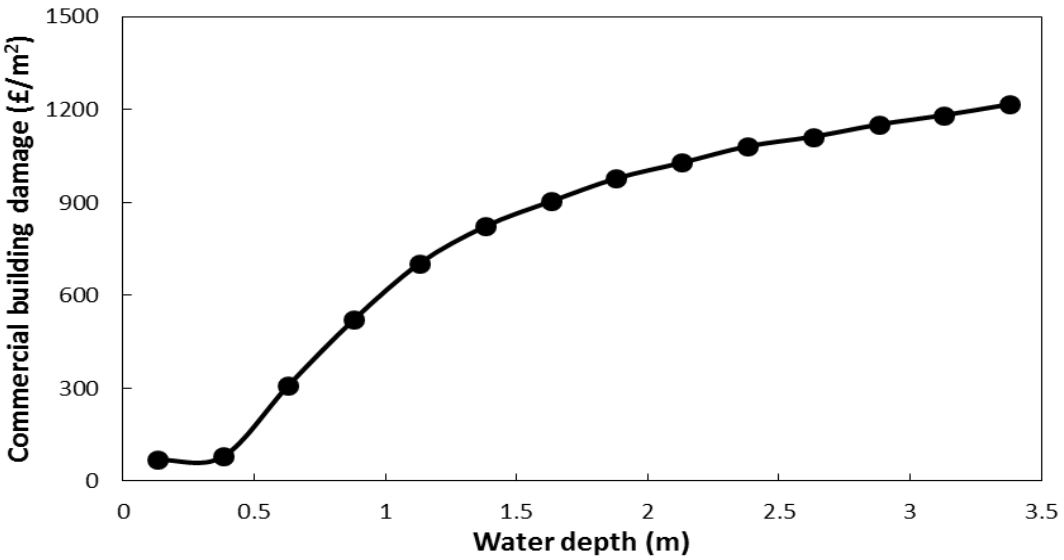

(b)

Figure 3.21 FHRC depth-damage curves for residential buildings (a) and commercial buildings (b).

The process of flood damage estimation is demonstrated in Figure 3.22. There are three steps: obtain land cover data, calculate the inundation depth and estimate flood damage through depth-damage curves.

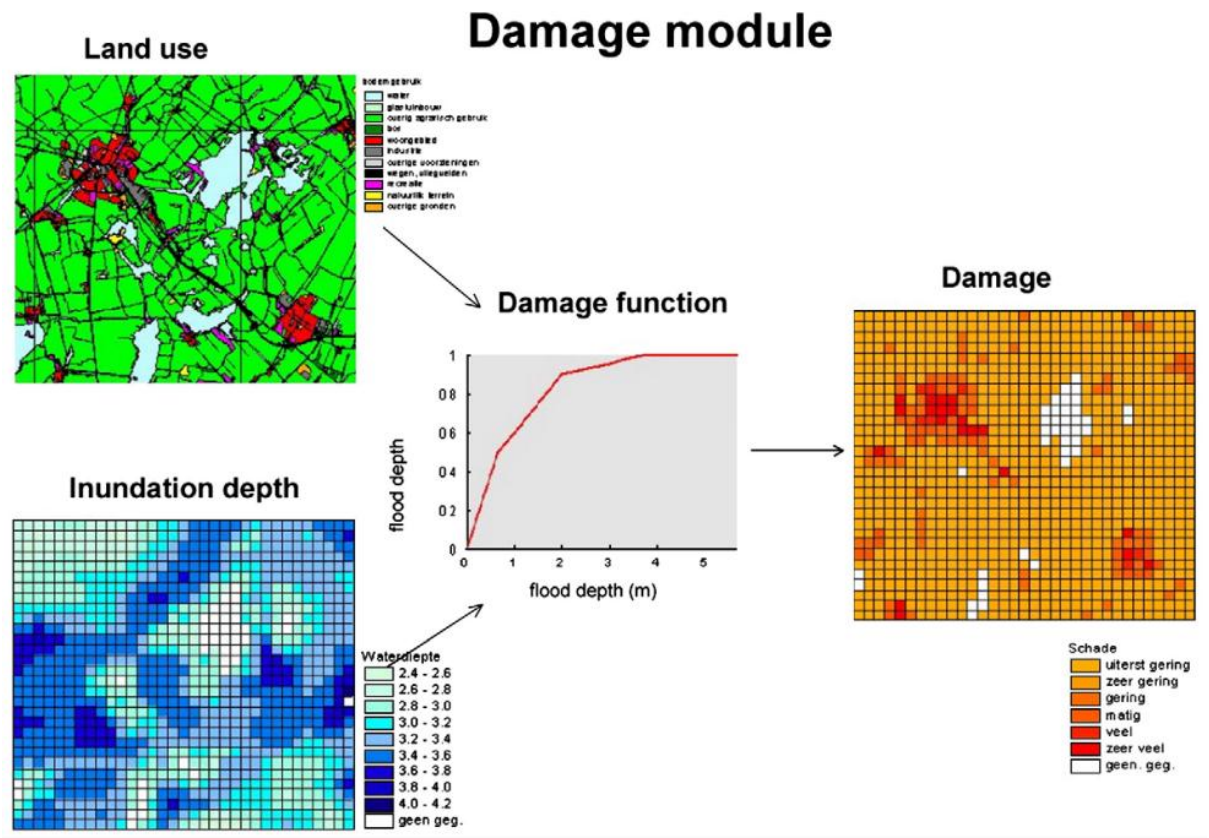

Figure 3.22 The schematization of the assessment of flood damage (Rijkswaterstaat, 2005).

3.10 Summary

This chapter has introduced the main methods that are involved in this work. The sub-catchments of interest can be extracted through hydrological analysis, and can be divided into hydraulic and hydrological zones, where the corresponding model is applied according to a design flood event and land cover data. The full 2D shallow flow model and WBM model have been selected for hydrodynamic and hydrological modelling, and are coupled by the 'UH' method. The coupled model speed can be increased by OpenMP parallel computing techniques. Finally, the FHRC depth-damage curve has been introduced to estimate flood damage.

Chapter 4 Research Site and Data

The research site of this study is Morpeth in North East England, UK. This chapter first introduces the background of Morpeth and the Wansbeck Catchment, where Morpeth is situated. The location of Morpeth means it is vulnerable to flooding, and it has suffered from many floods in history. The most severe flood event happened in September 2008, the details of which are also introduced in this chapter. Since this event, the Environment Agency has made investments to maintain, upgrade and build structural facilities across the town, in order to mitigate flood risks. In addition, many researchers have attempted to take non-structural measures to better simulate, predict, assess, and manage floods in this area, and this study is one such piece of work. In the rest of this chapter, the collection and processing of the relevant data used in this study are also presented.

4.1 Background of the Research Site

Morpeth is an ancient market town in North East England, UK. It is about 24 km north of Newcastle upon Tyne and 19 km west of the North Sea (Figure 4.1). Northumberland County Council has been located in Morpeth since 1981.The population is 14,403 according to the 2011 Census.

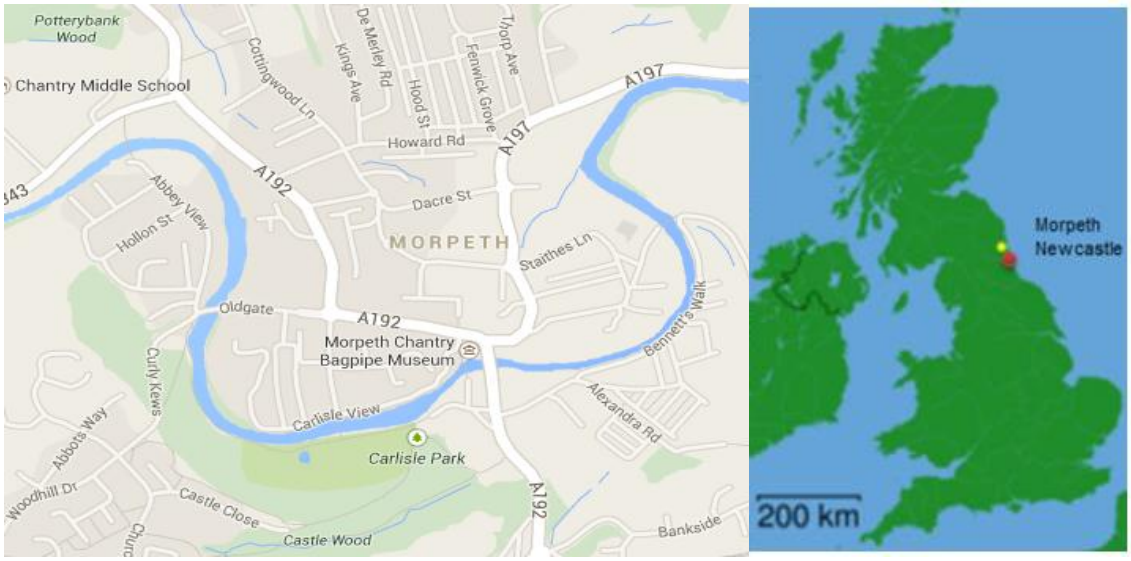

Figure 4.1 The location map of Morpeth .

The town was established in the 8th century in the loop of the Wansbeck River, for easy access to water and convenient transportation. The Wansbeck Catchment (Figure 4.2) covers 331 km^2, and the catchment area upstream of Morpeth is approximately 287.3

km^2 (CEH, 2014). The catchment has gentle topography and relatively low altitude with the mean elevation of 163 m above Ordnance datum (AOD), relative to the average sea level at Newlyn, Cornwall, UK. Other main descriptors of the catchment are listed in Table 4.1.

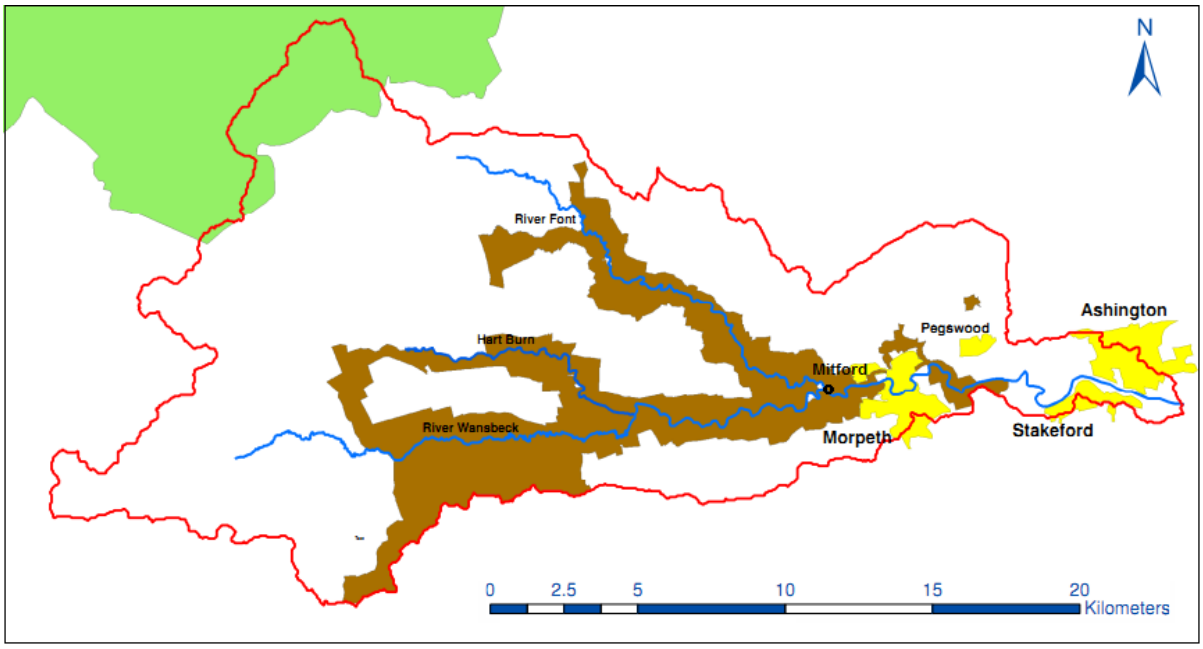

Figure 4.2 The location map of the Wansbeck Catchment (Environment Agency, 2005a).

Catchment descriptor	Wansbeck value
BFIHOST	0.34
DPLBAR	34.2 km
DPSBAR	49.6 m/km
PROPWET	0.42
SAAR	779 mm
$URBEXT_{1990}$	0.0119

Table 4.1 The descriptors of the Wansbeck Catchment (CEH, 2009).

The catchment average lag time, i.e. the time lapse between the gravity centre of rainfall and peak discharge, is only 11 hours as a result of rapid urbanisation and low permeability soil types in the Wansbeck Catchment (JBA Consulting, 2010). This is assumed by FEH, and may vary based on storm patterns. The Wansbeck River has two main tributaries: Font River and Hart Burn. Hart Burn flows into Upper Wansbeck River, and Upper Wansbeck River and Font River converge in the town of Mitford, forming the Lower Wansbeck which then travels through the towns of Morpeth and Ashington before flowing into the North Sea. In Morpeth itself, the Wansbeck River is joined by three small tributaries, i.e. Cotting Burn, Church Burn, and Postern Burn. The main reach of the Wansbeck River has an active floodplain ranging from 100 m to 300 m in width. Morpeth is located in this floodplain (Environment Agency, 2005b). The

town location means that it is vulnerable to flooding, and 1,407 properties have been identified as at risk in the town centre (Environment Agency, 2009b).

The flood risk map (Figure 4.3) provided by the Environment Agency demonstrates the area at risk of flooding, at two different levels of severity, if there were no flood defences in place. In the figure, dark blue shows the area that could be affected by 1 in 100 year fluvial floods or 1 in 200 year coastal floods; while light blue shows the additional area that could be affected by severe floods of 1 in 1000 years.

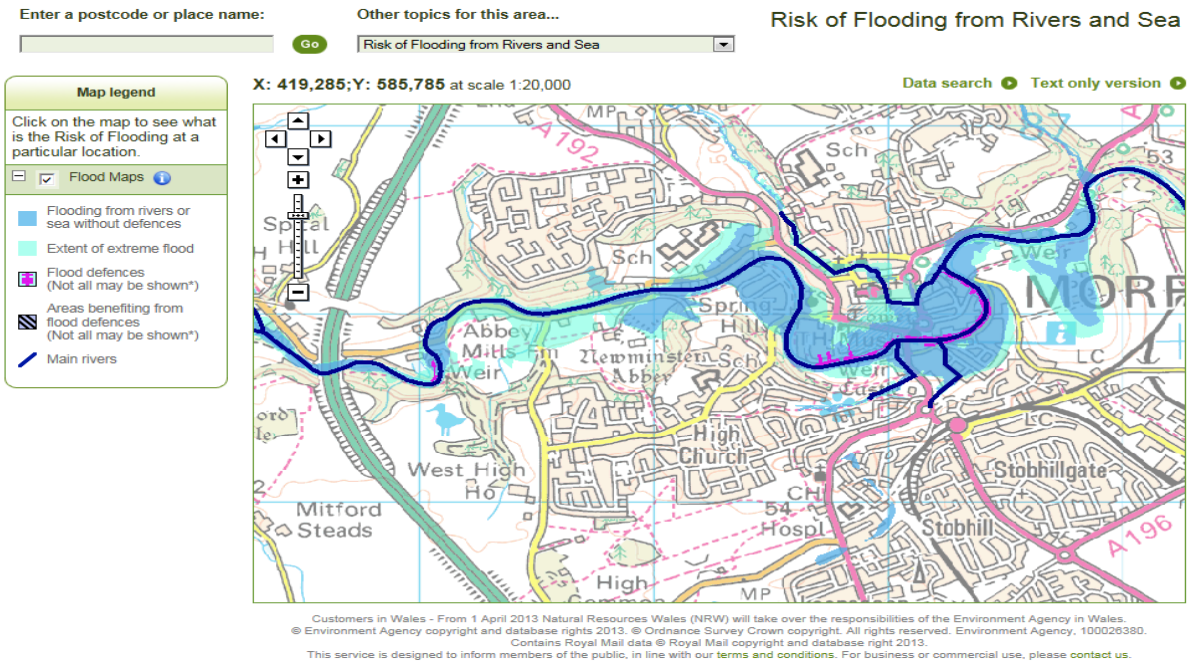

Figure 4.3 The flood risk map of Morpeth (Environment Agency, 2013b).

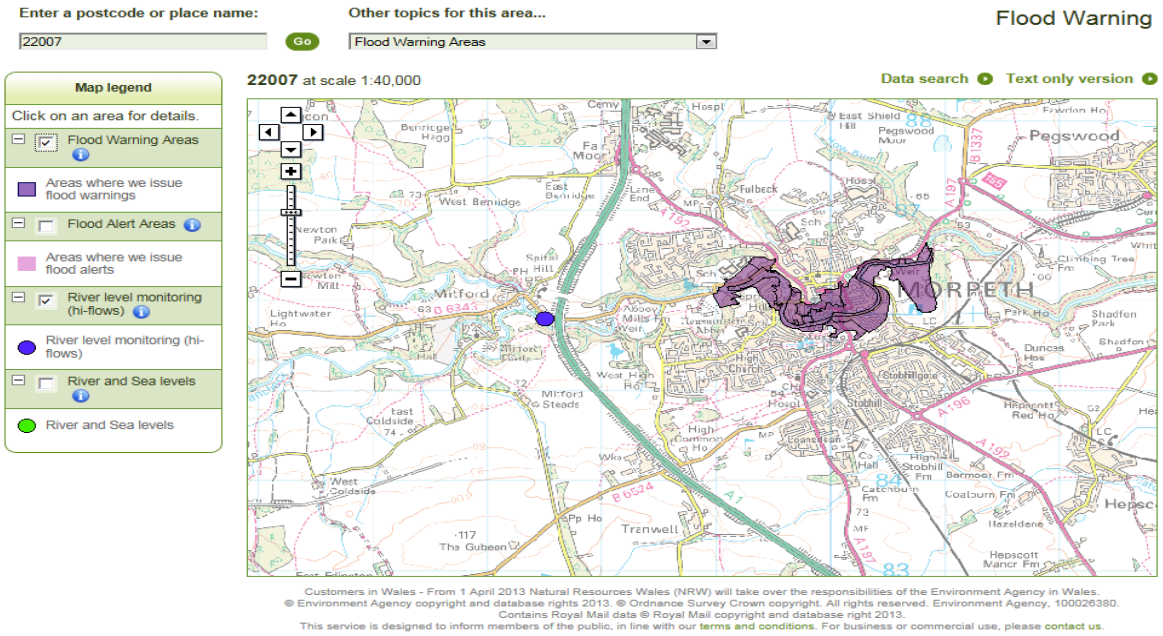

Figure 4.4 The flood warning map of Morpeth (Environment Agency, 2013a).

Combined with the flood risk map, the Environmental Agency has also provided a flood warning map (Figure 4.4) and a flood alert map (Figure 4.5). Flood warning areas are areas considered to be at particular risk from flooding, and residents who receive a flood warning should take immediate action. Flood alerts are issued when flooding is possible, and residents living in flood alert areas should prepare for flooding.

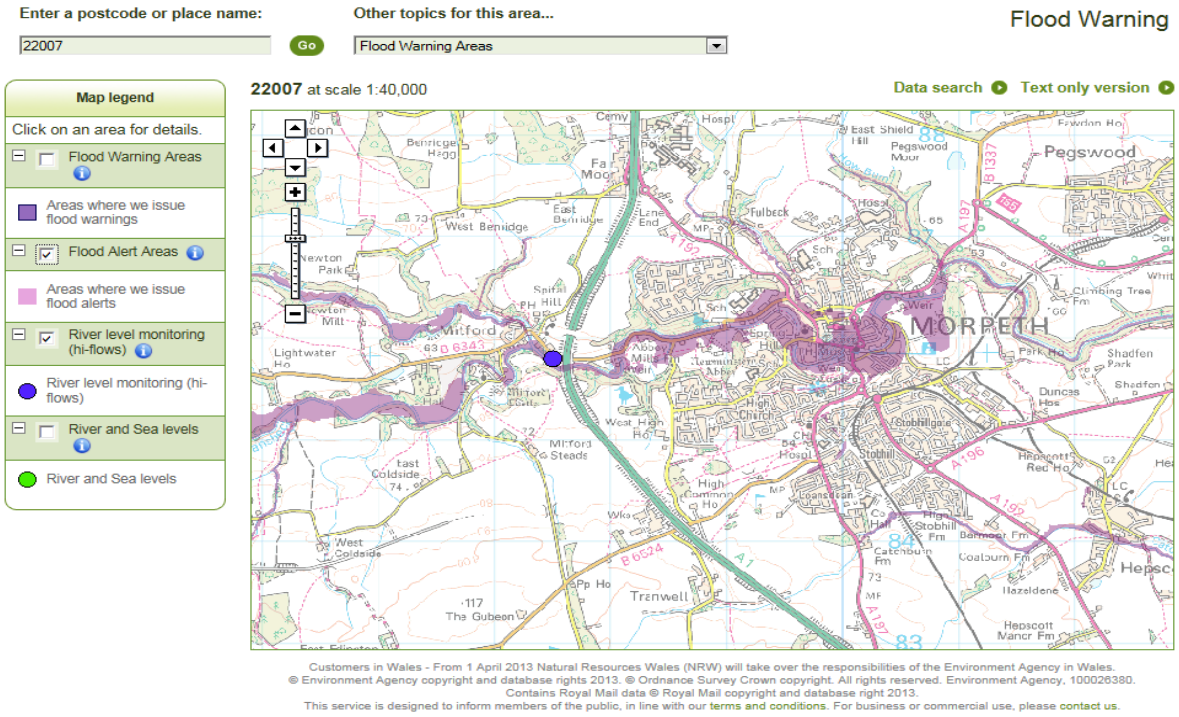

Figure 4.5 The flood alert map of Morpeth (Environment Agency, 2013a).

Throughout history, Morpeth has experienced many flood events with varying levels of severity. Between 1863 and 1903, buildings in the town were inundated on 12 occasions (Archer, 1992). After this, severe flood events did not happen until the 1960s. The most recent flood events occurred in 2008 and 2012. In 1963 a combination of rainfall and snowmelt resulted in severe inundations, which caused 482 flooded houses (Archer, 1992). Following this event, flood defences against 1 in 50 year flood event were built on the north bank to protect the main business district in Morpeth. Residential areas at Middle Greens on the south bank were also protected by flood defences (Environment Agency, 2007). However, with climate change and intensive human activities, this design standard of the flood defences is no longer high enough. In 2008 and 2012, these flood defences were overtopped by the more severe floods.

4.2 September 2008 Flood Event

Between 4th and 6th September 2008, North East England was hit by a very heavy storm, shown in Figure 4.6. Morpeth weather station recorded 152.3 mm of rainfall equivalent to 235% of the average rainfall for September (Met Office, 2008a).

The catchment was already almost saturated due to the antecedent rainfall of July and August, which caused more surface runoff and quickly rising river levels and discharges (JBA Consulting, 2009). The peak discharge reached 357 m^3/s at Mitford flow station, located about 2.2 km upstream of Morpeth. The high upstream discharge combined with local overland inflow led to the overtopping and damage of flood defences for the first time since they were built about 50 years ago. As a result, Morpeth experienced its worst flood on record, which was evaluated by the Environment Agency (2009a) as a 1 in 137 year flood event. The manhole near Church Burn was forced open, and Cotting Burn also flooded. A timeline of this flood event is shown in Figure 4.7.

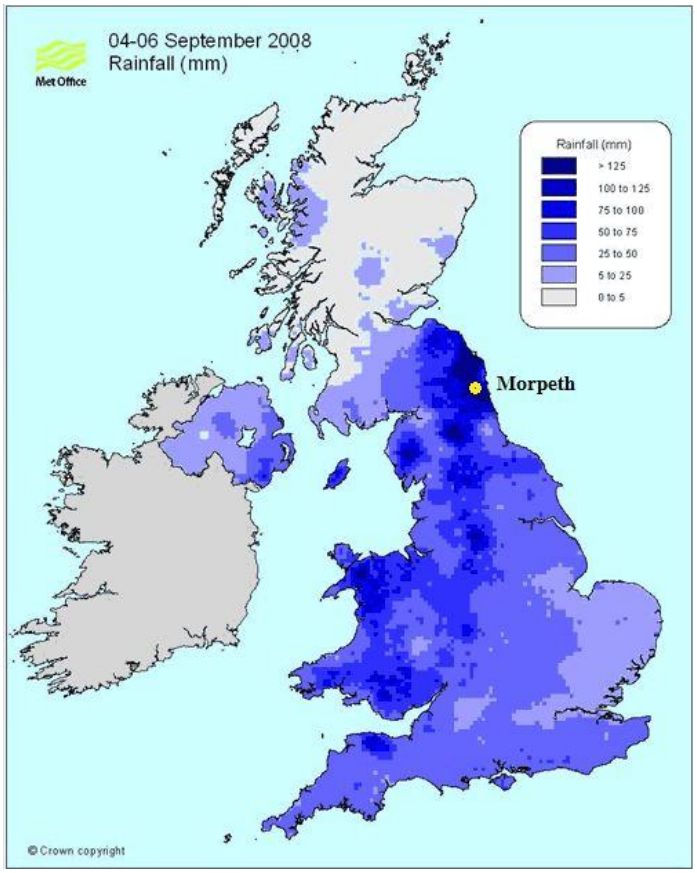

Figure 4.6 The rainfall map of UK during 04th-06th September 2008 (Met Office, 2008a).

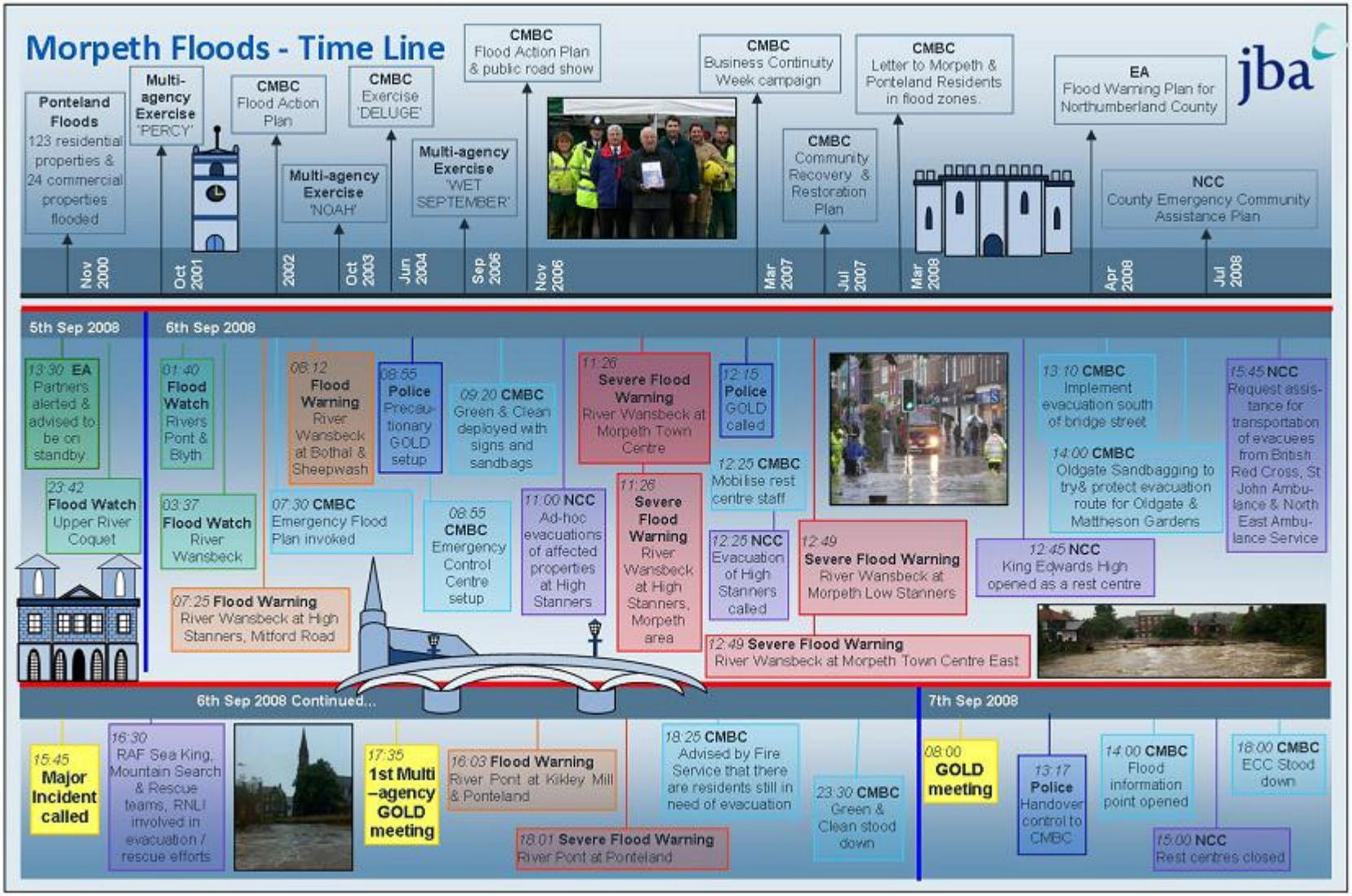

Figure 4.7 The summarised timeline of the September 2008 flood event in Morpeth (JBA Consulting, 2009).

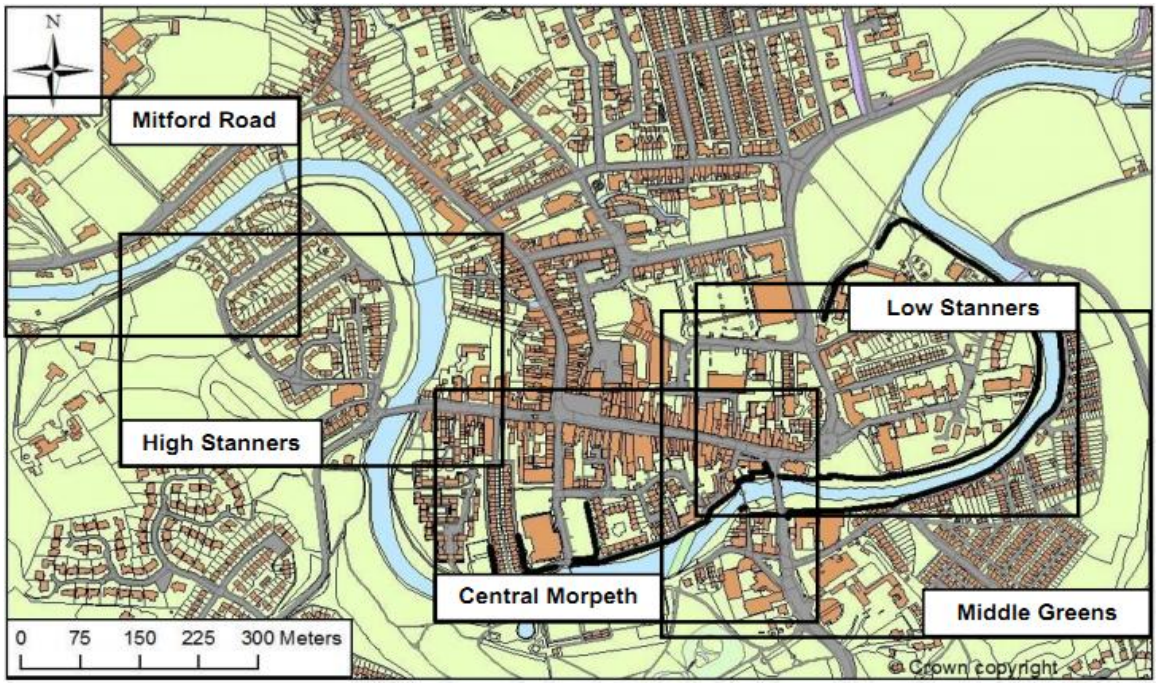

Figure 4.8 The main inundation areas in Morpeth during the September 2008 flood event (Parkin, 2010).

The town centre has been classified into five main areas according to different flooding mechanisms (Parkin, 2010).

- Mitford Road – Houses prevented water from draining to the river.
- High Stanners – Flooding limited the access to emergency services.
- Central Morpeth – The flood defences played an important part in the early stages of flooding.
- Middle Greens – Flooding occurred behind the flood defences.
- Low Stanners – Rapid flooding was caused by the overtopping of the flood defences.

A combination of pluvial, fluvial and sewer floods inundated more than 950 properties in the town centre, and another 90 properties throughout the borough. These properties included St George's Church, Riverside Leisure Centre, the town's main library, the emergency ambulance station and the health centre in Gashouse Lane, etc. All road networks within the town centre were largely affected. Emergency services including fire fighters, ambulance crews, the Royal Air Force (RAF), the Royal National Lifeboat Institution (RNLI) and the British Red Cross dealt with a huge number of calls for assistance from public. Hundreds of residents were forced to evacuate, and many of them were not able to live in their home for months. It was estimated that damage could exceed £10 million (Coolgeology, 2013) .

Figure 4.9 The selected pictures of Morpeth during the September 2008 flood event (Parkin, 2010).

After this flood event, the Environment Agency invested £2.25 million to maintain flood defences, strengthen culverts and remove deposited gravels (Environment Agency, 2011). A further flood alleviation scheme with £21 million investment is underway which involves building new defences, upgrading the existing defences and storing flood water upstream of Morpeth. The main purpose of this scheme is to mitigate flood problems from the Wansbeck River by raising the current design standard to protect the town against a 1 in 137 year flood event, the same as the September 2008 flood event in Morpeth.

4.3 Data

Data needed in the work are classified into two kinds: non-spatial data and spatial data. Non-spatial data include rainfall, discharge, water depth, etc.; while spatial data include DTM, land cover, soil type, etc. Table 4.2 shows the data used in this study. It should be aware of the data uncertainties in rainfall, flow, river bathymetry and field observation data, etc.

Data	Reference	Purpose
Rainfall	Environment Agency	Model input
Discharge	Environment Agency	Model input
DTM	Environment Agency	Providing basic topography
Buildings	OS MasterMap	Considering the effect of buildings on modelling results
Flood defences	Field work	Upgrading the basic topography
Land cover map	OS MasterMap	1, Classifying hydraulic and hydrological zones 2, Classifying permeable and impermeable surfaces
Soil type map	1, British Geological Society 2, National Soil Resources Institute	Obtaining general infiltration parameters
Water depth at critical points	2008 Morpeth Flood Summary Report	Model validation
Inundation extent map	2008 Morpeth Flood Summary Report	Model validation

Table 4.2 The data used in this study.

4.3.1 *Rainfall*

The rain gauges in the Wansbeck Catchment are illustrated in Figure 4.4, and detailed in Table 4.3.

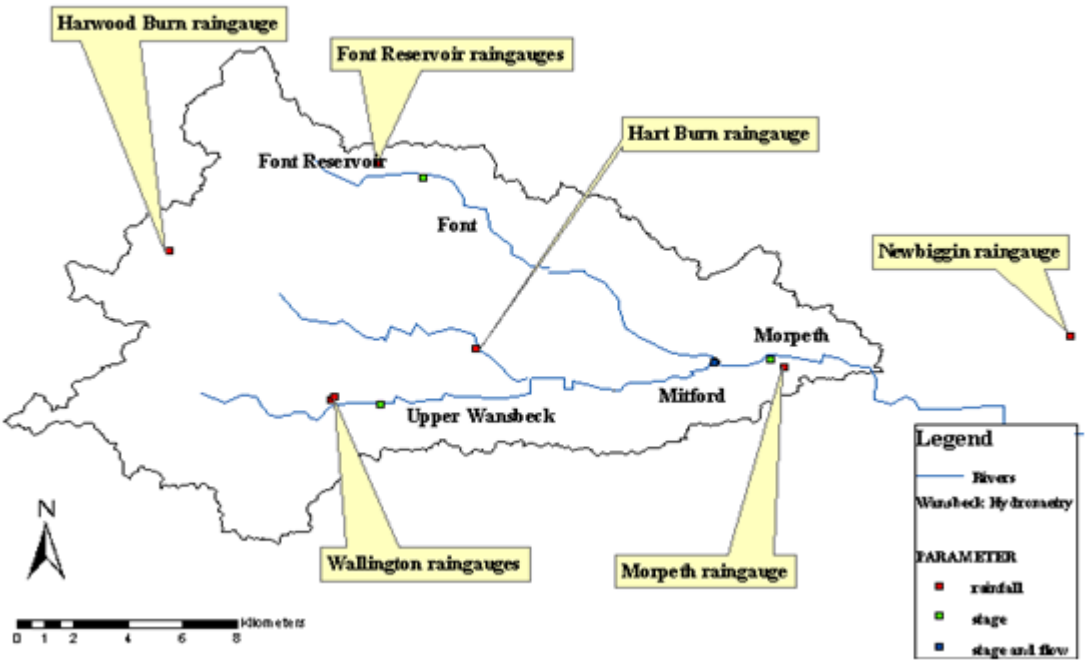

Figure 4.10 The location map of rain gauges in the Wansbeck Catchment (Ward, 2008).

Rain gauges	Start year	End year	Easting	Northing	Gauge Type	Average Rainfall (mm/a)	Collected Data
Hart Burn 006168	1968	1985	408800	586400	Storage	887	1968-1985
Wallington Hall 005784	1983	1994	403500	584300	TBR	663	1983-1994
Wallington Log 005782	1994	current	403636	584441	TBR	663	2008 .9 2009.7-2010.9
Harwood Burn 006076	2002	current	397585	590299	Storage	887	2002.11-2007.10
Harwood Burn 006077	2002	current	397585	590299	TBR	840	2002.11-2007.10 2008.9-2009.12
Font Reservoir 006403	1982	current	405208	593767	TBR	758	1982-2007 2008.9-2009.12
Font Reservoir 006404	1979	current	405208	593767	Storage	866	1979-2007
Morpeth Park 006734	1970	2007	420079	585656	Storage	712	1970-2007
Newbiggin STW 005588	1999	current	430534	586884	TBR	606	1999.4-2008.1 2008.9-2011.1

Table 4.3 The details of rain gauges in the Wansbeck Catchment (Ward, 2008).

From Table 4.3, it can be seen that some rain gauges were not in use during the September 2008 flood event. The available rainfall data for this event was mainly provided by four rain gauges: Wallington Log, Harwood Burn, Font Reservoir and Newbiggin STW. The inverse distance weighting method is utilised to obtain the rainfall data at Morpeth town centre. The resulting data is the weighted average of rainfall data from the four rain gauges, and the weight depends on their inverse distances from the town centre. The simplest form of the inverse distance weighing method is called Shepard's method (Shepard, 1968). The equation is shown as follows:

$$PP = \sum_{ii=1}^{nn} PP_{ii} w_{ii} \tag{4.1}$$

$$w_{ii} = \frac{dis_{ii}^{-pow}}{\sum_{ii=1}^{nn} dis_{ii}^{-pow}} \tag{4.2}$$

where *ii* is the index of rain gauges; *nn* is the total number of rain gauges; *dis* is the distance between rain gauges and Morpeth town centre; *w* is the weight of rain gauges; *pow* is power of inverse distance.

The resulting hourly rainfall is demonstrated in Figure 4.12.The highest daily rainfall of 72.75 mm occurred on 6th September corresponding to the day when the peak flow occurred.

4.3.2 *Discharge*

The discharge data was obtained from the nearest flow station (Mitford, 22007) about 2.2 km upstream of Morpeth town centre (Figure 4.2). It is located at the confluence point of Upper Wansbeck River and Font River with an upstream catchment area of approximately 282.03 km^2 (CEH, 2009).

A flat-V weir with a central flume at Mitford town has been in place since 1966. The side slope is 1:25, and overall width is 18 m with the central flume 3.0 m wide (HiFlows-UK, 2014). The structure of Mitford flow station is shown in Figure 4.11.

Figure 4.11 The structure of Mitford flow station (Ward, 2008).

The discharge data for the September 2008 flood event is available at 15 minute intervals. The peak discharge of 357 m^3/s was recorded on 6th September (Figure 4.12). These data sets are used as inflow for the research site, providing the upstream boundary of the model. Time zero in the model is set to be 16:00 on the 5th of September. Unfortunately, the discharge data for Cotting Burn, Church Burn, and Postern Burn are not avaible for this flood event.

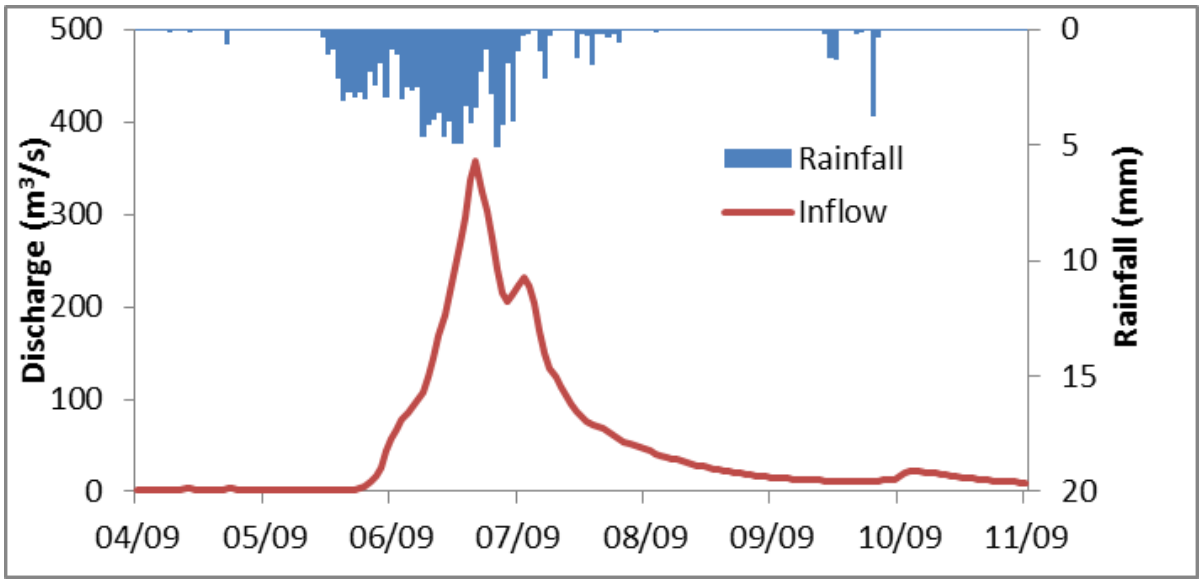

Figure 4.12 The rainfall and discharge data for Morpeth during 4th-11th September 2008.

4.3.3 *DTM and flood defences*

DTM data are provided by the Environment Agency with varying spatial resolutions. A 2 m × 2 m DTM is mainly used in this study as the basic topography representation of

the model, while other resolutions are also used to analyse the effects on modelling results from different spatial resolutions. The resulting DTM has been validated using two sets of ground control point data, showing the *RMSE* is only about 20 cm (Parkin, 2010).

In the DTM, river bed elevations are not well represented as the light reflects at water surfaces in the LiDAR technique. This problem has been solved by Asfaw (2010) who has improved the DTM with river cross section surveys. As well as this, the width of the flood defences is less than 1m, and may not be well represented in the 2 m × 2 m DTM. Field work has been carried out in order to measure the location and the height of the flood defences using a Trimble R8 GNSS device and the measuring tape (Figure 4.13). These flood defences were very important in retaining water inside the channel during the early stages of this flood event, and need to be added to the DTM (Figure 4.14).

Figure 4.13 The field work to measure the height of the flood defences in Morpeth.

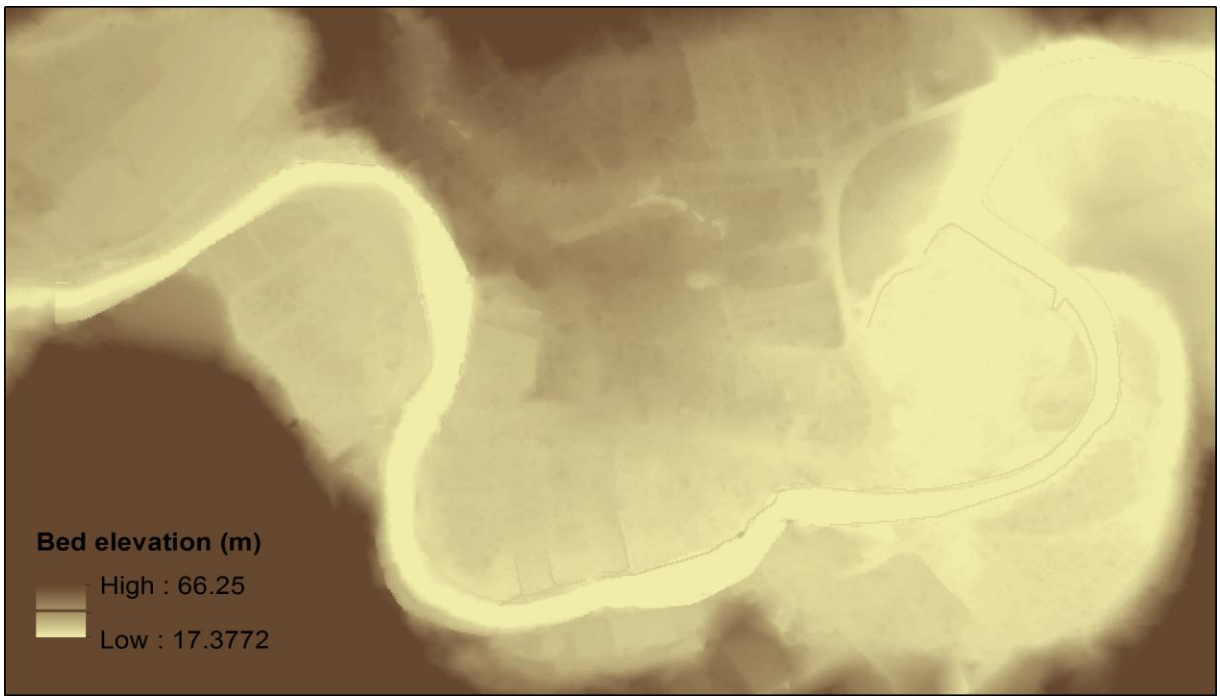

Figure 4.14 The improved DTM of Morpeth town centre with the representations of the river beds and the flood defences.

4.3.4 *Buildings*

Buildings play an important part during flood events in urban areas. Two methods of representing buildings in this study have been introduced in Section 3.5. Regardless of which method is used, building outlines and locations are required. This data can be obtained from OS MasterMap (Figure 4.15).

Figure 4.15 The outline and location of buildings in Morpeth.

Using the Analysis Tool, Data Management Tool and Conversion Tools in ArcGIS, building polygons can be converted into a raster, and allocated individual numbers (Figure 4.16) for further use in the model.

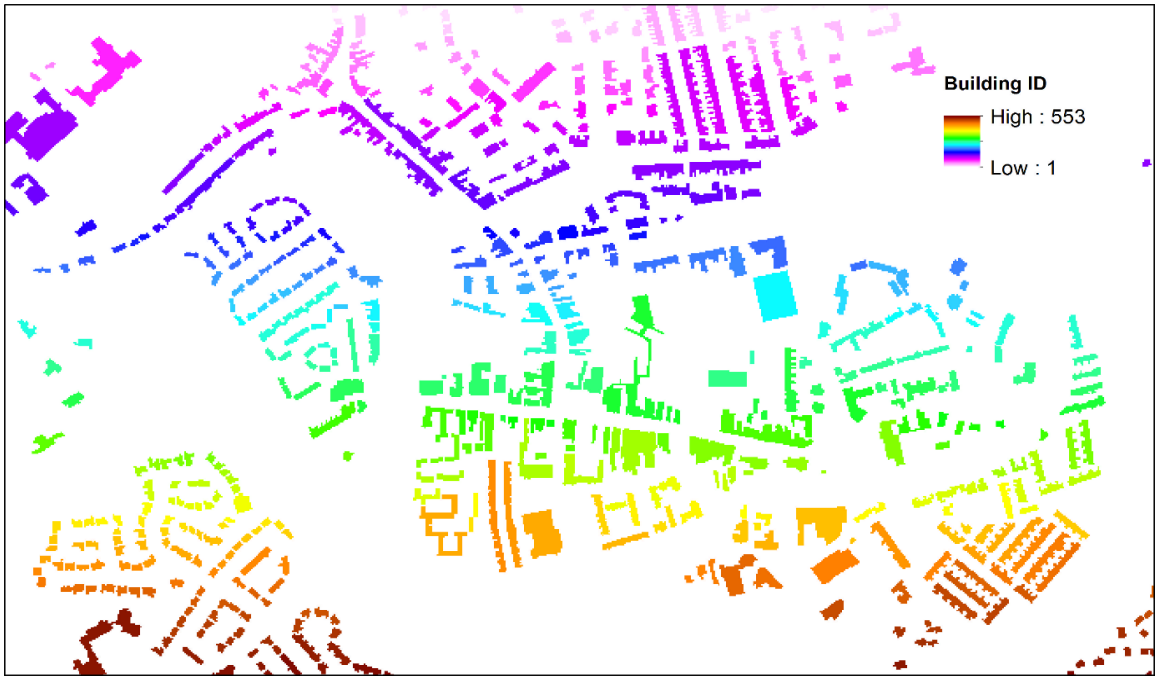

Figure 4.16 The building raster map of Morpeth with the individual number.

4.3.5 *Land cover*

Land cover data is obtained from OS MasterMap. The portal to download the MasterMap topography layer is shown in Figure 4.17. All available layers are downloaded to provide a detailed land cover of Morpeth.

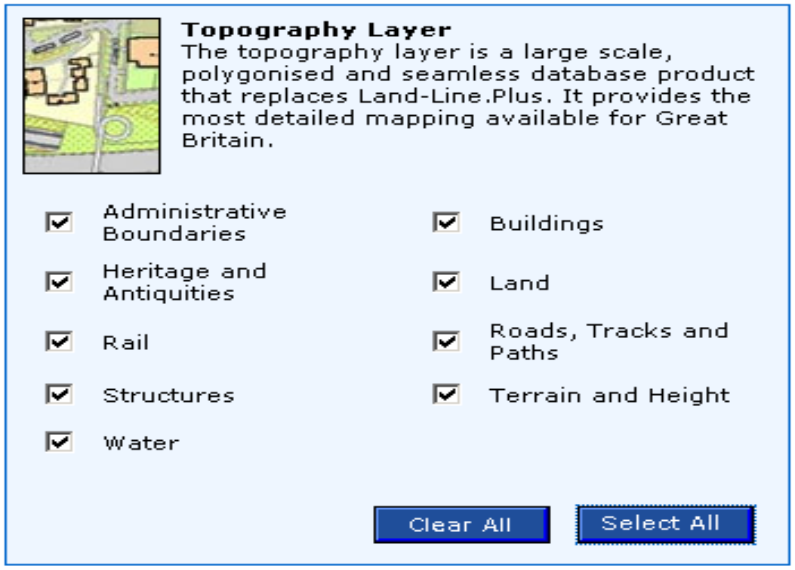

Figure 4.17 The land cover download interface (EDINA Digimap, 2013).

The downloaded data is visualised and analysed by InterpOSe and ArcGIS, and the resulting land cover raster map is shown in Figure 4.18. All green land, including natural surfaces, rough grassland, scrubs, marsh reeds, etc. are displayed in different shades of green ranging from light green to dark green. These areas are regarded as permeable areas, and possibly classified as hydrological zones if they are of relatively high elevation and steep slopes.

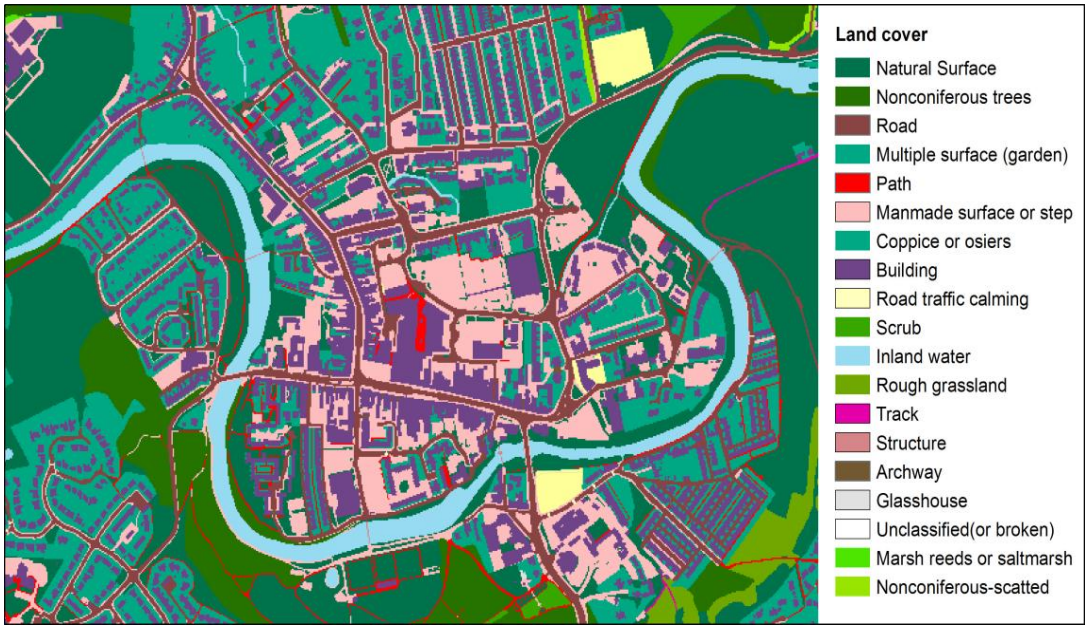

Figure 4.18 The land cover raster map of Morpeth.

4.3.6 *Soil type*

A digital map of soil types is not directly available, so a superficial geology map is used to infer soil types, because certain associations can be made between soil types and superficial geology (Ward, 2008).

The 1:625,000 superficial geology map is available at British Geological Society. Figure 4.19 shows that in Morpeth the superficial geology consists of ‘sand and gravel’, ‘clay, silt and sand’ and ‘diamicton’, and their distribution is also provided.

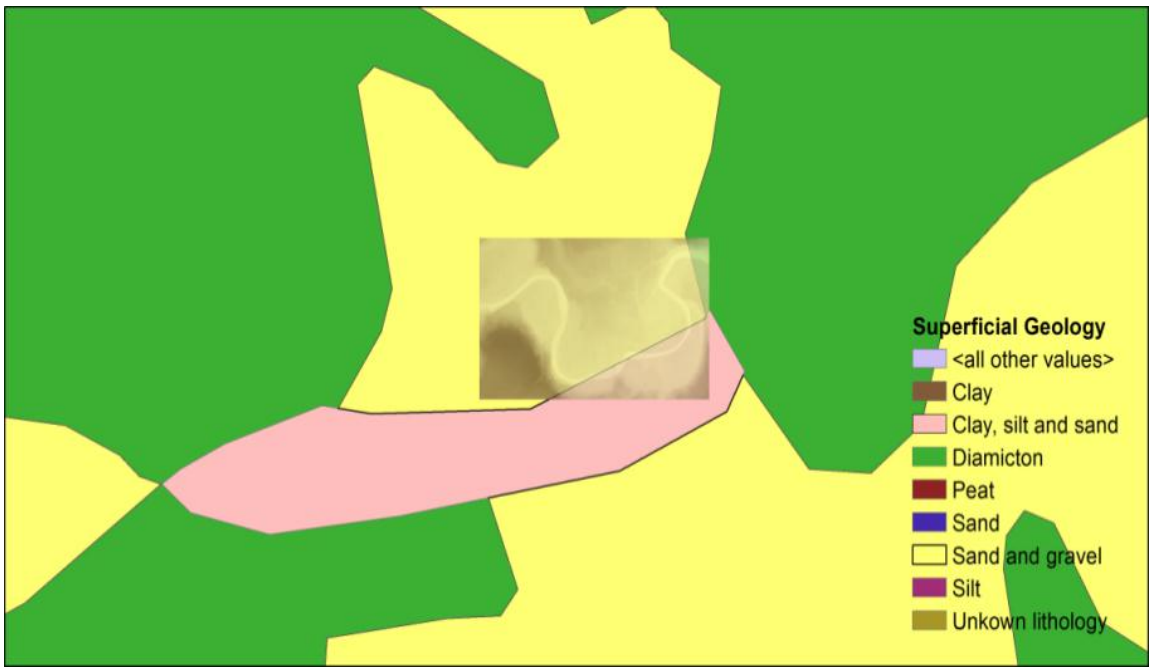

Figure 4.19 The superficial geology map of Morpeth.

The Soil Site Report of the National Soil Resources Institute is then downloaded and employed to provide the associated soil types for the superficial geology. From Figure 4.20 it can be seen that two types of soil are associated: dunkeswick and nercwys.

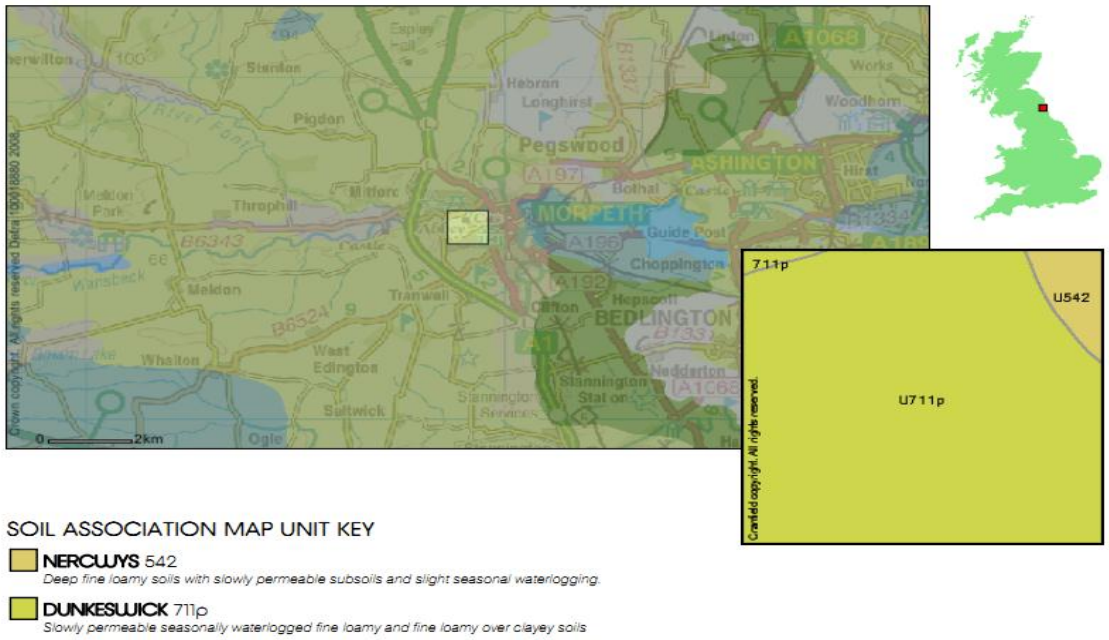

Figure 4.20 The soil association map of Morpeth.

According to the soil descriptions, these soil types can be thereafter associated with United States Department of Agriculture (USDA) soil texture (Figure 4.21). The process of soil type identification is shown in Table 4.4.

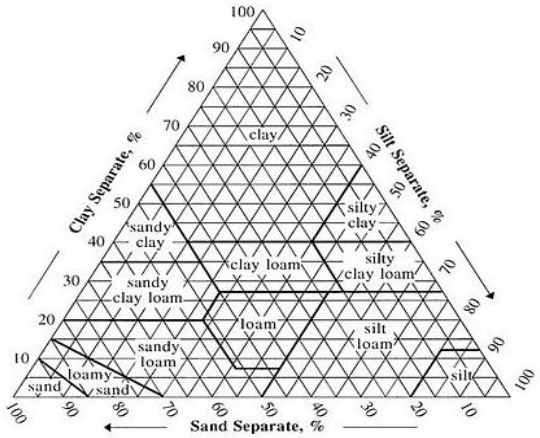

Figure 4.21 The USDA soil texture.

Geology type	Conversion to Soil	HOST	Soil description	USDA soil texture
Sand and gravel	Dunkswick	24	Slowly permeable seasonally waterlogged fine loamy and fine loamy over clayey soils	Clay loam
Clay, silt and sand	Dunkswick	24	Slowly permeable seasonally waterlogged fine loamy and fine loamy over clayey soils	Clay loam
Diamicton	Nercwys	21	Deep fine loamy soil with slowly permeate sub-soils and slight seasonal waterlogging	Sandy clay loam

Table 4.4 The soil type identification of Morpeth.

The resulting digital soil type map is illustrated in Figure 4.22.

Figure 4.22 The soil type raster map of Morpeth.

Based on the USDA soil texture, the general Green-Ampt infiltration parameters can be obtained (Rawls *et al.*, 1982; Rawls and Brakensiek, 1985), shown in Table 4.5. Due to the almost saturated soil prior to the flood event, the initial moisture content can be set the same as the saturated moisture content in the model.

USDA soil texture	Saturated moisture content θ_s (cm^3/cm^3)	Saturated hydraulic conductivity K_s (cm/h)	Matric pressure at the wetting front Ψ_f (cm)
Clay loam	0.464	0.10	20.88
Sandy clay loam	0.398	0.15	21.85

Table 4.5 Green- Ampt soil parameter estimates.

4.3.7 *Field observation data*

A post-event investigation has been carried out by Parkin (2010), and has provided flood water depth data and inundation extent maps at specific times throughout the flood event. About 2,000 pieces of information including photographs, videos and emails have been collected from the witnesses of the flood event. The best quality information is the photographs that clearly describe the date/time and location, and show measurable features to estimate water levels.

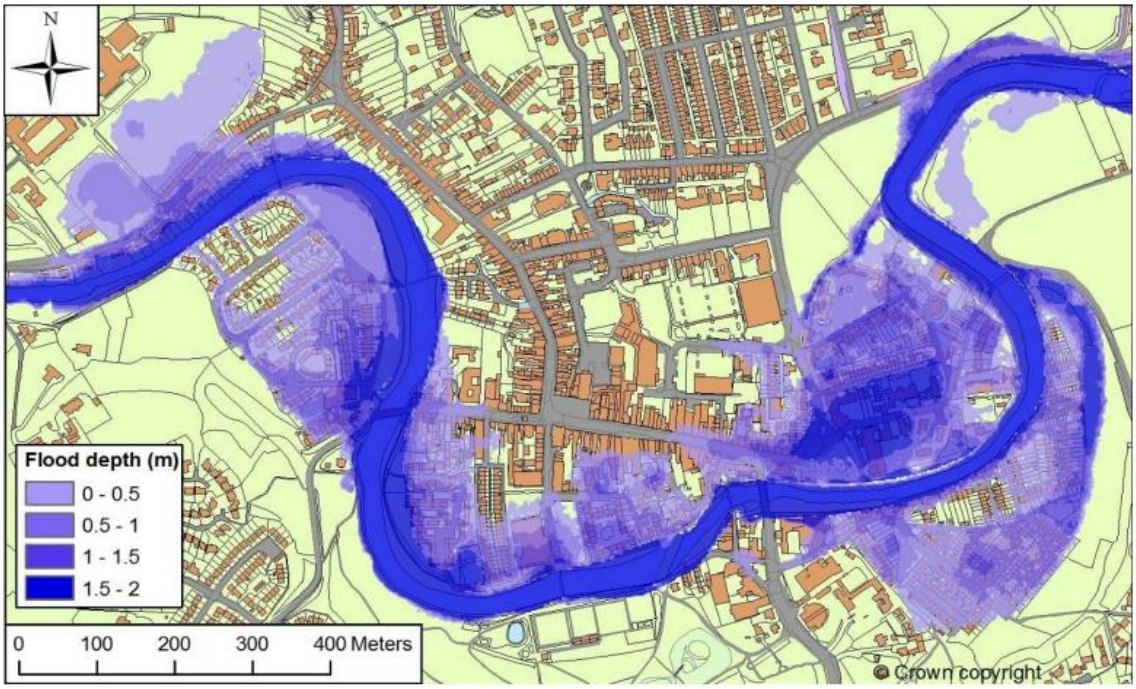

Figure 4.23 The reconstructed inundation extent map of Morpeth at 5pm 6th September, 2008 (Parkin, 2010).

In order to ensure there was enough data to interpolate water levels across the town centre, and obtain water surface maps, water levels were grouped and corrected to

specific times (11am, 1pm, 3pm, 5pm 6th September 2008) assuming the same rising rate with the available water level at Oldgate Bridge. The inverse distance weighting method was utilised to interpolate the corrected water levels, and obtain water surface maps. Water depths data and inundation extent maps at specific times were reconstructed using water surface maps together with DTM data. The inundation extent maps at intermediated times (12pm, 2pm, 4pm 6th September 2008) were averaged by the maps at the adjacent time.

Figure 4.23 shows one of these maps at 5pm 6th September. Morpeth Flood Action Group has reviewed the inundation extent maps and provided further clarifications. More details can be found in (Parkin, 2010).

The field observation data provided by the post-event investigation is useful to validate the model in this study. However, adequate scrutiny should be given to the accuracy of this data because false conclusions may be drawn resulting from inaccurate field observation data. It should be considered that there are several limitations in both collecting flood information and reconstructing inundation extent maps in the post-event investigation (Parkin, 2010; Erickson, 2011):

1. The quality of the collected information was not always good. Some did not have specific date/time or location attached, while some did not have identifiable features to estimate flood levels. These were not suitable for direct quantitative use, and needed further estimations by comparing with other information.
2. The spatial distribution of the collected information was unbalanced. The collected information was concentrated close to the river in the town centre where the interpolated flood levels obtained from the inverse distance weighting method were more reliable than other areas with limited pieces of information.
3. The level recorder used to obtain the observed data may introduce errors.
4. The assumption that flood levels rose at the same rate across the town centre may cause uncertainties in flood levels due to local topographic variations, especially in areas with dense buildings.
5. The post-event investigation was supported by the Environment Agency debris data reflecting the maximum inundation extent (at 5pm) which could be regarded most reliable. However, the debris data can not represent the progression of the flood, which

means the inundation extent maps at 11am, 1pm, 3pm are less accurate. The least accurate inundation extent maps are those at 2pm and 4pm due to the average of the maps at the adjacent time. The use of remote sensing data such as Synthetic Aperture Radar (SAR) imagery may provide more reliable inundation extent maps.

Chapter 5 Results and Discussion

This chapter presents and discusses the main modelling results. The sub-catchments of interest within the Wansbeck Catchment are firstly extracted. These are then divided into hydraulic zones and hydrological zones according to a 1 in 200 year flood event and land cover data. Model simulations using the full 2D shallow flow model and the coupled model are implemented and discussed in both Morpeth town centre and the extracted sub-catchments. Additionally, the coupled model is investigated and evaluated in Morpeth town centre, and is also employed to estimate flood damage under the Morpeth Flood Alleviation Scheme.

5.1 Sub-catchments Extraction

Morpeth is located in the lower part of the Wansbeck Catchment. A common way to demonstrate the advantages of the coupled model is to run it for the whole catchment, and compare the modelling results with either post-event measurement data or alternative numerical predictions, obtained from the full 2D shallow flow model. However, it usually incurs high computational cost for the full 2D shallow flow model to be implemented over such a large domain area especially when it is based on a relatively fine grid. Rather than using the whole Wansbeck Catchment, running these two models on the sub-catchments where Morpeth is located can produce a reasonable alternative method of validation. Furthermore, it may take much less computational time, and make the full 2D shallow flow model more practical due to the much smaller domain area.

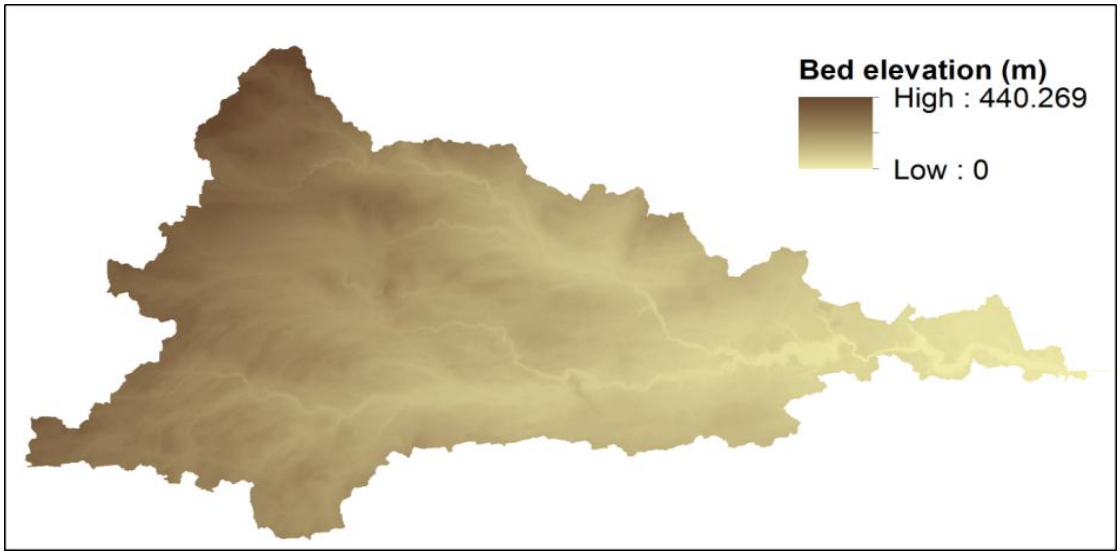

Figure 5.1 The filled 5 m × 5 m DTM of the Wansbeck Catchment.

In order to identify the relevant sub-catchments, the DTM for the Wansbeck Catchment is first extracted from a larger DTM map, and sinks in the DTM are filled in order to calculate the correct flow directions, as shown in Figure 5.1.

The flow direction in each cell can be evaluated by the 'D8 method' based on the filled DTM, as shown in Figure 5.2.

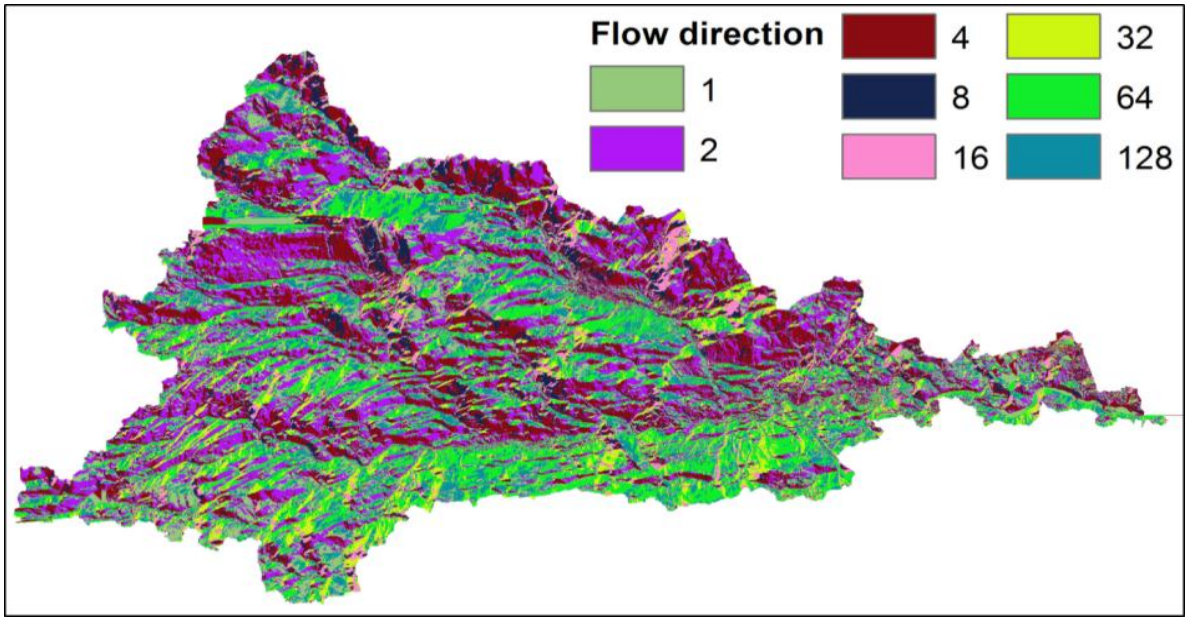

Figure 5.2 The flow directions of the Wansbeck Catchment.

Once the flow directions are obtained, the flow accumulation can then be derived. In order to create a stream network on the basis of the flow accumulation result, an accumulation threshold of 7,000 is set. If the accumulated flow value of a cell is above the threshold, the cell is then regarded as a stream cell. This threshold is obtained by trial and error so as to generate a more reasonable stream network, which includes main streams and tributaries and excludes some small tributaries. The resulting stream network is illustrated in Figure 5.3.

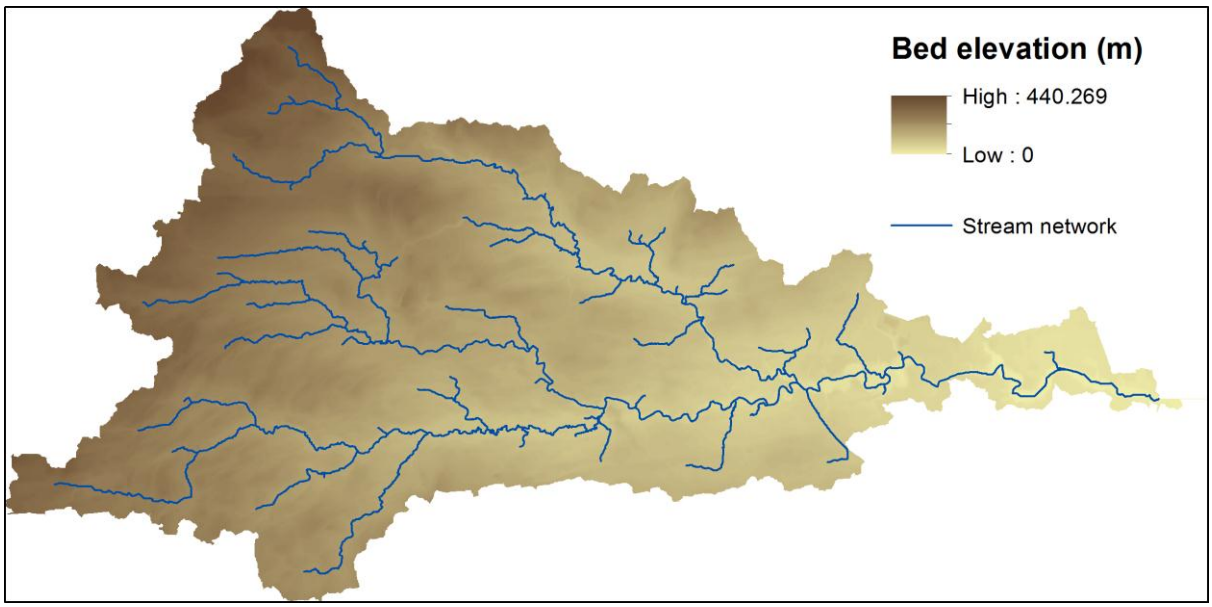

Figure 5.3 The stream network of the Wansbeck Catchment.

After this the stream network is integrated with the flow direction in order to calculate the stream link, which allocates each stream an individual number and links them by the stream order (Figure 5.4).

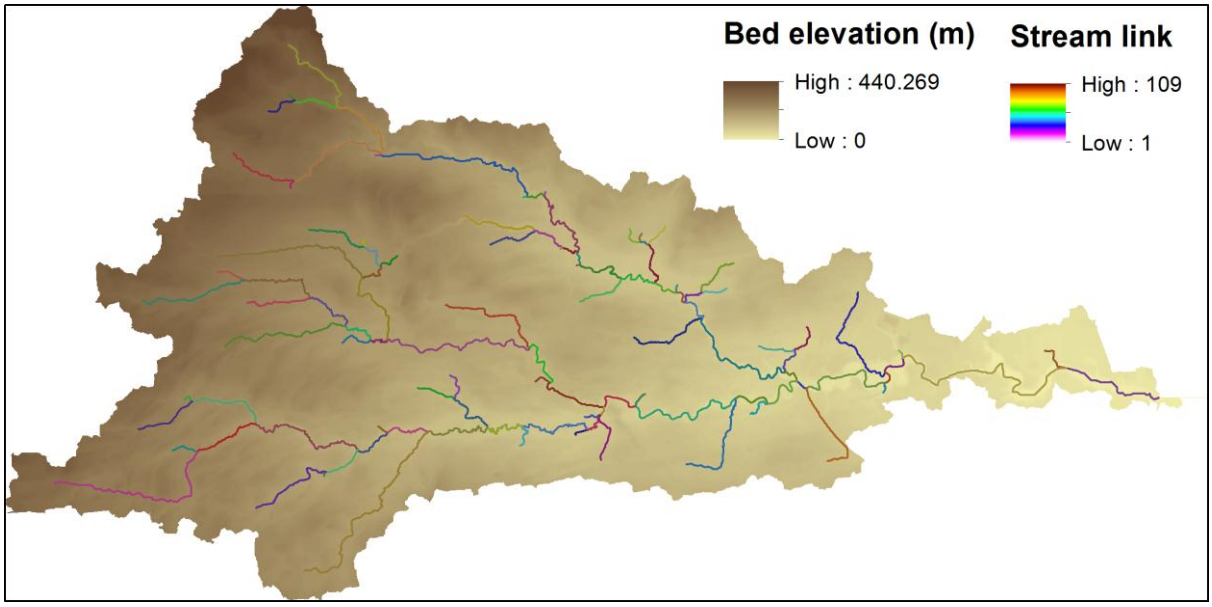

Figure 5.4 The stream link of the Wansbeck Catchment.

The sub-catchments can be generated using the stream link and the flow directions as illustrated in Figure 5.5.

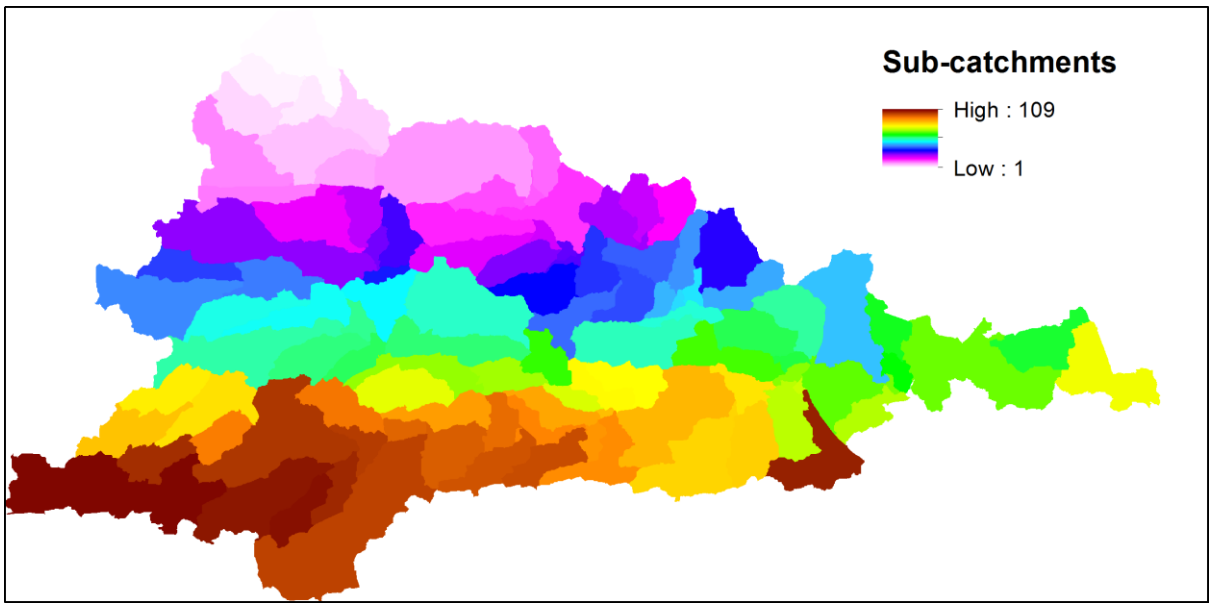

Figure 5.5 The sub-catchments of the Wansbeck Catchment.

There are 109 sub-catchments within the Wansbeck Catchment, seven of which directly affect Morpeth. From Figure 5.6, the effect of the sub-catchments upstream of point 'A' can be represented by the discharge at Mitford flow station. The sub-catchments downstream of point 'B' do not affect Morpeth. In this condition, the seven sub-catchments with the total area of 19.16 km^2 between point 'A' and 'B' are separated from the whole catchment, shown in the red outline in Figure 5.6. The coupled model and the full 2D shallow flow model will be run and compared in this selected catchment area.

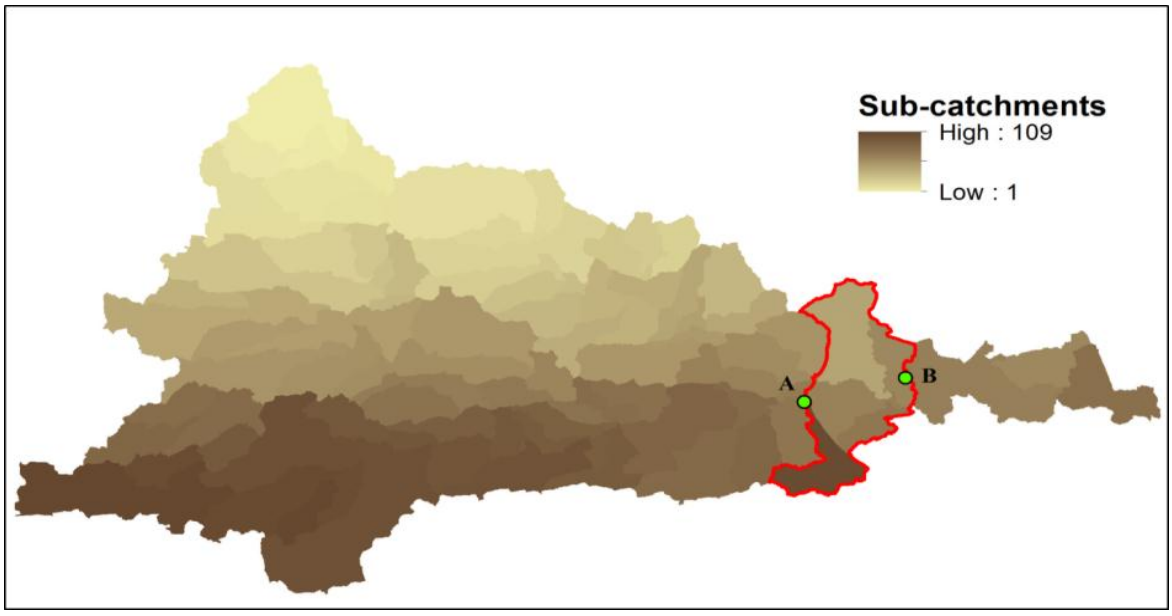

Figure 5.6 The extracted sub-catchments in the Wansbeck Catchment.

5.2 Catchment Division

The extracted sub-catchments should be divided into hydraulic and hydrological zones in which the corresponding models are applied. The design rainfall and design hydrograph, with the return period of 200 years, are first obtained using DDF curves and the ReFH model for the Wansbeck Catchment. A design flood event is then generated by the full 2D shallow flow model based on the design rainfall and design hydrograph. The resulting flood extent together with the land cover is employed as a reference to divide the catchment into hydraulic and hydrological zones. The estimated return period of the largest recorded flood event in Morpeth was 1 in 137 years, so the 1 in 200 year design flood event herein is appropriate to offer the catchment a division reference.

5.2.1 *Design rainfall*

The design rainfall can be acquired using DDF curves for the Wansbeck Catchment. It can be assumed that the extracted sub-catchments can be represented by a 1km grid point when calculating the rainfall for a certain duration and return period.

A point with the grid reference (419024, 586042) around the centre of the extracted sub-catchments has been selected, and its nearest 1 km grid point (419000, 586000) is used to obtain the rainfall DDF parameters, shown in Table 5.1.

DDF curve parameter	C	D_1	D_2	D_3	E	F
Value	-0.02	0.421	0.393	0.258	0.267	2.33

Table 5.1 The DDF parameters for the selected 1 km grid point.

The resulting DDF curves are illustrated in Figure 5.7. From these curves the DDF design rainfall for a certain duration and return period can be obtained. The parameters can be exported into the ReFH spreadsheet, and the DDF design rainfall is then discounted by multiplying an areal reduction factor (0.98) and a seasonal correction factor (0.74) to obtain the corrected design rainfall, shown in Table 5.2. The design rainfall hyetographs can be generated for a 13-hour duration, as shown in Figure 5.8. According to the aforementioned assumption, these hyetographs can represent the design rainfall in the extracted sub-catchments.

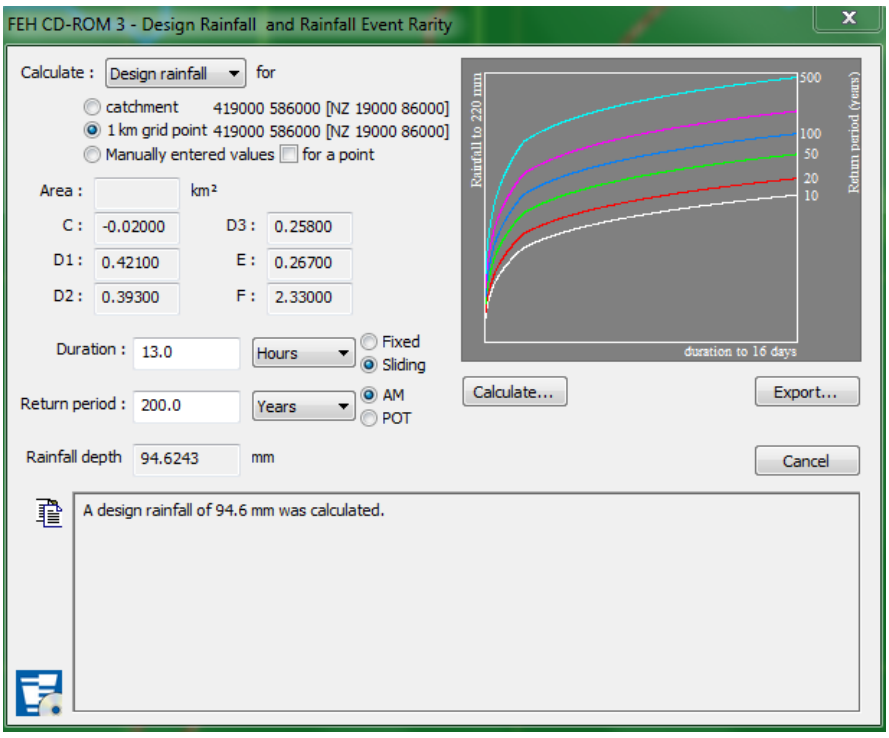

Figure 5.7 DDF curves for the selected 1 km grid point.

Return Period (a)	DDF design rainfall (mm)	Design rainfall (mm)	Peak rainfall (mm)
200	94.6	68.6	13.4

Table 5.2 The design rainfall depth for 13 hours in the extracted sub-catchments.

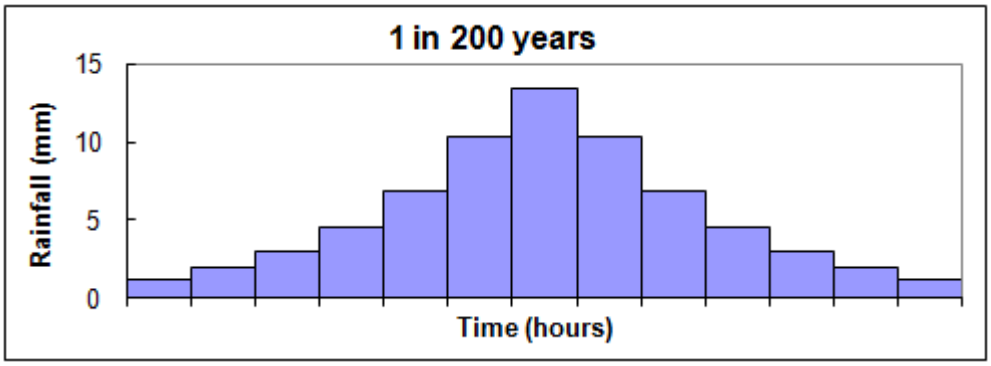

Figure 5.8 The design rainfall hyetograph in the extracted sub-catchments.

5.2.2 *Design hydrograph*

The design hydrograph at the Mitford flow station is acquired for the 1 in 200 year flood event. The design rainfall is first calculated according to the same method given in sub-section 5.2.1, for the catchment upstream of the Mitford flow station, as shown in Figure 5.9.

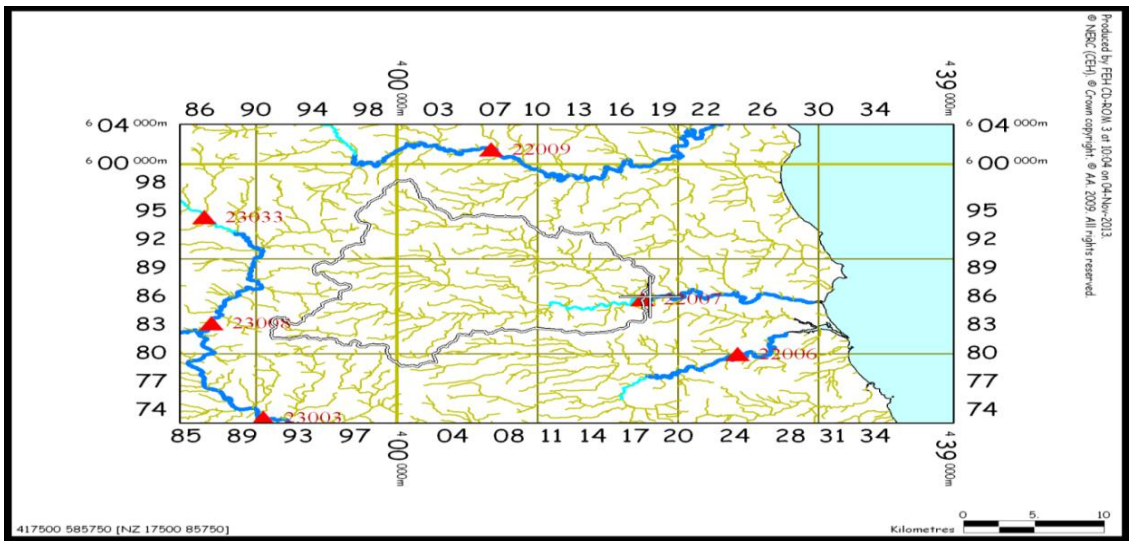

Figure 5.9 The catchment upstream of the Mitford flow station.

Based on the design rainfall, the ReFH model is employed to generate the design hydrograph with the catchment descriptors in Table 5.3. *AREA* is the catchment area (km), and other descriptors have been introduced in sub-section 3.2.1.

The September 2008 flood event, evaluated as 1 in 137 year event by the Environment Agency, is used here as a reference to adjust the resulting design hydrograph, illustrated in Figure 5.10.

Descriptors	*AREA*	*PROPWET*	*SAAR*	*BFIHOST*	*DPLBAR*	*DPSBAR*	$URBEXT_{1990}$
Value	282	0.45	794	0.347	20.15	50.8	0.0005

Table 5.3 The relevant descriptors for the catchment upstream of the Mitford flow station.

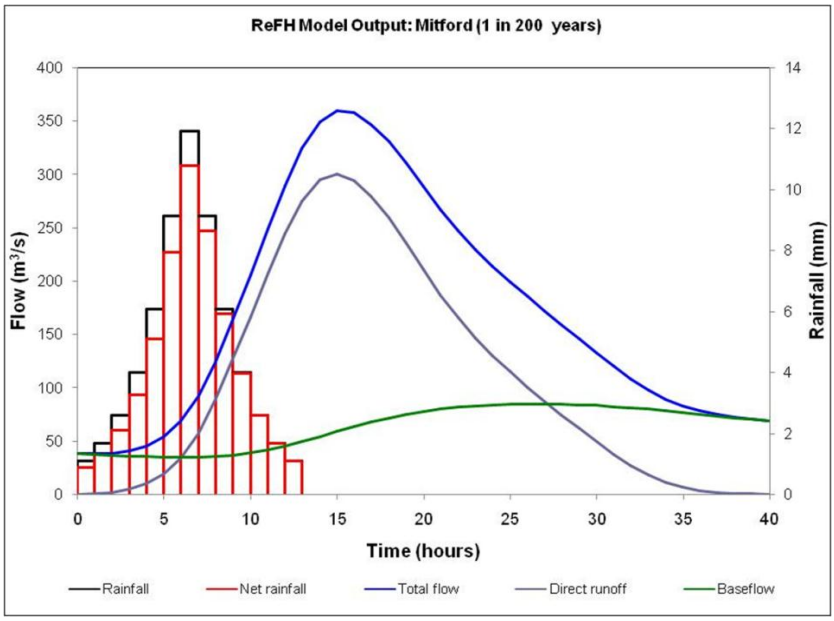

Figure 5.10 The design hydrograph at the Mitford flow station.

5.2.3 *Design flood event*

The design flood event can be produced by the full 2D shallow flow model based on the above design rainfall hyetograph and design inflow hydrograph to specify the hydraulic and hydrological zones on the extracted sub-catchments. When classifying the zones, only rough inundation extent is required and so simulations can be performed on coarse meshes of 5 m × 5 m resolution to reduce computational cost. Before running the full 2D shallow flow model, a steady state in the river channel, driven by a steady low inflow at the inlet is obtained as the initial condition for the full 2D shallow flow model. A global error is defined (Zhou *et al.*, 2001):

$$GE = \sqrt{\sum_{i,j}\left(\frac{h_{i,j}^{k} - h_{i,j}^{k-1}}{h_{i,j}^{k}}\right)^{2}} \quad . \tag{5.1}$$

where $h_{i,j}^{k}$ and $h_{i,j}^{k-1}$ represent the local water depth at the current and previous time level, and $GE < 5\times10^{-6}$ is taken as the convergence criterion for the steady state.

The steady state is achieved with 10 m^3/s of constant inflow after about 10 hours, and the initial water depth is displayed in Figure 5.11.

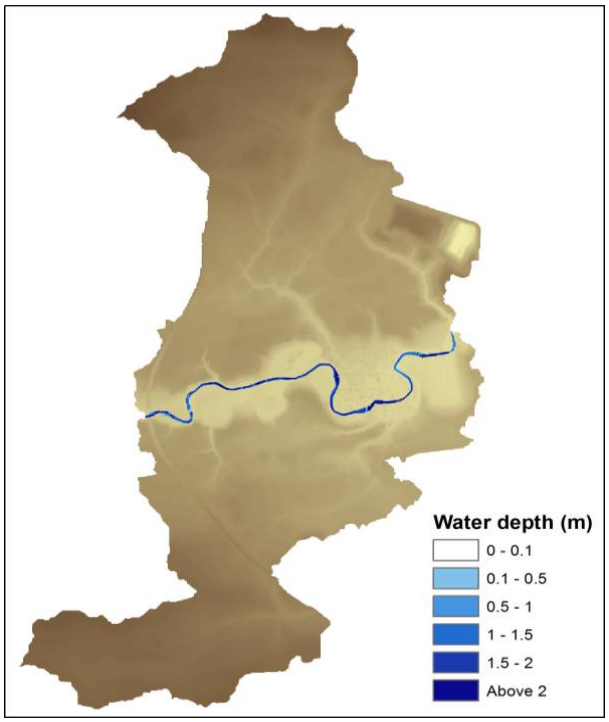

Figure 5.11 The water depth at the initial steady state in the extracted sub-catchments.

Based on the steady initial state, the 1 in 200 year design flood event is generated by the full 2D shallow flow model, and the inundation extent is displayed in Figure 5.12.

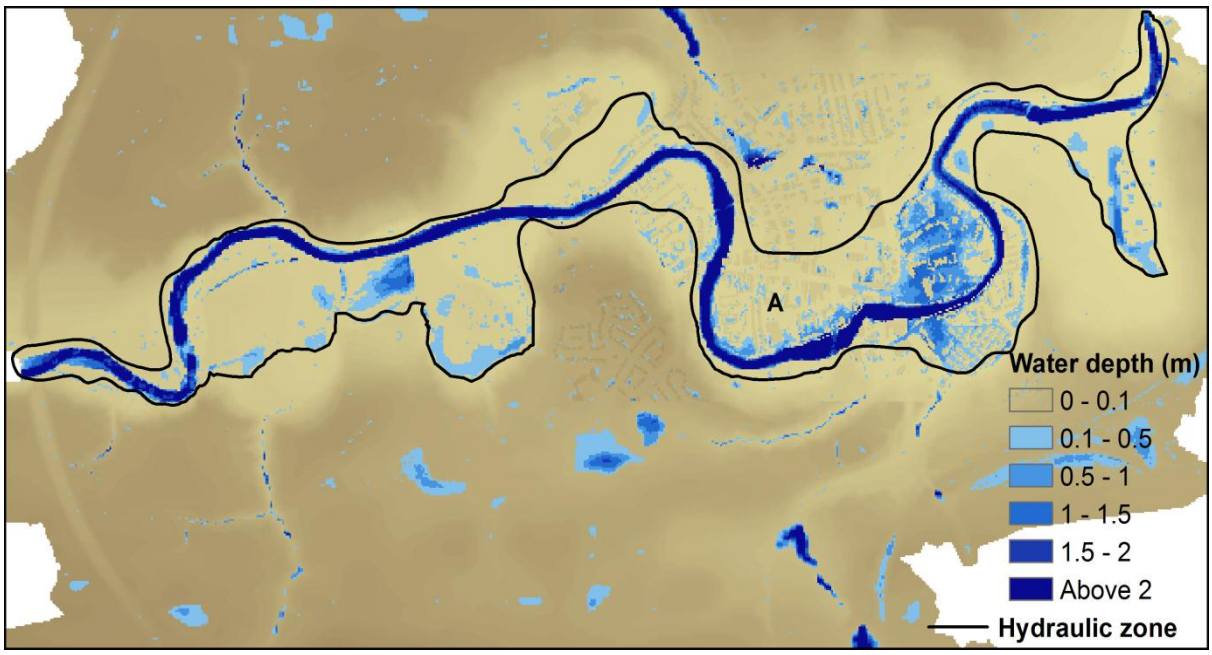

Figure 5.12 The inundation extent of the 1 in 200 year design flood event in the extracted sub-catchments.

The fluvial inundation area can be preliminarily regarded as a hydraulic zone, and local adjustments may be made according to the land cover. For example, in Figure 5.12, the inundation area around point 'A' may be caused by local rainfall, but it is still included in the hydraulic zone because it is mostly covered by buildings and close to the fluvial inundation area. As mentioned in sub-section 3.2.3, due to its subjective nature, there is no accurate solution for the division of the catchment, but the inundation extent map and land cover can act as important references. The hydraulic zone for the 1 in 200 year design flood event is outlined in Figure 5.12. The remaining areas in the domain are regarded as the hydrological zone.

5.3 Simulations in Morpeth Town Centre

The September 2008 flood event is used in this work to validate the full 2D shallow flow model as well as the coupled model. Post-event measurement data is taken as the reference. The extracted sub-catchments are discretised by a fine uniform grid with 2 m × 2 m resolution in order to represent the complex urban topography. This will inevitably incur a huge amount of computational time, especially for the full 2D shallow flow model, due to the size of the domain. In this section, the two models are applied to Morpeth town centre with domain dimensions of 1.45 km × 0.9 km. For validation, it has been assumed that the modelling results in the extracted sub-catchments' domain are not significantly affected by the reduction in domain size. Furthermore, it is also

assumed that the effects on the modelling results from buildings, Manning coefficient, etc. are consistent in the sub-catchments' domain and the town centre domain. Following this, further model validation will be conducted in the extracted sub-catchments' domain in Section 5.5.

Seven critical points throughout the town centre are selected to record the time history of water depths and flow velocities, shown in Figure 5.13. The points are located in the five main inundation areas as introduced in Section 4.2, in order to better represent the inundation process. More details of the critical points are documented in Table 5.4.

Critical point	Location	Easting	Northing	Description
1	Mitford Road	419223	586162	Between houses, to assess flow between buildings
2	High Stanners	419549	586138	River breaks out of banks across the green area and floods houses
3	High Stanners	419571	585979	Undefended area next to river and hydrological zone
4	Central Morpeth	419818	585764	Undefended area next to river
5	Low Stanner	420123	586085	Located in a small lane
6	Middle Greens	420222	585820	Extensive surface water flooding and leakage through flood defences

Table 5.4 The details of the critical points in Morpeth town centre.

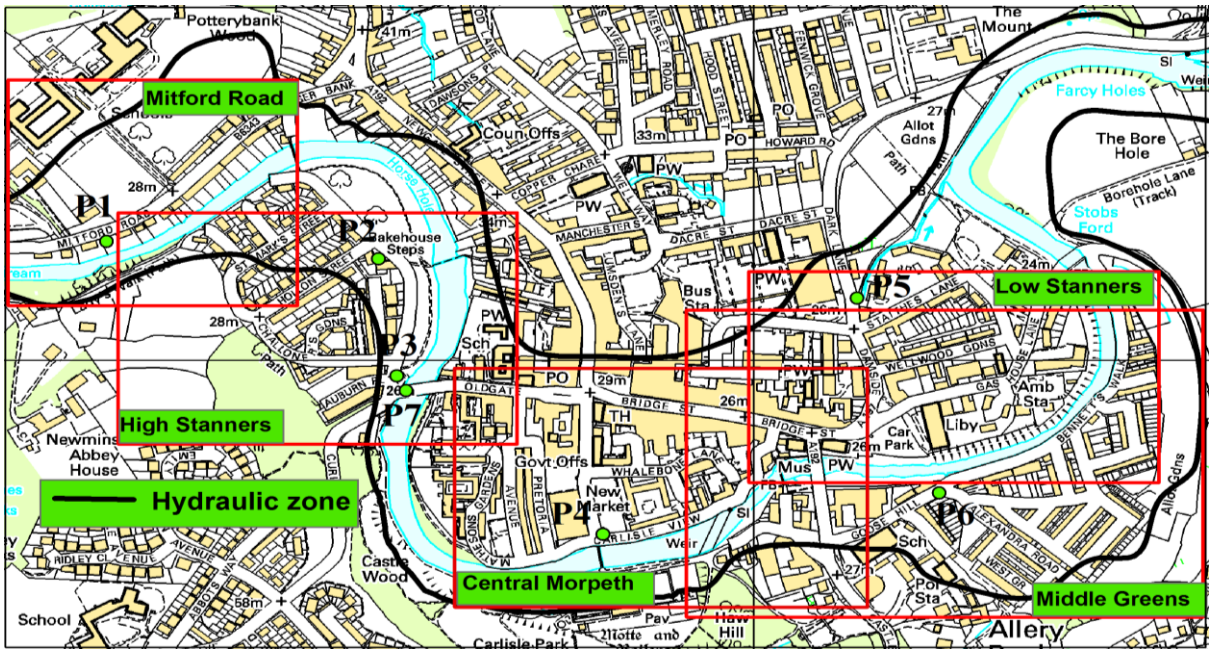

Figure 5.13 The location map of the critical points in Morpeth.

An initial steady state in the river channel is achieved with a 10 m^3/s constant inflow after approximately a 10-hour simulation. The convergence criterion for the steady state

has been described in sub-section 5.2.3. Since the return period of the September 2008 flood event is evaluated as 137 years, the catchment division scheme from the 1 in 200 year design flood event is considered suitable for the simulations. Buildings are represented by raising the bottom to a single elevation of 10 meters. An initial Manning coefficient of 0.02 $m^{-1/3}$ s and a Courant number of 0.8 are used. Infiltration is not considered at this stage. For all simulations, g = 9.81 m/s^2.

Before simulations, the full 2D shallow flow model is employed to record the 'unit hydrographs' at the hydraulic and hydrological zone border under a uniform net rainfall of 10 mm for 15 minutes in the hydrological zone of the town centre domain.

Figure 5.14 sketches an example of a 'unit hydrograph' at one bordering cell. The 'unit hydrograph' is then scaled and superimposed, according to the real net rainfall to generate an accumulative hydrograph at the zone border, shown in Figure 5.15. The observed rainfall in the catchment does not catch the rainfall intensity for the 'unit hydrograph', so the peak in the accumulative hydrograph is lower. There are a group of accumulative hydrographs at the zone border forming the lateral inflow from the hydrological zone to the hydraulic zone.

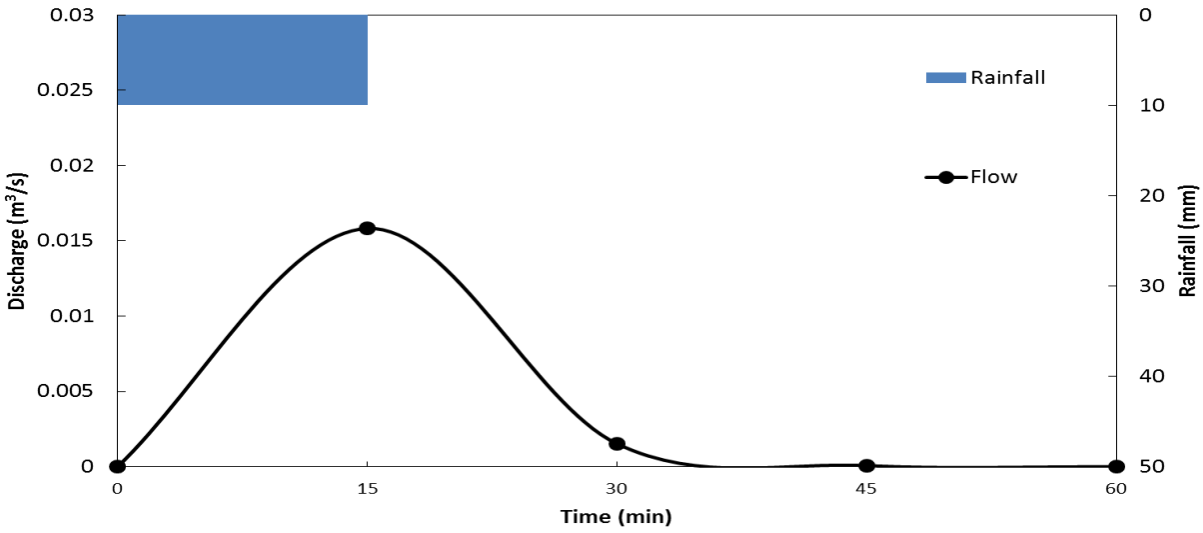

Figure 5.14 An example of the 'unit hydrograph' at the zone border in the town centre domain.

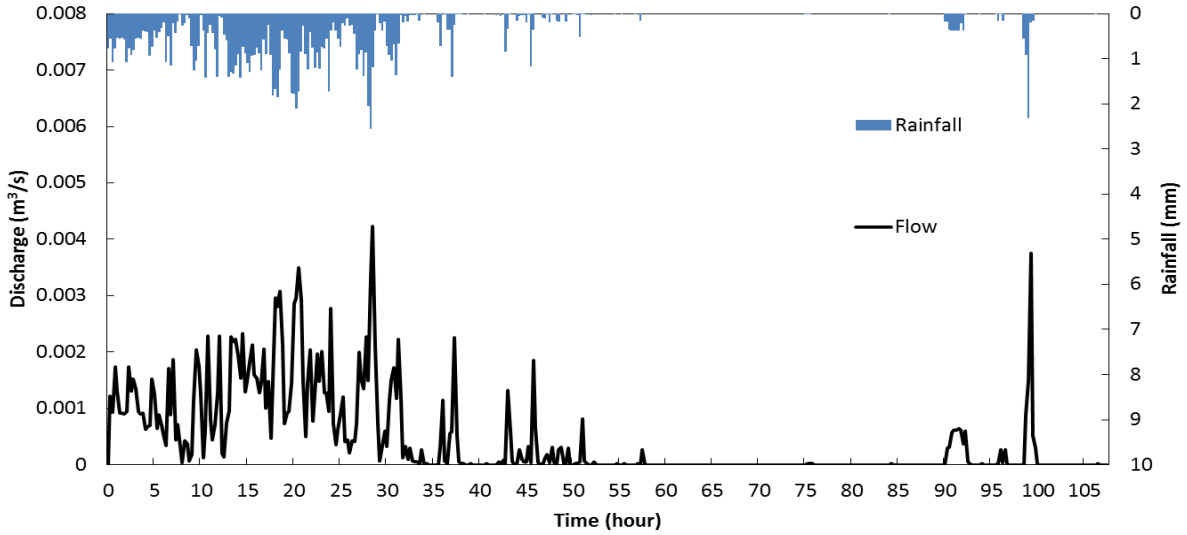

Figure 5.15 An example of the accumulative hydrograph at the zone border in the town centre domain.

Simulations for 50 hours starting at 4pm on the 5th September are implemented by the coupled model and the full 2D shallow flow model based on a standard desktop PC with an Intel(R) Core(TM) i5 CPU.

The inundation maps at 11am, 1pm, 3pm and 5pm on 6th September from the coupled model are compared with the ones from the post-event investigation and also the full 2D shallow flow model. These maps are illustrated in Figure 5.16-Figure 5.19.

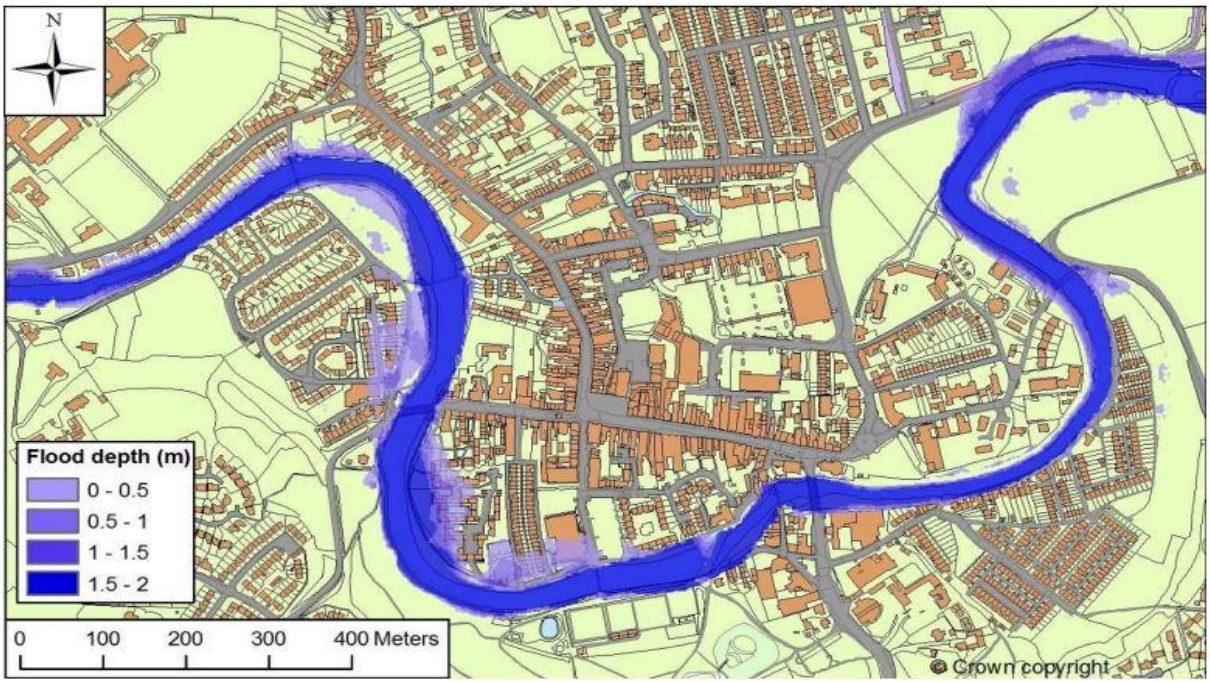

(a)

(b)

(c)

Figure 5.16 Inundation maps at 11 am in the town centre domain: (a) post-event investigation (Parkin, 2010), (b) full 2D model, (c) coupled model.

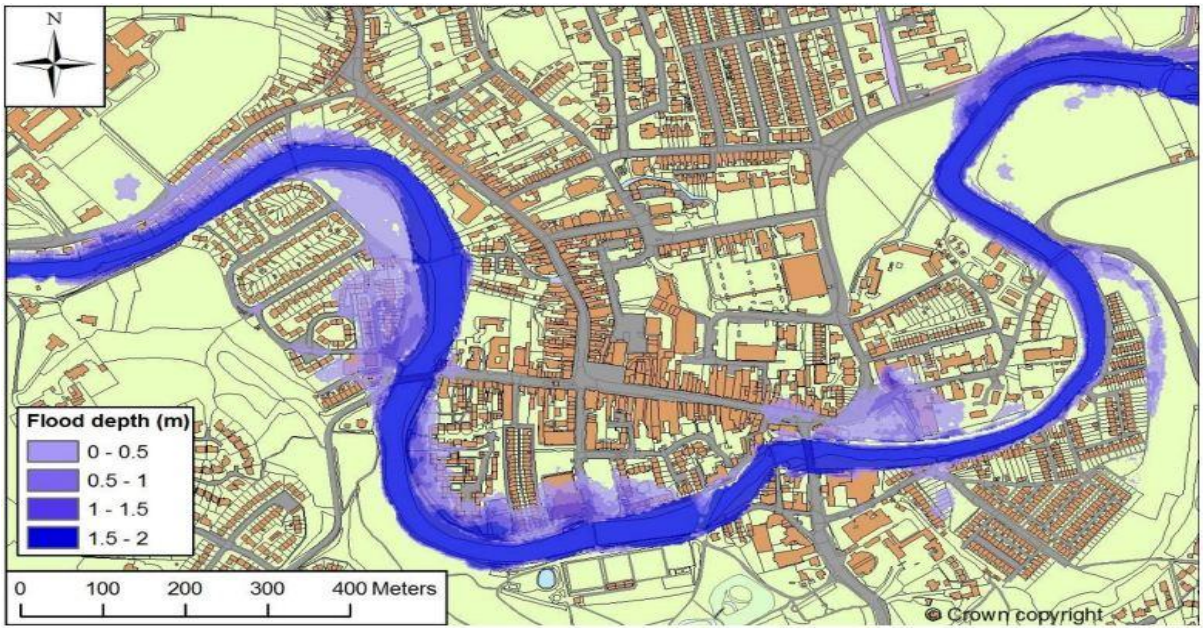
N
Flood depth (m)
0 - 0.5
0.5 - 1
1 - 1.5
1.5 - 2
0
100
200
300
400 Meters
© Crown copyright

(a)


Water depth (m)
0 - 0.1
0.1 - 0.5
0.5 - 1
1 - 1.5
1.5 - 2
Above 2
Hydraulic zone

(b)

(c)

Figure 5.17 Inundation maps at 1pm in the town centre domain: (a) post-event investigation (Parkin, 2010), (b) full 2D model, (c) coupled model.

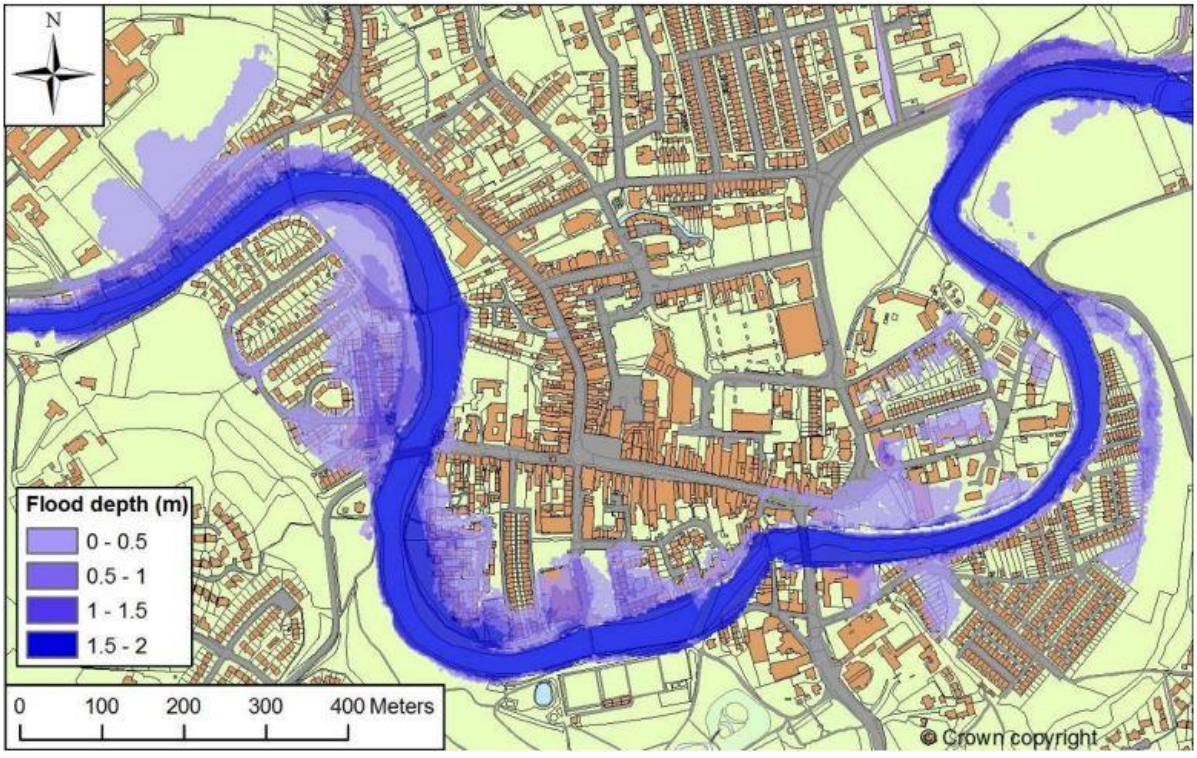

(a)

(b)

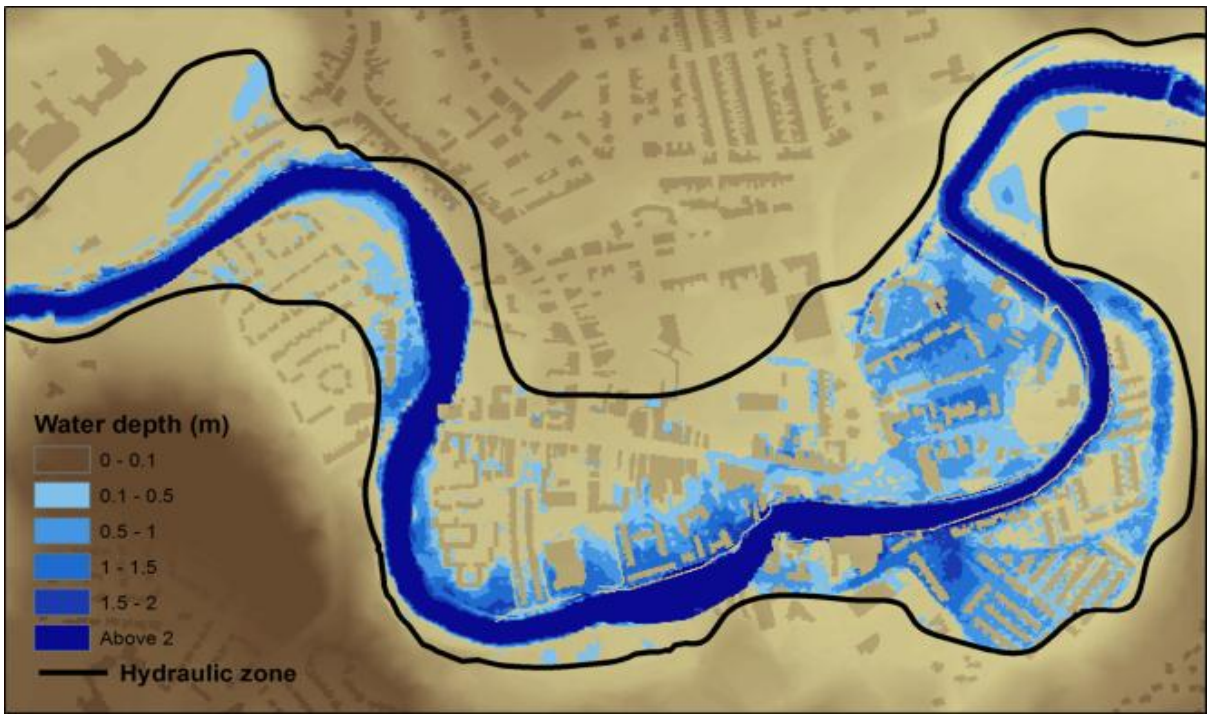

(c)

Figure 5.18 Inundation maps at 3pm in the town centre domain: (a) post-event investigation (Parkin, 2010), (b) full 2D model, (c) coupled model.

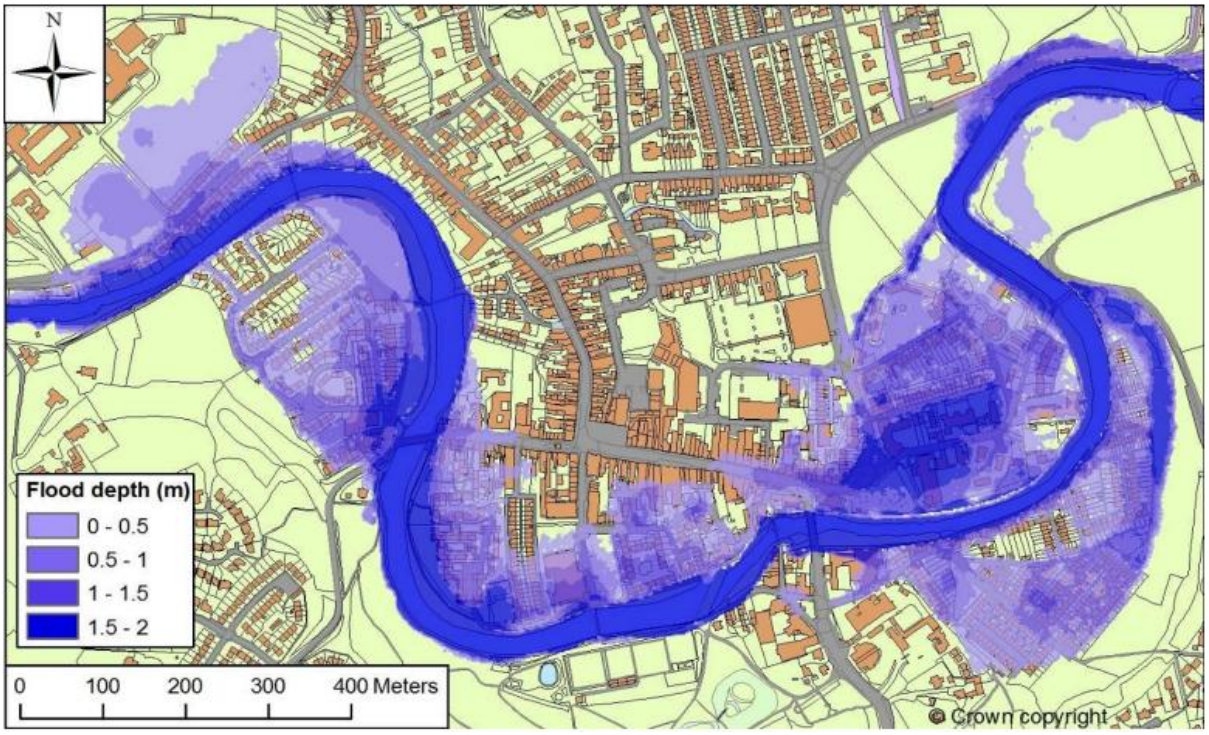
N
Flood depth (m)
0 - 0.5
0.5 - 1
1 - 1.5
1.5 - 2
0
100
200
300
400 Meters
© Crown copyright

(a)

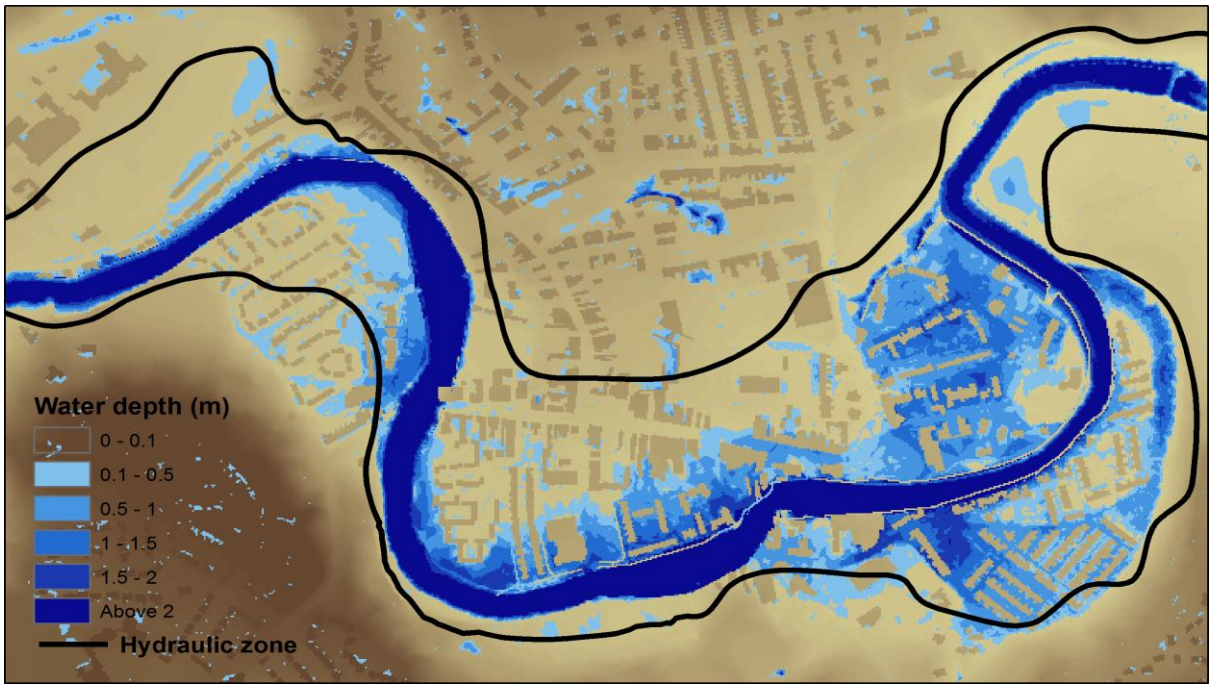
Water depth (m)
0 - 0.1
0.1 - 0.5
0.5 - 1
1 - 1.5
1.5 - 2
Above 2
Hydraulic zone

(b)

(c)

Figure 5.19 Inundation maps at 5pm in the town centre domain: (a) post-event investigation (Parkin, 2010), (b) full 2D model, (c) coupled model.

The full 2D shallow flow model has produced quite similar inundation extents with the coupled model within the hydraulic zone at 11am and 1pm. However, at 3pm the inundation extent from the coupled model is larger at the left bank in Central Morpeth and at the right bank in High Stanners. At 5pm, this difference becomes marginal again. This may be explained by the coupling method used in the coupled model. Using a 'unit hydrograph' in the coupled model may route the flow from the hydrological zone to the hydraulic zone faster than using shallow water equations within the full 2D shallow flow model, and therefore the flow from the hydrological zone predicted by the coupled model may join the fluvial flood in the hydraulic zone earlier, at around 3pm resulting in a larger inundation extent. However, this effect is less pronounced when the rainfall is reducing, and at 5pm the two inundation extents become similar again, after the intense rainfall terminates.

When compared with the post-event investigation inundation maps, the two simulated inundation extents, from both the coupled model and the full 2D shallow flow model are larger at 11am and 1pm. A closer match has been produced for flood extents at 3pm. At 5pm the simulated inundation extents from both models achieve the closest overall match with the post investigation survey. Generally, larger events have been predicted

than those recorded. This may be because both models do not account for the effects of infiltration or the drainage system. Both of these factors are significant in early hours of the inundation when the soil is not fully saturated and the drainage system is under capacity. Infiltration will be considered in sub-section 5.4.4., while the effects of the drainage system will be investigated in future work. Another cause of this discrepancy might be limitations in the measured data, as mentioned in sub-section 4.3.7. The EA debris data can not represent the full flood propagation process, and this means that the maximum inundation extent (at 5pm) is likely to be much more reliable than the records at other times.

Water depths at the seven critical points are recorded by both models, and sketched in Figure 5.20. For all the critical points, the water depths generally rise until reaching a peak, and then fall. After this, the water depths increase again to a second but smaller peak before a final decrease. The 'twin peak' shape of the water depths at critical points may be as a result of the similar shape of the inflow hydrograph, shown in Figure 4.12. The water depths from the coupled model match reasonably well with the ones from the full 2D shallow flow model at P1, P4, P6 and P7.

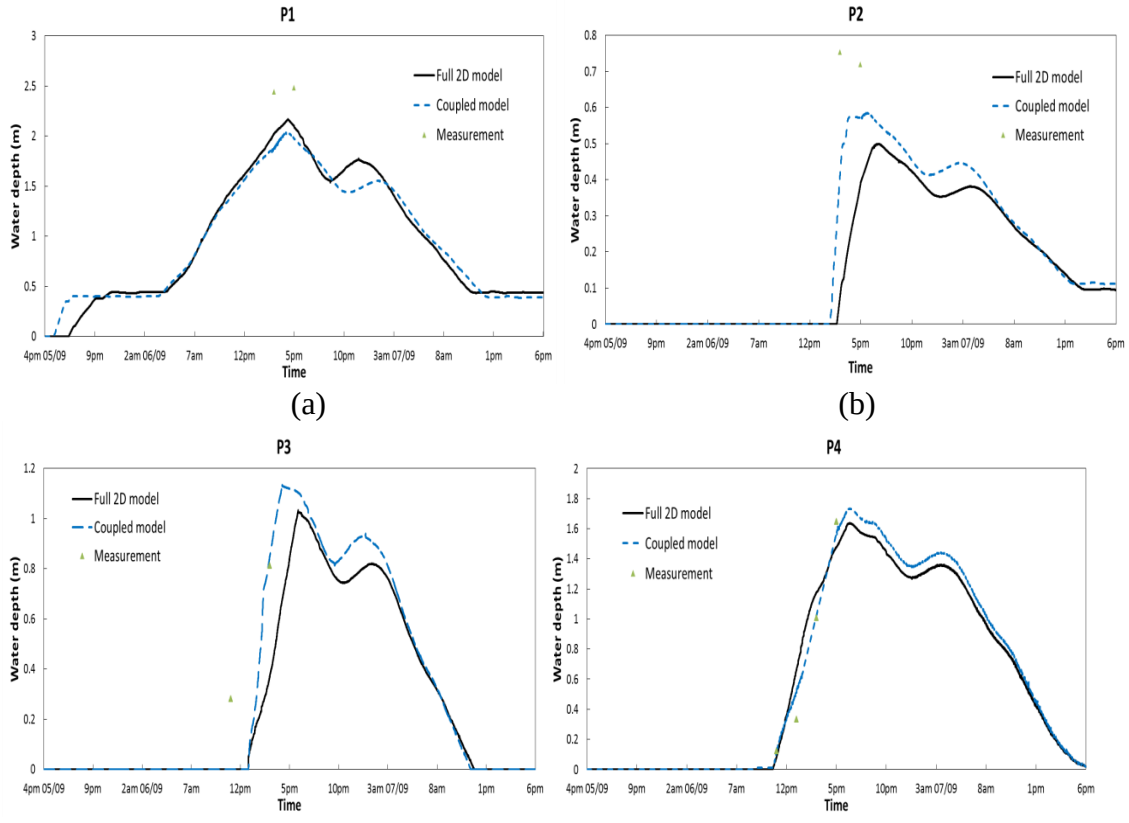

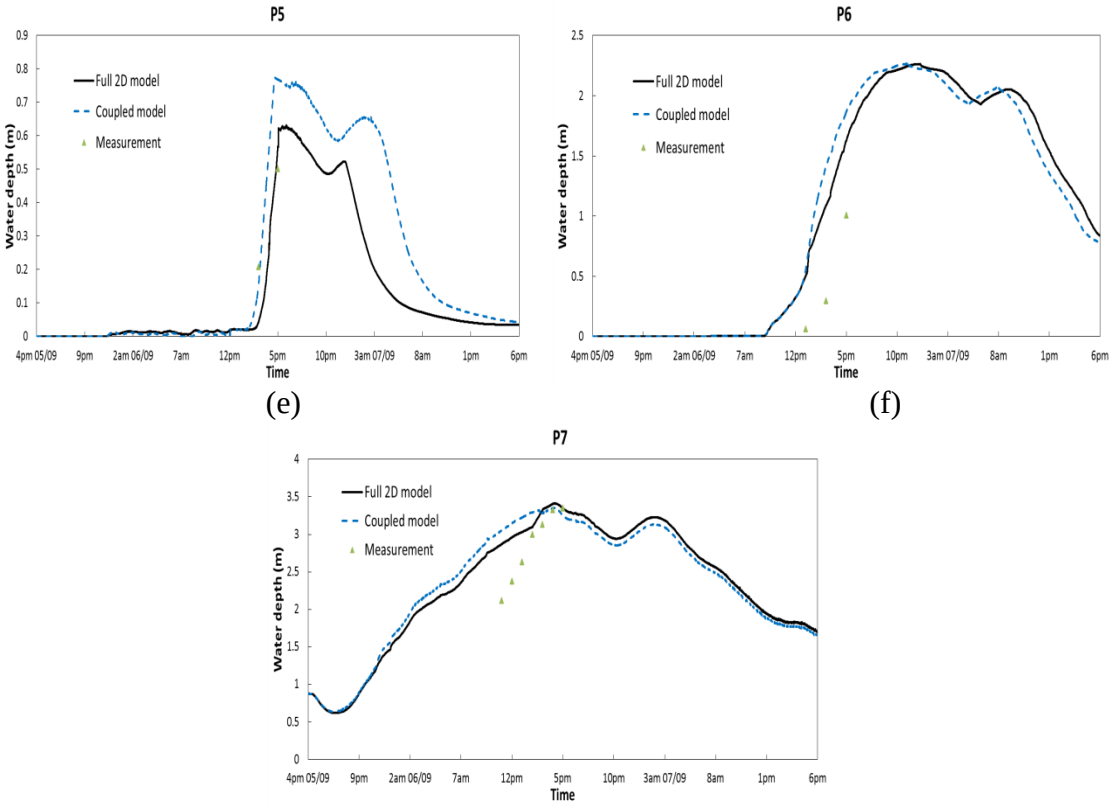

Figure 5.20 The time histories of water depth at the critical points in the town centre domain.

However, obvious deviations can be spotted in P2, P3 and P5, where the coupled model generally produces larger depths than the ones from the full 2D shallow flow model. As can be seen in Figure 5.13, P2, P3 and P5 are located relatively nearer to the zone border than the other critical points, and are therefore more influenced by lateral inflow from the hydrological zone. The faster routing method of 'unit hydrograph' may explain the larger depth as well as the shorter arrival time that are predicted by the coupled model. From Figure 5.21, the maximum water depths from the coupled model at P2, P3, P4, P5 are slightly larger than the ones from the full 2D shallow flow model. From Figure 5.22, the flood predicted by the coupled model arrives at P1, P2, P5 earlier.

When compared with the measured water depths in the post-event investigation, obvious discrepancy can be found. Results from both models are deeper than the measured data at P6 and P7, and shallower at P1 and P2. The full 2D shallow flow model performs better at P3 and P5, while the coupled model behaves better at P4. Negating elements of the draining process along with limitations of the measured data may be the reason for these differences.

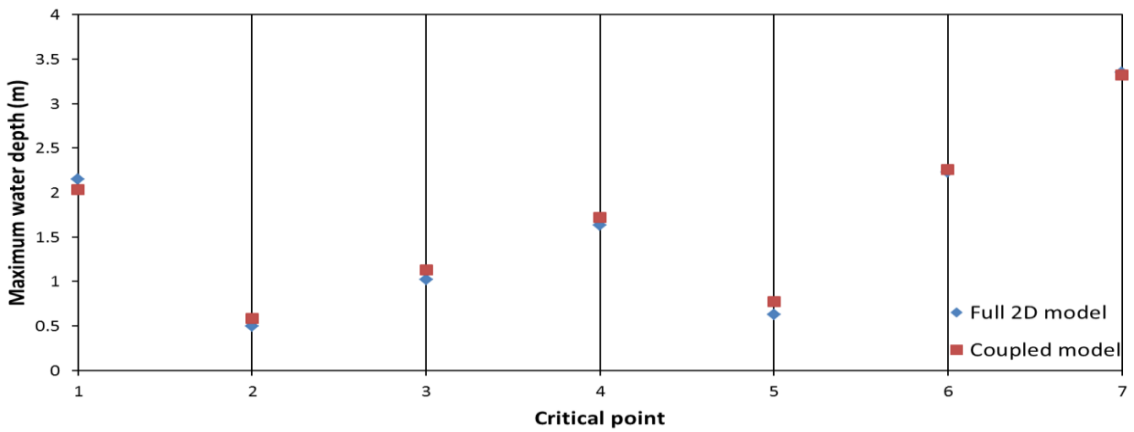

Figure 5.21 Maximum water depths at the critical points in the town centre domain.

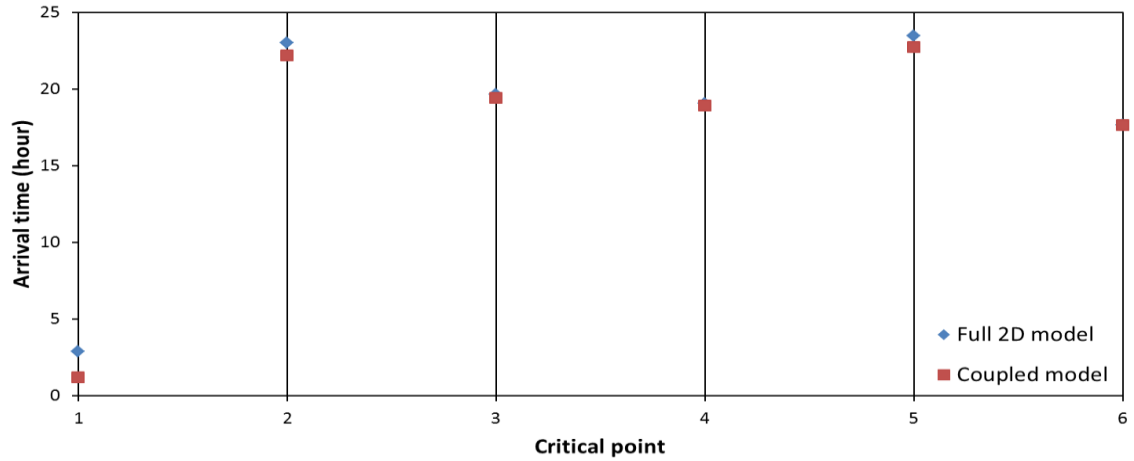

Figure 5.22 Arrival times for the critical points in the town centre domain.

Velocity field maps from both models at 5pm 6th September have been displayed in Figure 5.23, but no comparison was made due to the unavailability of field measurements. The results from the two models seem to be similar in the hydraulic zone. Two areas, 'A' and 'B' are selected to investigate the local velocities. The zoomed-in views of areas 'A' and 'B' are illustrated in Figure 5.24. Area 'A' is located in the meandering segment of the channel, and area 'B' is situated in the floodplain. As can be seen, in area 'A' the velocity produced by the coupled model matches quite well with those produced by the full 2D shallow flow model, in both magnitude and direction, because the flow regime in the river channel is primarily affected by the upstream inflow rather than by the lateral inflow from the hydrological zone. The velocity agreement in area 'B' is less satisfactory, as a discrepancy in flow direction can be found. With regard to magnitude, the velocity from the full 2D model is larger in the west part of the area, while the velocity from the coupled model is larger in the east part of the area after the 'L' turn.

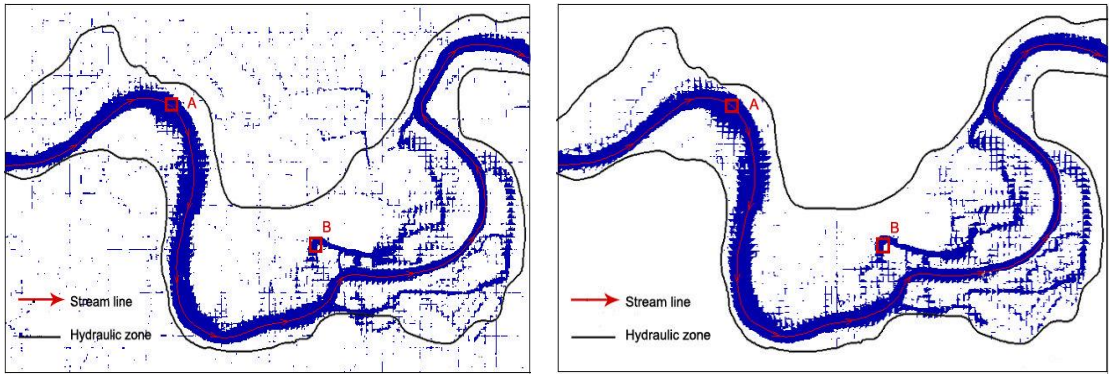

(a) (b)

Figure 5.23 Velocity field maps at 5pm in the town centre domain: (a) full 2D model, (b) coupled model.

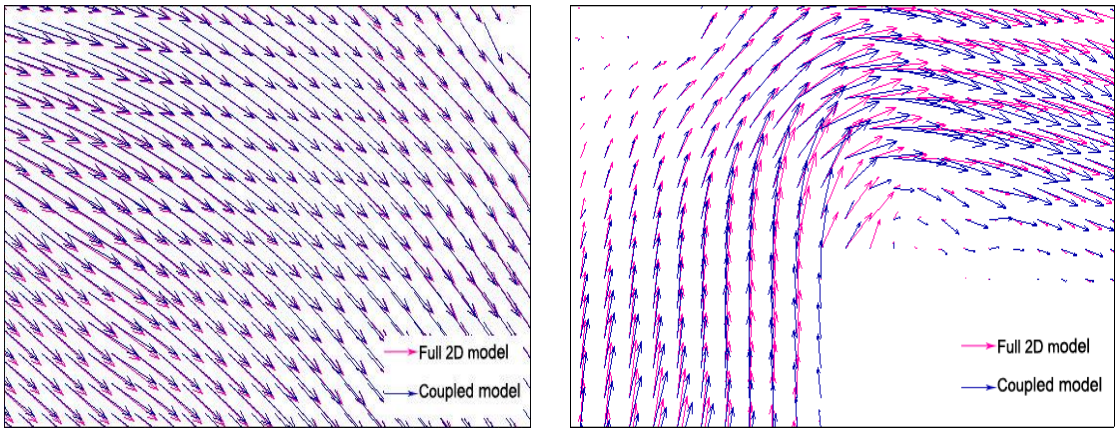

(a) (b)

Figure 5.24 The zoomed-in view of velocity field maps at 5pm in the town centre domain: (a) area 'A', (b) area 'B'.

Three typical critical points are selected to display the time history of velocities in Figure 5.25. The coupled model's results follow the same pattern with those of the full 2D shallow flow model, but the magnitude is relatively smaller. That may be because in the coupled model the direction of the lateral inflow at the zone border is neglected, and the inflow is treated just as a source point. However, the velocity simulated by the coupled model is not always smaller, as the flow in the hydrological zone is more quickly routed to the hydraulic zone by the 'unit hydrograph'. This has been confirmed by Figure 5.24(b). Evident deviations can be seen at the critical points located closer to the zone border, e.g. P3, and a good alignment can be achieved at those located far from the zone border, e.g. P4 or in the river channel, e.g. P7.

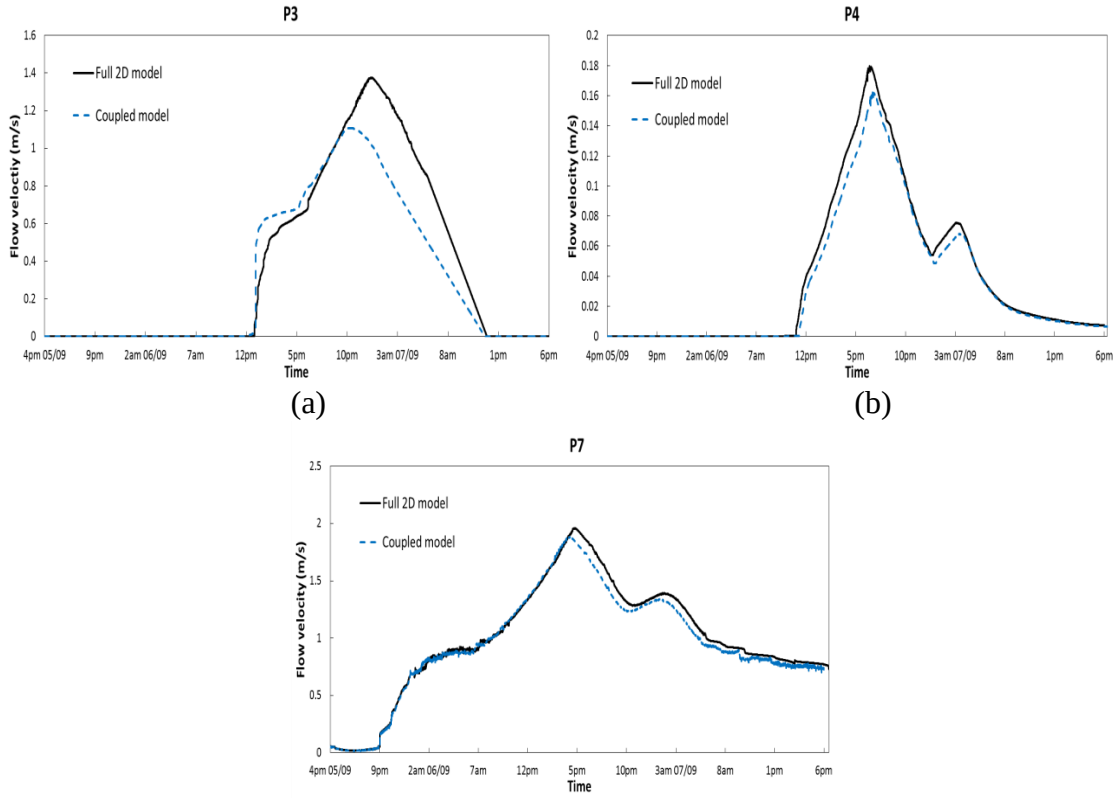

Figure 5.25 The time histories of flow velocity at the critical points in the town centre domain.

In order to globally evaluate the model performance in the town centre domain, statistics such as *RMSE*, F^1 and F^2 are calculated with the assumption that a water depth less than 0.1 m can be regarded as dry, and the absolute value of flow velocity smaller than 0.1 m/s can be treated as zero in order to prevent unreasonably large relative *RMSE*s. Table 5.5 shows the results from both models with the post-event investigation data as a reference. At 5pm when the measured data are considered most reliable, it can be seen that the relative *RMSE*s for water depth are below 25%. F^1 and F^2 are above 80% and 75%, respectively. However, at other times, the statistics are less satisfactory; the largest relative *RMSE* for water depth is over 40%, and the smallest F^1 and F^2 are below 76% and 50%, respectively. Apart from the aforementioned limitations in the measured data and the omission of the infiltration and drainage systems, the domain size might be another cause of this. The overland inflows from outside the town centre domain are not considered in both models, which will be avoided in Section 5.5 when taking the extracted sub-catchments as the computational domain.

Time	Model	Relative *RMSE*(h) (%)	F^1 (%)	F^2 (%)
11am	Full 2D model	39.2	87.7	51.7
	Coupled model	40.4	86.1	48.2
1pm	Full 2D model	34.0	83.8	61.3
	Coupled model	35.9	83.3	56.6
3pm	Full 2D model	28.8	76.5	66.9
	Coupled model	30.2	75.5	62.6
5pm	Full 2D model	22.8	85.1	78.4
	Coupled model	24.3	83.2	76.1

Table 5.5 Statistics of modelling results in the town centre domain (benchmark: post-event investigation data).

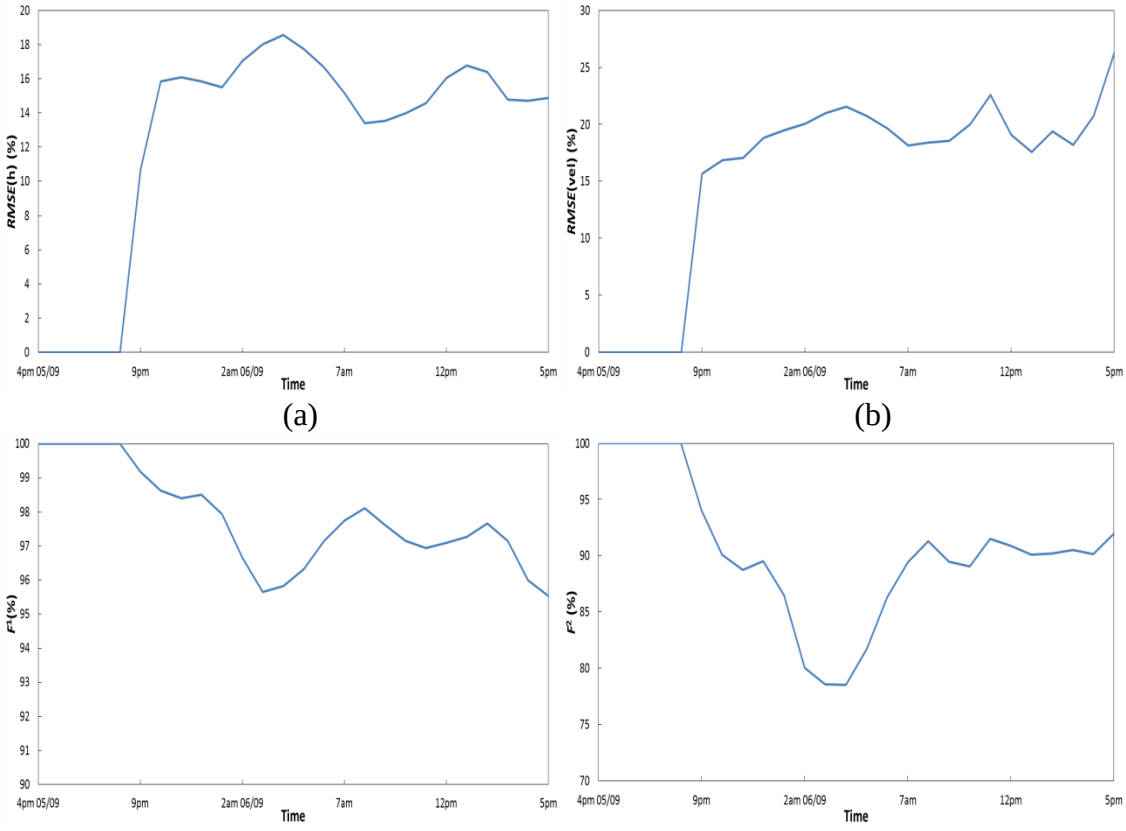

Figure 5.26 Statistics of the coupled model's results in the town centre domain: (a) Relative *RMSE* for water depth, (b) Relative *RMSE* for flow velocity, (c) F^1, (d) F^2 (benchmark: full 2D shallow flow model's results).

From Table 5.5, the coupled model performs less satisfactorily than the full 2D shallow flow model. The differences are sketched in Figure 5.26. The full 2D shallow flow model's results are taken as a reference. The *RMSE*s for water depth and flow velocity start to rise sharply before 9pm on 5th September to a certain value, and vary gradually, up and down, with maximum values of around 18% and 25%, respectively. F^1 and F^2 begin to fall before 9pm on 5th September followed by a rise, and then gradually

fluctuate with minimum values of around 95% and 80%, respectively. These errors, reflected by the statistics, are considered reasonable and acceptable.

In terms of computational time, the coupled model runs about twice as fast as the full 2D shallow flow model, shown in Table 5.7. This is reasonable as the number of computational cells used for the full 2D shallow flow model is about 2.3 times as many as the coupled model uses, shown in Table 5.6. Total cells include all cells inside and outside the computational domain. Domain cells include only cells inside the domain, and these are the computational cells for the full 2D shallow flow model. Hydraulic cells are the cells inside the hydraulic zone, and these are the computational cells for the coupled model. Hydrological cells are the cells inside the hydrological zone, which are usually treated as a lumped area.

Cell type	Cell number
Total cells	326,250
Domain cells	326,250
Hydraulic cells	144,124
Hydrological cells	182,126

Table 5.6 The number of cells in the town centre domain.

Simulation Time (hours)	CPU Time (hours)		Improved efficiency
	Full 2D model	Coupled model	
25	405.2	182.5	2.2x
50	744.6	368.6	2.0x

Table 5.7 Computational costs in the town centre domain.

The coupled model is hence preferable due to its high computational efficiency whilst maintaining the satisfactory accuracy.

In order to further save computational time, OpenMP is employed to implement parallel computations based on a dual-core CPU. With the same level of computational accuracy, parallel computations can achieve approximately 1.5 times acceleration compared to serial computations, as shown in Table 5.8. For this reason, OpenMP is used for all of the remaining simulations in this chapter.

Computing type	Model	CPU Time (hours)		Average improved efficiency by OpenMP
		25-hour simulation	50-hour simulation	
Serial computation	Full 2D model	405.2	744.6	-----
	Coupled model	182.5	368.6	-----
Parallel computation	Full 2D model	246.4	567.2	1.5x
	Coupled model	116.8	283.6	1.4x

Table 5.8 Computational cost comparison between serial and parallel computations in the town centre domain.

5.4 Evaluation of the Coupled Model in Morpeth Town Centre

In this section, the coupled model is evaluated in order to investigate the effects of temporal and spatial resolutions, Manning coefficient, rainfall, infiltration, buildings and coupling methods. For all statistical calculations, e.g. *RMSE*, F^1, F^2, the post-event measurement data at 5pm 6th September are utilised as the reference.

5.4.1 *Resolution*

The effect of the temporal and spatial resolution on the coupled model is researched in this sub-section. Three Courant numbers are selected, 0.2, 0.4, 0.8, to investigate the impact of temporal resolution, while three cell sizes are employed; 2 m × 2 m, 4 m × 4 m, 10 m × 10 m, to explore the influence of spatial resolution.

The inundation extents at 5pm on 6th September with different temporal resolutions match fairly well with each other. However, the ones with different spatial resolutions show some discrepancies, as shown in Figure 5.27. The inundation extent is larger with the increasing cell size, probably because the low spatial resolution may not be able to properly represent the urban topography, leading to more diffusive numerical results.

The relative *RMSE* for water depth listed in Table 5.9 indicates the model's performance under different resolutions. The temporal resolution has a marginal and consistent effect on water depth, while the spatial resolution influences the water depth dramatically. The order of accuracy for water depths with varied cell sizes is close to 1. This is the same as the order of the coupled model. The water depth error is plotted

against the cell size in a logarithmic coordinate axis (shown in Figure 5.28) to demonstrate the grid convergence.

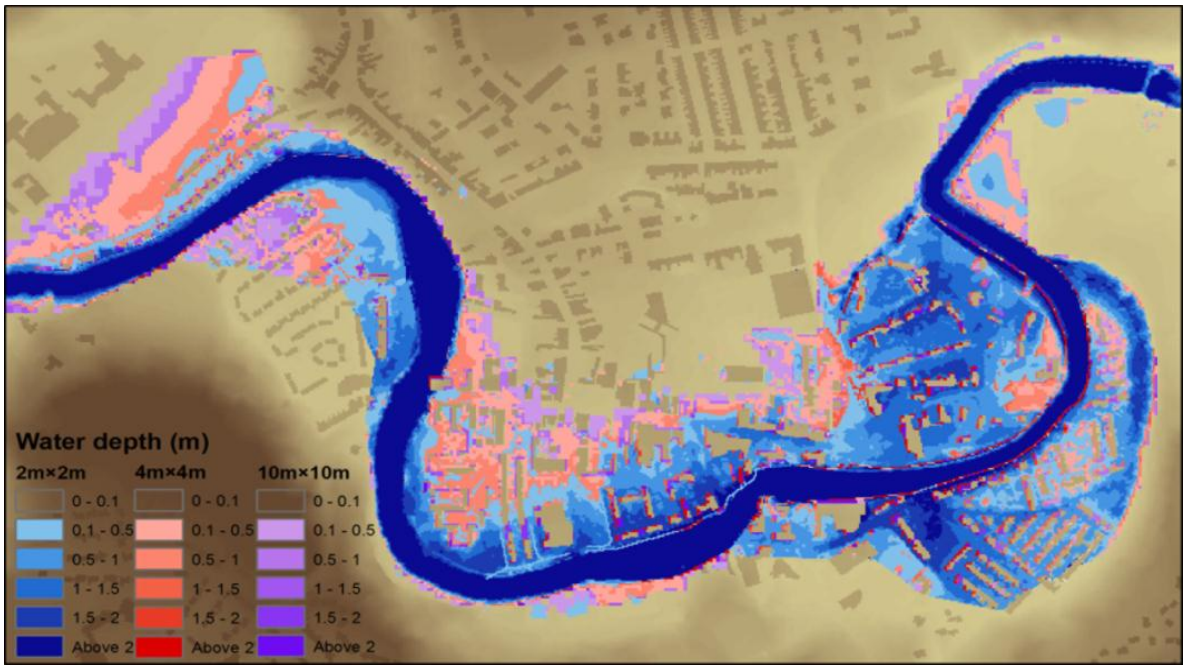

Figure 5.27 Inundation maps at 5pm with three different spatial resolutions in the town centre domain.

Courant number	Relative *RMSE*(h)	Cell size (m^2)	Relative *RMSE*(h)	Order
0.2	24.1%	2 × 2	24.3%	-----
0.4	24.2%	4 × 4	42.6%	0.81
0.8	24.3%	10 × 10	87.1%	0.78

Table 5.9 Statistics of the coupled model's results with different temporal and spatial resolutions in the town centre domain.

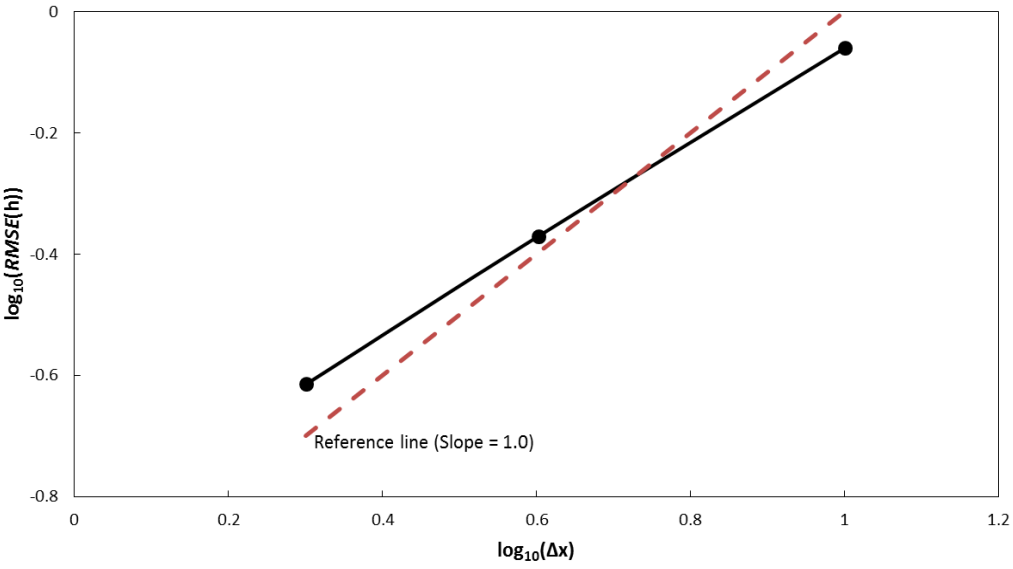

Figure 5.28 Grid convergence of the coupled model in the town centre domain.

In terms of computational efficiency, less time is required with a larger Courant number or larger cell size, because longer time steps can be achieved through Equation 3.11 and 3.12, and also fewer computational cells are used to discretise the domain when the cell size is larger, shown in Table 5.10 and Table 5.11. In order to balance accuracy and efficiency, a Courant number of 0.8 and the cell size of 2 m × 2 m are regarded to be the most favourable choices.

Courant number	Total cell number	Domain cell number	Hydraulic cell number	Hydrological cell number	CPU time (hours)	
					25-hour simulation	50-hour simulation
0.2	326,250	326,250	144,124	182,126	402.9	1029.2
0.4	326,250	326,250	144,124	182,126	219.2	552.5
0.8	326,250	326,250	144,124	182,126	116.8	283.6

Table 5.10 Computational costs for the coupled model with different temporal resolutions in the town centre domain.

Cell size (m^2)	Total cell number	Domain cell number	Hydraulic cell number	Hydrological cell number	CPU time (hours)	
					25-hour simulation	50-hour simulation
2 × 2	326,250	326,250	144,124	182,126	116.8	283.6
4 × 4	81,675	81,675	34,342	47,333	13.7	34.6
10 × 10	13,050	13,050	5,504	7,546	1.1	2.8

Table 5.11 Computational costs for the coupled model with different spatial resolutions in the town centre domain.

5.4.2 *Manning coefficient*

A uniform Manning coefficient of 0.02 $m^{-1/3}s$ has been initially selected for the whole town centre domain, but this selection is not sensible as the friction effect may vary depending on land cover. Ideally, a spatially distributed Manning coefficient would reflect the frictional variation throughout the domain. However, when implementing a sensitivity analysis, the Manning coefficient for each land cover type needs to be perturbed resulting in a huge number of combinations (Wilson and Atkinson, 2003). For simplicity, only two classes of land cover are employed for the sensitivity analysis in this work, i.e. channel and floodplain. For each land cover a range of Manning coefficients, from 0.02 $m^{-1/3}s$ to 0.08 $m^{-1/3}s$ with an increment of 0.02 $m^{-1/3}s$, are applied to explore how the coupled model's results are affected by friction.

As can be seen in Figure 5.29, the results are more sensitive to the Manning coefficient in the channel than in the floodplain. This is primarily because the flood wave development and propagation are influenced by the underlying elevation data more than the friction, as uneven topography creates or blocks flood pathways (Wilson and Atkinson, 2003; Ozdemir *et al.*, 2013). Compared with the floodplain, the river bed variation is relatively gentle, and thus the effect of friction is more pronounced. More satisfactory results are achieved with decreasing Manning coefficient in the river channel, as larger river conveyance can be realised which may compensate for the limitation of representing the meandering river channel with square cells. Additionally, compared to water depth, flood extent is less sensitive to friction as is concluded in the work of Ozdemir *et al.* (2013).

The Manning coefficients 0.02 $m^{-1/3}s$ for the river channel and 0.06 $m^{-1/3}s$ for the floodplain are recommended for the town centre domain in order to optimise simulations.

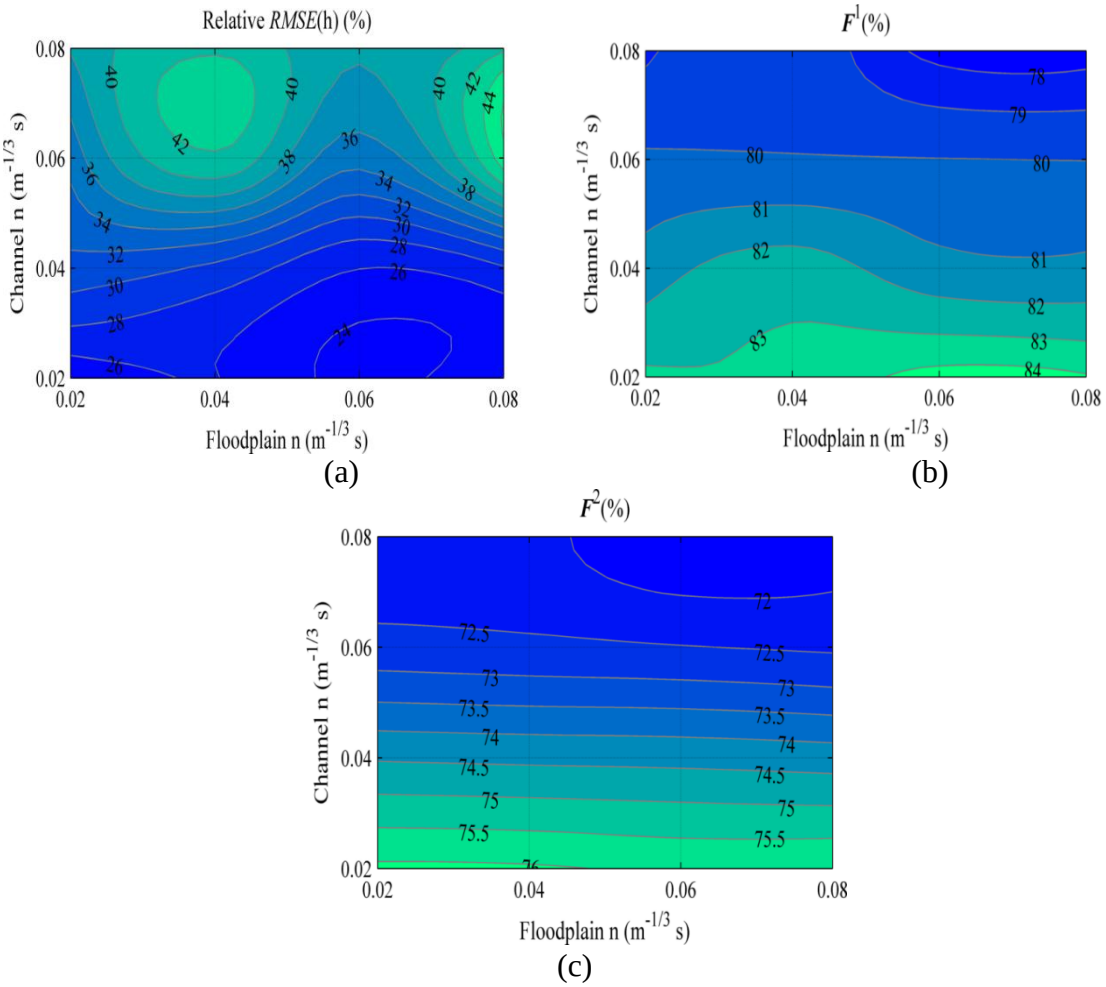

Figure 5.29 Statistics of the coupled model's results with different Manning coefficients in the town centre domain.

5.4.3 *Rainfall*

Uniform rainfall has been applied throughout the town centre domain for this work, as the flood event resulted from a prolonged frontal rainfall system over a large area (Met Office, 2008b), which reduced its spatial variations. Simulations are run with and without rainfall so as to investigate the effect of the rainfall on the modelling results.

As Figure 5.30 demonstrates, the inundation extent at 5pm is more extensive with the inclusion of rainfall. This is as expected as a larger volume of water is retained within the domain, shown in Figure 5.31. The average difference of 6.2% suggests that the pluvial flood has limited impact in comparison with the dominant fluvial flood. However, the consideration of rainfall can identify the localized risk from pluvial flooding. It is not that obvious in Figure 5.30 as inundation from the river may cover some localized pluvial flooding. An inundation extent map in the earlier time at 11am has been shown as Figure 5.32, where the purple colour may indicate the areas vulnerable to the pluvial flooding risk, e.g. Mitford Road, and the right bank of the river in Middle Green.

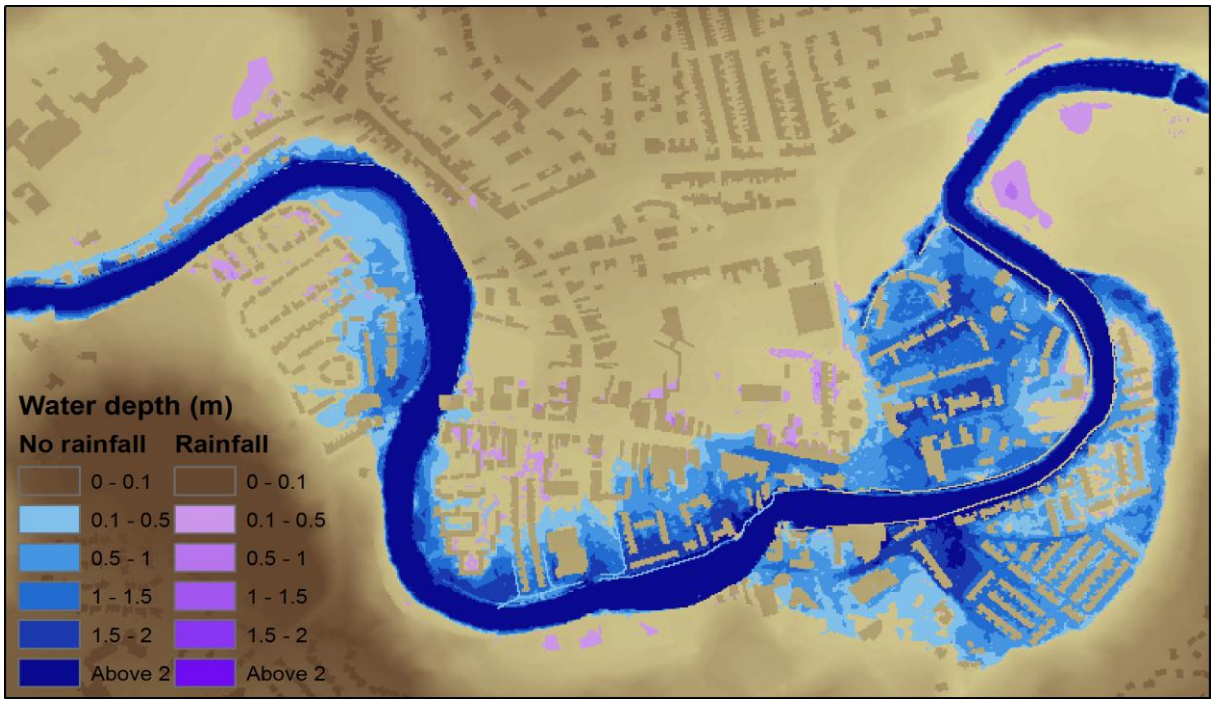

Figure 5.30 Inundation maps at 5pm with and without rainfall in the town centre domain.

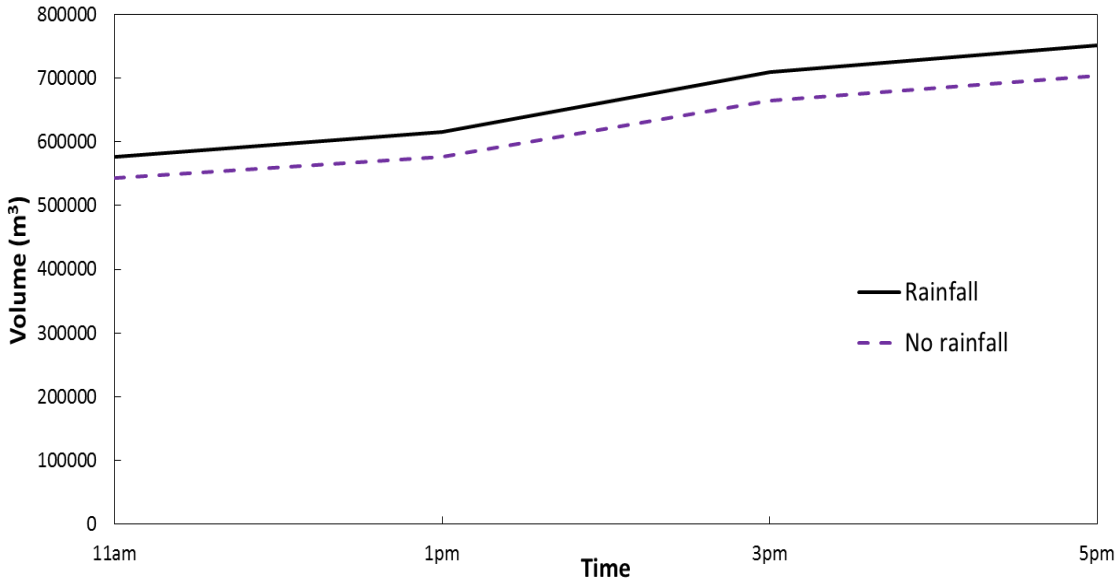

Figure 5.31 The water volume in the hydraulic zone with and without rainfall in the town centre domain.

Figure 5.32 Inundation maps at 11am with and without rainfall in the town centre domain.

5.4.4 *Infiltration*

Infiltration in the permeable surfaces may contribute to alleviate flooding as less runoff can be produced with water infiltrating into the subsurface. The Green-Ampt equation (Equation 3.37) is used in this work to calculate infiltration. There are four parameters in the equation, i.e. *Ks*, ψ_f, θ_s and θ_a. Initially, the domain is almost saturated due to the antecedent rainfall in July and August so θ_a is approximated as θ_s. In this case, the

only parameter that affects infiltration is *Ks*. As mentioned in sub-section 4.3.6, the domain consists of two soil types: clay loam and sandy clay loam. These correspond to two different saturated hydraulic conductivities, Ks_1 and Ks_2. The general values of *Ks* for the two soil types are listed in Table 4.5. A sensitivity analysis is conducted with *Ks* for each soil type ranging from 0.05 cm/h to 0.2 cm/h with an increment of 0.05 cm/h. This generates sixteen combinations for evaluating model results.

Figure 5.33 shows the coupled model's results are quite insensitive to Ks_2 because the sandy clay loam covers only the northeast corner of the domain, and the rest is covered by clay loam, as shown in Figure 4.22. With an increase in Ks_1, the F^1 and F^2 statistics also increase which indicates a better match between the coupled model's results and the post-event measurement data in terms of wet-dry states. The relative *RMSE* for water depth reduces first and thereafter increases with the smallest relative error of 23.5% when Ks_1 is around 0.1cm/h. Although the results are affected by the different Ks_1, they are not considered too sensitive. The changes are only 2.5%, 1.2% and 1.2% for the relative *RMSE*, F^1, and F^2 when Ks_1 varies from 0.05 cm/h to 0.2 cm/h. This is mainly due to the initially almost saturated soil.

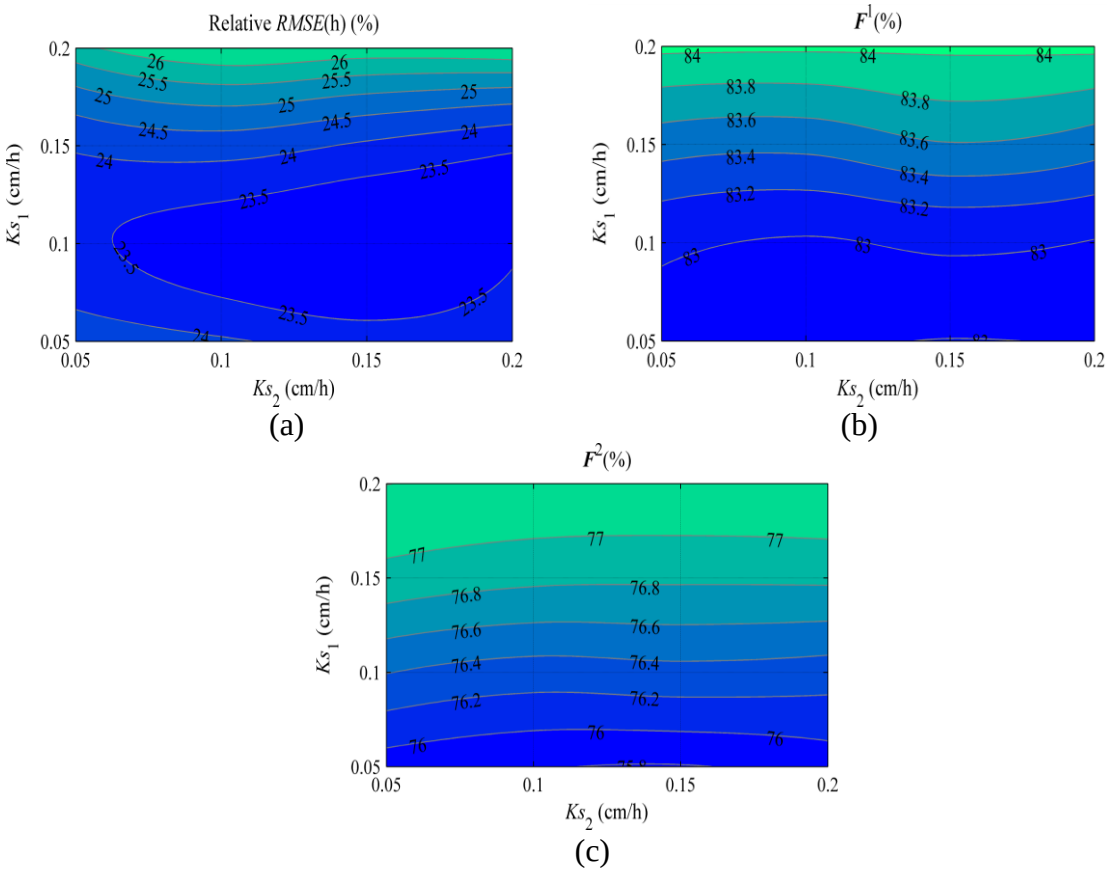

Figure 5.33 Statistics of the coupled model's results with different saturated hydraulic conductivity in the town centre domain.

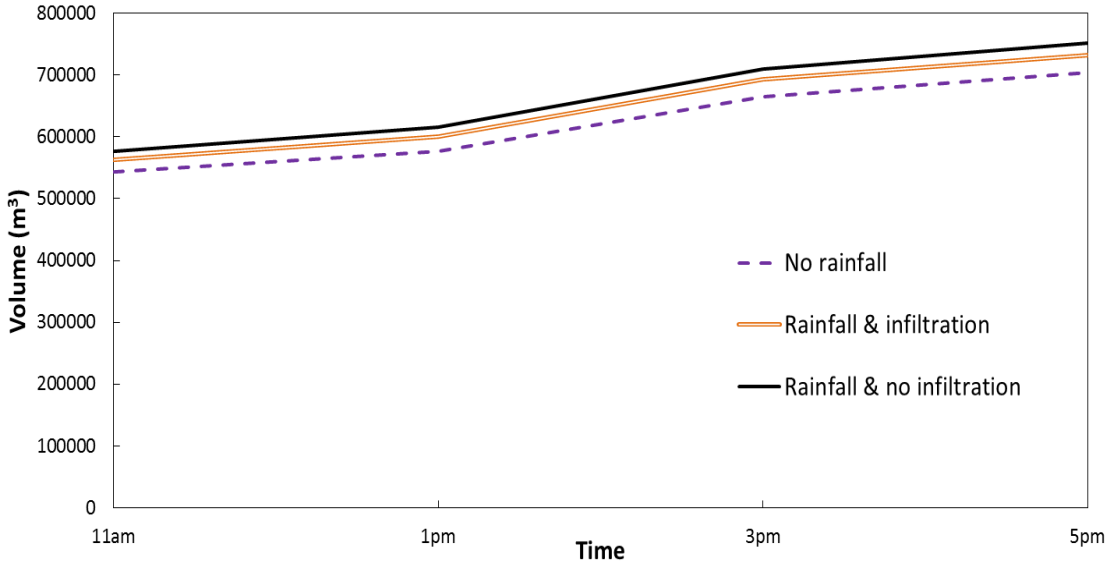

Figure 5.34 The water volume in the hydraulic zone with and without infiltration in the town centre domain.

The water volume in the hydraulic zone with and without infiltration is sketched in Figure 5.34. The average difference is merely 2.5%.

No evident differences can be found in the inundation map at 5pm with and without the consideration of infiltration, as fluvial flooding may mask the effects of infiltration, as shown in Figure 5.35. The inundation map at 11am provides a better understanding of the effect of infiltration. In Figure 5.36, slight difference can be noticed at the right bank in Middle Greens which can be recognised as a result of the infiltration.

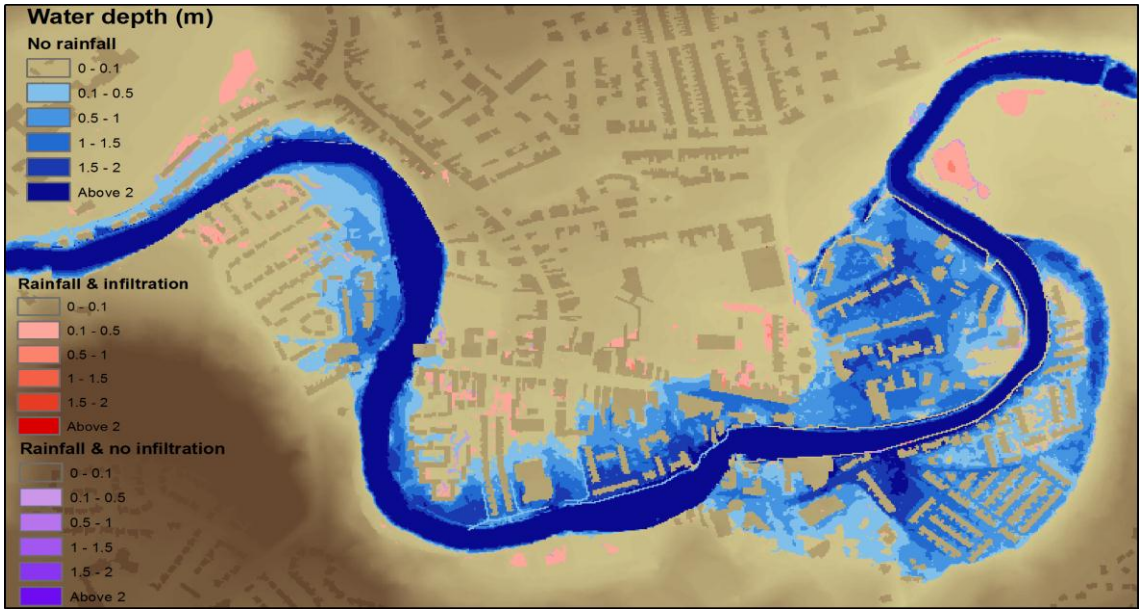

Figure 5.35 Inundation maps at 5pm with and without infiltration in the town centre domain.

Figure 5.36 Inundation maps at 11am with and without infiltration in the town centre domain.

5.4.5 *Buildings*

This sub-section discusses how building representations affect the accuracy and efficiency of the coupled model. Two kinds of building representations: raised buildings and blocked buildings, as introduced in Section 3.5 are employed here.

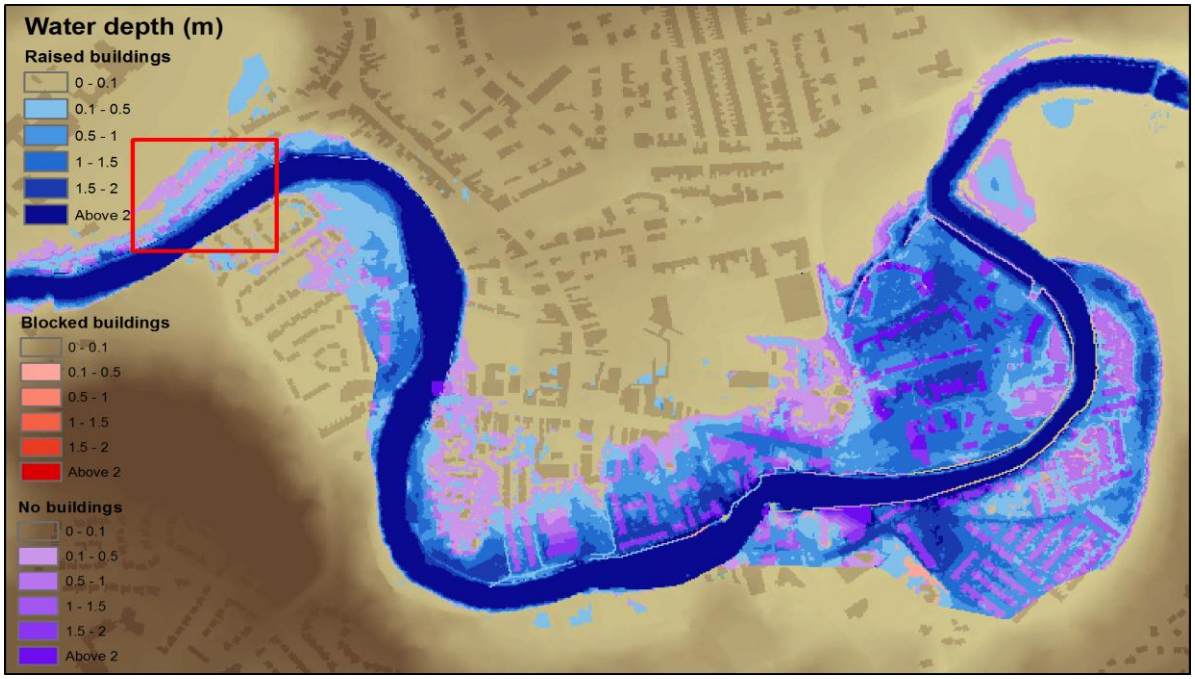

Figure 5.37 Inundation maps at 5pm with different building representations in the town centre domain.

From Figure 5.37, it is clear that the inundation is more extensive if there are no buildings, as the clear pathways can convey floods faster and further. Some areas where

buildings should be located are also inundated as the buildings have been removed from the domain. In general, the inundation extents are fairly similar between using raised buildings and blocked buildings. A local inundation at Mitford Road (highlighted in Figure 5.37) is illustrated in Figure 5.38. This inundation shows that blocked buildings may produce slightly larger inundation extents around buildings. The rainfall on the tops of blocked buildings is proportionally distributed to the neighbouring cells immediately, while the rainfall on the tops of raised buildings flows to the neighbouring cells naturally with a time delay, and this may explain the slightly larger inundation around the building.

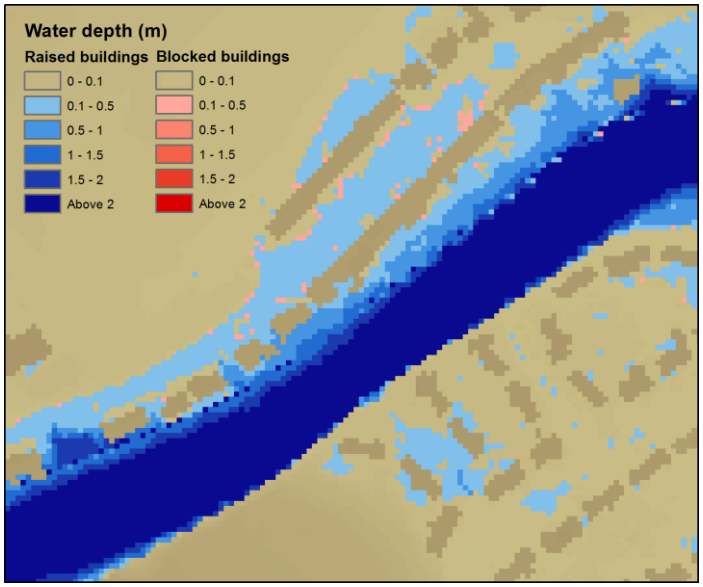

Figure 5.38 Local inundations at 5pm with different building representations in the town centre domain.

The critical point P1 is situated between two buildings, and is hence chosen to evaluate the local effect of the building representations. As can be seen in Figure 5.39, the arrival times for all simulations are similar, but it is slightly earlier if no buildings are considered in the domain as the flood can propagate faster without blockage. This could be the reason why the maximum water depth is smaller than the other two simulations. Furthermore, the maximum water depth using raised buildings is shallower than using blocked buildings as some rainfall may still be retained on the tops of the buildings.

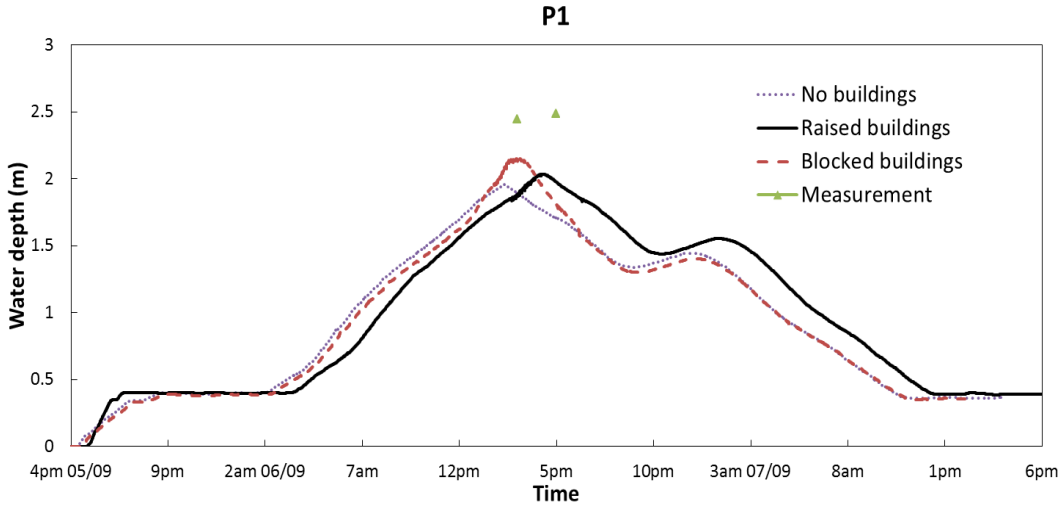

Figure 5.39 The time histories of water depth at the critical point P1 with different building representations in the town centre domain.

The statistics of the coupled model's results with different building representations are displayed in Table 5.12. The results using raised buildings are slightly better which can be attributed to the more sensible rainfall distribution compared to the blocked building method. The results when buildings are excluded match best with the post-event measurement data, and this was not anticipated. One possible reason may be that data for most areas in the post-event measurement inundation map are acquired from a limited number of measured data by interpolation, and no buildings are accounted during this process. As a result, some of the buildings in the post-event measurement inundation maps (Figure 5.16(a), Figure 5.17(a), Figure 5.18(a), Figure 5.19(a)) include flood water on the tops of the buildings, which in reality would not have occurred.

Building representation type	Relative *RMSE*(h) (%)	F^1 (%)	F^2 (%)
No buildings	21.8	86.5	79.2
Raised buildings	24.3	83.2	76.1
Blocked buildings	26.5	82.9	75.9

Table 5.12 Statistics of the coupled model's results with different building representations in the town centre domain.

When discussing the computational efficiency, the time cost by the full 2D shallow flow model using raised buildings is used as the reference. From Table 5.13, using blocked buildings is more efficient than using raised buildings as fewer hydraulic cells are involved in the computation. As a trade-off between accuracy and efficiency, blocked buildings are preferable. Additionally, with the same number of hydraulic cells, raised buildings consume more time than no buildings as local flow velocities around raised

buildings may be larger, causing smaller computational time steps through Equation 3.11 and 3.12.

Building type	Total cell number	Domain cell number	Hydraulic cell number	Hydrological cell number	CPU time (hours)		Average improved efficiency
					25-hour simulation	50-hour simulation	
No buildings	326,250	326,250	144,124	182,126	110.1	274.3	2.2x
Raised buildings	326,250	326,250	144,124	182,126	116.8	283.6	2.1x
Blocked buildings	326,250	326,250	127,484	198,766	103.2	241.7	2.4x
Raised buildings (Full 2D model)	326,250	326,250	326,250	0	246.4	567.2	-----

Table 5.13 Computational cost comparison between different building representations in the town centre domain.

5.4.6 *Coupling method*

Two coupling methods in Section 3.6 are assessed in this sub-section, in terms of the accuracy and efficiency of the coupled model. The ‘unit hydrograph’ method is referred as ‘coupling method 1’, while the method using the ArcGIS Hydrology Tool is referred as ‘coupling method 2’.

As shown in Figure 5.40, the inundation extents are quite similar using the two coupling methods. A local inundation at Mitford Road (highlighted in Figure 5.40) is displayed in Figure 5.41. Herein, ‘coupling method 2’ generates slightly a larger inundation extent near the zone border. This is because the rainfall in the hydrological zone is immediately distributed to border cells proportionally and travel time of runoff is negated. In ‘coupling method 1’ the propagation process is described by the ‘unit hydrograph’.

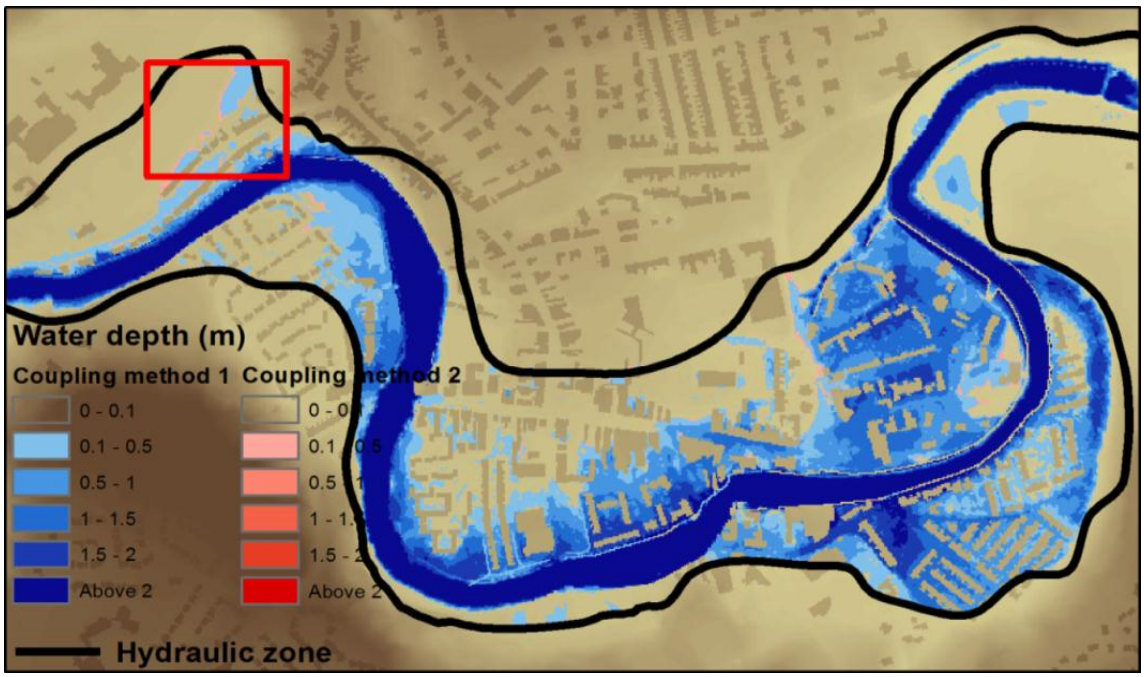

Figure 5.40 Inundation map at 5pm with different coupling methods in the town centre domain.

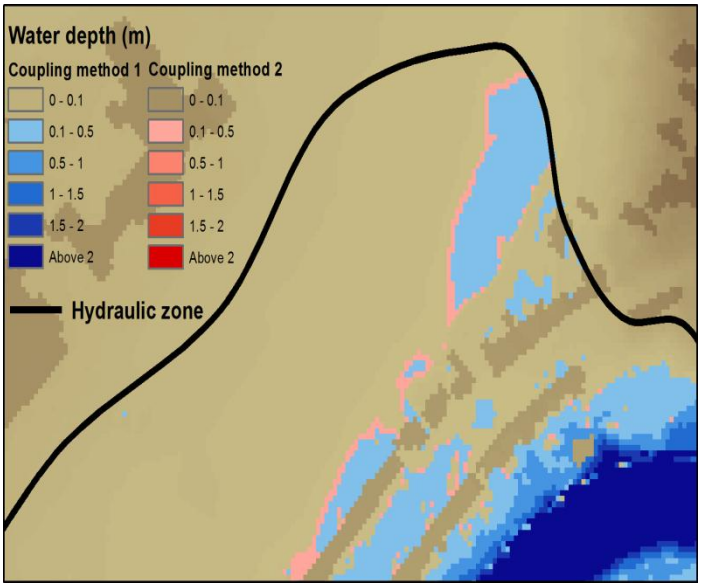

Figure 5.41 Local inundations at 5pm with different coupling methods in the town centre domain.

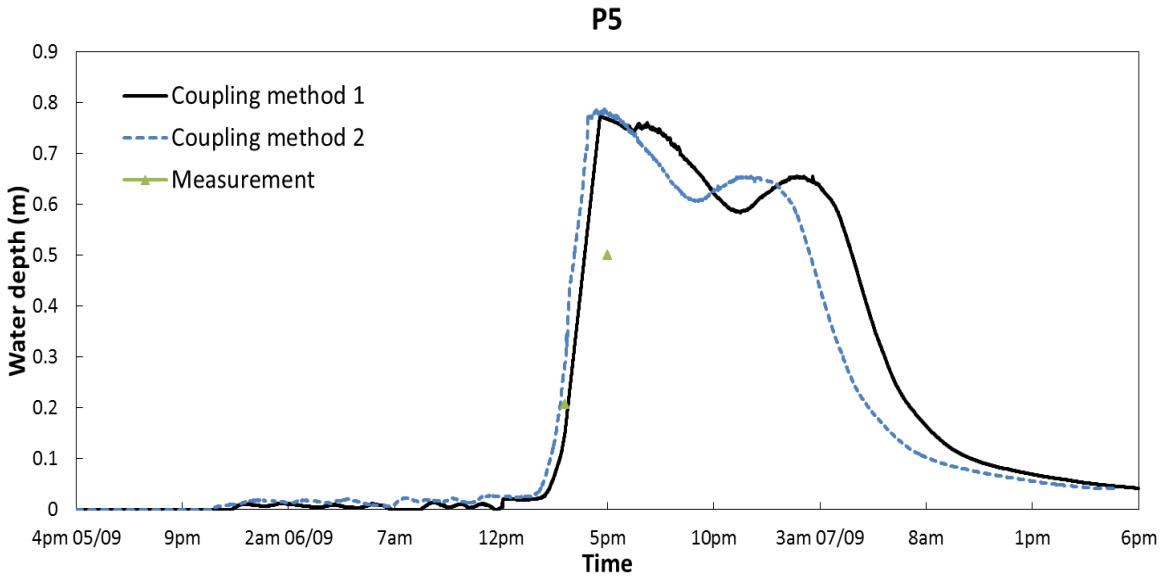

Figure 5.42 The time histories of water depth at the critical point P5 with different coupling methods in the town centre domain.

Critical point P5 is close to the zone border, and is hence suitable to investigate the local effect of the coupling methods. As can be seen in Figure 5.42, the water depth rises slightly earlier to a higher peak followed by a quick recession when using 'coupling method 2' as a result of the negation of the runoff travel time.

In order to obtain a global view, some statistics are calculated and listed in Table 5.14, which shows that using 'coupling method 1' can achieve better accuracy than using 'coupling method 2'. This is because the 'UH' routing method in the hydrological zone of 'coupling method 1' is more reasonable than the direct distributions of the rainfall in 'coupling method 2'.

Coupling method	Relative *RMSE*(h) (%)	F^1 (%)	F^2 (%)
Method 1	24.3	83.2	76.1
Method 2	25.9	82.9	75.3

Table 5.14 Statistics of the coupled model's results with different coupling methods in the town centre domain.

Coupling method	Total cell number	Domain cell number	Hydraulic cell number	Hydrological cell number	CPU time (hours)		Average improved efficiency
					25-hour simulation	50-hour simulation	
Method 1	326,250	326,250	144,124	182,126	116.8	283.6	2.1x
Method 2	326,250	326,250	144,124	182,126	115.9	283.1	2.1x
Full 2D model	326,250	326,250	326,250	0	246.4	567.2	----

Table 5.15 Computational cost comparison between different coupling methods in the town centre domain.

With regard to computational efficiency, the time cost by the full 2D shallow flow model is used as the reference. As can be seen in Table 5.15, using both coupling methods cost similar computational time due to the identical hydraulic cell number and almost equal complexity.

5.5 Simulations in the Extracted Sub-catchments

In Section 5.3 and Section 5.4, the coupled model has been preliminarily validated and evaluated. In order to save computational time, the simulations have been implemented in Morpeth town centre over 1.3 km^2 instead of the extracted sub-catchments, with the assumption that modelling results are not significantly affected by the reduced domain size, and the effect is consistent in the sub-catchments' domains and the town centre domain.

In this section, the assumption is examined by applying the full 2D shallow flow model and the coupled model in the extracted sub-catchments and comparing the modelling results. In addition, the coupled model can also be further validated. A resolution of 2 m × 2 m and 2,541 × 4,097 cells are used to discretise the extracted sub-catchments. The seven selected gauge points in Figure 5.13 are still used herein to record the time histories of the water depth and flow velocity. An initial steady state in the river channel is achieved with 10 m^3/s constant inflow after about 10-hour simulation. Other details such as the building representation, the catchment division scheme, computing power, etc. are all the same as the ones in Section 5.3 for fair companions.

Before simulations are carried out, the full 2D shallow flow model is used to record the 'unit hydrographs' at the hydraulic and hydrological zone border under a uniform net rainfall of 10 mm for 15 minutes in the hydrological zone. Figure 5.43 displays an

example of two sets of ‘unit hydrographs’ in one border cell which are produced by pre-running the full 2D shallow flow model with the extracted sub-catchments and the town centre as the domain, respectively. The unit hydrographs are then scaled and superimposed according to the real net rainfall to generate accumulative hydrographs from the hydrological zone to the hydraulic zone, as illustrated in Figure 5.44.

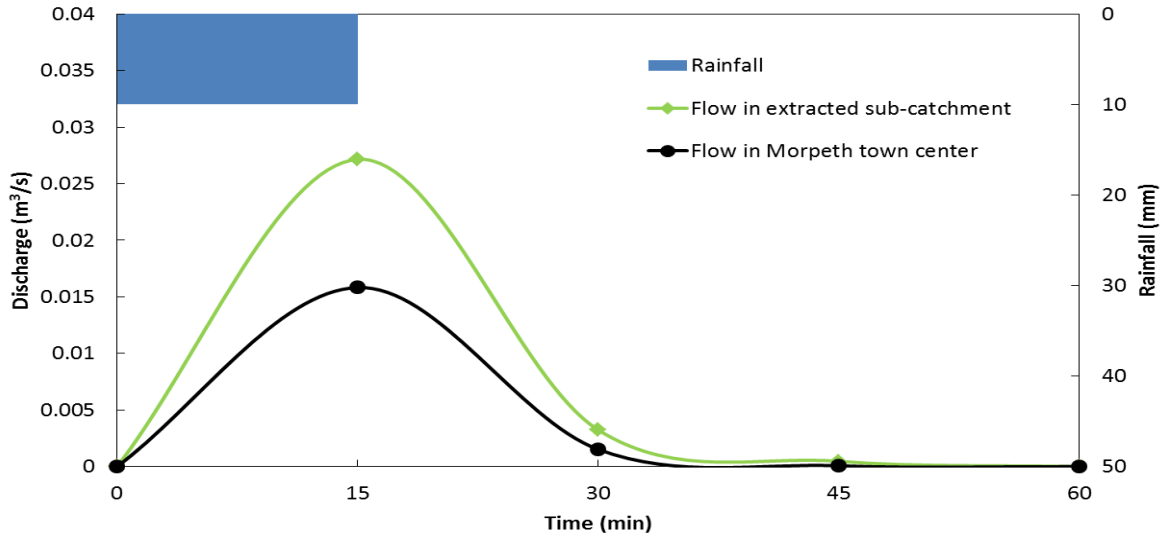

Figure 5.43 An example of the ‘unit hydrographs’ at the zone border in the extracted sub-catchments’ domain and the town centre domain.

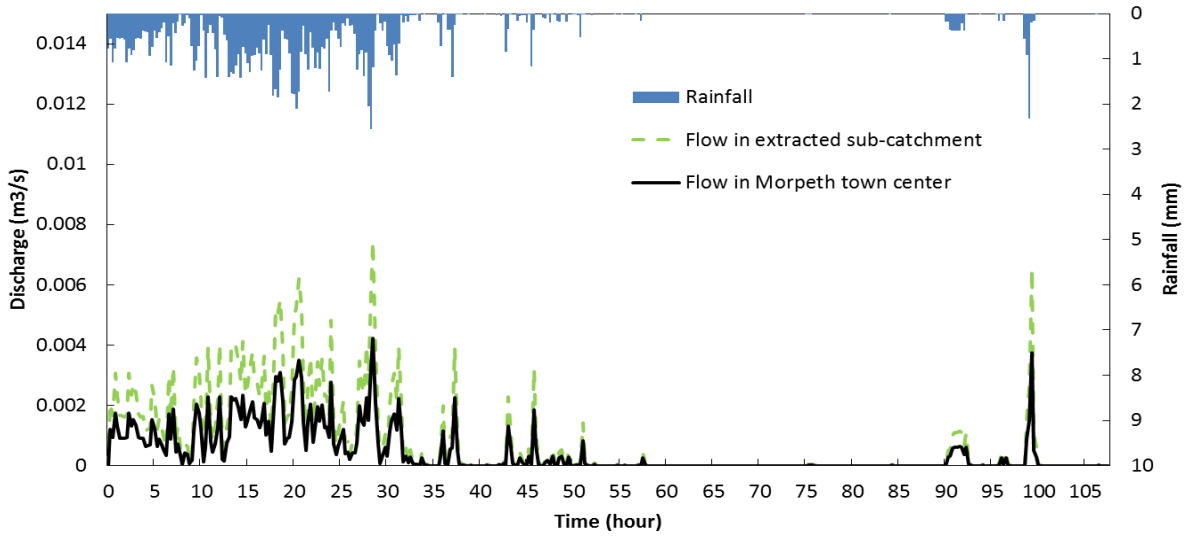

Figure 5.44 An example of the accumulative hydrographs at the zone border in the extracted sub-catchments’ domain and the town centre domain.

As can be seen in Figure 5.43 and Figure 5.44, the increase of domain size can accumulate a larger amount of flow into the hydraulic zone, which leads to larger ‘unit hydrographs' and subsequently larger accumulative hydrographs when using the extracted sub-catchments as the computational domain.

Since huge computational time is required when full 2D model is applied in the extracted sub-catchments, a 25-hour simulation is conducted for this condition to reproduce the rising limb of the flood. The inundation maps in the extracted sub-catchments at 11am, 1pm, 3pm and 5pm on 6th September produced by the full 2D shallow flow model and the coupled model are illustrated in Figure 5.45-Figure 5.48.

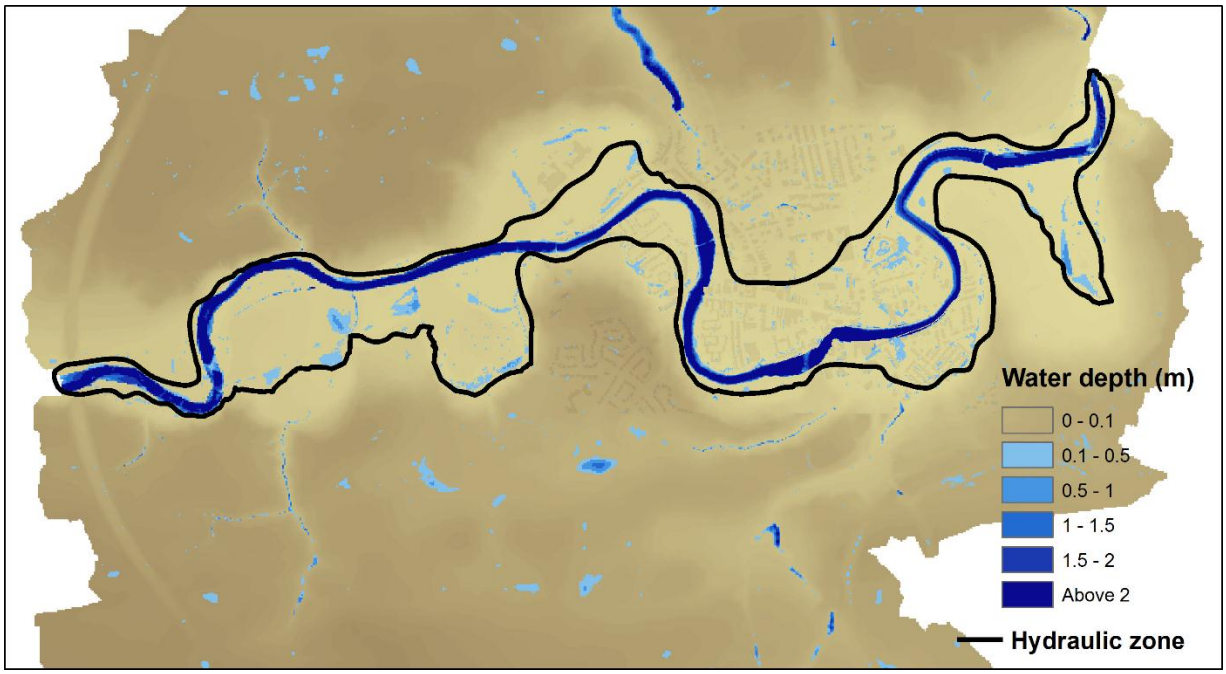

(a)

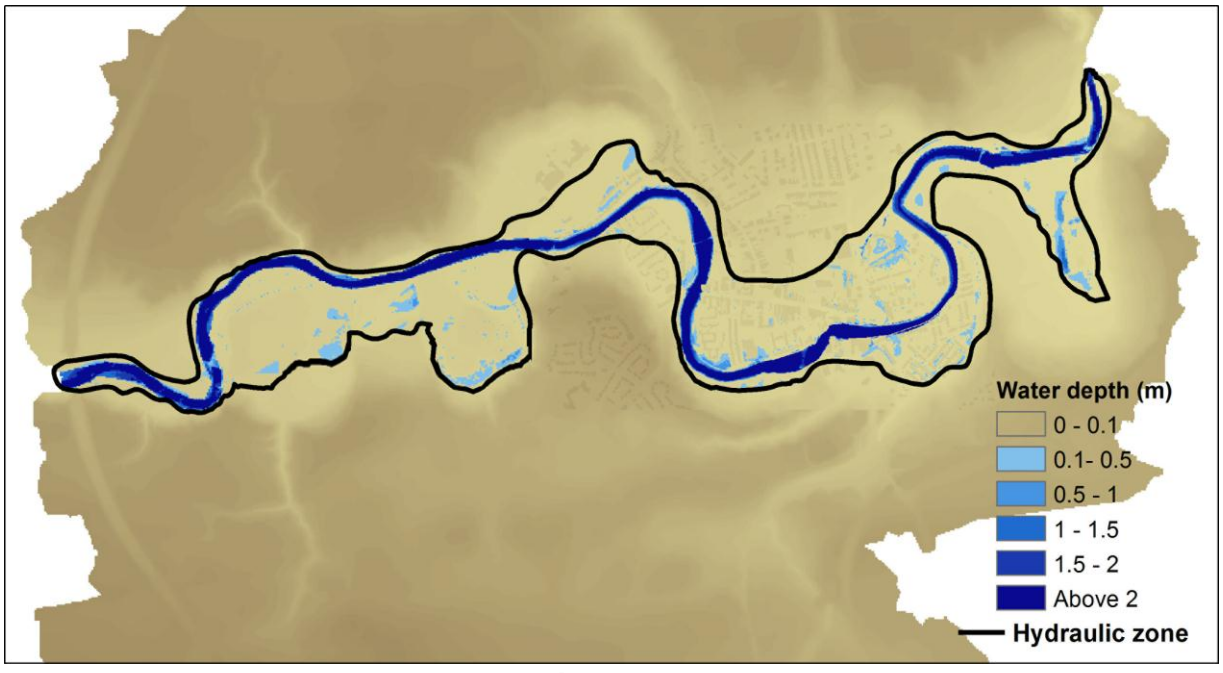

(b)

Figure 5.45 Inundation maps at 11 am in the extracted sub-catchments' domain: (a) full 2D model, (b) coupled model.

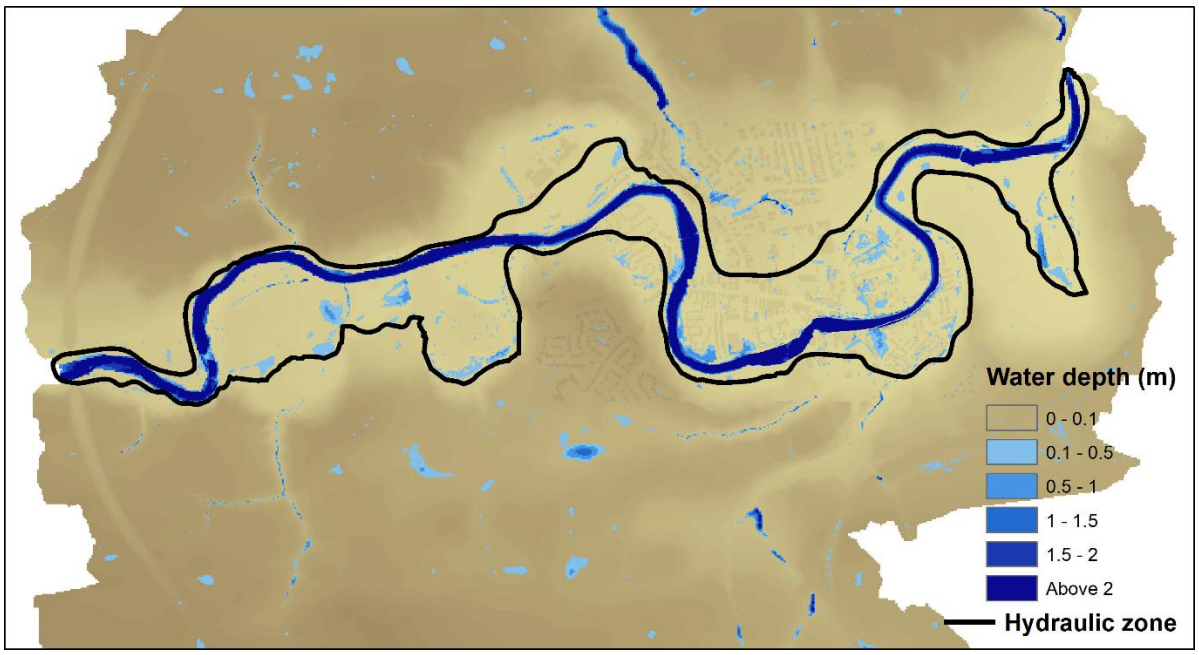

(a)

(b)

Figure 5.46 Inundation maps at 1pm in the extracted sub-catchments' domain: (a) full 2D model, (b) coupled model.

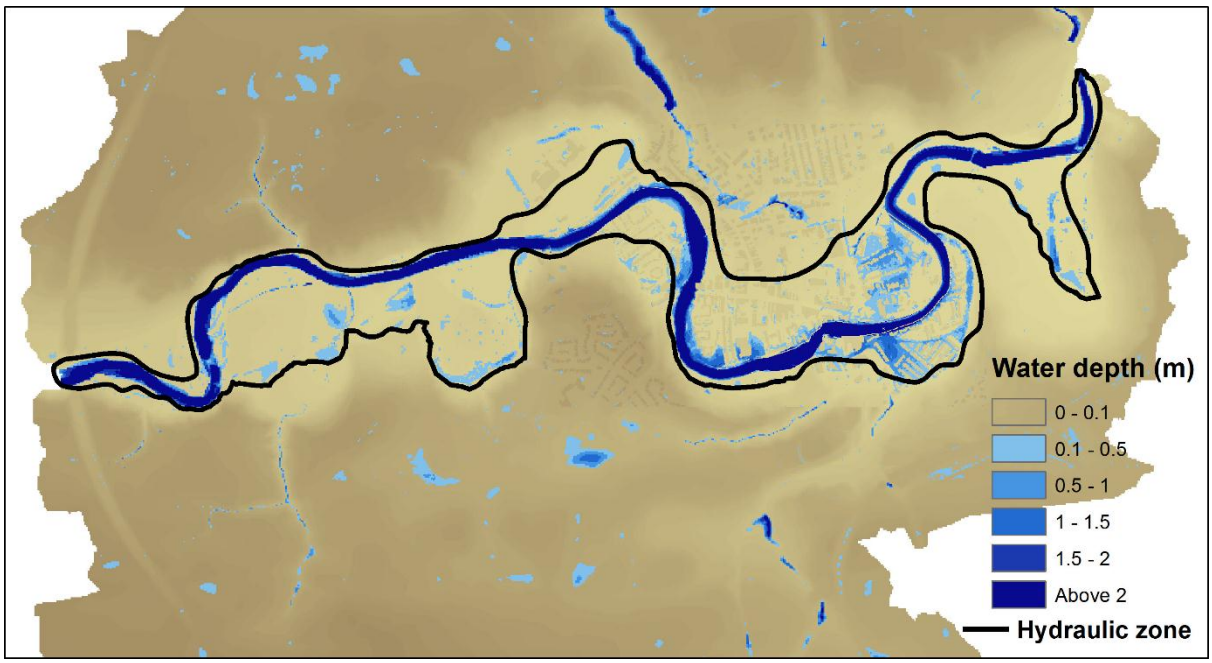

(a)

(b)

Figure 5.47 Inundation maps at 3pm in the extracted sub-catchments' domain: (a) full 2D model, (b) coupled model.

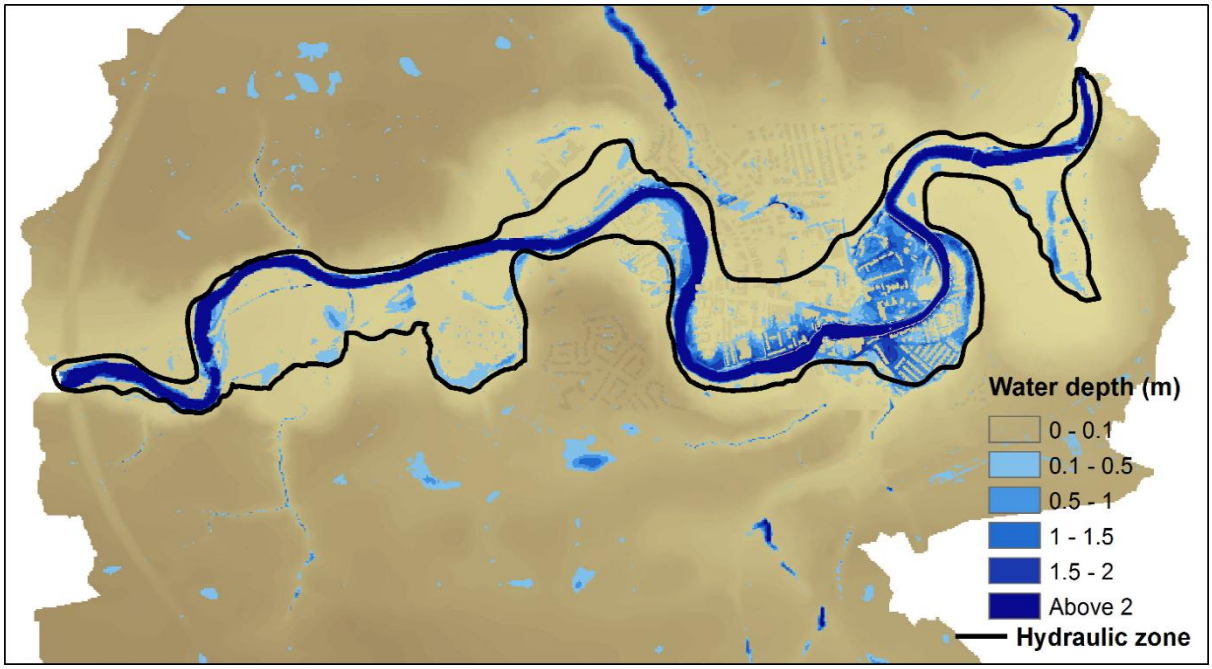

(a)

(b)

Figure 5.48 Inundation maps at 5pm in the extracted sub-catchments' domain: (a) full 2D model, (b) coupled model.

In the hydraulic zone, the inundation extents from the coupled model match reasonably well with the ones from the full 2D model at all times. Compared with the inundation maps interpolated from the measured data (Figure 5.16(a), Figure 5.17(a), Figure 5.18(a), Figure 5.19(a)), generally both modelling results seem to be slightly more extensive at 11am, 1pm and 3pm. The best agreement is achieved at 5pm. This is

consistent with the inundation maps in the town centre domain. The omission of the drainage system is the main reason for the larger inundation extents. Another reason may be the negation of infiltration, but it is quite limited as discussed in sub-section 5.4.4.

The effect of the changing domain size on the modelling inundation extent can be evaluated by comparing the inundation maps from the model with the town centre domain and the extracted sub-catchments' domain. For example, the comparison between Figure 5.19(c) and Figure 5.48(b) can assess the effect of the domain size on the inundation extent obtained by the coupled model. In general, both models produce less extensive flood extents when the sub-catchments are used as the computational domain than when the town centre is used. This is opposite to the anticipation that more extensive flood extents should be predicted in the extracted sub-catchments' domain, as more rainfall is considered. One possible reason to explain this phenomenon is that the same inflow hydrograph at Mitford flow station is employed for the two domain conditions. This is correct when the sub-catchments are used as the domain. However, the inlet of Morpeth town centre is actually approximately 2.2 km downstream of the flow station, and imposing the inflow hydrograph directly may cause earlier or larger inundations.

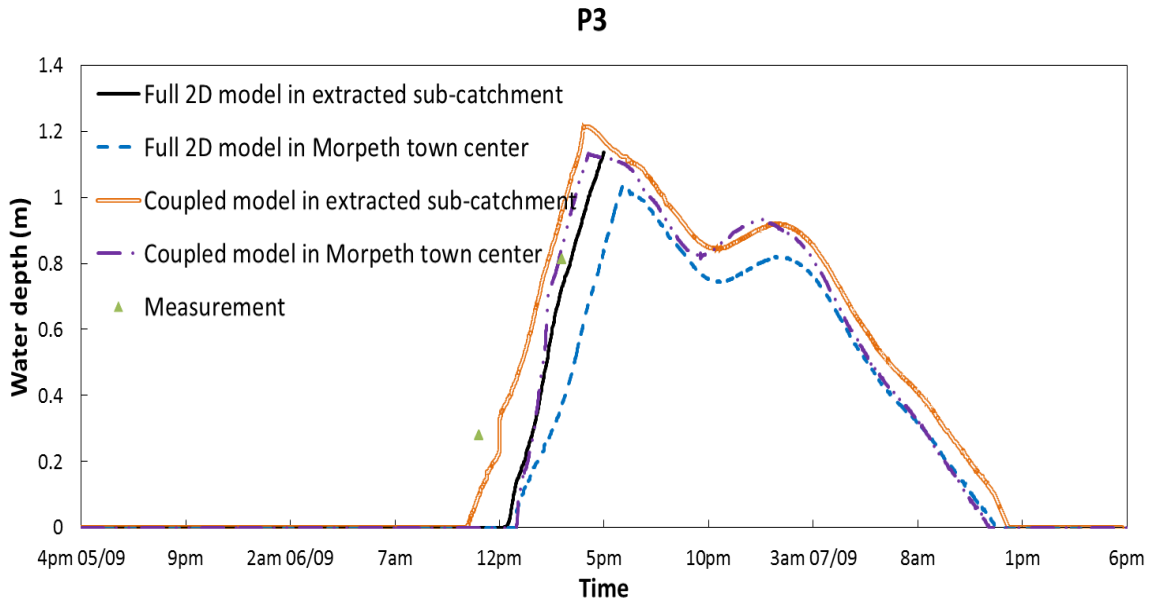

Figure 5.49 The time histories of water depth at the critical point P3 in the extracted sub-catchments' domain and the town centre domain.

The critical point P3 near the zone border is selected to investigate the local effect on the water depth and flow velocity from using the different domains. In Figure 5.49, in

the extracted sub-catchments' domain, the water depth predicted by the coupled model is generally larger than the one by the full 2D shallow flow model. This is because the flow in the hydrological zone can be routed to the zone border faster by the coupled model. Comparisons about the maximum water depth and arrival time in Table 5.16 confirm this, and also demonstrate the consistency of the effect on modelling results with using the model in the town centre domain.

	Extracted sub-catchments' domain		Town centre domain	
	Maximum depth (m)	Arrival time (hour)	Maximum depth (m)	Arrival time (hour)
Full 2D model	1.12	20.67	1.02	19.68
Coupled Model	1.21	19.01	1.13	19.44

Table 5.16 The maximum water depth and the arrival time at the critical point P3 in the extracted sub-catchments' domain and the town centre domain.

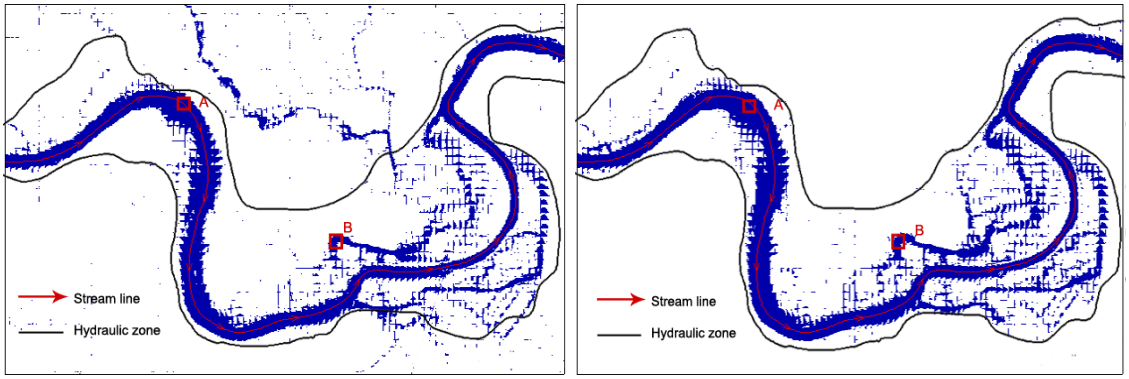

(a) (b)

Figure 5.50 Velocity field maps at 5pm in the extracted sub-catchments' domain: (a) full 2D model, (b) coupled model.

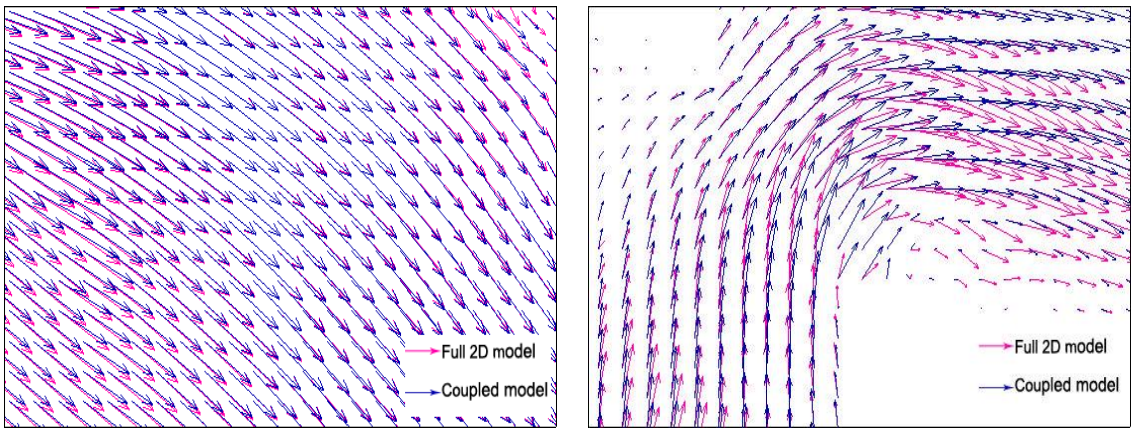

(a) (b)

Figure 5.51 The zoomed-in view of velocity field maps at 5pm in the extracted sub-catchments' domain: (a) area 'A', (b) area 'B'.

Velocity field maps from both models at 5pm 6th September are illustrated in Figure 5.50. Similar velocity fields can be found in the hydraulic zone. Local velocities at the

same areas 'A' and 'B' with Figure 5.23 are studied. The zoomed-in views are displayed in Figure 5.51. As it is located in the river channel, the flow regime of area 'A' is mainly affected by the upstream inflow. Therefore, marginal deviations of the velocities are predicted by the full 2D shallow flow model and by the coupled model. The velocity match in area 'B' is less satisfactory, as discrepancies in both magnitude and direction can be found. Generally, the velocity from the full 2D shallow flow model is larger in the whole area 'B'. This may be because in the coupled model the direction of the lateral inflow at the zone border is ignored, and the inflow is treated only as a source point. Figure 5.52 shows that at critical point P3, the velocities from the two models rise in the extracted sub-catchments' domain following a similar trend.

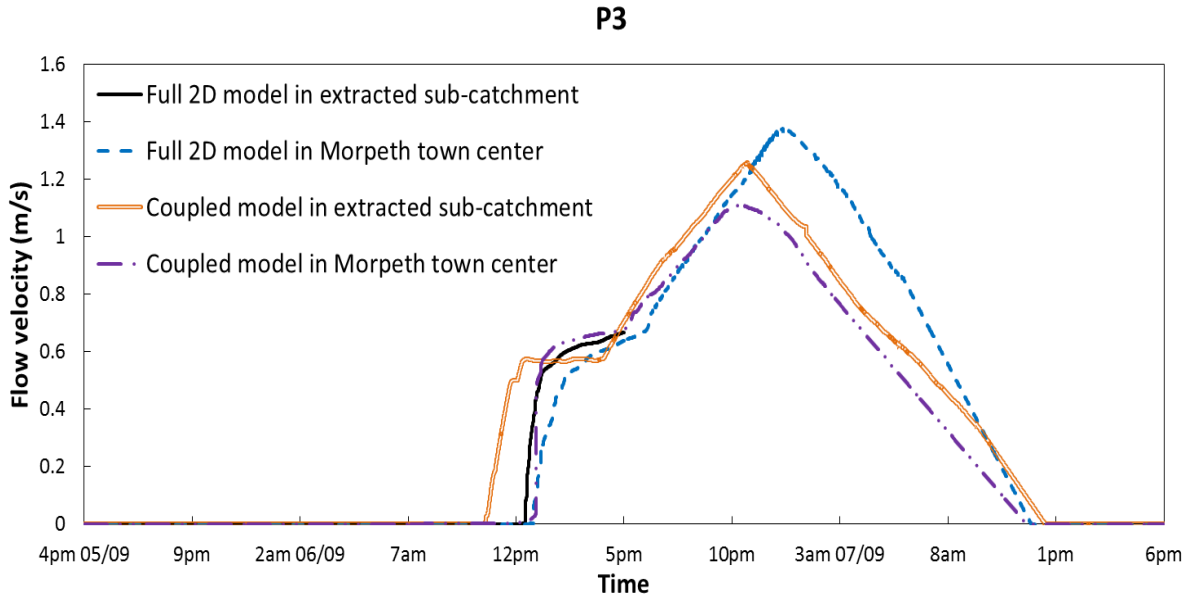

Figure 5.52 The time histories of flow velocity at the critical point P3 in the extracted sub-catchments' domain and the town centre domain.

Relative *RMSE* and Fit statistics (F^1 and F^2) are adopted in order to evaluate the global performance of the coupled model in the extracted sub-catchments' domain. As can be seen in Table 5.17, the full 2D shallow flow model performs better than the coupled model in the extracted sub-catchments' domain at all times, as physical details in the hydrological zone are considered. Compared with statistics obtained when the town centre is used as the domain, shown in Table 5.5, the changing size of the domain has a consistent impact on the models' results. Furthermore, the statistics for the sub-catchments' domain are better than the town centre domain, as all the rainfall in the sub-catchments is included and the flow station, where the inflow hydrograph is generated, is exactly located at the inlet of the sub-catchments' domain.

Time	Model	Relative *RMSE* (%)	F^1 (%)	F^2 (%)
11am	Full 2D model	33.2	92.1	64.2
	Coupled model	37.6	89.6	59.1
1pm	Full 2D model	27.5	88.2	69.9
	Coupled model	30.1	85.4	65.3
3pm	Full 2D model	21.7	82.1	74.8
	Coupled model	24.2	79.2	70.2
5pm	Full 2D model	16.2	89.3	83.4
	Coupled model	19.1	86.5	79.6

Table 5.17 Model comparison in the extracted sub-catchments' domain (benchmark: post-event investigation data)

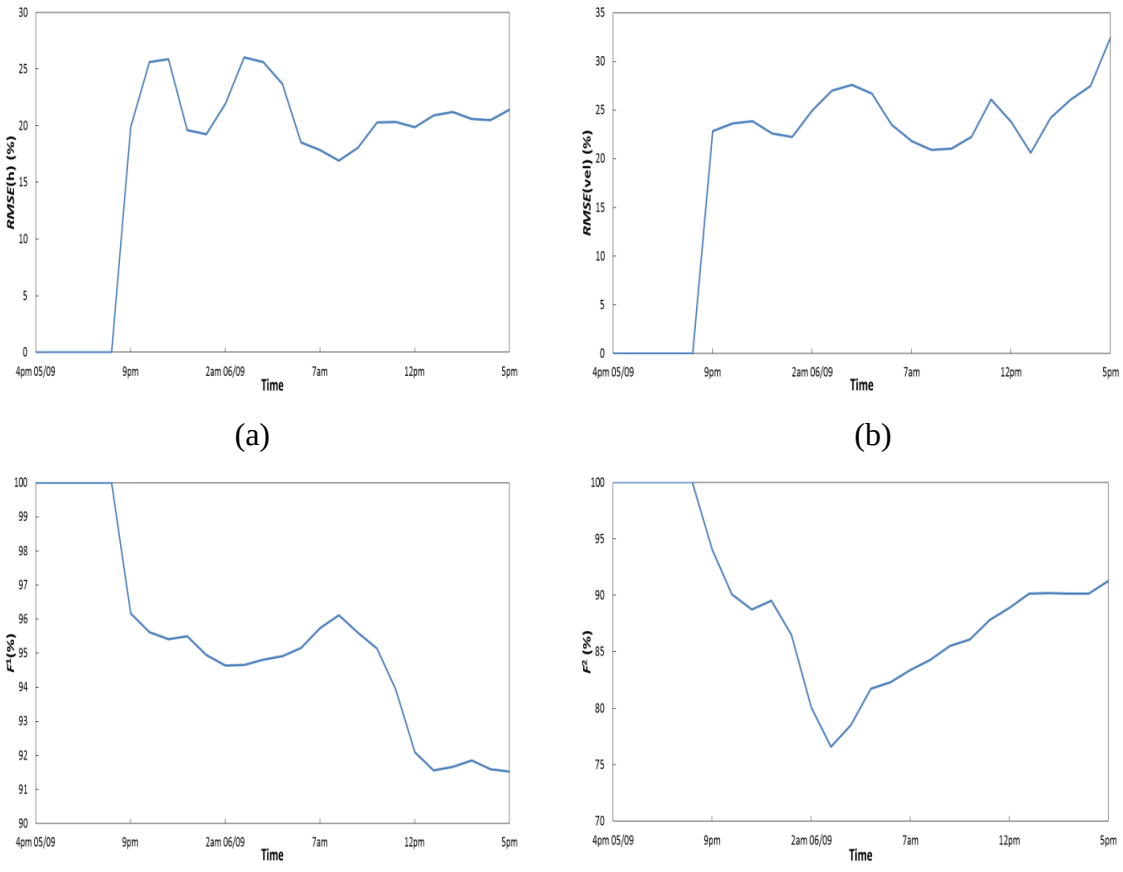

Figure 5.53 Statistics of the coupled model's results in the extracted sub-catchments' domain: (a) Relative *RMSE* for water depth, (b) Relative *RMSE* for flow velocity, (c) F^1, (d) F^2 (benchmark: full 2D model's results).

The differences between the coupled model and the full 2D shallow flow model in the extracted sub-catchments' domain are sketched in Figure 5.53 with the full 2D shallow flow model's results as the reference. The *RMSE*s for water depth and flow velocity begin to rise sharply before 9pm on 5th September to about 25%, and thereafter fluctuate

gradually with maximum values of around 25% and 30%, respectively. Generally, F^1 decreases with a minimum value about 92%, and F^2 decreases first and then increases with the minimum value about 75%. Although these errors shown by the statistics are acceptable, they are greater than those in the town centre domain as shown in Figure 5.26. In the extracted sub-catchments' domain, a larger area with relatively complicated topography and also the uncertainties introduced by rainfall and infiltration, may bring more errors to the models. It can therefore be expected that larger deviations are found compared to those found herein when using the town centre as the computational domain.

The full 2D shallow flow model costs a huge amount of time in the sub-catchments' domain to carry out a 25-hour simulation. Because of this the simulation is interrupted after reproducing the rising limb of the flood. As can be seen in Table 5.19, the efficiency of the coupled model has been dramatically improved against the full 2D shallow flow model when compared with the one in the town centre domain, due to the larger percentage of hydrological cells, shown in Table 5.18.

Cell type	Cell number
Total cells	10,410,477
Domain cells	4,789,781
Hydraulic cells	269,480
Hydrological cells	4,520,301

Table 5.18 The number of cells in the extracted sub-catchments' domain.

Simulation Time (hours)	CPU Time (hours)		Improved efficiency
	Full 2D model	Coupled model	
25	2137.4	175.2	12.2x
50	------	397.0	-----

Table 5.19 Computational costs in the extracted sub-catchments' domain.

5.6 Damage Estimations under the Morpeth Flood Alleviation Scheme

A flood alleviation scheme is currently underway in Morpeth and is being carried out by the Environment Agency. It mainly includes constructing a storage facility to store flood water upstream of Morpeth, and building/refurbishing flood defences in the town centre alongside the Wansbeck River. In this section, flood damages to buildings, including building fabric and household inventory, etc. are roughly estimated before and after the flood alleviation scheme. The estimation is based on limited information about

the storage and flood defences being built, and is intended to demonstrate how this construction may mitigate floods and reduce damages.

5.6.1 *Damage estimation under three inflow scenarios with upstream storage*

The design volume of the upstream storage is 1.4 million m^3, of which the flood control volume can be used to regulate the inflow hydrograph by reducing the peak discharge. It is assumed that the outflow from the storage is equal to the river flow until a certain large discharge is reached. After this the outflow rate is limited in order to store flood water (Ward, 2008). Based on the actual inflow hydrograph in the September 2008 flood event, three control volume percentages, 60%, 80%, 100%, are selected leading to three corresponding inflow scenarios, i.e. 'inflow scenario 1', 'inflow scenario 2', 'inflow scenario 3', shown in Figure 5.54. The percentage is set to be as high as possible because the storage is mainly designed for the purpose of flood storage.

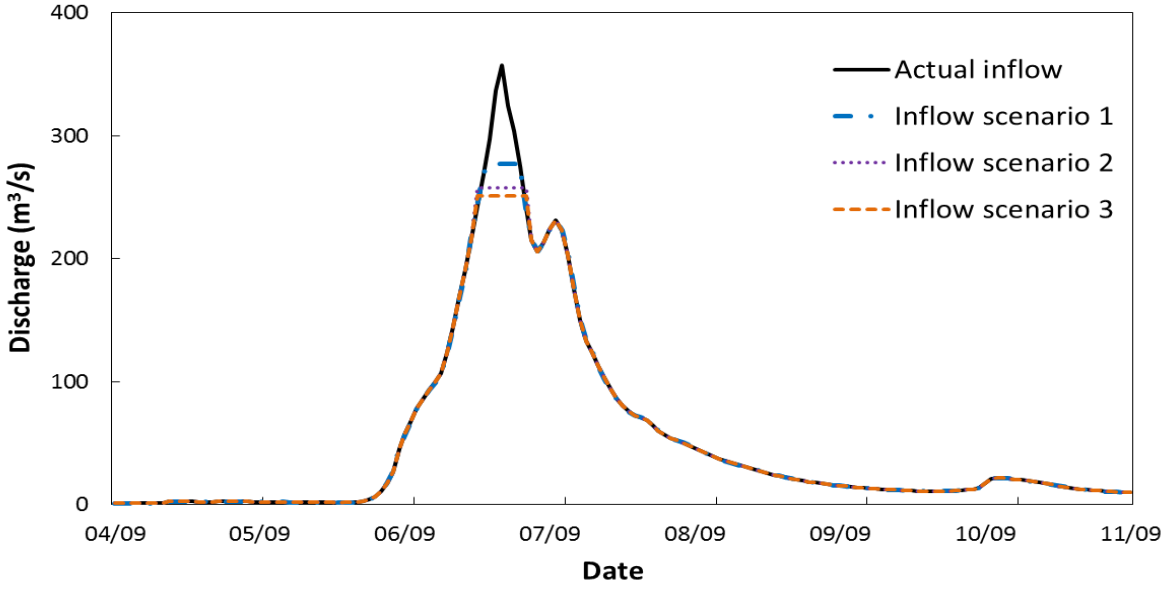

Figure 5.54 Three inflow scenarios under Morpeth flood alleviation scheme.

A 50-hour simulation has been carried out by the coupled model in the Morpeth town centre domain, under the three inflow scenarios, with all other modelling conditions kept the same as the ones in Section 5.3. The flood inundation maps at 5pm are illustrated in Figure 5.55. The inundation extent reduces with the increasing control volume of the storage, especially when the percentage reaches 100% of the total volume.

The FHRC depth-damage curves are employed to estimate the flood damages to buildings under the actual inflow and the three inflow scenarios, and evaluate the effect of the storage on alleviating flood damages. The economic losses caused by the building damage are listed in Table 5.20.

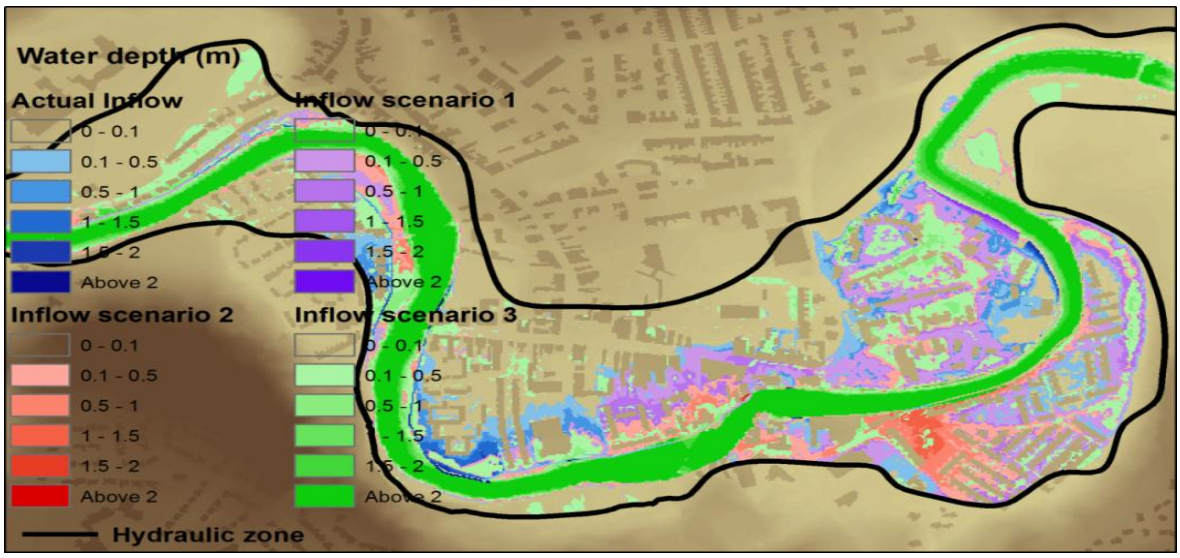

Figure 5.55 Inundation maps at 5pm with different inflow scenarios in the town centre domain.

Scenarios	Peak discharge (m^3/s)	Affected building areas (m^2)		Economic losses (£: million)		Total economic losses (£: million)
		Residential building	Commercial building	Residential building	Commercial building	
Actual inflow	357	50,360	24,012	7.97	2.62	10.59
Inflow scenario 1	277	42,832	23,102	6.42	2.31	8.73
Inflow scenario 2	258	37,841	17,674	5.68	1.77	7.45
Inflow scenario 3	251	21,143	15,018	3.17	1.5	4.67

Table 5.20 The economic losses caused by the building damages with three inflow scenarios in the town centre domain.

The total economic losses with the actual inflow is £10.59 million, which is generally in line with the estimation in Section 4.2. Flood damage can be alleviated after the construction of the storage, and a larger flood control volume may achieve lesser flood damage, consequently causing smaller economic losses. The improvement between 'inflow scenario 3' and 'inflow scenario 2' is significant, 100% flood control volume is therefore recommended.

5.6.2 *Damage estimation under three flood defence scenarios*

The location of the design flood defences, under the Morpeth flood alleviation scheme, can be seen in Figure 5.56. As no data about the height of the design flood defences is currently available, three scenarios: 'flood defence scenario 1', 'flood defence scenario 2', and 'flood defence scenario 3' are set up for the design flood defence height of 0.5 m, 1 m and 1.5 m, respectively.

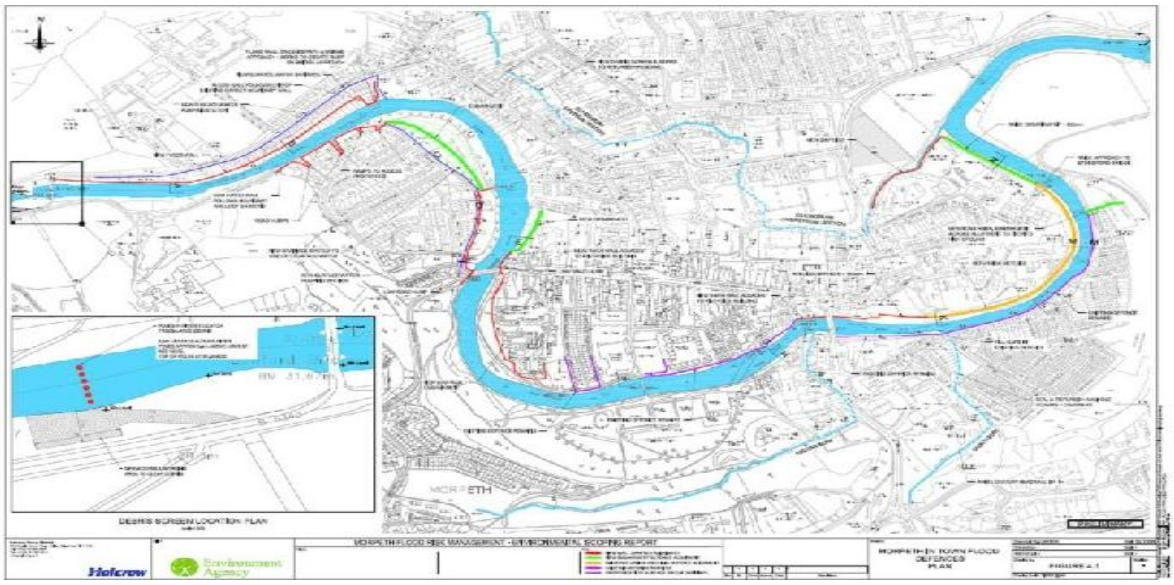

(a)

(b)

Figure 5.56 The location of the design flood defences under Morpeth flood alleviation scheme: (a) engineering map (Morpeth Flood Action Group), (b) schematization.

The simulation has been implemented by the coupled model for 50 hours in Morpeth town centre domain, under the three flood defence scenarios, with all other modelling conditions kept the same as the ones in Section 5.3. The flood inundation maps at 5pm

are displayed in Figure 5.57. The inundation extent decreases with the increasing height of the flood defences, and an impressive improvement can be found when the height is 1.5 m.

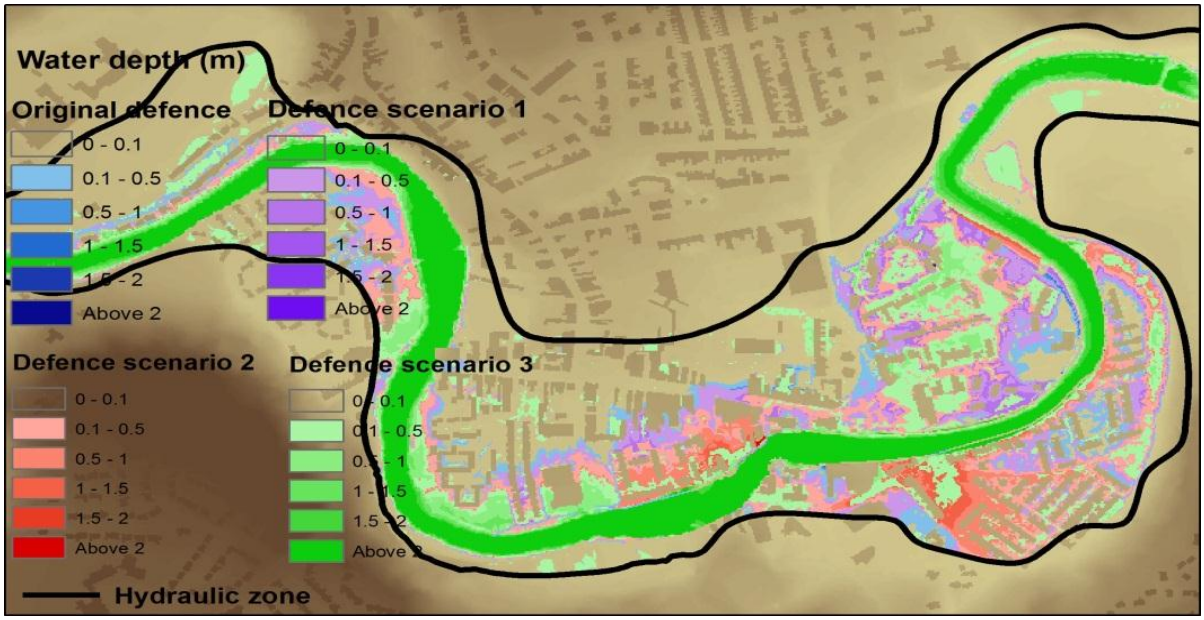

Figure 5.57 Inundation maps at 5pm with different flood defence scenarios in the town centre domain.

The FHRC depth-damage curves are utilised to estimate damages to buildings from inundations under the three flood defence scenarios as well as the scenario with the original flood defences. The economic losses caused by building damage are listed in Table 5.21.

Scenarios	Design flood defence height (m)	Affected building areas (m^2)		Economic losses (£: million)		Total economic losses (£: million)
		Residential building	Commercial building	Residential building	Commercial building	
Original flood defence	-----	50,360	24,012	7.97	2.62	10.59
Flood defence scenario 1	0.5	48,152	21,448	7.62	2.34	9.96
Flood defence scenario 2	1	46,148	16,644	7.31	1.81	9.12
Flood defence scenario 3	1.5	38,712	13,884	6.13	1.51	7.64

Table 5.21 The economic losses caused by the building damages with three flood defence scenarios in the town centre domain.

The newly built flood defences can mitigate fluvial flooding, and thus reduce the economic losses. Larger flood defence height leads to smaller damages to the buildings, and thereby fewer economic losses. When compared with the effect of the upstream storage, flood defences seem to perform less effectively in reducing economic losses.

5.6.3 *Damage estimation under the combination of upstream storage and flood defences*

The inflow scenario with a control volume of 100% and the flood defence scenario with a height of 1.5 m are combined as a new scenario as both have shown the most satisfactory performance when investigated separately. The coupled model is used to simulate the September 2008 flood event in Morpeth town centre domain for 50 hours. No fluvial inundations have been found in the town centre during the simulation, which suggests the combination of the newly built storage and flood defences may be capable of protecting the town centre from the flood event of at least this level, i.e. 1 in 137 years.

5.7 Summary

The full 2D shallow flow model and the coupled model have been applied to simulate the real flood event in both Morpeth town centre and the extracted sub-catchments. Both models have performed reasonably well when compared with the post-event investigation data. The coupled model can save a lot of computational time compared to the full 2D shallow flow model while keeping a reasonable level of accuracy. The coupled model has been investigated and evaluated in terms of the effects from modelling resolution, bed friction, rainfall, infiltration, buildings and coupling methods in the town centre domain. Finally, the coupled model has also been employed to estimate the flood damage under the Morpeth Flood Alleviation Scheme.

Chapter 6 Conclusions and Future Work

Despite the advantages of the full 2D hydrodynamic models, in representing the physics of flood waves and delivering the required flow details with relatively high accuracy, they usually necessitate sophisticated numerical methods, and thus incur high computational burdens. Therefore, techniques for improving computational efficiency are required to provide reasonable numerical solutions within manageable and practical timescales.

A number of mathematical, numerical and computing methods have been implemented to improve full 2D hydrodynamic models, in order to balance the modelling accuracy and efficiency. Coupling the full 2D hydrodynamic models with hydrological models represents one of these approaches, which achieves a more efficient performance at a cost of sacrificing detailed physical descriptions of certain parts of a catchment.

This work has developed a new modelling system by routing the surface runoff, which is produced by a lumped conceptual model WBM, in the hydrological zone through a group of pre-acquired 'unit hydrographs' to the border cells. High-resolution simulations are carried out later in the hydraulic zone by the full 2D hydrodynamic model. The coupled model has accounted for the contribution of the surface runoff in hydrological zone rather than only the runoff through the river to the inundation in hydraulic zone.

In this work, an approach to specify hydraulic and hydrological zones has been developed according to the design flood event and land cover. Based on this division approach, the full 2D hydrodynamic model and the coupled model, equipped with OpenMP for parallel computation, have been validated through a real flood event in both an urban area and larger-scale catchment. Furthermore, the coupled model has been adequately investigated and evaluated with regard to the effects of modelling resolutions, bed friction, rainfall, infiltration, buildings and coupling methods. Finally, the coupled model has been employed to estimate the flood damage under different scenarios, for the upstream storage and flood defences in the town centre.

The rest of this chapter will conclude the results of the work, indicate the main capabilities and limitations of the newly developed coupled model, and recommend future work.

6.1 Conclusions

6.1.1 *Model validation*

The full 2D shallow flow model and the coupled model have been applied to simulate a real flood event, in both the town centre and the larger-scale sub-catchments for model validation.

In the town centre domain, both models have performed reasonably well when compared with post-event investigation data, even if more extensive inundation extents have been produced, due to the omission of the drainage system effect. With regards to modelling accuracy, the coupled model has been found less satisfactory than the full 2D shallow flow model, and deviations near the zone border are larger than in the rest of the domain. In general, larger water depths as well as shorter arrival times near the zone border have been predicted by the coupled model as a faster routing speed may be caused when using 'unit hydrographs'. In addition, the coupled model has generally produced smaller flow velocities because the direction of the lateral inflow at the zone border is omitted, and the inflow is treated just as a source point with no initial velocity. However, these discrepancies between the two models are not significant. In terms of modelling efficiency, the coupled model has achieved 2 times acceleration against the full 2D shallow flow model, which can be attributed to the use of the hydrological model in parts of the domain.

In the sub-catchments' domain, the conclusions are consistent with the ones drawn from the town centre domain. Furthermore, in the sub-catchments' domain both models have performed better when compared with the post-event investigation data because all rainfall over the sub-catchments has been considered, and the inflow hydrograph is more accurate. However, the deviations between the shallow flow model and the coupled model are greater than those in the town centre domain, which indicates that in the sub-catchments' domain, a larger area with relatively complicated topography and uncertainties introduced by rainfall and infiltration may bring more uncertainties to the models. The coupled model runs about 12 times as fast as the full 2D shallow flow model in the sub-catchments' domain because a larger percentage of the area in the domain has been specified as a hydrological zone where a hydrological model is applied. This indicates that the coupled model can be used in a large-scale catchment with relatively high efficiency. In addition, the benefit will become more obvious if more of

the flooding is due to surface runoff from hydrological zone rather than fluvial inundation.

6.1.2 *Model evaluation*

The coupled model has been further investigated and evaluated with regard to the effects of modelling resolutions, bed friction, rainfall, infiltration, buildings and coupling methods in the town centre domain.

The temporal resolution has a marginal and consistent effect on modelling results, while the spatial resolution significantly affects the results. Coarser spatial resolutions lead to larger modelling errors due to the limitation of representing urban topography, and the error converges with a decrease in cell size. In addition, finer temporal or spatial resolutions usually cost higher computational time.

In terms of bed friction, the results are less sensitive to the Manning coefficients in the floodplain than in the channel, which is because in the floodplain the dramatically changing bed elevation rather than the bed friction plays the most important part in the flood routing. Better results are obtained with the decreasing Manning coefficients in the river channel as larger river conveyance can be achieved which may compensate the limitation of representing the meandering river channel with square cells. Furthermore, flood extent is less sensitive than water depths to the bed friction.

Inclusion of rainfall during the flood event can result in a slightly larger inundation extent, and the effect is limited by the dominant fluvial inundation. However, the consideration of rainfall can assist in identifying the localized risk from pluvial flooding. With regard to infiltration, the coupled model's results are not quite sensitive to the saturated hydraulic conductivity, which suggests the limited effect from infiltration in a flood event with initially almost saturated soil.

Exclusion of buildings leads to earlier flood arrivals, smaller maximum water depths and more extensive inundation extents as the clear pathways can route floods faster and further. In general, the inundation extents agree favourably between using raised buildings and blocked buildings, and using blocked buildings may produce slightly larger inundation extents around buildings and also larger water depths, due to the immediate distribution of the rainfall on building tops. As a result of the more sensible rainfall distribution method, the coupled model using raised buildings performs more

satisfactorily than the one using blocked buildings. With respect to computational efficiency, using blocked buildings is more efficient than using raised buildings as the number of hydraulic cells is reduced in the computation.

Two coupling methods have been assessed in this work. The one using 'unit hydrographs' is referred as 'coupling method 1'; while the one adopting ArcGIS Hydrology Tool is referred as 'coupling method 2'. The inundation extents match closely between using the two coupling methods, but slightly larger inundation extents and earlier flood arrivals, as well as larger water depths near the zone border, can be predicted by using 'coupling method 2'. This is due to the distribution of rainfall in the hydrological zone to bordering cells, without considering the travel time of the runoff. Compared with the post-event investigation data, using 'coupling method 1'can achieve better accuracy than using 'coupling method 2' owing to the more reasonable routing method in the hydrological zone. Using both coupling methods cost similar computational time as a result of the identical hydraulic cell number and the almost equal complexity.

6.1.3 *Damage estimations*

Finally, the coupled model has been employed to implement damage estimations under different scenarios of upstream storage and flood defences in the town centre. In general, a larger percentage of the flood control volume for the upstream storage, or larger height of the design flood defences can produce a lesser inundation extent, and thus result in smaller economic losses. The effect of upstream storage may be more impressive than flood defences. Moreover, the combination of upstream storage and flood defences can significantly reduce flood risks.

In summary, the new modelling system could provide a robust and efficient tool for practitioners to perform flood modelling, damage estimation, risk assessment and flood management in urban areas and large-scale catchments.

6.2 Recommendations and Future Work

The coupled model is recommended to be used in other site following the steps below:

1) Collect spatial and non-spatial data, and implement hydrological analysis to separate the relevant catchment. DTM and rainfall data are of the most

importance. From experience, buildings are recommended to be represented by 'blocked building' method.

2) Run the full 2D shallow flow model on a coarse grid to work out the initial inundation extent for a design flood event.
3) Divide hydrological zone and hydraulic zone by the above inundation extent and land cover data/ urban area map.
4) Run the full 2D shallow flow model with 10 mm effective rainfall as the input for 15 minutes to obtain a group of 'unit hydrographs' at the zone border.
5) Run the coupled model for your observed/design event.

Although considerable work has been done to develop, validate and evaluate the coupled model, there is still some future work required to further improve its modelling accuracy and efficiency.

With respect to enhancing modelling accuracy, the following work may be worth investing future efforts:

1) Developing a more robust method for the catchment division.

In this work, the catchment is divided into hydraulic and hydrological zones according to the design flood event and land cover. However, due to subjectivity, there is no accurate solution for this division. Actually, in some aforementioned simulations the fluvial flood in the hydraulic zone has reached the zone border, which should be avoided by either resorting to a larger hydraulic zone or developing a more robust catchment division method.

2) Coupling the current models with a sewer model to consider the flow in the drainage systems.

Both the full 2D shallow flow model and the coupled model have produced larger inundation extents than the post-event measurement data in either the town centre domain or the sub-catchments' domain due to the omission of the drainage system's effect. In future work, a sewer model to simulate flows in drainage systems is necessary.

3) Improving the hydrological model and upgrading the coupling method accordingly.

In this work, local pluvial flooding in the hydrological zone can not be recognised as the lumped hydrological model is employed. A physically based and fully distributed

hydrological model might be a better choice for this purpose, but the improvement in efficiency may not be significant as this type of model also costs much computational time. The coupling method may need to be upgraded according to the features of the new hydrological model.

Other recommendations to improve modelling accuracy may involve including more features in the DEM, considering the spatial variability of rainfall and evaluating the effect from tributaries, etc.

With respect to improving computational efficiency, the coupled model is suggested to combine with high-performance computing hardware, e.g. GPU, and advanced computational techniques, e.g. adaptive grids, to achieve further accelerations.

In summary, the author would recommend this model of use by the flood modelling community. This model could be of great use in large catchment across the world where large cities are prone to fluvial flooding. The ability to represent a range of flood management options is made easier with this model.

References

Abbott, M.B., Bathurst, J.C., Cunge, J.A., O'Connell, P.E. and Rasmussen, J. (1986) 'An introduction to the European Hydrological System -Systeme Hydrologique Europeen, "SHE", 2: Structure of a physically-based, distributed modelling system', *Journal of Hydrology*, 87(1-2), pp. 61-77.

Ai, C.F. and Jin, S. (2009) 'Solution of the 2D shallow water equations using the high-resolution finite-volume method on unstructured meshes', *Jisuan Lixue Xuebao/Chinese Journal of Computational Mechanics*, 26(6), pp. 900-905.

Alcrudo, F. and Garcia-Navarro, P. (1993) 'A high-resolution Godunov-type scheme in finite volumes for the 2D shallow-water equations', *International Journal for Numerical Methods in Fluids*, 16(6), pp. 489-505.

Ambroise, B., Beven, K. and Freer, J. (1996) 'Toward a generalization of the TOPMODEL concepts: Topographic indices of hydrological similarity', *Water Resources Research*, 32(7), pp. 2135-2145.

Anastasiou, K. and Chan, C.T. (1997) 'Solution of the 2D shallow water equations using the finite volume method on unstructured triangular meshes', *International Journal for Numerical Methods in Fluids*, 24(11), pp. 1225-1245.

Anselmo, V., Galeati, G., Palmieri, S., Rossi, U. and Todini, E. (1996) 'Flood risk assessment using an integrated hydrological and hydraulic modelling approach: a case study', *Journal of Hydrology*, 175(1-4), pp. 533-554.

Archer, D. (1992) *Land of Singing Waters: Rivers and Great Floods of Northumbria*. Stocksfield: Spredden Press.

Ariff, N.M., Jemain, A.A., Ibrahim, K. and Wan Zin, W.Z. (2012) 'IDF relationships using bivariate copula for storm events in Peninsular Malaysia', *Journal of Hydrology*, 470-471, pp. 158-171.

Arnold, J.G., Srinivasan, R., Muttiah, R.S. and Williams, J.R. (1998) 'Large area hydrological modelling and assessment part I: Model development', *Journal of the American Water Resources Association*, 34(1), pp. 73-89.

Aronica, G., Bates, P.D. and Horritt, M.S. (2002) 'Assessing the uncertainty in distributed model predictions using observed binary pattern information within GLUE', *Hydrological Processes*, 16(10), pp. 2001-2016.

Asfaw, A.S. (2010) *Flood hazard assessment using geographic information system and 1D river model in Morpeth, England*. Newcastle University: MSc Dissertation.

Ashley, R., Garvin, S., Pasche, E., Vassilopoulos, A. and Zevenbergen, C. (2007) *Advances in urban flood management*. London, UK: Taylor & Francis.

Association of British Insurers (2007) *Summer floods 2007: Learning the lessons*. London, UK.

Audusse, E., Bouchut, F., Bristeau, M.O., Klein, R. and Perthame, B. (2004) 'A fast and stable well-balanced scheme with hydrostatic reconstruction for shallow water flows', *SIAM Journal on Scientific Computing*, 25(6), pp. 2050-2065.

Baeza, A. and Mulet, P. (2006) 'Adaptive mesh refinement techniques for high-order shock capturing schemes for multi-dimensional hydrodynamic simulations', *International Journal for Numerical Methods in Fluids*, 52(4), pp. 455-471.

Barber, C.P. and Shortridge, A. (2005) 'LiDAR elevation data for surface hydrologic modeling: Resolution and representation issues', *Cartography and Geographic Information Science*, 32(4), pp. 401-410.

Bates, P.D. and Anderson, M.G. (1993) 'A two-dimensional finite-element model for river flow inundation', *Proceedings of the Royal Society of London. Series A: Mathematical and Physical Sciences*, 440(1909), pp. 481-491.

Bates, P.D. and de Roo, A.P.J. (2000) 'A simple raster-based model for flood inundation simulation', *Journal of Hydrology*, 236(1-2), pp. 54-77.

Bates, P.D., Horritt, M.S. and Fewtrell, T.J. (2010) 'A simple inertial formulation of the shallow water equations for efficient two-dimensional flood inundation modelling', *Journal of Hydrology*, 387(1-2), pp. 33-45.

Begnudelli, L. and Sanders, B.F. (2007) 'Conservative wetting and drying methodology for quadrilateral grid finite-volume models', *Journal of Hydraulic Engineering*, 133(3), pp. 312-322.

Berger, M.J. and Colella, P. (1989) 'Local adaptive mesh refinement for shock hydrodynamics', *Journal of Computational Physics*, 82(1), pp. 64-84.

Berger, M.J. and Oliger, J. (1984) 'Adaptive mesh refinement for hyperbolic partial differential equations', *Journal of Computational Physics*, 53(3), pp. 484-512.

Bergström, S. (1995) 'The HBV model', in Singh, V.P. (ed.) *Computer Models of Watershed Hydrology.* Colorado, US: Water Resources Publications, pp. 443-476.

Beven, K. (2012) *Rainfall-Runoff Modelling*. Lancaster University, UK: John Wiley & Sons.

Beven, K., Calver, A. and Morris, E.M. (1987) *The Institute of Hydrology distributed model* (No.98). Wallingford, UK.

Beven, K. and Kirkby, M.J. (1979) 'A physically based, variable contributing area model of basin hydrology', *Hydrological Sciences Bulletin*, 24(1), pp. 43-69.

BMT WBM (2010) *TUFLOW User mannual*. Brisbane, Australia.

Bonnifait, L., Delrieu, G., Lay, M.L., Boudevillain, B., Masson, A., Belleudy, P., Gaume, E. and Saulnier, G.M. (2009) 'Distributed hydrologic and hydraulic modelling with radar rainfall input: Reconstruction of the 8-9 September 2002 catastrophic flood event in the Gard region, France', *Advances in Water Resources*, 32(7), pp. 1077-1089.

Boorman, D.B., Hollis, J.M. and Lilly, A. (1995) *Hydrology of soil types: a hydrologically-based classification of the soils of the United Kingdom*. Wallingford, UK.

Boughton, W. and Droop, O. (2003) 'Continuous simulation for design flood estimation - A review', *Environmental Modelling and Software*, 18(4), pp. 309-318.

Bradbrook, K.F., Lane, S.N., Waller, S.G. and Bates, P.D. (2004) 'Two dimensional diffusion wave modelling of flood inundation using a simplified channel representation', *International Journal of River Basin Management*, 2(3), pp. 211-223.

Bravo, J., Allasia, D., Paz, A., Collischonn, W. and Tucci, C. (2012) 'Coupled hydrologic-hydraulic modeling of the upper Paraguay River basin', *Journal of Hydrologic Engineering*, 17(5), pp. 635-646.

Brufau, P. and García-Navarro, P. (2003) 'Unsteady free surface flow simulation over complex topography with a multidimensional upwind technique', *Journal of Computational Physics*, 186(2), pp. 503-526.

Bussing, T.R.A. and Murman, E.M. (1988) 'Finite-volume method for the calculation of compressible chemically reacting flows', *AIAA journal*, 26(9), pp. 1070-1078.

Caleffi, V., Valiani, A. and Zanni, A. (2003) 'Finite volume method for simulating extreme flood events in natural channels', *Journal of Hydraulic Research*, 41(2), pp. 167-177.

CEH (2005) *User guidance to spreadsheet implementation of the Revitalised FEH rainfall-runoff method*. Wallingford, UK.

CEH (2009) *FEH CD-ROM 3*. Wallingford, UK.

CEH (2014) *National River Flow Archive: 22007-Wansbeck at Mitford*. Available at: http://www.ceh.ac.uk/data/nrfa/data/station.html?22007 (Accessed: 28/01/2014).

Chen, A.S., Evans, B., Djordjević, S. and Savić, D.A. (2012) 'A coarse-grid approach to representing building blockage effects in 2D urban flood modelling', *Journal of Hydrology*, 426-427, pp. 1-16.

Chow, V.T. (1973) *Open Channel Hydraulics*. New York: McGraw-Hill Book Company.

Coe, M.T. (2000) 'Modeling terrestrial hydrological systems at the continental scale: Testing the accuracy of an atmospheric GCM', *Journal of Climate*, 13(4), pp. 686-704.

Coolgeology (2013) *Morpeth floods of 2008*. Available at: http://www.coolgeography.co.uk/GCSE/AQA/Water%20on%20the%20Land/Morpeth/Morpeth.htm (Accessed: 28/12/2013).

Correia, F.N., Rego, F.C., Saraiva, M.D.G. and Ramos, I. (1998) 'Coupling GIS with hydrologic and hydraulic flood modelling', *Water Resources Management*, 12(3), pp. 229-249.

Courant, R., Friedrichs, K. and Lewy, H. (1967) 'On the partial difference equations of mathematical physics', *IBM Journal of Research and Development*, 11(2), pp. 215-234.

Crawford, N.H. and Linsley, R.K. (1966) *Digital simulation in hydrology: Stanford watershed model IV* (No. 39). Stanford, US.

Cunge, J.A., Holly, F.M. and Verwey, A. (1980) *Practical Aspects of Computational River Hydraulics*. London: Pitman Publishing Ltd.

Dale, M. (2005) 'Impact of climate change on UK flooding and future predictions', *Proceedings of the Institution of Civil Engineers: Water Management*, 158(4), pp. 135-140.

Danish Hydraulic Institute (2001) *MIKE 11 A modelling system for rivers and channels Referecne manual*. Hørsholm, Denmark.

Danish Hydraulic Institute (2011) *MIKE 21 & MIKE 3 flow model, hydrodynamic and transport module, scientific documentation*. Hørsholm, Denmark.

de Almeida, G.A.M. and Bates, P.D. (2013) 'Applicability of the local inertial approximation of the shallow water equations to flood modeling', *Water Resources Research*, 49(8), pp. 4833-4844.

de Almeida, G.A.M., Bates, P.D., Freer, J.E. and Souvignet, M. (2012) 'Improving the stability of a simple formulation of the shallow water equations for 2-D flood modeling', *Water Resources Research*, 48(5), p. W05528.

Debele, B., Srinivasan, R. and Parlange, J.Y. (2008) 'Coupling upland watershed and downstream waterbody hydrodynamic and water quality models (SWAT and CE-QUAL-W2) for better water resources management in complex river basins', *Environmental Modeling and Assessment*, 13(1), pp. 135-153.

DEFRA (2005) *Making space for water: First government response to the autumn 2004 making space for water consultation exercise*. London, UK.

DEFRA (2011) *The national flood and coastal erosion risk management strategy for England*. London, UK.

Dillon, P.J. (1988) *DIVAST: Diffuse source vertical analytical solute transport model User manual*. Melbourne, Australia: CSIRO, Institute of Natural Resources and Environment, Division of Water Resources Research.

Division for Research and Development of the French Electricity Board (2000) *2D hydrodynamics TELEMAC-2D Version 5.0 validation document*. Moret-sur-Loing, France.

Dottori, F. and Todini, E. (2011) 'Developments of a flood inundation model based on the cellular automata approach: Testing different methods to improve model performance', *Physics and Chemistry of The Earth*, 36(7-8), pp. 266-280.

EDINA Digimap (2013) *Data download*. Available at: http://digimap.edina.ac.uk/datadownload/osdownload (Accessed: 14/02/2013).

Environment Agency (2005a) *River Wansbeck Scheme Viability Note*. Bristol, UK.

Environment Agency (2005b) *Wansbeck and Blyth Catchment flood management plan*. Bristol, UK.

Environment Agency (2007) *Catchment flood management plan: History for Wansbeck at Mitford*. Bristol, UK.

Environment Agency (2009a) *Flooding in England: A national assessment of flood risk*. Bristol, UK.

Environment Agency (2009b) *Wansbeck and Blyth Catchment flood management plan*. Leeds, UK.

Environment Agency (2011) *Work continues to cut Morpeth flood risk, September 2010.* Available at: www.environment-agency.gov.uk/news/123207.aspx?month=9&year=2010&coverage=North+East (Accessed: 29/06/2011).

Environment Agency (2013a) *Flood warning*. Available at: http://maps.environment-agency.gov.uk/wiyby/wiybyController?value=Morpeth&lang=_e&ep=map&topic=fwa&layerGroups=default&scale=9&textonly=off&submit.x=12&submit.y=3#x=419976&y=586061&lg=1,&scale=9 (Accessed: 10/12/2013).

Environment Agency (2013b) *Risk of flooding from rivers and sea* Available at: http://watermaps.environment-agency.gov.uk/wiyby/wiyby.aspx?topic=floodmap#x=419920&y=585604&scale=9 (Accessed: 10/12/2013).

Erickson, V. (2011) *An evaluation of the CityCAT modelling tool: an application to the town of Morpeth, Northumberland*. Newcastle University: MSc Dissertation.

Evans, B. (2010) *A multilayered approach to two-dimensional urban flood modelling*. University of Exeter: PhD thesis.

Evans, E., Ashley, R., Hall, J., Penning-Rowsell, E., Sayers, P., Thome, C. and Watkinson, A. (2004) *Foresight: Future flooding Volume II: Managing future risks*. London, UK.

Faulkner, D. (1999) *Flood Estimation Handbook. Volume 2*. Wallingford, UK: Institute of Hydrology.

Fennema, R. and Chaudhry, M. (1990) 'Explicit methods for 2-D transient free surface flows', *Journal of Hydraulic Engineering*, 116(8), pp. 1013-1034.

Fewtrell, T., Duncan, A., Sampson, C., Neal, J. and Bates, P.D. (2011) 'Benchmarking urban flood models of varying complexity and scale using high resolution terrestrial LiDAR data', *Physics and Chemistry of The Earth*, 36(7-8), pp. 281-291.

Fewtrell, T.J., Bates, P.D., Horritt, M. and Hunter, N.M. (2008) 'Evaluating the effect of scale in flood inundation modelling in urban environments', *Hydrological Processes*, 22(26), pp. 5107-5118.

Fiedler, F.R. and Ramirez, J.A. (2000) 'A numerical method for simulating discontinuous shallow flow over an infiltrating surface', *International Journal for Numerical Methods in Fluids*, 32(2), pp. 219-239.

Fluent Incorporated Company (2006) *FLUENT 6.3 User's guide,*. Lebanon, US.

Foresight (2014) *General Reports*. Available at: http://www.dti.gov.uk/foresight/our-work/projects/published-projects/flood-and-coastal-defence/general-reports (Accessed: 30/04/2014).

Froehlich, D.C. (2010) 'Short-duration rainfall intensity equations for urban drainage design', *Journal of Irrigation and Drainage Engineering*, 136(8), pp. 519-526.

Govindaraju, R.S., Jones, S.E. and Kavvas, M.L. (1988a) 'On the diffusion wave model for overland flow: 1. Solution for steep slopes', *Water Resources Research*, 24(5), pp. 734-744.

Govindaraju, R.S., Jones, S.E. and Kavvas, M.L. (1988b) 'On the diffusion wave model for overland flow: 2. Steady state analysis', *Water Resources Research*, 24(5), pp. 745-754.

Greenberg, J.M. and Leroux, A.Y. (1996) 'A well-balanced scheme for the numerical processing of source terms in hyperbolic equations', *SIAM Journal on Numerical Analysis*, 33(1), pp. 1-16.

Grimaldi, S., Petroselli, A. and Serinaldi, F. (2012) 'Design hydrograph estimation in small and ungauged watersheds: Continuous simulation method versus event-based approach', *Hydrological Processes*, 26(20), pp. 3124-3134.

Gül, G.O., Harmancioğlu, N. and Gül, A. (2010) 'A combined hydrologic and hydraulic modeling approach for testing efficiency of structural flood control measures', *Natural Hazards*, 54(2), pp. 245-260.

Halcrow & Wallingford (1997) *ISIS Flow - User manual*. UK.

Heber Green, W. and Ampt, G.A. (1911) 'Studies on soil physics', *The Journal of Agricultural Science*, 4(1), pp. 1-24.

Hermanns, M. (2002) *Parallel programming in Fortran 95 using OpenMP*. Madrid, Spain.

HiFlows-UK (2014) *Wansbeck at Mitford* Available at: http://www.environment-agency.gov.uk/hiflows/station.aspx?22007 (Accessed: 28/01/2014).

Horritt, M.S. and Bates, P.D. (2001) 'Predicting floodplain inundation: Raster-based modelling versus the finite-element approach', *Hydrological Processes*, 15(5), pp. 825-842.

Horritt, M.S. and Bates, P.D. (2002) 'Evaluation of 1D and 2D numerical models for predicting river flood inundation', *Journal of Hydrology*, 268(1-4), pp. 87-99.

Hou, J., Liang, Q., Simons, F. and Hinkelmann, R. (2013) 'A 2D well-balanced shallow flow model for unstructured grids with novel slope source term treatment', *Advances in Water Resources*, 52(0), pp. 107-131.

Hou, J., Zhang, H. and Liang, Q. (2014) 'Flood simulation using effcient non-uniform structured grids with automatically captured local high-resolution', *Journal of Hydrology*, Submitted.

Houghton-Carr, H. (1999) *Flood Estimation Handbook. Volume 4*. Wallingford, UK: Institute of Hydrology.

Hsu, K., Gupta, H.V. and Sorooshian, S. (1995) 'Artificial Neural Network Modeling of the Rainfall-Runoff Process', *Water Resources Research*, 31(10), pp. 2517-2530.

Hughes, D.A. and Sami, K. (1994) 'A semi-distributed, variable time interval model of catchment hydrology - structure and parameter estimation procedures', *Journal of Hydrology*, 155(1-2), pp. 265-291.

Hundecha, Y. and Bárdossy, A. (2004) 'Modeling of the effect of land use changes on the runoff generation of a river basin through parameter regionalization of a watershed model', *Journal of Hydrology*, 292(1-4), pp. 281-295.

Hunt, J.C.R. (2002) 'Floods in a changing climate: A review', *Philosophical Transactions of the Royal Society A: Mathematical, Physical and Engineering Sciences*, 360(1796), pp. 1531-1543.

Hunter, N.M., Bates, P.D., Horritt, M.S. and Wilson, M.D. (2006) 'Improved simulation of flood flows using storage cell models', *Proceedings of the Institution of Civil Engineers: Water Management*, 159(1), pp. 9-18.

Hunter, N.M., Bates, P.D., Horritt, M.S. and Wilson, M.D. (2007) 'Simple spatially-distributed models for predicting flood inundation: A review', *Geomorphology*, 90(3-4), pp. 208-225.

Hunter, N.M., Bates, P.D., Neelz, S., Pender, G., Villanueva, I., Wright, N.G., Liang, D., Falconer, R.A., Lin, B., Waller, S., Crossley, A.J. and Mason, D.C. (2008) 'Benchmarking 2D hydraulic models for urban flooding', *Proceedings of the Institution of Civil Engineers: Water Management*, 161(1), pp. 13-30.

Hunter, N.M., Horritt, M.S., Bates, P.D., Wilson, M.D. and Werner, M.G.F. (2005) 'An adaptive time step solution for raster-based storage cell modelling of floodplain inundation', *Advances in Water Resources*, 28(9), pp. 975-991.

IPCC (2007) *Climate Change 2007: Synthesis Report*. Valencia, Spain.

Ivanenko, S.A. and Muratova, G.V. (2000) 'Adaptive grid shallow water modeling', *Applied Numerical Mathematics*, 32(4), pp. 447-482.

Iwagaki, Y. (1955) 'Fundamental studies on the runoff analysis by characteristics', *Bulletins - Disaster Prevention Research Institute, Kyoto University*, 10, pp. 1-25.

JBA Consulting (2009) *Flooding in Castle Morpeth 6 & 7 September 2008: Independent Review*. Northampton, UK.

JBA Consulting (2010) *Morpeth flood hazard study*. Newcastle upon Tyne, UK.

Jenson, S.K. and Domingue, J.O. (1988) 'Extracting topographic structure from digital elevation data for geographic information system analysis', *Photogrammetric Engineering and Remote Sensing*, 54(11), pp. 1593-1600.

Ji, H., Lien, F.S. and Yee, E. (2010) 'A new adaptive mesh refinement data structure with an application to detonation', *Journal of Computational Physics*, 229(23), pp. 8981-8993.

Jonkman, S.N., Bočkarjovab, I.M., Kokc, M. and Bernardinid, P. (2008) 'Integrated hydrodynamic and economic modelling of flood damage in the Netherlands', *Ecological Economics* (66), pp. 77-90.

Jonkman, S.N. and Kelman, I. (2005) 'An analysis of the causes and circumstances of flood disaster deaths', *Disasters*, 29(1), pp. 95-97.

Kesserwani, G. and Liang, Q. (2010) 'A discontinuous Galerkin algorithm for the two-dimensional shallow water equations', *Computer Methods in Applied Mechanics and Engineering*, 199(49-52), pp. 3356-3368.

Kim, J., Warnock, A., Ivanov, V.Y. and Katopodes, N.D. (2012) 'Coupled modeling of hydrologic and hydrodynamic processes including overland and channel flow', *Advances in Water Resources*, 37, pp. 104-126.

Kite, G.W. and Kouwen, N. (1992) 'Watershed modeling using land classifications', *Water Resources Research*, 28(12), pp. 3193-3200.

Kjeldsen, T.R. (2007a) *Flood Estimation Handbook. Supplementary Report No.1*. Wallingford, UK: Centre for Ecology and Hydrology.

Kjeldsen, T.R. (2007b) *Flood Estimation Handbook. Supplementary Report No.1*. Centre for Ecology and Hydrology, Wallingford, UK.

König, A., Sægrov, S. and Schilling, W. (2002) 'Damage assessment for urban flooding.', *The 9th International Conference on Urban Drainage*. Oregon, U.S. pp. 1-11.

Kowalik, J. (1994) *PVM: Parallel Virtual Machine*. London, UK: The MIT Press.

Krámer, T. and Józsa, J. (2007) 'Solution-adaptivity in modelling complex shallow flows', *Computers & Fluids*, 36(3), pp. 562-577.

Kumar, D., Bhishm, S.K. and Khati, S. (2012) 'Black box model for flood forecasting', *Journal of Civil Engineering (IEB)*, 40(1), pp. 47-59.

Lastra, J., Fernández, E., Díez-Herrero, A. and Marquínez, J. (2008) 'Flood hazard delineation combining geomorphological and hydrological methods: An example in the Northern Iberian Peninsula', *Natural Hazards*, 45(2), pp. 277-293.

Lehner, B., Döll, P., Alcamo, J., Henrichs, T. and Kaspar, F. (2006) 'Estimating the impact of global change on flood and drought risks in Europe: A continental, integrated analysis', *Climatic Change*, 75(3), pp. 273-299.

Lerat, J., Perrin, C., Andréassian, V., Loumagne, C. and Ribstein, P. (2012) 'Towards robust methods to couple lumped rainfall-runoff models and hydraulic models: A sensitivity analysis on the Illinois River', *Journal of Hydrology*, 418-419, pp. 123-135.

Lian, Y., Chan, I.C., Singh, J., Demissie, M., Knapp, V. and Xie, H. (2007) 'Coupling of hydrologic and hydraulic models for the Illinois River Basin', *Journal of Hydrology*, 344(3-4), pp. 210-222.

Liang, D., Falconer, R.A. and Lin, B. (2007a) 'Coupling surface and subsurface flows in a depth averaged flood wave model', *Journal of Hydrology*, 337(1-2), pp. 147-158.

Liang, D., Falconer, R.A. and Lin, B. (2007b) 'Linking one- and two-dimensional models for free surface flows', *Proceedings of the Institution of Civil Engineers: Water Management*, 160(3), pp. 145-151.

Liang, D., Lin, B. and Falconer, R.A. (2007c) 'Simulation of rapidly varying flow using an efficient TVD–MacCormack scheme', *International Journal for Numerical Methods in Fluids*, 53(5), pp. 811-826.

Liang, Q. (2010) 'Flood simulation using a well-balanced shallow flow model', *Journal of Hydraulic Engineering*, 136(9), pp. 669-675.

Liang, Q. (2011) 'A structured but non-uniform Cartesian grid-based model for the shallow water equations', *International Journal for Numerical Methods in Fluids*, 66(5), pp. 537-554.

Liang, Q. (2012) 'A simplified adaptive Cartesian grid system for solving the 2D shallow water equations', *International Journal for Numerical Methods in Fluids*, 69(2), pp. 442-458.

Liang, Q. and Borthwick, A.G.L. (2009) 'Adaptive quadtree simulation of shallow flows with wet-dry fronts over complex topography', *Computers and Fluids*, 38(2), pp. 221-234.

Liang, Q., Borthwick, A.G.L. and Stelling, G. (2004) 'Simulation of dam- and dyke-break hydrodynamics on dynamically adaptive quadtree grids', *International Journal for Numerical Methods in Fluids*, 46(2), pp. 127-162.

Liang, Q., Du, G., Hall, J. and Borthwick, A.G.L. (2008) 'Flood inundation modeling with an adaptive quadtree grid shallow water equation solver', *Journal of Hydraulic Engineering - ASCE*, 134(11), pp. 1603-1610.

Liang, Q. and Marche, F. (2009) 'Numerical resolution of well-balanced shallow water equations with complex source terms', *Advances in Water Resources*, 32(6), pp. 873-884.

Lighthill, M.J. and Whitham, G.B. (1955a) 'On kinematic waves. I. Flood movement in long rivers', *Proceedings of the Royal Society of London. Series A, Mathematical and Physical Sciences*, 229(1178), pp. 281-316.

Lighthill, M.J. and Whitham, G.B. (1955b) 'On kinematic waves. II. A theory of traffic flow on long crowded roads', *Proceedings of the Royal Society of London. Series A, Mathematical and Physical Sciences*, 229(1178), pp. 317-345.

Ma, J., Lin, G., Chen, J. and Yang, L. (2010) 'An improved topographic wetness index considering topographic position', *18th International Conference on Geoinformatics*. Beijing, China.

Madsen, H., Mikkelsen, P.S., Rosbjerg, D. and Harremoës, P. (2002) 'Regional estimation of rainfall intensity-duration-frequency curves using generalized least squares regression of partial duration series statistics', *Water Resources Research*, 38(11), pp. 211-2111.

Mark, O., Weesakul, S., Apirumanekul, C., Aroonnet, S.B. and Djordjević, S. (2004) 'Potential and limitations of 1D modelling of urban flooding', *Journal of Hydrology*, 299(3-4), pp. 284-299.

Marsh, T.J. and Hannaford, J. (2007) *The summer 2007 floods in England and Wales - a hydrological appraisal*. Wallingford, U.K.

Mediero, L., Jiménez-Álvarez, A. and Garrote, L. (2010) 'Design flood hydrographs from the relationship between flood peak and volume', *Hydrology and Earth System Sciences*, 14(12), pp. 2495-2505.

Mejia, A.I. and Reed, S.M. (2011) 'Evaluating the effects of parameterized cross section shapes and simplified routing with a coupled distributed hydrologic and hydraulic model', *Journal of Hydrology*, 409(1-2), pp. 512-524.

Met Office (2008a) *Heavy rainfall early Septembe 2008*. Available at: http://www.metoffice.gov.uk/climate/uk/interesting/sep2008/ (Accessed: 08/12/2013).

Met Office (2008b) *Heavy rainfall early September 2008*. Available at: http://www.metoffice.gov.uk/climate/uk/interesting/sep2008/ (Accessed: 08/12/2013).

Met Office (2009) *Warming – climate change: the facts*. Exeter, UK.

Met Office (2014) *The Recent Storms and Floods in the UK*. Exeter, UK.

Moramarco, T., Melone, F. and Singh, V.P. (2005) 'Assessment of flooding in urbanized ungauged basins: a case study in the Upper Tiber area, Italy', *Hydrological Processes*, 19(10), pp. 1909-1924.

Morita, M. and Yen, B.C. (2002) 'Modeling of conjunctive two-dimensional surface-three-dimensional subsurface flows', *Journal of Hydraulic Engineering*, 128(2), pp. 184-200.

Morpeth Flood Action Group *Alleviation Scheme*. Available at: http://www.morpethfloodaction.org.uk/fas.html (Accessed: 01/03/2014).

Nash, J.E. and Sutcliffe, J.V. (1970) 'River flow forecasting through conceptual models part I - A discussion of principles', *Journal of Hydrology*, 10(3), pp. 282-290.

Neal, J., Fewtrell, T. and Trigg, M. (2009) 'Parallelisation of storage cell flood models using OpenMP', *Environmental Modelling & Software*, 24(7), pp. 872-877.

Neal, J., Schumann, G., Fewtrell, T., Budimir, M., Bates, P.D. and Mason, D. (2011) 'Evaluating a new LISFLOOD-FP formulation with data from the summer 2007 floods in Tewkesbury, UK', *Journal of Flood Risk Management*, 4(2), pp. 88-95.

Newcastle City Council (2013) *Summer 2012 Flooding in Newcastle upon Tyne: A report on the experiences of residents and non-residential property managers*. Newcastle upton Tyne, UK.

Ozdemir, H., Sampson, C.C., de Almeida, G.A.M. and Bates, P.D. (2013) 'Evaluating scale and roughness effects in urban flood modelling using terrestrial LIDAR data', *Hydrology and Earth System Sciences*, 17(10), pp. 4015-4030.

Paiva, R.C.D., Collischonn, W. and Tucci, C.E.M. (2011) 'Large scale hydrologic and hydrodynamic modeling using limited data and a GIS based approach', *Journal of Hydrology*, 406(3-4), pp. 170-181.

Parkin, G. (2010) *The September 2008 Morpeth flood: Information gathering for dynamic flood reconstruction.* Newcastle upon Tyne: Newcastle University.

Parlange, J.Y., Hogarth, W.L., Sander, G.C., Surin, A. and Haverkamp, R. (1989) 'Comment on "On the diffusion wave model for overland flow: 2. Steady state analysis" by R. S. Govindaraju, S. E. Jones, and M. L. Kauvas', *Water Resources Research*, 25(8), pp. 1923-1924.

Pau, J. and Sanders, B. (2006a) 'Performance of parallel implementations of an explicit finite-volume shallow-water model', *Journal of Computing in Civil Engineering*, 20(2), pp. 99-110.

Pau, J.C. and Sanders, B.F. (2006b) 'Performance of parallel implementations of an explicit finite-volume shallow-water model', *Journal of Computing in Civil Engineering*, 20(2), pp. 99-110.

Penning-Rowsell, E., Viavattene, C., Pardoe, J., Chatterton, J., Parker, D. and Morris, J. (2010) *The benefits of flood and coastal risk management: A handbook of assessment techniques*. London: Flood Hazard Research Centre.

Pitt, M. (2008) *The Pitt Review: lessons learned from the 2007 floods*. London, UK.

Popinet, S. (2012) 'Adaptive modelling of long-distance wave propagation and fine-scale flooding during the Tohoku tsunami', *Natural Hazards and Earth System Sciences*, 12(4), pp. 1213-1227.

Prinsen, G.F. and Becker, B.P.J. (2011) 'Application of sobek hydraulic surface water models in the Netherlands hydrological modelling instrument', *Irrigation and Drainage*, 60(SUPPL. 1), pp. 35-41.

Rabenseifner, R., Hager, G. and Jost, G. (2009) 'Hybrid MPI/OpenMP parallel programming on clusters of multi-core SMP nodes', *17th Euromicro International Conference on Parallel, Distributed and Network-Based Processing*. Weimar, Germany. pp. 427-436.

Raber, G.T., Jensen, J.R., Hodgson, M.E., Tullis, J.A., Davis, B.A. and Berglund, J. (2007) 'Impact of LiDAR nominal post-spacing on DEM accuracy and flood zone delineation', *Photogrammetric Engineering and Remote Sensing*, 73(7), pp. 793-804.

Rahman, A., Weinmann, P.E., Hoang, T.M.T. and Laurenson, E.M. (2002) 'Monte Carlo simulation of flood frequency curves from rainfall', *Journal of Hydrology*, 256(3-4), pp. 196-210.

Rawls, W.J., Brakensiek, C.L. and Saxton, K.E. (1982) 'Estimation of soil water properties', *Transactions - American Society of Agricultural Engineers*, 25(5), pp. 1316-1320, 1328.

Rawls, W.J. and Brakensiek, D.L. (1985) 'Prediction of soil water properties for hydrologic modelling', *Proceeding of Symposium on Wathershed Management in the Eighties*, pp. 293-299.

Refsgaard, J.C. and Storm, B. (1995) *Computer Models of Watershed Hydrology*. Highlands Park, CO, US: Water Resources Publication.

Reich, B.M. (1963) 'Short-duration rainfall-intensity estimates and other design aids for regions of sparse data', *Journal of Hydrology*, 1(1), pp. 3-28.

Rijkswaterstaat (2005) *Flood risks and safety in the Netherlands-full report*. Delft: Ministry of Transport and Public Works and Water Management.

Robson, A. and Reed, D. (1999) *Flood Estimation Handbook. Volume 3*. Wallingford, UK: Institute of Hydrology.

Rogers, B., Fujihara, M. and Borthwick, A.G.L. (2001) 'Adaptive Q-tree Godunov-type scheme for shallow water equations', *International Journal for Numerical Methods in Fluids*, 35(3), pp. 247-280.

Rogers, B.D., Borthwick, A.G.L. and Taylor, P.H. (2003) 'Mathematical balancing of flux gradient and source terms prior to using Roe's approximate Riemann solver', *Journal of Computational Physics*, 192(2), pp. 422-451.

Sampson, C.C., Bates, P.D., Neal, J.C. and Horritt, M.S. (2013) 'An automated routing methodology to enable direct rainfall in high resolution shallow water models', *Hydrological Processes*, 27(3), pp. 467-476.

Schubert, J.E. and Sanders, B.F. (2012) 'Building treatments for urban flood inundation models and implications for predictive skill and modeling efficiency', *Advances in Water Resources*, 41, pp. 49-64.

Schubert, J.E., Sanders, B.F., Smith, M.J. and Wright, N.G. (2008) 'Unstructured mesh generation and landcover-based resistance for hydrodynamic modeling of urban flooding', *Advances in Water Resources*, 31(12), pp. 1603-1621.

Shankar, S., Kalyanapu, A.J., Hansen, C.D., Burian, S.J. and (2010) 'A GPU-based flood simulation framework', *Symposium on Application Accelerators in High Performance Computing*. Tennessee, US.

Shepard, D. (1968) 'Two-dimensional interpolation function for irregularly-spaced data', *Proceeding of 23rd ACM National Conference*, pp. 517-524.

Singh, V.P. (1996) *Kinematic Wave Modeling in Water Resources: Surface Water Hydrology*. New York: Wiley.

Singh, V.P. (2001) 'Kinematic wave modelling in water resources: A historical perspective', *Hydrological Processes*, 15(4), pp. 671-706.

Skoula, Z.D., Borthwick, A.G.L. and Moutzouris, C.I. (2006) 'Godunov-type solution of the shallow water equations on adaptive unstructured triangular grids', *International Journal of Computational Fluid Dynamics*, 20(9), pp. 621-636.

Sleigh, P.A., Gaskell, P.H., Berzins, M. and Wright, N.G. (1998) 'An unstructured finite-volume algorithm for predicting flow in rivers and estuaries', *Computers and Fluids*, 27(4), pp. 479-508.

SMHI (2006) *HBV model*. Available at: http://www.smhi.se/sgn0106/if/hydrologi/hbv.htm (Accessed: 19/07/2014).

Smith, L.S. and Liang, Q. (2013) 'Towards a generalised GPU/CPU shallow-flow modelling tool', *Computers & Fluids*, 88, pp. 334-343.

Soares-Frazão, S., Lhomme, J., Guinot, V. and Zech, Y. (2008) 'Two-dimensional shallow-water model with porosity for urban flood modelling', *Journal of Hydraulic Research*, 46(1), pp. 45-64.

Song, L., Zhou, J., Guo, J., Zou, Q. and Liu, Y. (2011) 'A robust well-balanced finite volume model for shallow water flows with wetting and drying over irregular terrain', *Advances in Water Resources*, 34(7), pp. 915-932.

Strahler, A.N. (1952) 'Hypsometric (area-altitude) analysis of erosional topology ', *Geological Society of America Bulletin* 63 (11), pp. 1117-1142.

Syme, W.J. (2008) 'Flooding in urban areas - 2D modelling approaches for buildings and fences', *Engineers Australia, 9th National Conference on Hydraulics in Water Engineering*. Darwin, Australia.

Tesfaye, Y.G., Meerschaert, M.M. and Anderson, P.L. (2006) 'Identification of periodic autoregressive moving average models and their application to the modeling of river flows', *Water Resources Research*, 42(1), p. W01419.

The European Union (2007) 'Directive 2007/60/EC of the European Parliament and of the Council of 23 October 2007 on the assessment and management of flood risks', *Official Journal of the European Union*, (L 288/27).

Thompson, J. (2004) 'Simulation of wetland water-level manipulation using coupled hydrological/hydraulic modeling', *Physical Geography*, 25(1), pp. 39-67.

Toro, E.F. (2001) *Shock-Capturing Methods for Free-Surface Shallow Flows*. Chichester: John Wiley & Sons.

Toro, E.F., Spruce, M. and Speares, W. (1994) 'Restoration of the contact surface in the HLL-Riemann solver', *Shock Waves*, 4(1), pp. 25-34.

Tran, V. and Hluchy, L. (2004) 'Parallelizing flood models with MPI: Approaches and experiences', in Bubak, M., Albada, G., Sloot, P.A. and Dongarra, J. (eds.) *Computational Science - ICCS 2004*. Berlin, Germany: Springer, pp. 425-428.

US Army Corps of Engineers (2010) *HEC-RAS river analysis system User's Manual*. Washington, DC, US.

US Army Engineer Research and Development Center (2006) *Users guide to RMA2 WES version 4.5*. Vicksburg, US.

VICAIRE (2006) *Engineering Hydrology*. Available at: http://echo2.epfl.ch/VICAIRE/mod_1b/chapt_10/main.htm (Accessed: 21/01/2014).

Waheed, A.A. and Chukwuemeka, A.J. (2010) 'The impacts of urbanization on Kaduna River flooding', *Journal of American Science*, 6(5), pp. 28-35.

Walker, G.R. and Zhang, L. (2002) 'Plot scale models and their application to recharge studies', in Walker, G.R. and Zhang, L. (eds.) *Studies in Catchment Hydrology: the basics of recharge and discharge.* Melbourne, Australia: CSIRO.

Wang, Y., Liang, Q., Kesserwani, G. and Hall, J.W. (2011a) 'A 2D shallow flow model for practical dam-break simulations', *Journal of Hydraulic Research*, 49(3), pp. 307-316.

Wang, Y., Liang, Q., Kesserwani, G. and Hall, J.W. (2011b) 'A positivity-preserving zero-inertia model for flood simulation', *Computers and Fluids*, 46(1), pp. 505-511.

Ward, E. (2008) *Development of a continuous simulation approach for flood risk estimation applied to the Wansbeck Catchment*. Newcastle University: MSc Dissertation.

Whiteaker, T.L., Robayo, O., Maidment, D.R. and Obenour, D. (2006) 'From a NEXRAD rainfall map to a flood inundation map', *Journal of Hydrologic Engineering*, 11(1), pp. 37-45.

Wilson, M.D. and Atkinson, P.M. (2003) 'Sensitivity of a flood inundation model to spatially-distributed friction', *Geoscience and Remote Sensing Symposium Proceedings*, 3, pp. 1579-1581.

Xia, J., Falconer, R.A., Lin, B. and Tan, G. (2011) 'Numerical assessment of flood hazard risk to people and vehicles in flash floods', *Environmental Modelling & Software*, (26), pp. 987-998.

Yu, D. (2005) *Diffusion-based modelling of flood inundation over complex floodplains*. University of Leeds: PhD thesis.

Yu, D. (2010) 'Parallelization of a two-dimensional flood inundation model based on domain decomposition', *Environmental Modelling & Software*, 25(8), pp. 935-945.

Yu, D. and Lane, S.N. (2006a) 'Urban fluvial flood modelling using a two-dimensional diffusion-wave treatment, part 1: Mesh resolution effects', *Hydrological Processes*, 20(7), pp. 1541-1565.

Yu, D. and Lane, S.N. (2006b) 'Urban fluvial flood modelling using a two-dimensional diffusion-wave treatment, part 2: Development of a sub-grid-scale treatment', *Hydrological Processes*, 20(7), pp. 1567-1583.

Zhang, C., Liang, Q. and Yin, J. (2013) 'A first-order adaptive solution to rapidly spreading flood waves', *Progress in Computational Fluid Dynamics*, 13(1), pp. 1-10.

Zhang, H., Wang, Y., Liang, Q., Smith, L.S. and Kilsby, C.G. (2014) 'Non-negative depth reconstruction for a two-dimensional partial inertial inundation model ', *Journal of Hydroinformatics*, In press.

Zhao, D., Shen, H., Tabios, G., Lai, J. and Tan, W. (1994) 'Finite-volume two-dimensional unsteady fow model for river basins', *Journal of Hydraulic Engineering*, 120(7), pp. 863-883.

Zhou, J.G., Causon, D.M., Mingham, C.G. and Ingram, D.M. (2001) 'The surface gradient method for the treatment of source terms in the shallow-water equations', *Journal of Computational Physics*, 168(1), pp. 1-25.